INEEL/EXT-02-00300

Key Differences in the Fabrication, Irradiation and Safety Testing of U.S. and German TRISO-coated Particle Fuel and Their Implications on Fuel Performance

David A. Petti
John T. Maki
Jacopo Buongiorno
Richard R. Hobbins
Gregory K. Miller

June 2002

Idaho National Engineering and Environmental Laboratory
Bechtel BWXT Idaho, LLC

INEEL/EXT-02-00300

Key Differences in the Fabrication, Irradiation and Safety Testing of U.S. and German TRISO-coated Particle Fuel and Their Implications on Fuel Performance

David A. Petti
John T. Maki
Jacopo Buongiorno
Richard R. Hobbins
Gregory K. Miller

June 2002

Idaho National Engineering and Environmental Laboratory

Idaho Falls, Idaho 83415

Prepared for
Bechtel National and for the
U.S. Department of Energy
Through the INEEL Bechtel Corporate Funded R&D (CFRD) Program
Under DOE Idaho Operations Office
Contract DE-AC07-99ID13727

EXECUTIVE SUMMARY

High temperature gas reactor technology is achieving a renaissance around the world. This technology relies on high quality production and performance of coated particle fuel. Historically, the irradiation performance of TRISO-coated gas reactor particle fuel in Germany has been superior to that in the United States. German fuel generally displayed in-pile gas release values that were three orders of magnitude lower than U.S. fuel. Thus, we have critically examined the TRISO-coated fuel fabrication processes in the U.S. and Germany and the associated irradiation database with a goal of understanding why the German fuel behaves acceptably, why the U.S. fuel has not faired as well, and what process/ production parameters impart the reliable performance to this fuel form. The postirradiation examination results are also reviewed to identify failure mechanisms that may be the cause of the poorer U.S. irradiation performance. This comparison will help determine the roles that particle fuel process/product attributes and irradiation conditions (burnup, fast neutron fluence, temperature, and degree of acceleration) have on the behavior of the fuel during irradiation and provide a more quantitative linkage between acceptable processing parameters, as-fabricated fuel properties and subsequent in-reactor performance.

Fabrication

A review of the fabrication processes used in Germany and the U.S. to make coated particle fuel indicates that the scale of fuel fabrication and development efforts in the last 25 years were quite different. German fabrication of modern TRISO-coated fuel was industrial/production scale incorporating improvements from fuel produced for the German AVR and THTR reactors. Strict process control was used to adhere to a process specification that produced high quality fuel. Only ~ 100 defects were found in 3.3 million particles produced. By contrast, the U.S. program post Fort St. Vrain was a mixture of lab scale and larger scale fabrication with some fuel fabrication done by GA and some done by Oak Ridge National Laboratory. Furthermore, different fuel and coating types, different fabrication process parameters, and different coaters and compact fabrication techniques were used in an attempt to produce high quality fuel. The result was an initial defect level in U.S. fuel that varied greatly and was much greater than those produced in Germany. Table E-1 compares each of the steps in the fabrication of German and U.S. TRISO-coated fuel. The U.S. entries are based on the fabrication of fuel for the New Production Reactor (NPR) program in the early 1990s. It is important to note that many of the

steps used to make this fuel were unique to the program and are not considered part of the traditional U.S. fabrication effort. Nevertheless, the NPR experience was used in this report primarily because it was the last manufacturing campaign in the U.S. and represents the most complete manufacturing pedigree and testing campaign of modern U.S. TRISO fuel, albeit HEU, aimed at commercial scale deployment. Furthermore, because the U.S. did not have a highly focused goal like the Germans, kernel and coating types varied which made selection of a U.S. "reference" fabrication process for this comparison problematic.

Table E-1. Comparison of U.S. and German TRISO-coated Particle Fuel Fabrication

		U.S. NPR	GERMAN
KERNEL FABRICATION			
Kernel Material		HEU-UCO	LEU-UO_2
Gel-Precipitation		Internal	External
Broth Composition		Aqueous solution of uranyl nitrate, carbon-black, Tamol, urea, Hexamethylene Tetramine	Aqueous solution of uranyl nitrate, Polyvinyl Alcohol, and other non-specified additives
Droplet Formation		Vibrating nozzle	Vibrating nozzle
Gelation Medium		Trichloroethylene	Ammonia gas and ammonia solution
Washing		Ammonia solution and clean water	Ammonia solution and isopropanol
Drying		Air at 60°C	80°C
Calcination		Ar at 350°C	Air at 300°C
Reduction		H_2 at 1600°C	na
Sintering		CO at 1800°C	H_2 at 1600-1700°C
COATING			
Coating Process		Discontinuous	Continuous
Buffer	Gas Composition	Ar-C_2H_2	Ar-C_2H_2
	Coating Temp.	1300°C	1250°C
	Coating Rate	na	6-10 μm/min
Seal	Gas Composition	Ar-C_3H_6	na
	Coating Temp.	1200°C	na
IPyC	Gas Composition	Ar-C_2H_2-C_3H_6	Ar-C_2H_2-C_3H_6
	Coating Temp.	1230°C	1300°C
	Coating Conc. & Rate	Low/<4 μm/min	Higher/4-6 μm/min
SiC	Gas Composition	H_2-CH_3SiCl_3	H_2-CH_3SiCl_3
	Coating Temp.	1650°C	1500°C
	Coating Rate	0.2-0.4 μm/min	0.2 μm/min
OPyC	Gas Composition	Ar-C_2H_2-C_3H_6	Ar-C_2H_2-C_3H_6
	Coating Temp.	>1300°C	1300°C
	Coating Conc. &Rate	Low/<4 μm/min	Higher/4-6 μm/min
Seal	Gas Composition	Ar-C_3H_6	na
	Coating Temp.	1200°C	na
PPyC	Gas Composition	Ar-C_2H_2	na
	Coating Temp.	1300°C	na
	Coating Rate	na	na
Seal	Gas Composition	Ar-C_3H_6	na
	Coating Temp.	1200°C	na
FUEL ELEMENT MANUFACTURE			
Fuel Element		Compact	Pebble
Matrix Materials		Graphite flour, graphite shim octadecanol, polystyrene	Graphite powder
Binders		Petroleum pitch	Phenol, hexamethylene-tetramine
Matrix State		Liquid	Powder
Overcoating		na	200 μm
Pre-Pressing		na	25°C, 30 MPa
Pressing		160°C, 6.9 MPa	25°C, 300-350 MPa
Lathing		na	Yes
Carbonization		900°C in alumina powder	800-900°C in inert gas
Leaching		HCl	na
Heat Treatment		1650°C in Ar	1950°C in vacuum

Both German and U.S. fuel fabrication processes consist of a number of similar steps. Kernels are made via a traditional sol-gel process, followed by washing, drying and calcining to produce UO_2 kernels in Germany and UCO kernels in the U.S. The major differences in kernel production are the addition of carbon black to the broth and a sintering step using CO in the U.S. process to ensure appropriate C/O stoichiometry in the UCO kernel. The coating processes for the buffer are similar, based on chemical vapor deposition from a mixture of Ar and acetylene in a coater between 1250 and 1300°C. A 5μm seal coat is produced in the U.S. to seal off the buffer; this step does not occur in the German process.

Major differences in the production of the TRISO coating are the coater design and the fact that all three layers are coated in a continuous manner in the German process, whereas in the U.S. process the fuel particles are unloaded after each coating layer to perform QC measurements. The inner pyrocarbon layer in both cases is deposited from a mixture of acetylene, propylene, and argon. The temperature in the U.S. process is somewhat lower than in German process and coating gas concentrations are different, producing a different microstructure for the IPyC. The SiC layer is deposited from a mixture of hydrogen and methyltrichlorosilane, at similar coating rates although the temperature for U.S. coating is about 150°C higher than that used in the German process. The OPyC layers are coated in a manner similar to the IPyC layer. In the U.S., seal coats and protective pyrocarbon (PPyC) were added which is not standard in U.S. fabrication. Neither is used in the German process.

The fuel pebble in Germany uses graphite powder and man-made organic binders to produce a powder matrix that is used to overcoat the particles and to create the fuel pebble. In the U.S., a liquid matrix composed of graphite flour, graphite shim, and additives, mixed with petroleum pitch binder is used to make the fuel compact. Both fuel forms are pressed and then carbonized at high temperature (800-900°C). HCl is used to leach impurities from the U.S. compact. Ultra high purity systems and feedstock are used in the manufacture of pebbles in Germany to ensure adequate control of impurities. Both fuel forms undergo a final heat treatment with the U.S. compact heated at 1650°C with an Ar purge and the German pebble at 1950°C in vacuum. (The report also discusses the fabrication process for Chinese and Japanese TRISO-coated fuel.).

It appears that the major difference in as-manufactured fuel quality between the German and U.S. fuel, expressed as heavy metal contamination and SiC defects, arises from differences in fabrication of the fuel bodies (German pebbles vs. U.S. compacts). Figure E-1 compares the

beginning of life Kr-85m R/B for German and U.S. irradiations discussed earlier in this section. This measurement was selected as a metric of as-manufactured quality. The results show that German fuel had consistently lower initial defects than the U.S. fuel in the 1980s and further that it improved over that time as was the case for fuel used in AVR; in fact the lowest ever R/B measured in an in-reactor irradiation is from German fuel (~ 10^{-10}). The initial defect level in U.S. fuel was much higher and showed great variability in the time from 1970-1980. The level did not significantly change until the early 1990s when serious effects at reduction of initial contamination were undertaken in the fabrication campaign. Unfortunately, those very low levels of contamination were followed by in-reactor fuel failures at the percent level.

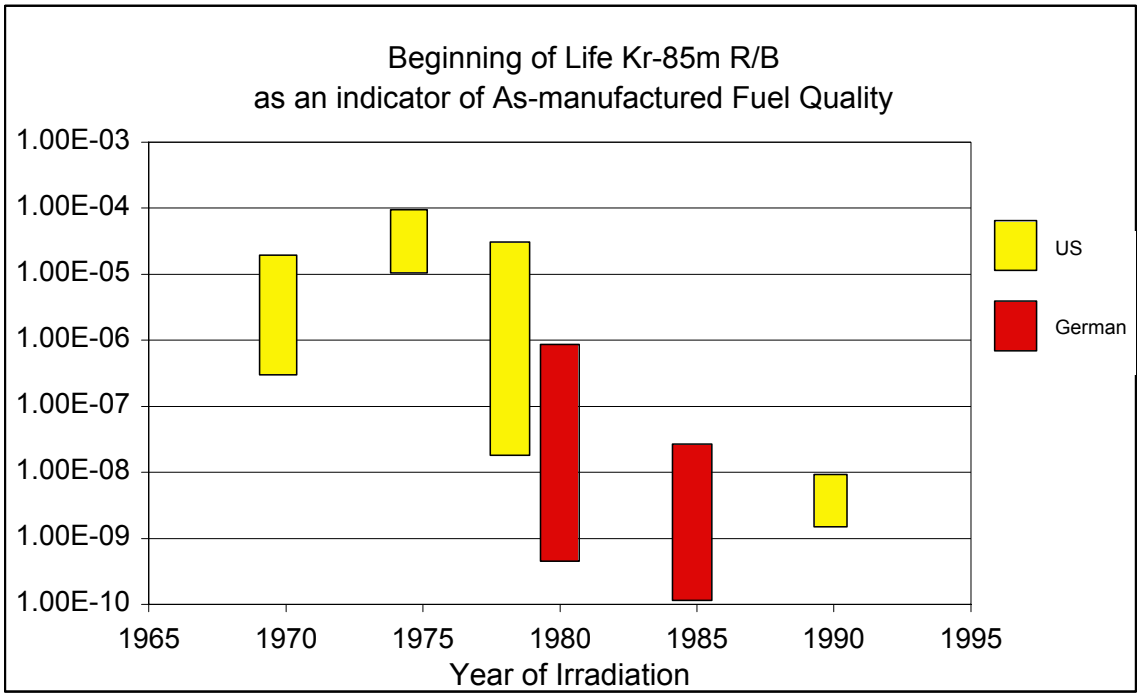

Figure E-1. Comparison of BOL Kr-85m R/B from German and U.S. irradiations.

Irradiation Performance

Numerous in-pile irradiation experiments have been conducted in both the U.S. and Europe as part of the U.S. and German TRISO-coated particle fuel development efforts. These irradiations were conducted at a variety of burnups, temperatures, and fluences. The rate of accumulation of burnup and fast fluence (i.e., the degree of acceleration) in the irradiation relative to that expected in the reactor may also be an important difference. Note that for most of these fuels, the time to reach goal burnup and fast fluence is ~ 1095 days (3 years) whereas in the irradiations the time to reach peak conditions were accelerated by factor of 3 to 10. A summary of salient features of the irradiations is found in Table E-2.

Table E-2. Summary of Particle Fuel Irradiation Experiments.

Test/cell	Fuel forms	Irrad.time (d)/ Accel. Level	Peak temp. (°C)	Peak fissile & fertile burnup (%FIMA)	Peak fluence (10^{25} n/m^2)	EOL Kr-85m R/B (10^{-6})
U.S. Experiments						
F-30/1	HEU (Th,U)C_2 TRISO & ThC_2 TRISO	269/4x	1100	15.0 / 3.0	8.0	8
F-30/2			1100	19.0 / 4.5	10.5	100
F-30/3			1120	20.0 / 5.0	11.5	10
F-30/4			1100	18.0 / 4.0	9.5	20
F-30/5			1200	12.0 / 1.5	12.0	20
HRB-4	LEU WAR UC_2 TRISO & ThO_2 BISO	244/4.5x	1250	27.7 / 13.4	10.5	320
HRB-5	LEU WAR UC_2 TRISO & ThO_2 BISO	107/10x	1250	15.7 / 4.3	4.7	100
HRB-6	HEU (Th,U)C_2 TRISO & ThO_2 BISO	183/6x	1100	26.6 / 9.3	7.9	270
OF-2/1	WAR UCO UC_2 (Th,U)O_2 TRISO & ThO_2 BISO	352/3x	1350	79.6 / 4.3	8.9	100
OF-2/2			1350	79.5 / 4.3	8.4	5
HRB-14	LEU UCO UO_2 (Th,U)O_2 TRISO & ThO_2 BISO	214/5x	1190	28.6 / 8.5	8.3	300
HRB-15B	LEU UCO UC_2 (Th,U)O_2 UO_2 TRISO and Si BISO & ThO_2 TRISO, BISO, and Si-BISO	169/6.5x	915	26.7 / 6.0	6.6	5
R2-K13/2	LEU UCO TRISO & ThO_2 TRISO	517/2x	1190	22.5 / 4.6	7.8	80
R2-K13/3			985	22.1 / 4.5	7.4	8
HRB-15A	LEU UCO UC_2 UO_2 TRISO and ZrC-TRISO & ThO_2 TRISO and Si-BISO	174/6.3x	1150	29.0 / 6.4	6.5	380
HRB-16	LEU UCO UC_2 UO_2 (Th,U)O_2 TRISO and ZrC-TRISO & ThC_2 ThO_2 TRISO and BISO	170/6.3x	1150	28.7 / 6.1	6.3	210
HRB-21	LEU UCO & ThO_2 TRISO-P	105/10x	1300	22.0 / 2.2	3.5	200
NPR-1	HEU UCO TRISO-P	170/6.3x	1240	79.0	3.8	300
NPR-2	HEU UCO TRISO-P	172/6.3x	1030	79.0	3.8	60
NPR-1A	HEU UCO TRISO-P	64/6.3x	1220	64.0	2.1	18
German Experiments						
R2-K12/1	HEU (Th,U)O_2 TRISO	308/3x	1100	11.1	5.6	0.300
R2-K12/2			1280	12.4	6.9	0.200
R2-K13/1	HEU (Th,U)O_2 TRISO	517/2x	1170	10.2	8.5	0.070
R2-K13/4			980	9.8	6.8	0.050
BR2-P25	HEU (Th,U)O_2 TRISO	350/3x	1070	15.6	8.1	1.000
HFR-P4/1	LEU UO_2 TRISO	351/3x	940	14.7	8.0	0.080
HFR-P4/2			945	14.9	8.0	0.080
HFR-P4/3			1075	14.0	8.0	0.008
SL-P1	LEU UO_2 TRISO	330/3x	794	11.3	6.8	1.200
HFR-K3/1	LEU UO_2 TRISO	359/3x	1200	7.5	4.0	0.200
HFR-K3/2			920	10.0	5.8	0.100
HFR-K3/3			920	10.6	5.9	0.100
HFR-K3/4			1220	9.0	4.9	0.300
FRJ2-K13/1	LEU UO_2 TRISO	396/2.75x	1125	7.5	0.2	0.020
FRJ2-K13/2			1150	8.0	0.2	0.020
FRJ2-K13/3			1150	7.9	0.2	0.007
FRJ2-K13/4			1120	7.6	0.2	0.007
FRJ2-K15/1	LEU UO_2 TRISO	533/2x	970	13.2	0.2	0.010
FRJ2-K15/2			1150	14.6	0.2	0.005
FRJ2-K15/3			990	13.9	0.1	0.003
FRJ2-P27/1	LEU UO_2 TRISO	232/4.7x	1080	7.6	1.4	1.600
FRJ2-P27/1			1320	8.0	1.7	10.000
FRJ2-P27/1			1130	7.6	1.3	0.120
HFR-K5/1	LEU UO_2 TRISO	563/2x	Cycled Proof Test	6.7	2.9	<0.3
HFR-K5/2				8.8	<4.3	<0.3
HFR-K5/3				9.1	4.3	<0.3
HFR-K5/4				8.7	< 4.3	<0.3
HFR-K6/1	LEU UO_2 TRISO	634/1.7x	Cycled Proof Test	7.2	3.2	<0.3
HFR-K6/2				9.3	< 4.8	<0.3
HFR-K6/3				9.7	4.8	<0.3
HFR-K6/4				9.2	<4.8	<0.3

Note: U.S. fluence is for E > 0.18 MeV and German fluence is for E > 0.10 MeV.

Our detailed review indicates that the U.S. and German irradiation programs were implemented quite differently with very different results. The German program's focus was on UO_2-TRISO fuel for AVR and all future designs such as HTR Modul, whereas the U.S. program examined many different variants (different coatings, different kernels). Figure E-2 presents the maximum on-line Kr-85m release to birth ratio (R/B) measured in the U.S. and German irradiations. (In most cases, the maximum R/B was measured at the end of life, however, in some irradiations, the final portion of the experiment was conducted at lower temperatures which caused the R/B to decrease.) The R/B results indicate that the German fuel exhibits about a factor of 1000 less fission gas release under irradiation than U.S. fuel under a broad range of conditions (temperature, burnup, fluence).

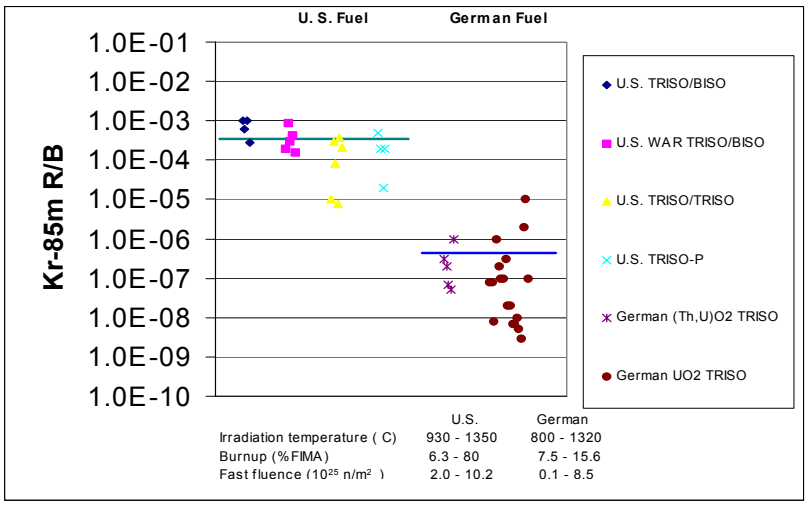

Figure E-2. Comparison of end-of-life Kr-85m R/B from historic German and U.S. irradiations.

Plots of gas release versus temperature, burnup, and fast fluence in Figure E-3 show no definitive trend. However, it is important to note that the German irradiations were generally performed at 1100°C whereas the U.S. irradiation temperatures were usually higher reflecting the higher maximum operating temperature in U.S. prismatic designs.

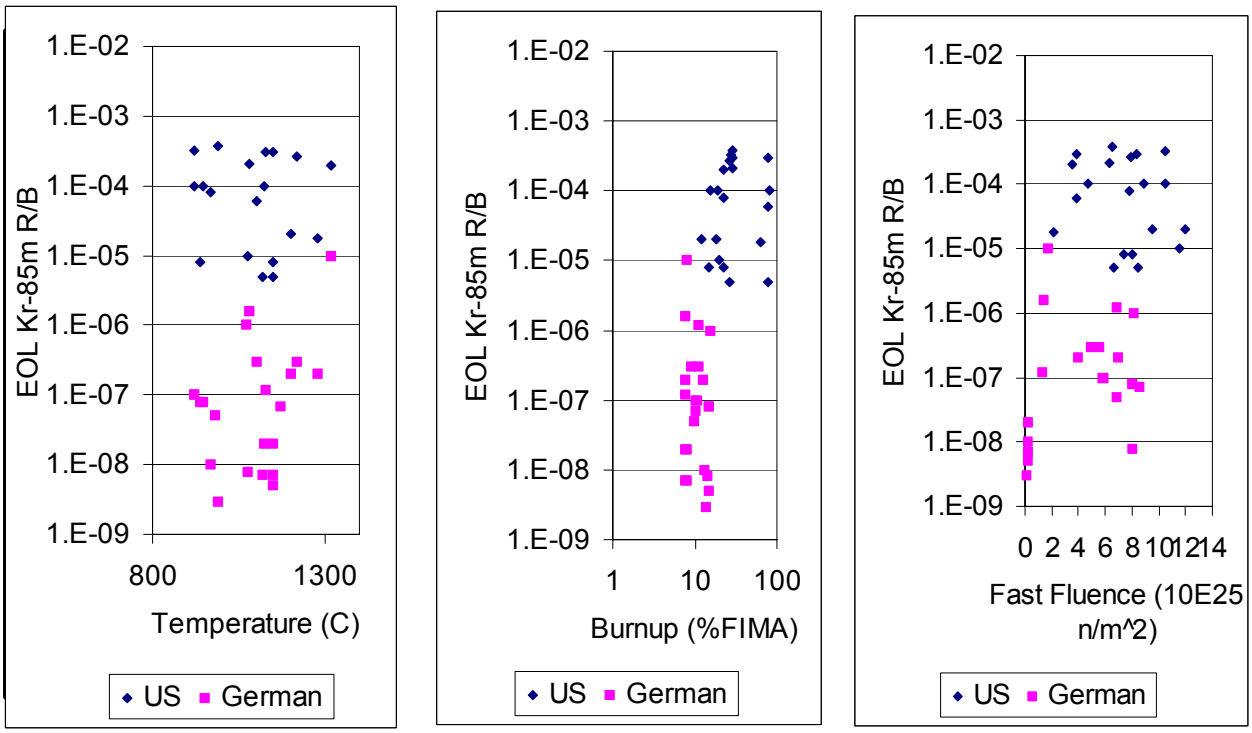

Figure E-3. Comparisons of release-to-birth ratios from German and U.S. Fuel Irradiations as functions of temperature, burnup and fast fluence.

Furthermore, the results from the postirradiation examinations confirm the more extensive gas release data. German fuel is excellent. Out of ~ 380,000 LEU UO_2 and ~ 80,000 HEU $(Th,U)O_2$ particles tested, there were no in-pile failures and only a few "damaged" particles due to experimental anomalies. Gas release was attributed only to as-manufactured defects and heavy metal contamination. By contrast, percent level failures of fuel and in many cases very high levels of failures of individual layers of the TRISO coated were observed following irradiation of U.S. fuel in most experiments. Figure E-4 presents the layer failures observed during postirradiation examination of U.S. coated particle fuel. The values in the figure represent the maximum observed layer failure across all batches in the experiment. The lack of a bar in the figure in most cases signifies that no data were tabulated for that layer. In rare instances, no failures were observed.

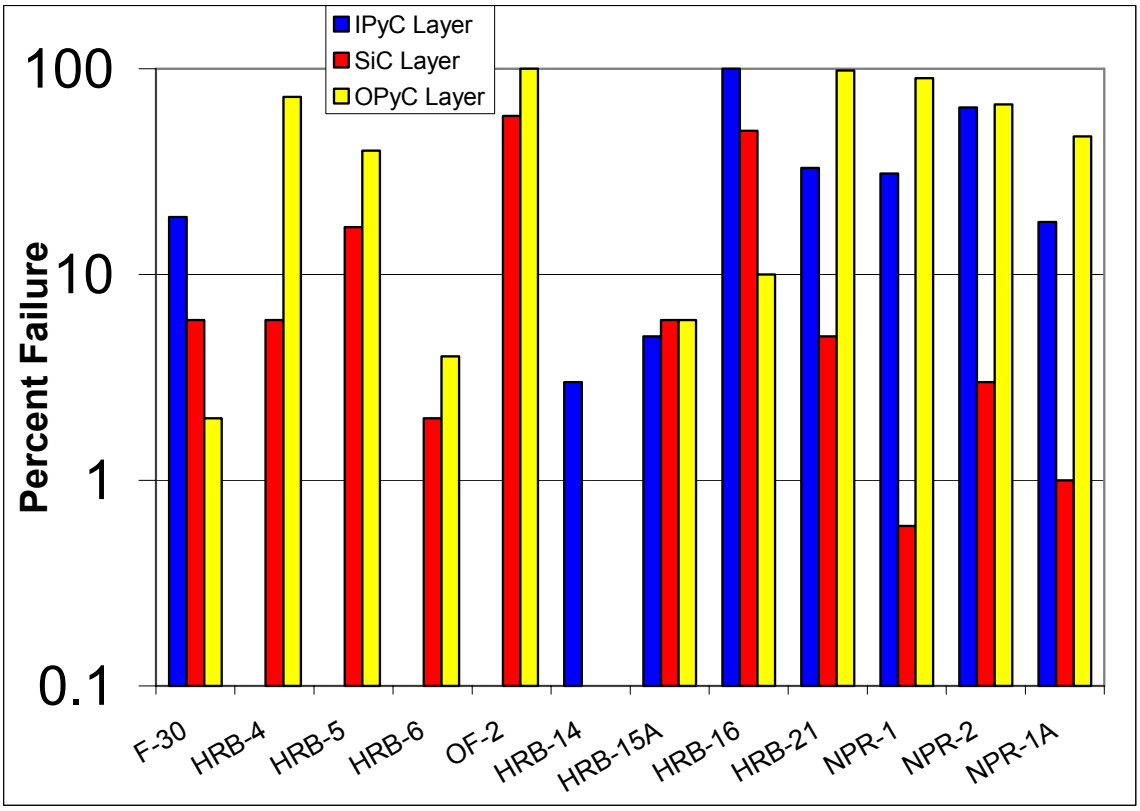

Figure E-4. Failures observed during postirradiation examination of U.S. coated particle fuel over the past 25 years.

Detailed review of the U.S. irradiation database indicates a number of different failure mechanisms of the individual layers of the TRISO coating contributed to the less than satisfactory U.S. fuel performance. Failures of the coating layers were attributed to: (a) pressure vessel failure (b) kernel migration (amoeba effect), (c) fission product attack of the SiC layer, (d) irradiation-induced IPyC cracking and/or debonding leading to cracking in the SiC layer, and (e) matrix-OPyC interaction and irradiation-induced OPyC failure. The PyC related mechanisms are strongly related to the anisotropy and porosity in the coatings. The anisotropy has a strong influence on the shrinkage and swelling behavior of the PyC layers under irradiation. The porosity of the layer has an impact on the strength of the interfacial bond between the SiC and PyC. Fission product and impurity attack of the SiC and kernel migration are thermally driven phenomena that are strongly influenced by the burnup temperature and temperature gradient across the particle. The temperature gradient is a strong function of the power density in the fuel body. A U.S. fuel compact has a higher packing fraction of particles (up to 50%) than German pebbles (~ 10%) and the U.S. core design uses a higher fuel power density than the German core designs. This difference requires more severe testing conditions for the U.S. fuel. In addition, the

U.S. irradiations were accelerated 3 to 10 times real time compared to the 2 to 3 times acceleration generally used for most of the German irradiations. Thus, some of the phenomena that were observed in U.S. irradiations may be attributed to the more demanding U.S. core design and the accelerated nature of the irradiation. These differences in power density in each reactor drove the fuel designs. The Germans could use oxide fuel with little threat to fuel integrity by kernel migration or fission product attack because of the lower temperatures and temperature gradients in the fuel. By contrast, the U.S. prismatic design with its high fuel operating temperature and power density (and resulting higher temperature gradient) resulted in the development of UCO kernel to minimize kernel migration and fission product mobility in the fuel. Had the U.S. and German irradiations been conducted under similar conditions, the disparity in results may have been less but these differences certainly cannot entirely account for the factor of 1000 in performance indicated in Figure E-2.

Impact on In-Reactor Performance

A comparison of the microstructures of the layers of the TRISO coatings in German and U.S. fuel and a detailed review of the fabrication processes have revealed many differences. There were three specific technical differences in the coating layers produced by the respective fabrication processes that have important impacts in terms of performance under irradiation and accident conditions: pyrocarbon anisotropy and density, IPyC/SiC interface structure, and SiC micro-structure. Each has important implications on the behavior of the fuel under irradiation and safety testing.

Pyrocarbon anisotropy and density. The density and anisotropy of PyC is determined by the conditions in the coater. German pyrocarbon is deposited at a higher coating gas concentration, which in turn results in a high coating rate (~ 4-6 μm/minute). This pyrocarbon is very isotropic and thus survives irradiation quite well. However, the conditions appear to lead to somewhat greater surface porosity than in U.S. pyrocarbon. U.S. pyrocarbon has been coated under a variety of conditions. In some cases it has been coated at very low coating gas concentrations, which results in a lower coating rate (1-4 μm/minute) and leads not only to a very dense and impermeable IPyC layer (which protects the kernel from attack by HCl during SiC deposition), but also to excessive anisotropy that can cause cracking of the PyC under irradiation. Post-irradiation examination of many of the U.S. capsules indicate large shrinkage cracks in the inner pyrocarbon layer which has been shown to lead to stress concentrations in the SiC layer and subsequent failure of the SiC layer. Photographs of such irradiation-induced shrinkage cracks in the F-30 and NPR-1 irradiations are shown in Figure E-5. This review has also indicated that

anisotropy measurements on PyC, especially by optical methods, fail to adequately correlate processing parameters to PyC isotropy, and furthermore are very unreliable as a predictor of in-reactor PyC failure. More reliable methods on anisotropy characterization are needed to ensure a link between acceptable processing parameters and satisfactory PyC in-reactor behavior.

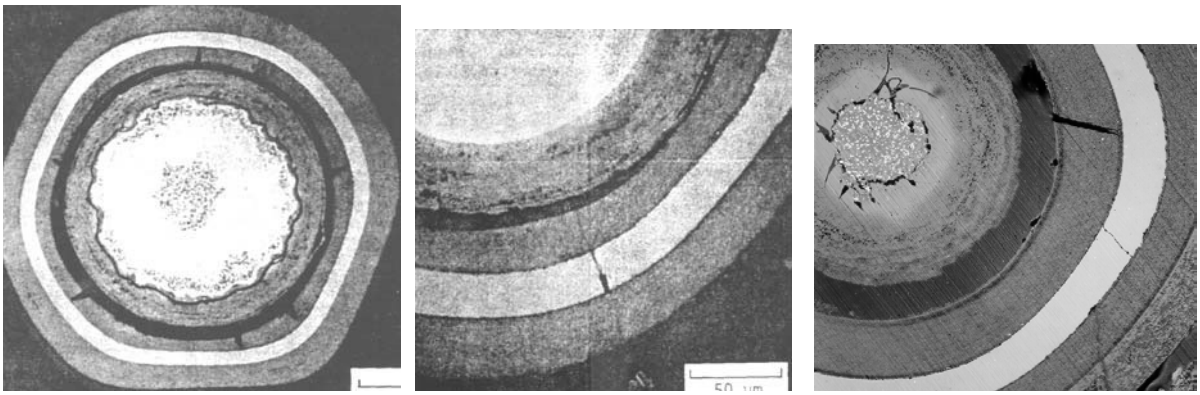

Figure E-5. Irradiation induced cracking of inner PyC in F-30 irradiation (left and center photomicrographs) and NPR irradiation [4,5].

Nature of the IPyC/ SiC interface. The difference in the microstructure and surface porosity between the German and U.S. IPyC leads to differences in the nature of bond that exist between the layers. Photomicrographs of the IPyC/SiC interface in German and U.S. fuel are shown in Figure E-6. This figure shows that the interface in German fuel is more tightly bonded because SiC is deposited into a PyC with apparently greater surface porosity. For the U.S. fuel, the denser, less porous surface of the IPyC results in a smoother, less strong bond. The TRISO coating of German fuel never exhibits debonding under irradiation whereas a review of the irradiation results indicates that the TRISO coating in U.S. fuel debonds quite frequently. The debonding is believed to be related to the strength of the IPyC/SiC interface. Localized debonding can lead to stress intensification in the SiC layer that may cause failure.

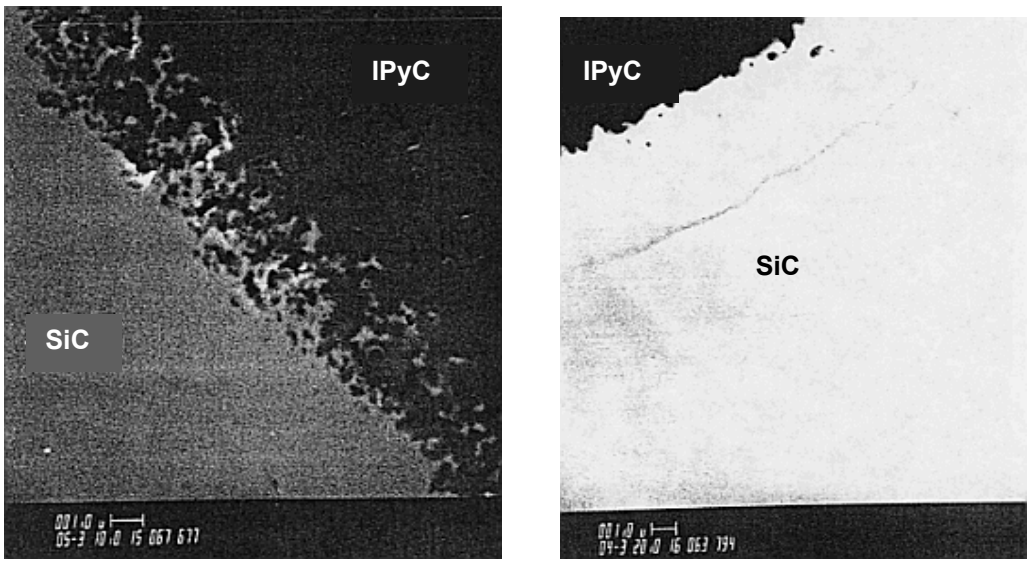

Figure E-6. Comparison of SiC/IPyC interface in German (left) and U.S. (right) fuel (The difference in contrast in the two pictures are associated with lighting techniques used in the examination.)

SiC microstructure. The microstructures of German and U.S. SiC are different. The German process results in small equiaxed grains whereas the U.S. process produces larger columnar thru-wall grained SiC. This difference in microstructure is believed to be primarily a function of temperature used during the SiC coating phase in the coaters, with the U.S. coater producing SiC at a higher temperature in some or all regions of the coater compared to the German process. A comparison of the microstructures is shown in E-7. These differences could be important from a performance perspective because the smaller-grained German SiC with its higher grain boundary tortuosity should in principle retain metallic fission products better than the large columnar grains of the U.S. SiC with more direct grain boundary pathways through the layer. Data from the HRB-15A irradiation experiment and from U.S. heatup tests of individual particles suggest that Ag and Cs release is a function of the SiC microstructure. Figure E-8 compares photomicrographs of two different types of SiC morphologies produced on U.S. UCO fuel. The fuel was irradiated to 26%FIMA and a peak fluence of 5.4 x 10^{25} n/m^2 at a temperature of ~ 1100°C. Approximately 90% of the Ag was released from the large columnar grained SiC whereas only ~ 30% was released in the smaller grained SiC microstructure. Figure E-9 is a photomontage of different SiC microstructures of U.S. coated particles with different kernels heated at 1500°C following irradiation. Release of Ag was 100% from the UO_2 particles with large columnar grained SiC and 24% for cesium. The weaker laminar SiC structure associated with the UC_2 kernel also showed very high Ag (82%) and Cs (12%) releases. The laminar SiC microstructures associated with UCO showed very little release of Ag and none for Cs. The ability of make definitive

statements about the role of SiC microstructure in fission product release from the coated particle is complicated by the fact that these data were obtained on fuels with different kernel types whose ability to retain metallic fission products may be different. While clearly not conclusive, grain structure appears to be important to fission product retention. Recently proposed experiments at MIT will attempt to answer this question more definitively.

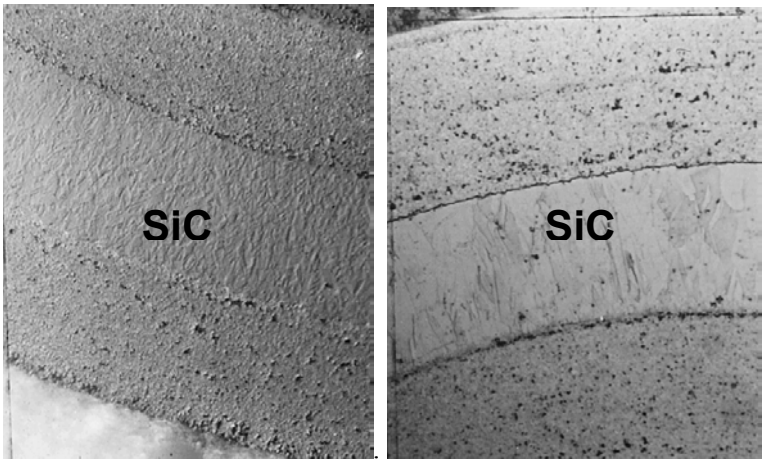

Figure E-7. Comparison of microstructure of German (left) and U.S. (right) produced SiC.

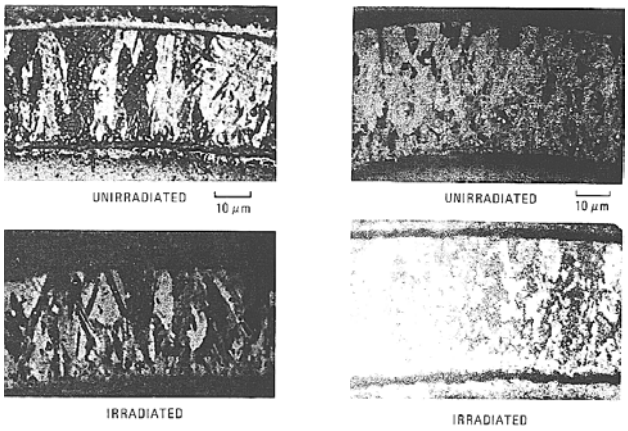

Figure E-8. Photomicrographs of large thru-wall columnar SiC grains and smaller SiC grains produced in UCO fuel irradiated in U.S. HRB-15A. Ag releases from these two fuels were different.

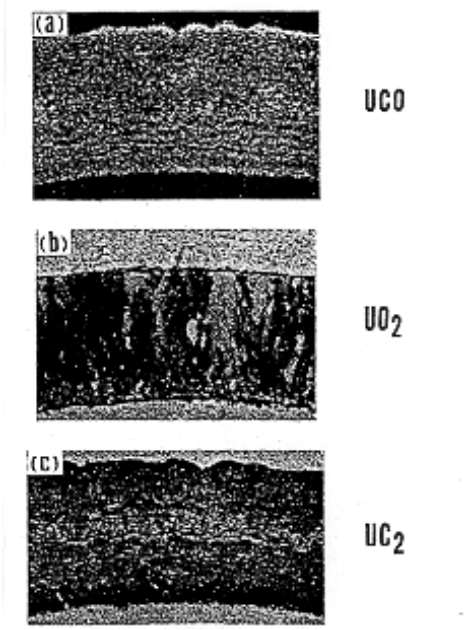

Figure E-9. Microstructures of different SiC layers on coated particles.

Accident Testing

Extensive testing has been done on German TRISO-coated fuel to characterize the behavior under long term depressurized conduction cooldown conditions. Much less work has been done on U.S. UCO fuel. The German data show excellent high temperature behavior for fuel irradiated to burnups less than 9%FIMA and fast fluences less than 4×10^{25} n/m^2. Greater releases during high temperature anneals were observed in fuel irradiated to 14%FIMA and fluences up to 4.6×10^{25} n/m^2. The work has also resulted in (a) a better understanding of the mechanisms that challenge the integrity of SiC with respect to retention of fission products (b) definition of the expected source term from the fuel for such events.

Summary

Our review has concluded that there have historically been differences in the quality of U.S. and German fuel as evidenced by the level of initial as-manufactured defects and the fuel performance results from many U.S. and German irradiations. These differences in as-manufactured defects appear to be related to differences in the manufacture of the fuel body (pebble vs. compact). The differences in irradiation performance have in part been traced to technical differences in the microstructures of the PyC and SiC layers in the TRISO coating and the bonding of those layers, which in turn are related to differences in the fabrication processes used in Germany and the U.S. In addition, part of the difference in the performance of these fuels has been attributed to the

different philosophies and approaches used to implement the irradiation and testing programs in the two countries. German fabrication was industrial/production scale with a focus on UO_2-TRISO fuel form. By contrast, the U.S. program post Fort St. Vrain consisted of a mixture of lab scale and larger scale fabrication of many different variants of TRISO coated particle fuel (i.e., different coatings, different kernels) on coaters of different designs. These fuel types were irradiated with apparently few lessons learned from one irradiation to the next and insufficient feedback to the fabrication process. The U.S. fuel was generally irradiated under very accelerated conditions, which may have overly stressed the fuel leading to a number of thermally-activated failure mechanisms.

ACKNOWLEDGMENTS

The authors are deeply appreciative of the review of this report by:

Martin Becker, KAPL
Gary Bell, ORNL
Jim Hollenbeck, Bettis
Frank Homan, Retired ORNL
Michael Kania, KAPL
Jim Kendall, Consultant formerly IAEA
Phil MacDonald, INEEL
Dick McCardell, Retired INEEL
Donald McEachern, GA
Heinz Nabielek, FzJ
Bill Scheffel, GA
Finis Southworth, INEEL
Stan Stansfield, Retired ORNL

Their comments were invaluable in improving the overall quality of the report. The authors also gratefully acknowledge the financial support of Bechtel Nuclear for this research.

CONTENTS

FIGURES

TABLES

ACRONYMS

ACRONYM	DEFINITION
ABAQUS	Finite-element code for structural analysis
BAF	Bacon Anisotropy Factor
BOL	Beginning of Life
B & W	Babcox & Wilcox
CVD	Chemical Vapor Deposition
DOE	Department Of Energy
EBC	Equivalent Boron Concentration
EOL	End of Life
FIMA	Fissions of Initial Metal Atoms
GA	General Atomics
HEU	High-Enrichment Uranium
HFIR	High Flux Isotope Reactor
HMTA	Hexamethylene Tetramine
HRB	HFIR Removable Beryllium
HTGR	High Temperature Gas Reactor
HTR-10	10-MW High Temperature Reactor
HTTR	High Temperature Test Reactor
IAEA	International Atomic Energy Agency
ID	Internal Diameter
IMGA	Irradiated Microsphere Gamma Analyses
INEEL	Idaho National Engineering and Environmental Laboratory
INET	Institute of Nuclear Energy Technology
IPyC	Inner Pyrocarbon
JAERI	Japan Atomic Energy Research Institute
KFA	KernForschungsAnlage
LEU	Low-Enrichment Uranium

ACRONYM	DEFINITION
LHTGR	Large HTGR
MTS	Methyltrichlorosilane
na	Not Available or Not Applicable
NFI	Nuclear Fuel Industry
NP-MHTGR	New Production Modular High Temperature Gas Reactor
NPR	New Production Reactor
OPTAF	OPTical Anisotropy Factor
OPyC	Outer Pyrocarbon
ORNL	Oak Ridge National Laboratory
ORR	Oak Ridge Research Reactor
PBMR	Pebble Bed Modular Reactor
PPyC	Protective Pyrocarbon
PTF	Performance Test Fuel
PVA	Polyvinyl Alcohol
PyC	Pyrocarbon
QC	Quality Control
R/B	Release-to-Birth Ratio
R&D	Research and Development
TD	Theoretical Density
TRIGA	Testing Research Isotopes General Atomics
TRISO	TRI ISOtropic
TRISO-P	TRISO Protective
U.S.	United States
WAR	Weak Acid Resin
4-HF	Tetrahydrogen furfurylalcohol

1. INTRODUCTION, BACKGROUND AND PURPOSE

High-temperature gas-reactor technology is achieving a renaissance around the world. Preliminary research has concluded that this technology has an excellent opportunity to satisfy the safety, economic, proliferation and waste disposal concerns that face all nuclear electric generating technologies. The potential economics of gas reactors are attractive enough that development continues in a number of countries. Small gas research reactors have been built in Germany, Japan, and China. Russia and the United States have a project to develop a Modular High Temperature Gas Reactor (prismatic type) to burn excess plutonium. The most ambitious project in this area is being pursued by a large utility in South Africa (ESKOM). They are proposing to build a 110- MWe pebble-bed gas reactor for commercial electric generation within the next 5 years.

The success of gas reactors depends critically upon the safety and high quality of the coated particle fuel. In a pebble bed gas reactor, graphite spheres (pebbles) of approximately 60 mm in diameter containing fuel particles are loaded into a bed-type arrangement into the reactor core. In prismatic cores, fuel compacts approximately 5 cm long and 1.2 cm in diameter are loaded into graphite hexagonal blocks. The basic fuel unit consists of fuel microspheres approximately 500-1000 μm in diameter. Figure 1-1 schematically represents a typical TRISO gas reactor fuel microsphere. A variety of fissile and fertile kernels have been used in particles including ThC_2, ThO_2, PuO_2, (Th, U) O_2, UC_2, UO_2, and UCO. Nominal fuel kernel diameters range between 100 and 500 microns. The fuel kernel is surrounded by a porous graphite buffer layer that absorbs fission recoils, and allows space for fission gases produced during irradiation. The buffer layer is generally about 100 μm thick. Surrounding this inner buffer layer is a layer of dense pyrolytic carbon, a SiC layer, and one dense outer pyrolytic carbon layer. The pyrolytic carbon layers act to protect the SiC layer, which is the pressure boundary for the microsphere; the inner pyrolytic carbon layer also protects the kernel from corrosive gases that are present during the deposition of the SiC layer. The pyrolytic carbon layers are approximately 40μm; the SiC layer is usually about 35μm thick. This layer arrangement is known as the TRISO coating system. Each microsphere acts as a mini pressure vessel. This feature is designed to impart robustness to the gas reactor fuel system.

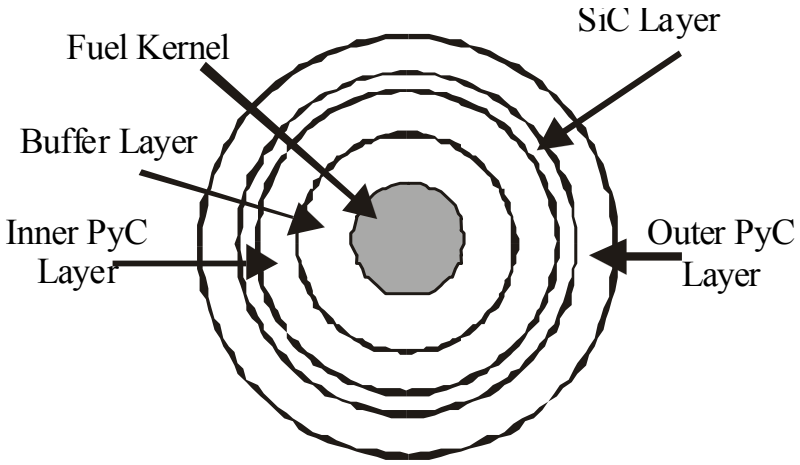

Figure 1-1. A typical gas reactor fuel microsphere.

Fuel development for this fuel form has included traditional in-reactor experiments followed by safety testing and postirradiation examination, as well as operation of both pebble bed and prismatic gas reactors in the U.S. and abroad. Although many of the variables critical to obtaining acceptable particle fuel performance are known, it is not clear that all of the important phenomena have been identified and that all the fabrication attributes needed to make acceptable fuel have been established. The irradiation behavior of particle fuel over the past three decades has been quite mixed. For example, the irradiation performance of German particle fuel has been very good, whereas for nominally the same processing parameters, U.S. gas reactor particle fuel performance has been much worse.

The reasons for these differences in irradiation performance have been subject to debate and speculation in the gas reactor community. It is important to know from a more first principles approach why the German fuel behaves acceptably, why the U.S. fuel has not faired as well, and what process/product parameters impart reliable performance to this fuel form. Thus, this report presents a critical re-examination of the historical fuel fabrication methods, and the irradiation and safety performance databases from the U.S. and German gas reactor programs to try to understand the reasons for the differences in observed performance. Thus, we propose to develop a more quantitative and less empirical linkage between acceptable processing parameters, as-fabricated fuel properties, and subsequent in-reactor performance. This will help to improve the confidence level associated with the use of this fuel in a gas reactor, and ultimately assist those associated with the new generation of gas reactors in understanding that the historic U.S. and German fuels presented in the literature are different both in their manufacture and performance.

Additionally, we hope to demonstrate the importance that fuel fabrication, quality control, and the nature of irradiation and safety testing have on TRISO-coated gas reactor fuel performance.

Section 2 compares the fabrication processes used in the U.S., Germany, China and Japan. The irradiation databases for U.S. and German fuel are presented in Section 3. Section 4 reviews the safety testing performed around the world for this fuel. In Section 5, the important differences in the German and U.S. fabrication processes are discussed in terms of their impact on fuel performance. In addition, the fuel failure mechanisms observed in gas reactor irradiations are reviewed. Our summary and conclusions are the subject of Section 6. The results presented here are largely based on information in the open literature and discussion with coated particle fuel researchers around the world when possible.

The authors believe that the reader will appreciate the magnitude of the scope of our work given the vast amount of information and its highly distributed nature. Given this fuel form has its origins in the late 1950s in the United Kingdom, a key issue was to decide the starting point for our historical comparison. A natural starting point that was considered was the development of modern TRISO fuel in the U.S. (LEU UCO) and in German (LEU UO_2). The amount of information available from Germany was adequate for this purpose. However, the amount of information on LEU UCO TRISO fuel in the U.S. is quite limited by comparison. Thus, the authors felt the need to consider US fuel performance as far back as the Fort St. Vrain fuel qualification effort (ca. 1975) which we knew would encompass other fuel forms (e.g., $(U,Th)O_2$, UC_2) but which we felt would still yield valuable information about the performance of the TRISO coating. Furthermore, we did not try to be complete and review every irradiation done since 1975. Many readers who are familiar with the worldwide gas reactor program will notice that many irradiations are missing (e.g., OF-1, SSL-1, SSL-2, GF-4, HRB 17/18). This lack of completeness was not intentional. Given the overall similarity in irradiation performance of U.S. TRISO coated fuel over the past 25 years, out intent was to examine a representative set of irradiations. We also recognize that some readers may consider the resulting comparison as “unbalanced” or “inconsistent” because of the wide range of U.S. fuel type examined. The authors felt on balance that the need to determine if there were some “common threads” to the U.S. fuel performance problems outweighed the need for consistency in the comparison in this case. Finally, some of the conclusions in the report are less quantitative than we had hoped for at the beginning of this effort and are sometimes based on anecdotal evidence and discussions with experts. Such conclusions are duly noted in the report. In many cases, the data needed to strengthen or substantiate the claims might be found in more detailed fabrication records, which may be proprietary, if they even still exist, and thus were unavailable to the authors. Furthermore, in much of this historical “detective” work, it is difficult to obtain all of the critical fabrication pedigree and tie it directly to each fuel batch used in each and every irradiation over the past 25 years. In other cases, such as irradiation testing and postirradiation examination, some results were not reported consistently. This might not be unexpected when performing a

historical review that spans three decades. Such an effort, however noble and useful in strengthening certain conclusions, was beyond the available resources for this work.

2. REVIEW AND COMPARISON OF THE FABRICATION PROCESSES OF U.S., GERMAN, JAPANESE AND CHINESE TRISO-COATED PARTICLE FUEL

2. 1 Introduction

The objective of this section is to analyze the fabrication process of TRISO-coated particle fuel that was developed in different countries for high-temperature gas-cooled reactors. TRISO-coated particle fuel was originally proposed in the U.K. and has been or is currently being developed mainly in six countries: the U.S., Germany, Japan, China, South Africa and Russia. Although in the 60's and 70's thorium-based and carbide kernels were explored, modern TRISO-particle kernels are usually made of Low Enrichment Uranium (LEU) dioxide. An exception to this is the U.S. where uranium oxycarbide kernels have been adopted as the mainline fuel form. In the U.S. commercial gas reactor program LEU UCO was used. In the New Production Modular High Temperature Gas Reactor (NP-MHTGR) program, High-Enrichment Uranium (HEU) was used. The fuel form is a spherical pebble in the German, Chinese, South African, and Russian reactor designs. Cylindrical compacts are used in the U.S., Japan, and also more recently Russia.

The focus in the following sections will be restricted to the U.S., Germany, Japan and China because little information is available in the open literature about the Russian fabrication process. As of this writing, the South African fabrication activities are just beginning and will not be considered further. Their fuel is not expected to differ significantly from the German fuel. In Section 2.2 a description of the fabrication process in the four countries is presented, while in Section 2.3 the key differences are identified and discussed.

2.2 Description of the Fabrication Process

The fabrication process for TRISO-coated particle fuel exhibits some general characteristics common to all countries. The kernels are manufactured according to the gel-precipitation process, either in the so-called internal gelation, external gelation or total gelation version. The pyrocarbon and silicon carbide layers are deposited in a high-temperature coater by Chemical Vapor Deposition (CVD). Finally, the fuel form is manufactured by mixing the fuel particles with matrix materials (e.g., graphite filler and binder) and then pressing and heat-treating the final fuel form.

The U.S. NPR Fuel

The U.S. New Production-Modular High-Temperature Gas-Cooled Reactor (NP-MHTGR or, briefly, NPR) was designed with prismatic graphite blocks loaded with cylindrical graphite-

matrix compacts containing TRISO-coated HEU uranium oxycarbide (UCO) particles. Similar LEU UCO fuel was fabricated and irradiated during the same time frame for the U.S. commercial MHGTR program. Our choice of using the NPR fabrication process for comparison stems from the greater amount of information available to the authors, although we recognize that significant differences exist in the characteristics of the NPR and German fuels (i.e., HEU vs. LEU kernel, oxicarbide vs. oxide kernel, 8-layers vs. 4-layers coating, thick vs. thin IPyC). Furthermore, the NPR experience was the last U.S. manufacturing campaign and represents the most complete manufacturing pedigree and testing campaign of modern TRISO fuel in the U.S. albeit HEU, aimed at commercial scale deployment. In addition, because the U.S. did not have a highly focused goal like the Germans, kernel and coating types varied, which made selection of a U.S. "reference" fabrication process for this comparison problematic.

In this section, a detailed description of the fabrication process of the Performance Test Fuel (PTF) produced by General Atomics (GA) and its subcontractor Babcock & Wilcox (B&W) for the NPR program is presented. At that time, the PTF fuel was labeled "the best as-manufactured particle fuel ever produced in the U.S." (Hobbins et al. 1993), as it met or exceeded over 60 strict quality specifications on the kernel, coated particle and compact properties (Bryan 1992). Nevertheless, as discussed in Section 3, upon irradiation of both this fuel and LEU UCO fuel in the U.S. commercial program, significant failures occurred. The NPR and commercial U.S. programs however, ramped down in the early 1990's and no new coated particle fuel has since been fabricated or irradiated in the U.S. ORNL developed the original concept for production of UCO_2 kernels (Stinton et al 1982).

UCO - Kernel Fabrication.

ORNL developed the original concept for production of UCO kernels (Stinton et al. 1982). The starting material is high-surface area UO_3 or U_3O_8 powder, which is acquired from the Oak Ridge Isotopic Y-12 Sales. The powder is dissolved in nitric acid to form uranyl nitrate ($UO_2(NO_3)_2$) (McCardell et al. 1990, Hobbins et al. 1993). Carbon-black powder and a dispersant, Tamol (Caldwell 1993) are added to the solution to provide the carbon needed for the final UCO form (Hobbins et al. 1993). Also, urea (H_2NCONH_2) is added to form a broth (Hobbins et al. 1993, McCardell et al. 1992). The broth is slowly cooled to below 0°C. Hexamethylene tetramine (HMTA, $C_6H_{12}N_4$) is added (Hobbins et al. 1993). The broth is pulsed through needle orifices to produce spherical droplets (Hobbins et al. 1993, McCardell et al. 1992) that fall into a hot (60°C) column of trichloroethylene (CH_3CCl_3) (Hobbins et al. 1993). Alternative organic liquids were

explored for utilization in the hot column including propylene carbonate, silicone oil and hexane (McCardell et al. 1992). As the temperature of the falling droplets rises, the HMTA contained in the droplets (which is unstable above 0°C) decomposes to yield formaldehyde and ammonia (Spence 1982). The ammonia induces precipitation of the uranyl nitrite, thus gelating the droplet (Hobbins et al. 1993). The gelated particles are then washed in aqueous ammonia solution at room temperature and finally water-washed (Hobbins et al. 1993) and air dried at 60°C (Hobbins et al. 1993, McCardell et al. 1992, Caldwell 1993).

The particles are then calcined in pure argon at 350°C (Caldwell 1993) to remove the residual ammonia, urea and water (Spence 1982). At this point of the process, the particles are made of pure UO_3+C (Hobbins et al. 1993, McCardell et al. 1992). The next step is sintering: the particles are heated in pure Ar at 800°C, then treated with a Ar-4%H_2 mixture at 1600°C to reduce UO_3+C to UO_2+UC_2 (Caldwell 1993) and finally with a Ar-10 CO mixture at 1800°C to increase the density and adjust the oxygen-carbon stoichiometry (Hobbins et al. 1993, McCardell et al. 1992, Caldwell 1993).

An external gel-precipitation process similar to that adopted by the Germans and Japanese for their respective particle fuel was initially explored within the NPR program. This process was subsequently abandoned in favor of the internal gel-precipitation process because it failed to yield high-density, symmetric particles (Hobbins et al. 1993).

Coating Deposition. The coating process takes place in a furnace with a conical graphite distributor (see Figure 2-1). The coating gases and the fluidizing gas are supplied through a 2" ID nozzle by a manifold at the bottom of the graphite cone[1] (Hobbins et al. 1993). It was noticed that large amounts of PyC would deposit on the surfaces of the nozzle, to the point of plugging the nozzle hole (Besenbruch 1993). This deposition was due to undesirable early pyrolysis of the coating gas in the nozzle tube (Besenbruch 1993, Lackey et al. 1977), which could become very hot (e.g., >1000°C) by heat conduction from the coater region or improper heater design. This problem prevented adequate control of the coating conditions in the coater (i.e., gas concentration, temperature, and flow). After termination of the NPR program, GA considered improving the nozzle design by insulating the nozzle tube from the coater, reducing the nozzle

[1]Oak Ridge National Laboratory developed a coater design with a fritted gas distributor to make the gas flow through the particles more uniform (Lackey et al. 1977, Nickel 1981). However, this design was not adopted by GA because plugging could not be prevented.

tube diameter to decrease the gas residence time in the tube, and reducing the exposed nozzle surface area (Besenbruch 1993).

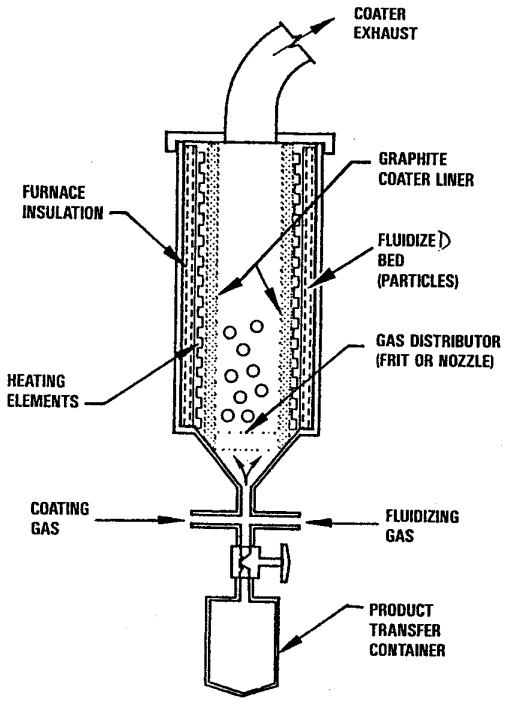

Figure 2-1. Schematic of the GA coater (Noren 1991) used for NPR fuel.

The porous buffer coating is deposited by decomposition of acetylene (C_2H_2) in an argon-acetylene mixture at about 1300°C (Hobbins et al. 1993). Other references report a wider coating temperature range, i.e., 1200-1450°C (McCardell et al. 1992) and 1150-1400°C (McCardell et al. 1990). The coating gas composition was ~ 60-80% C_2H_2 by volume while the exact value of the coating rate could be found in the literature. A high-density seal coating (1-5μm) is deposited on the buffer layer by pyrolysis of propylene (C_3H_6) at 1200°C (McCardell et al. 1992).

The IPyC is deposited from a mixture of acetylene, propylene and argon at 1300°C. Pure propylene would provide the highest density, but the addition of acetylene minimizes the temperature depression induced in the coating region by the endothermic propylene pyrolysis (Hobbins et al. 1993). High temperatures and high coating-gas concentrations in the mixture, resulting in high coating rates at the particle surface, promote agglomeration of pyrocarbon in the gas mixture and deposition of very-isotropic, but lower-density, clusters of pyrocarbon on the

particle surface (Goodin 1993). Low temperatures and low coating-gas concentrations result in molecular deposition of pyrocarbon and ultimately in a more ordered, higher-density, IPyC coating with a highly anisotropic structure (Goodin 1993). A reasonable compromise between high density, needed to protect the kernel against HCl attack during the SiC deposition and isotropy, needed for adequate fuel performance under irradiation, can be achieved by proper selection of the coating gas concentration, coating rate, and temperature. References (Besenbruch 1993, Goodin 1993) indicate that the coating rate, the coating gas volumetric concentration, and the coating temperature for the NPR IPyC were 2.2 μm/min, 16%, and 1230°C, respectively, which should result in a high-density, high-anisotropy coating (Goodin 1993), (see Figure 2-2). Personal communications with GA staff confirmed that the GA pyrocarbons have often been deposited at coating rates between 1 and 4 μm/min. It should be noted that the anisotropy measurements conducted at GA at the time the NPR fuel was produced showed acceptable values of the anistropy (i.e., BAF index) for the IPyC (Bryan 1992). However, these measurements, based on optical methods, are in contradiction with the larger body of data showing that low coating rates and temperatures result in anisotropic PyC coatings (IAEA 1997). Moreover, GA staff themselves have historically doubted the accuracy of measurements as numerous memorandums and references emphasize the need for depositing more isotropic PyC layers (Stansfield 1970, Scheffel 1993, Goodin 1993, Besenbruch 1993, Bullock 1993, Adams 1994). The implications of this subject on the irradiation performance of the U.S. fuel will be discussed in Section 4.

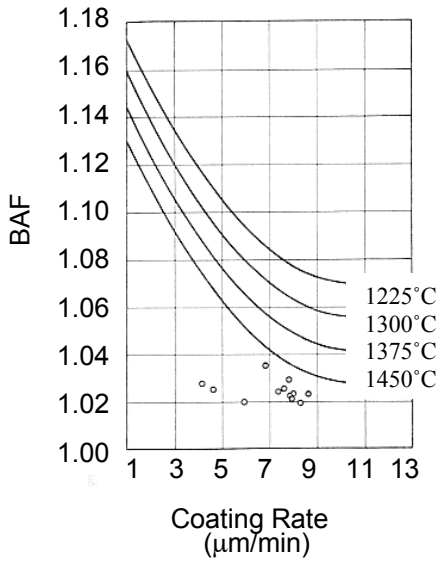

Figure 2-2. Effect of the coating temperature and rate on the PyC anisotropy (adapted from Lackey et al 1977).

An example of the larger body of data on the role of PyC coating conditions on anisotropy is illustrated in Figure 2-2. The figure demonstrates that at low coating rates, anisotropy increases. While the general trends illustrated in Figure 2-2 (i.e., the BAF increase with decreasing coating temperature and rate) should be valid for all coaters, the absolute values in Figure 2-2 are valid only for the particular coater described by Lackey et al. (1977).

The SiC coating gas needed for the deposition of the SiC layer is picked up by a H_2 stream passing over a bath of methyltrichlorosilane (MTS, CH_3SiCl_3) according to the reaction $CH_3SiCl_3+H_2 \rightarrow SiC+3HCl+H_2$ (Voice and Lamb 1969, Hobbins et al. 1993, McCardell et al. 1992). The MTS/H_2 steam is mixed with more H_2 and taken into the coater where the MTS decomposes. Columnar beta-phase SiC deposits on the particle surface at 0.2-0.4 μm/min and temperature in the 1500-1650°C range (Hobbins et al. 1993). To obtain maximum SiC density, the upper temperature (1650°C) and excess H_2 (1.5 vol.% MTS, 98.5 vol.% in H_2) should be selected (McCardell et al. 1992, 1990). To obtain maximum SiC strength and small grain size, the lower temperature (1500°C) should be adopted. Hobbins et al. (1993) report that the PTF fuel SiC coating was optimized for maximum density (i.e., 1650°C and excess H_2). Note that these trends are not general. For example, Xu reports (Xu, 1995) that both density and strength exhibit a maximum at 1550° C for SiC deposited by the Chinese.

The OPyC is deposited from a mixture of acetylene, propylene, and argon at temperatures above 1300°C. Isotropy of the OPyC, which is desirable under irradiation because it results in uniform compressive stressing of the SiC and ultimately in lower failure probabilities of the SiC (McCardell et al. 1992), could be achieved with high coating rates of 4-6 μm/ min. However, as with the IPyC, the OPyC for the NPR PTF was deposited at low coating gas concentrations (16 vol.% coating gas) and hence low coating rates (i.e., <4 μm/min). A high-density seal coating (1-5 μm) is deposited on the OPyC by pyrolysis of C_3H_6 at 1200°C (McCardell et al. 1992).

An additional protective layer (PPyC) is deposited on the second seal to minimize particle/particle interaction during fabrication of the fuel compacts (Hobbins et al. 1993). The PPyC coating is deposited with the same process parameters of the buffer layer (Hobbins et al, 1993). Note that this protective coating was used in the NPR program only and the last commercial U.S. LEU fabrication campaign, but not in older "historic" U.S. fuel. Finally, a third high-density seal coating (1-5μm) is deposited on the PPyC by pyrolysis of C_3H_6 at 1200°C (McCardell et al. 1992). Because it was revealed that the seal and PPyC layers contributed to particle failure, GA subsequently decided not to use them again, but to retain standard TRISO particle design.

It is also very important to emphasize that the U.S.-fuel coating process is not continuous. Unloading of the partially coated particles is performed three times for a single batch, i.e., after the deposition of the IPyC, SiC and PPyC layers (Johnson 1993, Gallix 1993), to perform various QA measurements. The implications of this coating approach on the irradiation performance of the fuel will be discussed in Section 4.

Fabrication of the Fuel Compacts. The fuel compacts are fabricated by injection of a hot liquid carbon base matrix (graphite flour, petroleum pitch, octadecanol, polystyrene (Hobbins et al. 1993, McCardell et al. 1992)) at 160°C and 6.9 MPa (Hobbins et al. 1993) into a mold cavity containing the coated particles and graphite shim material, which provides the desired average fuel loading in the compact (Hobbins et al. 1993). The compacts are cooled to room temperature to solidify the matrix and then are packed in alumina powder for carbonization at 900°C (Hobbins et al. 1993, McCardell et al. 1992), which decomposes the organic compounds leaving only pure carbon. The compacts are then surface-leached with HCl to remove traces of iron and free uranium (Hobbins et al. 1993). Finally, heat treatment at 1650°C in a graphite furnace with an Ar purge for a short time drives off the residual volatiles and stabilizes the carbon matrix (Hobbins et

al. 1993, McCardell et al. 1992). The high level of as-manufactured defects in GA fuel is believed to be related to the introduction of impurities from the graphite furnace that subsequently attacked the SiC layer during this final heat treatment (McEachern 2002).

Fuel Specifications and Quality Control. The specifications (to be met with 95% confidence) for the NPR PTF fuel, along with the actual data obtained for the as-manufactured fuel, are reported in Table 2-1. Two separate limits are specified for the free uranium (i.e., uranium outside the intact SiC coating) from matrix contamination and particles with defective SiC, 1×10^{-5} and 5×10^{-5}, respectively (EG&G 1991). Both specifications were met with significant margin (Bryan 1992), i.e., the mean uranium contamination fraction was measured to be 7×10^{-7}, while the fraction of particles with defective SiC was 1.43×10^{-5}. Note that the dominant contribution to the total free uranium fraction is from the particles with defective SiC.

QC activities for the U.S. fuel include measurements of the coatings thickness by radiographic techniques, measurements of the coatings density by hydrostatic techniques, measurements of the PyC anisotropy by an optical microphotometer, and evaluation of the fraction of particles with defective SiC with the burn-leach method (Saurwein 1994).

It should be emphasized that the fabrication process parameters were not specified or tightly controlled for the NPR fuel (Shaber 1992), while they were for both the Fort St. Vrain fuel (Shaber 1992) and German fuel (Saurwein 1994). At the end of the NPR program several flaws related to the lack of control of the process were hypothesized as a possible explanation for less than expected coating performance.

Table 2-1. Specifications for the NPR fuel (EG&G 1991) and actual data for the as-manufactured fuel (Bryan 1992).

	SPECIFICATION	AS-MANUFACTURED*
FUEL KERNEL		
Material	UCO	UCO
Enrichment	$93.15^{+0.15}_{-1.00}$ wt%	93.147±0.007 wt%
Impurities	≤5,000 wt-ppm	1800±120 wt-ppm
C/U Atomic Ratio	≤0.5	0.3618±0.0008
O/U Atomic Ratio	1.4-1.7	1.5098±0.0066
Diameter	195^{+10}_{-50} μm	200±5 μm
Density	≥10.3 g/cm^3	10.51±0.01 g/cm^3
COATED PARTICLE		
Buffer Layer Thickness	90-110 μm	101.7±10.2 μm
Buffer Layer Density	0.80-1.10 g/cm^3	0.958±0.005 g/cm^3
IPyC Thickness	40-60 μm	52.9±3.7 μm
IPyC Density	1.85-1.95 g/cm^3	1.923±0.008 g/cm^3
IPyC BAF	≤1.20	1.058±0.005
SiC Thickness	35-40 μm	35.3±3.1 μm
SiC Density	≥3.18 g/cm^3	3.2278±0.0007 g/cm^3
OPyC Thickness	30-50 μm	39.1±4.0 μm
OPyC Density	1.80-1.95 g/cm^3	1.85±0.01 g/cm^3
OPyC BAF	Not Specified	1.052±0.006
PPyC Thickness	40-60 μm	47.0±11.3 μm
PPyC Density	0.80-1.10 g/cm^3	1.06 g/cm^3
FUEL COMPACT		
Length	49.30±0.50 mm	49.33±0.11 mm
Diameter	12.37-12.62 mm	12.37-12.51 mm
Burnable Impurities (B, Cd, Eu, Gd, Li, Sm)	≤5 ppm EBC**	0.77±0.50 ppm EBC**
Non-Burnable Impurities (Na, S, Ca, Yb, Ti, V, Cr, Lu, Mn, Fe, Co, Al, In, Ta, Cs, La, Ce, W, Pr, Nd, Tb, Ho, Er, Tm)	≤1 ppm EBC**	0.56±0.13 ppm EBC**
Total free uranium fraction	6 x 10^{-5}	1.4 x 10^{-5}

* Data mostly reported in terms of the mean value and the standard deviation.
** EBC = Equivalent Boron Concentration

The calibration of the sensors measuring the temperature in the coater was questioned, as was the control of the coating-gas mass flow rate in the coater, which was inferred from flow rate measurements and knowledge of the coating gas density based on the (possibly erroneous) temperature (Gallix 1993). Moreover, it was found that non-uniform circulation of the particles within the coater would result in different coated-particle properties for the same coating conditions (Gallix 1993). The screening and tabling parameters were not strictly controlled (Gallix 1993), and the guidelines for maintenance of the fabrication equipment were vague and subjective (Gallix 1993). This likely resulted in a large variability of the GA fabrication process, which might have affected the quality of the fuel.

German Fuel

The reference fuel for all modern German HTGR designs consists of spherical graphite pebbles containing several thousands of TRISO-coated LEU uranium dioxide (UO_2) particles. Fabrication of pebble-type fuel had been developed in Germany over a period of thirty years within the framework of a collaboration between the companies Nukem/Hobeg and Hochtemperature Reaktor Bau, and the research laboratory FzJ in Jülich. However, prior to 1980, mostly HEU Th-U-based coated particles of the BISO type (i.e., particles without the SiC layer) were produced. When it was decided to adopt a LEU U-based fuel, it took about two years to re-develop and optimize the fabrication process (Nabielek et al. 1984).

The UO_2 kernels for this fuel are manufactured by the external gel-precipitation process, while the particle coating is deposited by means of a Chemical-Vapor Deposition (CVD) technique. Finally, fabrication of the pebbles is accomplished by particle overcoating, cold-pressing and heat treatment.

UO_2-Kernel Fabrication. The starting material is an aqueous solution of uranyl nitrate, to which polyvinyl alcohol (PVA) and other non-specified additives are added to form a broth (Mehner et al. 1990, Heit et al. 1985). Droplets of the broth are generated by a 600Hz vibrator (Huschka and Vygen 1977) and fall through ammonia gas, which induces gelation of the droplet surface by PVA precipitation (Wolf et al. 1975). The partially gelated droplets finally fall into a concentrated aqueous solution of ammonia for bulk gelation (Heit et al. 1985, Mehner et al. 1990). At this stage of the fabrication process, uranium is in the form of ammonium diuranate (Huschka and Vygen 1977).

The gel-droplets are then washed in aqueous solution of ammonia and isopropanol (Heit et al. 1985, Huschka and Vygen 1977) to remove reaction products like ammonium nitrite (Mehner et al. 1990). The droplets are dried at 80°C to remove the isopropanol (Heit et al. 1985, Huschka and Vygen 1977) and are calcined in air at 300°C to remove CO_2, ammonia, and water (Huschka and Vygen 1977, Heit et al. 1985). At this point in the process, the chemical form of uranium is UO_3 (Mehner et al. 1990), which is reduced to UO_2 by a H_2 stream at 1600-1700°C (Heit et al. 1985, Huschka and Vygen 1977). During this step the kernel density increases to its final value ranging from 10.8 to 10.9 g/cm^3 (Mehner et al. 1990, Heit et al. 1985) or, assuming a UO_2 theoretical density of 10.97g/cm^3 (Todreas and Kazimi 1990), to between 98 and 99% TD. All

kernels are classified by means of vibrating tables to eliminate the odd-shaped particles (Mehner 1990).

Coating Deposition. Deposition of the PyC and SiC protecting layers is performed by a CVD process that takes place in a coater consisting of a 400 mm-ID tube (with a cone-shaped gas distributor) where the particles are fluidized and exposed to the pyrolitically-decomposed coating gases. This coater can handle batches of UO_2 kernels up to 10 kg. However, it was not operated with batches above 5 kg because of criticality concerns. A 240-mm ID coater was also used in the past for batches up to 5 kg and an even smaller coater of 0.5 kg capacity was used as well. The coating process is continuous, i.e., deposition of the four coating layers takes place in a single pass of the particles through the coater without loading and unloading after deposition of each layer (Mehner et al. 1990), although a few particles are siphoned out of the coater for QC. Argon is the gas used to fluidize the particles for PyC coating (Mehner et al. 1990). Two configurations of the gas injection system were explored: one in which both Ar and the coating gas are injected from the bottom of the coater, and one in which Ar and the coating gas are injected from the bottom and top of the coater, respectively (Huschka and Vygen 1977). The reference configuration is the one in which both gases are injected from the bottom of the coater, and is illustrated in Figure 2-3. The internal furnace components were thoroughly cleaned or replaced after each coating run to remove any soot or debris that might have been left behind from the coating process.

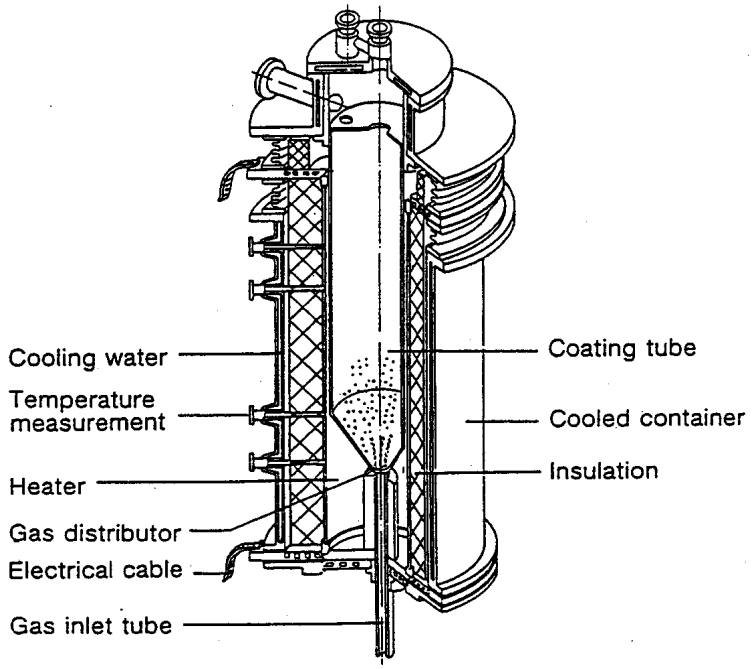

Figure 2-3. A German coater (Gontard and Nabielek 1990).

The buffer layer is deposited from a mixture of C_2H_2 and Ar at 1250°C at a rate of 6-10 μm/min (Huschka and Vygen 1977). The IPyC layer is deposited from a mixture of C_2H_2, C_3H_6 and Ar at 1300°C at coating gas concentrations resulting in a coating rate of 4-6 μm/min (Huschka and Vygen 1977). The SiC layer is deposited from a mixture of CH_3SiCl_3, and H_2 at 1500°C at a rate of 0.2 μm/min (Huschka and Vygen 1977). The OPyC is also deposited from a mixture of C_2H_2, C_3H_6 and Ar at 1300°C at a rate of 4-6 μm/min (Huschka and Vygen 1977). Finally, the odd-shaped coated particles are eliminated by means of vibrating tables (Heit et al. 1985).

It should be emphasized that the above temperature and deposition rate data were reported for the early coater of smaller capacity (i.e., 0.5 kg batches). Similar information for the intermediate 5 kg coater and for the more recent industrial-scale coater (i.e., 10 kg batches) could not be found in the literature, as they are Nukem proprietary information.

The coating process described above, initially developed for mixed Th-U-oxide kernels, was retained for UO_2 kernels as well. Deposition of the PyC layers from a mixture of methane (CH_4) and Ar at higher temperature (1900-2100°C) was considered early in the R&D program, but was later discarded in favor of the C_3H_6 process (Wolf et al. 1975) because of the:

- Irradiation induced PyC cracking due to high anisotropy
- High costs associated with maintaining the higher temperature,
- Slower deposition rates achievable,
- Larger uranium contamination of the layers,
- Larger radial gradients of properties induced by the high temperature,
- PyC/kernel chemical interaction (Allen et al. 1977).

Fabrication of the Fuel Pebbles. A resinated powder is formed by warm-mixing of graphite powder with phenol and hexamethylene-tetramine (both resin binders), which is ground to a controlled but non-specified size (Heit et al. 1985). Earlier, a mixture of 75% natural flake graphite, 15% petroleum coke, and 10% phenol was used (Wolf et al. 1975).

The resinated powder is used to deposit a 200 μm overcoating on the coated particles (Heit et al. 1985). Overcoated particles are classified to eliminate odd-shaped particles (Heit et al. 1985). The overcoated particles are mixed with more resinated powder and premolded in silicone rubber molds at about 30 MPa and room temperature to form the 5-cm fuel region of the pebbles (Heit et al. 1985, Wolf et al. 1975). Additional resinated powder is loaded in the molds to form the fuel-free zone (Heit et al. 1985). Final molding takes place at room temperature by isostatic pressing at 300 MPa in silicone rubber molds (Heit et al. 1985, Nabielek et al. 1984, Mehner et al. 1990, Wolf et al. 1975). The spheres are machined to final shape and size (i.e., 6 cm diameter (Mehner et al. 1990, Heit et al. 1985)). Resin binder carbonization is induced at 800-900°C in inert gas and finally the pebbles are heat-treated at 1950°C under vacuum to extract residual gases and other unspecified impurities (Nickel et al. 2001, Heit et al. 1985, Mehner et al. 1990, Wolf et al. 1975).

Fuel Specifications and Quality Control. A list of specifications for the German fuel for the 170 MWth MODUL reactor (Gontard and Nabielek 1990) is presented in Table 2-2, along with some as-manufactured properties of earlier German fuel taken from Heit et al (1985). The most important specification for the German fuel is the total fraction of free uranium (i.e., matrix contamination + particles with defective SiC), whose limit is specified at 6×10^{-5} (Gontard and Nabielek 1990). Note that this is effectively the same limit as for the U.S. fuel, i.e., two separate limits were specified for the U.S. fuel on matrix contamination and particles with defective SiC, respectively, the sum of which is 6×10^{-5}. Actual values of the free uranium fraction in the German fuel range from 0.8×10^{-5} to 5.0×10^{-5} (Nabielek et al. 1990), with the dominant contribution being from particles with defective SiC (as in the U.S. fuel).

QC activities for the German fuel done at Nukem include measurements of the buffer and IPyC thickness by ceramography techniques, measurements of the SiC and OPyC thickness by radiography, measurements of the coatings density by hydrostatic techniques, and measurements of the PyC anisotropy by an optical microphotometer (Saurwein 1994). The free uranium fraction is measured with the burn-leach method (Nabielek et al. 1990, Saurwein 1994), which enables detection of uranium contamination in the fuel-element matrix and in the particle OPyC, uranium from particles with completely cracked coatings, and uranium from particles with cracked SiC but intact PyC layers. Note that QC of these key fuel parameters is performed in the German and U.S. fabrication processes using similar technologies. Nevertheless, an important difference exists. The Germans, on the premise that conformance with fuel-particle specifications alone could not guarantee fabrication of high-quality fuel, relied on process specifications, as well (Saurwein 1994), while GA did not. However, the actual process specifications are proprietary information of Nukem and are not available in the open literature.

Table 2-2. Specifications for the 170 MWth MODUL reactor fuel (from Gontard and Nabielek 1990), and the as-manufactured properties of an earlier German fuel (Heit et al. 1985).

	SPECIFICATION	AS-MANUFACTURED
FUEL KERNEL		
Material	UO_2	UO_2
Enrichment	8.0±0.1 wt%	
Diameter	480-520 μm	500±11 μm
Density	≥10.4 g/cm^3	10.9±0.08 g/cm^3
Sphericity		<1.07
Fraction of odd-shaped kernels		5×10^{-4} (before tabling) 10^{-5} (after tabling)
COATED PARTICLE		
Buffer Layer Thickness	72-108 μm	92±14 μm
Buffer Layer Density	≤1.05 g/cm^3	0.97 g/cm^3
IPyC Thickness	30-50 μm	39±4 μm
IPyC Density	1.91±0.1 g/cm^3	1.91±0.02 g/cm^3
IPyC BAF	≤1.1	
IPyC OPTAF		1.054±0.012
SiC Thickness	31-39 μm	35±2.5 μm
SiC Density	≥3.18 g/cm^3	3.20±0.003 g/cm^3
OPyC Thickness	25-45 μm	40±3 μm
OPyC Density	1.91±0.1 g/cm^3	1.91±0.02 g/cm^3
IPyC BAF	≤1.1	
OPyC OPTAF		1.024±0.005
FUEL ELEMENT MATRIX		
Density	1.75±0.02 g/cm^3	1.75±0.004 g/cm^3
Ash Content		40 ppm
Thermal Conductivity, @ 1,000°C	≥25 W/cm·K	39 W/cm·K, ⊥ * 40 W/cm·K, || *
Standard Specific Corrosion Rate	≤1.3 mg/cm^2·h @ 1,000°C	0.62±0.08 mg/cm^2·h
Standard Abrasion Rate		2.9±0.7 mg/ cm^2·h
Crushing Strength	≥18 kN	23.7±0.3 kN, ⊥ * 26.3±0.4 kN, || *
Total free uranium fraction	6 x 10^{-5}	<5 x 10-5

⊥ and || indicate perpendicular to and parallel to the graphite granules in the sphere

Japanese Fuel

The Japanese High Temperature Test Reactor (HTTR) uses prismatic graphite assemblies loaded with compacts made of TRISO-coated LEU uranium dioxide (UO_2) particles. Fabrication of this type of fuel has been developed in Japan over a period of thirty years within the framework of a collaborative program between the Japan Atomic Energy Research Institute (JAERI) and the Nuclear Fuel Industries, Ltd. (NFI) (Minato et al. 1997).

The UO_2 kernels for this fuel are manufactured by the external gel-precipitation process while the particle coating is deposited by CVD. Finally, fabrication of the compacts consists of particle overcoating, warm pressing and heat treatment.

UO_2-Kernel Fabrication. The starting LEU uranium (4-10 wt% (Sawa et al. 1999)) is in the form of aqueous uranyl nitrate solution and is handled in batches of 4 kg at a time. A broth is prepared by adding methanol and an unspecified additive (Sawa et al. 1999, Yoshimuta et al. 1991).

Droplets of the broth are generated by a vibrator and fall through ammonia gas (which provides droplet surface gelation) into a concentrated solution of ammonia (NH_3) for bulk gelation. At the end of this process, the gel droplets are ammonium diuranate (Yoshimuta et al. 1991). The droplets are then washed in water and alcohol, dried, calcined to form UO_3 and sintered in H_2 atmosphere to increase density and reduce the UO_3 to UO_2. The exact process parameters for drying, calcining and sintering of UO_2 kernels could not be found in the open literature. However, the process parameters for drying and sintering of $(Th,U)O_2$ kernels were found in (Fukuda et al. 1989) and they are as follows: drying in humidified air at 200°C, sintering in Ar+4%H_2 at 1300°C. All UO_2 kernels are classified by means of a vibrating table to exclude the odd-shape particles (Sawa et al. 1999).

Coating Deposition. Deposition of the PyC and SiC protecting layers is performed by a CVD process that takes place in a coater consisting of a graphite tube (ID 160-200 mm) and a gas nozzle where the particles are fluidized and exposed to the coating gases. The porous buffer layer is deposited from pyrolytic decomposition of C_2H_2 in a gaseous mixture of C_2H_2 and Ar at 1380°C (Minato et al. 1997). The IPyC layer is deposited from a gaseous mixture of C_3H_6 and Ar also at 1380°C (Minato et al. 1997). The SiC layer is deposited from a mixture of MTS and hydrogen at 1600°C for 60-200 min (Minato et al. 1995). Finally, the OPyC layer is deposited

from propylene and argon at 1380°C (Minato et al. 1997). Note that the coating time for the buffer, IPyC and OPyC layers, although not specified in the literature, is said to be less than for the SiC layer.

The presence of radial regions of lower density within the SiC was noted in some of the coated particles (Minato et al. 1994). This would result in debonding within the SiC. It was speculated that these flaws were due to violent spouting of the particles upon fluidization. This would cause some particles to fly out of the region of the coater where uniform temperature and MTS concentration conditions are maintained and into the upper region, where the different temperatures and lower MTS concentrations would result in irregular coating.

The gas flow rate, nozzle shape and size were varied systematically to assess their effect on the mode of fluidization. It was found by visual observations of the fluidized particles that there exists an intermediate range of gas flow rate values that generate a stable and gentle fluidization. At lower flow rates no fluidization is observed while at higher flow rates violent spouting results in impact of the particles with the coater wall. The effect of the nozzle shape and size was not as important, although better results were obtained with constant diameter nozzles than with converging nozzles (Minato et al. 1994). Implementation of these improvements resulted in the elimination of the SiC flaws.

The coating process was originally performed with loading and unloading of the particles after deposition of each coating layer, i.e., for each layer the following steps were performed:

- Loading of the particles
- Fluidization and coating of the particles with the coating gas
- Replacement of the coating gas with pure Ar
- Cooling of the coater
- Unloading of the particles
- Cleaning of the coater
- Start again from the first step

These steps were repeated four times for TRISO-coated particles (Minato et al. 1995). However, this process produced significant amounts of particles with cracked PyC and SiC coatings. It was assumed that these defects were caused by particle/particle or particle/wall impact during the repeated fluidization and unloading (Minato et al. 1995). An additional failure mechanism was

identified for the SiC layer that is caused by an underlying cracked IPyC, as follows. The kernel carbonization reaction $UO_2+3C \rightarrow UC+2CO$ (Minato et al. 1995) normally would not proceed during the high-temperature SiC deposition process because the CO is retained within the IPyC. However, if the IPyC is cracked, the CO is released through the crack and the reaction can actually take place at a fast rate. The flow of CO through the crack blows the coating gas away and effectively prevents the SiC from depositing in the region around the crack. Interestingly, it was observed that deposition of the OPyC on the failed SiC particles could be successfully performed because the PyC coating temperature and time are lower, which prevents kernel carbonization.

To eliminate these failure mechanisms, continuous coating of the particles (with just one loading prior to buffer deposition and one unloading after OPyC deposition) was successfully adopted in 1994 (Minato et al. 1995). All coated particles are classified to exclude the odd-shape particles (Sawa et al. 1999).

Fabrication of the Fuel Compacts. The coated particles are overcoated by a resinated graphite powder with alcohol to prevent mechanical damage of the coating during pressing (Sawa et al. 1999). The resinated graphite is prepared by grinding a mixture of 64 wt% natural graphite powder, 16 wt% electrographite powder and 20 wt% phenol resin (which acts as a binder). Originally, the overcoating process comprised a single-step overcoating of 200 μm. It was observed that the overcoating would not effectively stick to the particles and would allow particle/particle mechanical contact during warm-pressing of the compacts. It was decided to break the overcoating in two steps (Minato et al. 1997): (a) an 80 μm overcoating and curing at 180°C and (b) an additional 120 μm overcoating. Curing of the inner thinner layer ensures good adhesion of the overcoating to the coated particle and ensures maintenance of an acceptable distance during warm pressing. All overcoated particles are classified by means of a vibrating table to exclude the odd-shape particles (Sawa et al. 1999).

Overcoated particles are warm-pressed in metal dies to form annular compacts. Carbonization of the binder is performed in flowing N_2 at 800°C (Sawa et al. 1999). Additional heat treatment is provided at 1800°C for 1 hour in vacuum to degas compacts. The final fuel particle loading fraction in the compacts is 30 ± 3 vol.% (Sawa et al. 1999, Yoshimuta et al. 1991). Failure of particles was observed during warm pressing, which led to decreasing the pressing load by reducing the pressing speed and decreasing the pressing temperature (Minato et al. 1997).

Fuel Specifications and Quality Control. The specifications for the first-loading fuel of the Japanese HTTR are reported in Table 2-3, taken from Sawa et al. 1999. Exhaustive data for the as-manufactured fuel could not be found in the literature, but it is reported by Sawa et al. (1999) that the first HTTR fuel load meets all specifications of Table 2-3. The design limit for the total free uranium fraction, i.e., matrix contamination + uranium in SiC defective particles, is specified at 2×10^{-3} (IAEA 1997). This is based on the exposure limits for the plant staff and public during normal operating conditions, and was met by a large margin, i.e., the expected free uranium fraction is 5.5×10^{-4} (IAEA 1997).

The QC activities performed during the fabrication process are described in Figure 2-4. Note that the process itself, and not just the product, is controlled. QC testing to detect uranium contamination is done by deconsolidation and acid leaching of 4 out of 700 compacts. Testing to detect as-fabricated failed SiC in the compacts is done by burn/leach of 6 out of 700 compacts. This process comprises the oxidation of the graphite matrix and OPyC at 900°C in air as well as acid leaching of the exposed kernels (Sawa et al. 1999).

Table 2-3. Specifications for the Japanese HTTR fuel.

FUEL KERNEL	
Material	UO_2
Diameter	600±55 μm
Enrichment	6 wt%
Density	10.63±0.26 g/cm^3
Impurity	<3 ppm EBC*
COATING LAYERS	
Buffer Layer Thickness	60±12 μm
Buffer Layer Density	1.1±0.1 g/cm^3
IPyC Thickness	30±6 μm
IPyC Density	$1.85^{+0.10}_{-0.05}$ g/cm^3
SiC Thickness	25^{+12}_{-0} μm
SiC Density	≥3.2 g/cm^3
OPyC Thickness	45±6 μm
OPyC Density	$1.85^{+0.10}_{-0.05}$ g/cm^3
IPyC/OPyC OPTAF	≤1.03
COATED FUEL PARTICLE	
Diameter	920^{+50}_{-30} μm
Sphericity	≤1.2
ANNULAR FUEL COMPACT	
Particle Packing Factor	30±3 vol.%
Impurity	≤5 ppm EBC*
OD	26.0±0.1 mm
ID	10.0±0.1 mm
Height	39.0±0.5 mm
Matrix Density	1.70±0.05 g/cm^3
Compressive Strength	≥4,900 N
Total Free Uranium Fraction	2 x 10^{-3}

* EBC = Equivalent Boron Content

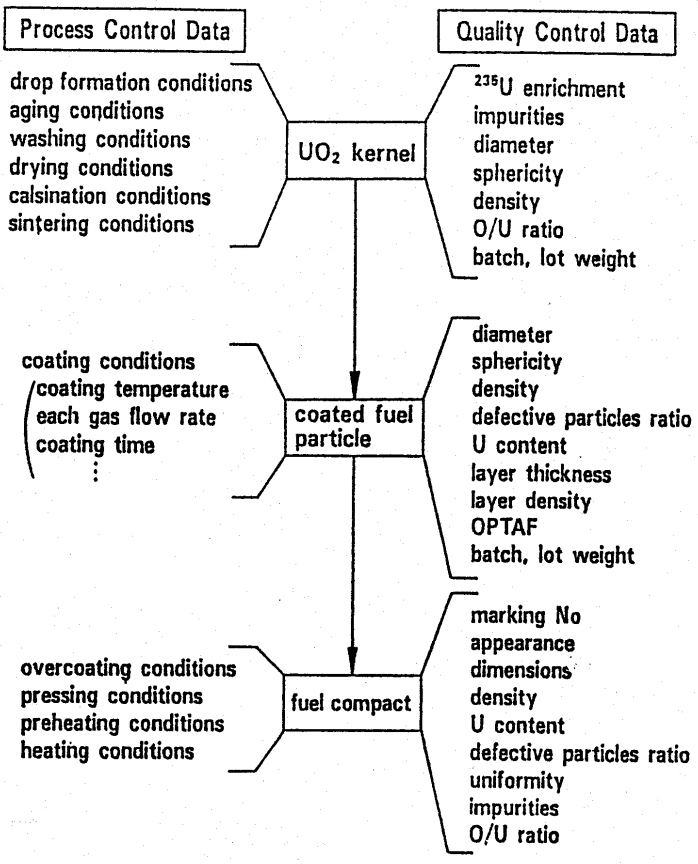

Figure 2-4. QC activities for the Japanese fuel (from Yoshimuta et al. 1991).

Chinese Fuel

The reference fuel for the Chinese demonstration High-Temperature Reactor (HTR-10) consists of spherical graphite pebbles containing about 8,300 TRISO-coated LEU uranium dioxide (UO_2) particles. Pebble-type fuel for gas-cooled reactors has been developed in China over a period of twenty-five years under the leadership of the Institute of Nuclear Energy Technology (INET). In 1991 the INET was put in charge of the fabrication of the first fuel load for the core of the HTR-10 reactor, which achieved its first criticality on December 1, 2000 (Nuclear News 2000).

The UO_2 kernels for this fuel are manufactured by the so-called "total" gel-precipitation process. The particle coatings are deposited by CVD. Finally, fabrication of the pebbles is realized by particle overcoating, pressing, and heat treatment.

UO_2 - Kernel Fabrication. The starting material is an aqueous solution of uranyl nitrate and urea (Tang et al. 2000), which is boiled at 93-95°C for about 60 minutes (Xu et al. 1993). An effect of the boiling time and initial uranium concentration was observed on the final shape of the kernels (Xu et al. 1993): specifically, a higher degree of sphericity is obtained with long boiling times (≥60 minutes) and high uranium concentration (>1.2*M*) (Xu et al. 1993). Then a solution of tetrahydrogen furfurylalcohol (4-HF) and PVA is added to increase viscosity (Xu et al. 1993, Tang et al. 2000). Finally, HMTA is added to the broth just before the droplets are generated by compressed-air pushing through a vibrating nozzle (for 500 μm kernels, the nozzle diameter is 700 μm (Xu et al. 1993) with pre-set (but unspecified) frequency (Tang et al. 2000)). The droplets are generated at a rate of 90-100 per second per nozzle and fall through a gas mixture of air and ammonia for external gelation (Xu et al. 1993), and into a room temperature ammonia solution bath (concentration > 4.0 *M*) for bulk gelation (Tang et al. 2000, Xu et al. 1993). This process is called total gelation because PVA precipitation on the droplet surface provides external gelation, while decomposition of the HMTA provides internal gelation. The total gelation process is thought to produce kernels with better sphericity (Xu et al. 1993). Complete hardening of the droplets is obtained by immersion in 4.0 *M* ammonia solution at 90°C, during which the droplets also shrink by 50% in volume (Xu et al. 1993). Consequently, the droplets are washed for 10-15 minutes in diluted ammonia solution (concentration 0.5 *M*) at 60-90°C to remove the ammonium nitrate from the kernels, and then dried with infrared light (Xu et al. 1993). Calcination takes place in air at 500°C to form UO_3 and remove the residual organic additives (Xu et al. 1993, Tang et al. 2000). UO_3 is reduced to UO_2 in an Ar-4%H_2 stream at 900°C (Tang et al. 2000). Finally, the kernels are sintered at 1550°C in H_2 atmosphere to obtain at least 98% TD (Tang et al. 2000). Oversized and undersized kernels are eliminated with a vibrator sieve (Tang et al. 2000). An inclined vibrating table eliminates fractured and irregular-shape particles (Tang et al. 2000).

Coating Deposition. Deposition of the PyC and SiC protecting layers is performed by a CVD process that takes place in a coater consisting of a 150-mm-ID tube with a cone-shaped distributor at the bottom, where the particles are fluidized and exposed to the coating gases (Tang et al. 2000). This coater can handle batches of UO_2 kernels up to 3 kg (Tang et al. 2000).

The auxiliary systems of the coater such as the gas supply cabinet, the regulating transformer, the control panel and the off-gas purification system were obtained from Germany (Tang et al. 2000). The heaters, coater tube and distributor, and the MTS evaporator were developed in China (Tang et al. 2000).

The kernels are injected from the top into the argon flow rising from the conical distributor (Tang et al. 2000). The buffer layer is deposited from a mixture of acetylene and argon at 1100-1400°C (IAEA 1997, Tang et al. 2000). The IPyC layer is deposited from a mixture of acetylene and propylene with argon as the carrying gas at 1370-1420°C (IAEA 1997, Tang et al. 2000). The SiC layer is deposited from MTS pyrolysis at 1500-1570°C using an equal mixture of H_2 and Ar as the carrying gases (IAEA 1997). Finally, the OPyC layer is also deposited from a mixture of acetylene and propylene with argon as the carrying gas at 1370-1420°C (IAEA 1997, Tang et al. 2000). No information on the coating rates of the pyrocarbons and silicon carbide could be found in the literature. Odd shaped particles are screened off by means of an inclined vibrating table.

Fabrication of the Fuel Pebbles. The basic materials for the pebble matrix are natural flake graphite (64 wt%), electrographite (16 wt%) and phenolic resin binder (20 wt%) (Tang et al. 2000). Natural flake graphite is normally impure and is purified by immersion in acids like HF, HCl and H_2SO_4 (Tang et al. 2000). The final impurities are as follows: 100 ppm ashes, <0.005 ppm lithium and <1 ppm boron (Tang et al. 2000).

The matrix materials are mixed, kneaded, dried and ground (Tang et al. 2000). Part of the mixture is used in an overcoating drum to overcoat the particles (200 μm thickness) (Tang et al. 2000). Then the overcoated particles are pre-molded at 30-50 MPa in silicon rubber molds with more matrix mixture to form the 5-cm fuel zone of the pebbles (Tang et al. 2000, IAEA 1997). The final molding is performed in silicon rubber molds at 300 MPa with more matrix mixture to make the 6cm-diameter pebbles Tang et al. 2000). Finally, the pebbles are lathed to sphericity (Tang et al. 2000), carbonized in Ar atmosphere at 800°C (IAEA 1997) and heat-treated at 1950°C in vacuum to remove residual impurities (IAEA 1997) and make the spheres corrosion resistant.

Fuel Specifications and Quality Control. The specifications for the Chinese HTR-10 particle fuel, along with the actual data for the as-manufactured fuel data, are reported in Table 2-4, taken from (Tang et al. 2000). Note that the geometry of the coated particle is specified at 95% confidence. The specified limit for the total free uranium content in the fuel elements is 3×10^{-4}. It is reported by Tang et al. (2000) that the measured free uranium in the first load of the as-manufactured HTR-10 fuel ranged from 3.7×10^{-5} to 5.5×10^{-4}, which therefore does not entirely meet the specification. The QC activities for the Chinese fuel are described in Figure 2-5.

Table 2-4. Specifications for the Chinese HTR-10.

	SPECIFICATION	AS-MANUFACTURED
FUEL KERNEL		
Material	UO_2	UO_2
Diameter*	500±50 μm	501.0±4.7 μm
Density	≥10.4 g/cm^3	10.77±0.05 g/cm^3
Sphericity	<1.2	1.05±0.01
O/U Ratio	≤2.01	2.000±0.001
Fraction of odd-shaped kernels	≤5×10^{-4}	2.6×10^{-4}±1.4×10^{-4}
COATED PARTICLE		
Buffer Layer Thickness*	90±36 μm	84.8±5.9 μm
Buffer Layer Density	≤1.10 g/cm^3	1.05±0.04 g/cm^3
IPyC Thickness*	40±20 μm	43.0±1.2 μm
IPyC Density	1.9±0.1 g/cm^3	1.8±0.02 g/cm^3
IPyC/OPyC OPTAF	≤1.03	1.02±0.006
SiC Thickness*	35±10 μm	40.0±1.4 μm
SiC Density	≥3.18 g/cm^3	3.200±0.003 g/cm^3
OPyC Thickness*	40±20 μm	38.5±1.5 μm
OPyC Density	1.9±0.1 g/cm^3	1.80±0.02 g/cm^3
GRAPHITE MATRIX		
Density	≥1.70 g/cm^3	1.72 g/cm^3
Total Ash	≤300 ppm	89 ppm
Li Content	≤0.3 ppm	<0.02 ppm
Impurity	≤3.0 ppm EBC**	<1.0 ppm EBC**
Thermal Conductivity	≥0.25 W/cm·K @ 1,000°C	0.31 W/cm·K, ⊥ *** 0.28 W/cm·K, || ***
Corrosion Rate	≤1.3 mg/cm^2·h @ 1,000°C in He + 1 vol.% H_2O	0.95 mg/cm^2·
Erosion Rate	≤6 mg/h per fuel element	3.2 mg/h
Breaking Loading	≥18 kN	22.7 kN, ⊥ *** 21.6 kN, || ***
FUEL ELEMENT		
Diameter	59.6-60.2 mm	59.6-60.2 mm
Thickness of Fuel-Free Shell	4.0-6.0 mm	4.0-6.0 mm
Total Free Uranium Fraction	3 x 10^{-4}	3.7-5.5 x 10^{-4}

* At 95% confidence

** EBC = Equivalent Boron Content

*** ⊥ and || indicate perpendicular to and parallel to the C-axis orientation, respectively.

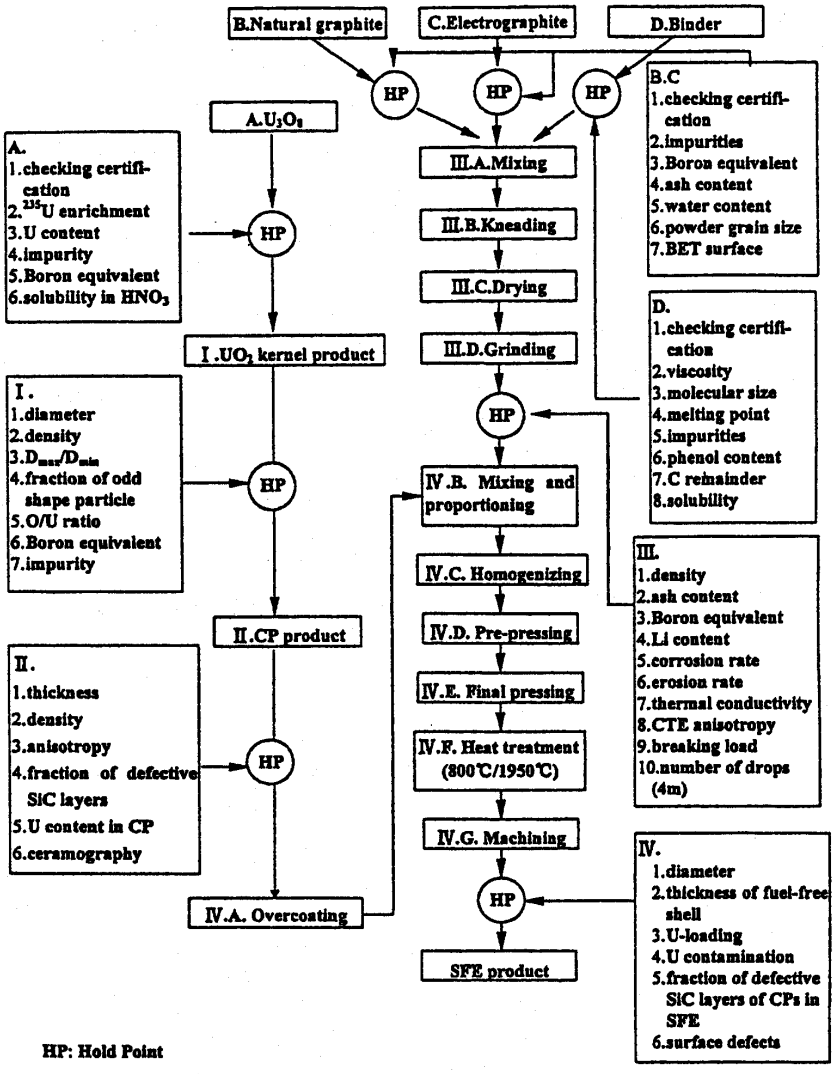

Figure 2-5. QC activities for the Chinese fuel (from Tang et al. 2000).

2.3 Discussion

The main characteristics of the kernel fabrication, coating process and fuel element fabrication are summarized in Tables 2-5 and 2-6, respectively. In these tables "na" stands for either "not available" or "not applicable".

Table 2-5. Characteristics of the kernel fabrication and coating processes.

COUNTRY		U.S.	GERMANY	JAPAN	CHINA
KERNEL MATERIAL		HEU-UCO	LEU-UO_2	LEU-UO_2	LEU-UO_2
GEL-PRECIPITATION		Internal	External	External	Total
BROTH COMPOSITION		Aqueous solution of uranyl nitrate, carbon-black, Tamol, urea, HMTA	Aqueous solution of uranyl nitrate, PVA and other non-specified additives	Aqueous solution of uranyl nitrate, methanol and other non-specified additives	Aqueous solution of uranyl nitrate, urea, 4-HF, PVA and HMTA
DROPLET FORMATION		Vibrating nozzle	Vibrating nozzle	Vibrating nozzle	Vibrating nozzle
GELATION		Trichloroethylene	Ammonia gas and ammonia solution	Ammonia gas and ammonia solution	Air, ammonia gas and ammonia solution
WASHING		Ammonia solution and clean water	Ammonia solution and isopropanol	Water and alcohol	Ammonia solution
DRYING		Air at 60°C	80°C	Air at 200°C	Infra-red
CALCINATION		Ar at 350°C	Air at 300°C	na	Air at 500°C
REDUCTION		H_2 at 1600°C	na	na	H_2 at 900°C
SINTERING		CO at 1800°C	H_2 at 1600-1700°C	H_2 at 1300°C	H_2 at 1550°C
COATING PROCESS		Discontinuous	Continuous	Continuous	Continuous
BUFFER	Gas	Ar-C_2H_2	Ar-C_2H_2	Ar-C_2H_2	Ar-C_2H_2
	Coating	1300°C	1250°C	1380°C	1100-1400°C
	Coating Rate	na	6-10 μm/min	na	na
SEAL*	Gas	Ar-C_3H_6	na	na	na
	Coating	1200°C	na	na	na
IPyC	Gas	Ar-C_2H_2-C_3H_6	Ar-C_2H_2-C_3H_6	Ar-C_3H_6	Ar-C_2H_2-C_3H_6
	Coating	1230°C	1300°C	1380°C	1370-1420°C
	Coating Rate	<4 μm/min	4-6 μm/min	na	na
SiC	Gas	H_2-CH_3SiCl_3	H_2-CH_3SiCl_3	H_2-CH_3SiCl_3	Ar-H_2-CH_3SiCl_3
	Coating	1650°C	1500°C	1600°C	1500-1570°C
	Coating Rate	0.2-0.4 μm/min	0.2 μm/min	0.1-0.4 μm/min	na
OPyC	Gas	Ar-C_2H_2-C_3H_6	Ar-C_2H_2-C_3H_6	Ar-C_3H_6	Ar-C_2H_2-C_3H_6
	Coating	>1300°C	1300°C	1380°C	1370-1420°C
	Coating Rate	<4 μm/min	4-6 μm/min	na	na
SEAL*	Gas	Ar-C_3H_6	na	na	na
	Coating	1200°C	na	na	na
PPyC	Gas	Ar-C_2H_2	na	na	na
	Coating	1300°C	na	na	na
	Coating Rate	na	na	na	na
SEAL*	Gas	Ar-C_3H_6	na	na	na
	Coating	1200°C	na	na	na

* Fabrication process for the NPR fuel only.

Table 2-6. Characteristics of the fuel-element fabrication process.

COUNTRY	U.S.*	GERMANY	JAPAN	CHINA
FUEL ELEMENT	Compact	Pebble	Compact	Pebble
MATRIX MATERIALS	Graphite flour, graphite shim, octadecanol, polystyrene	Graphite powder	Natural graphite, electrographite	Natural flake graphite, electrographite
BINDERS	Petroleum pitch	Phenol, hexamethylene-tetramine	Phenol	Phenol
MATRIX STATE	Liquid	Powder	Powder	Powder
OVERCOATING	Na	200 μm	80 μm, 180˚C +120 μm	200 μm
PRE-PRESSING	na	25˚C, 30 MPa	na	25˚C, 30-50 MPa
PRESSING	160˚C, 6.9 MPa	25˚C, 300 MPa	Warm-pressing	25˚C, 300 MPa
LATHING	na	Yes	na	Yes
CARBONIZATION	900˚C in alumina powder and N_2	800-900˚C in inert gas	800˚C in N_2	800˚C in Ar
LEACHING	HCl	na	na	na
HEAT TREATMENT	1650˚C in Ar	1950˚C in vacuum	1800 ˚C in vacuum	1950˚C in vacuum

* Fabrication process for the NPR fuel, only.

It can be seen that the U.S. (or GA) fuel fabrication process significantly differs from that of the other countries in all three steps: kernel fabrication, coating and fuel element fabrication. Differences in kernel fabrication stem from the different kernel composition (although GA did use UO_2 and Nukem used UCO in the past) and from selection of different gelation processes. The initial broth in the GA process contains carbon black that supplies the carbon needed to form the UCO kernel. Also, gelation of the broth droplets in the GA process occurs in a hot organic bath and ammonia is derived from additives to the broth not externally from ammonia gas or ammonium hydroxide solutions. Finally, sintering of the GA kernels is performed in CO atmosphere to prevent excessive reduction of the carbides, whereas hydrogen is utilized for the UO_2 kernels in other countries. Differences also exist in the coating parameters used to produce PyC and SiC. These different conditions result in differences in the microstructure, anisotropies and densities of the coatings. In addition, the U.S. coating process is discontinuous with the fuel particle unloaded after each layer to perform QC measurements. German, Japanese, and Chinese TRISO-coating is done in one pass or a continuous manner. The implications of these differences on the irradiation performance of this fuel are discussed in Section 4.

Several differences are apparent in the fuel element fabrication process. The U.S. process differs in the lack of overcoating of the particles prior to pressing, the use of the liquid matrix, a higher pressing temperature for the matrix material, and the leaching of the compacts with HCl before heat treatment. In the final heat treatment, the U.S. used graphite furnaces purged with inert gases while all others are in vacuum. In addition, a lower temperature is used for the final heat treatment in the U.S. These differences in fabrication of the fuel body are believed to lead to differences in the observed as-manufactured defects in the two fuel types.

Anecdotal discussions with experts in the U.S. and Germany indicate other potentially important differences in fabrication. In Germany, strict process control was adopted and systematic process improvement was used to develop high quality fuel. Once high quality fuel was manufactured, changes in the process were rare. The effort was significant in terms of financial and personnel resources. By contrast, the U.S. lacked the level of financial resources in the area of fuel fabrication. This was further complicated by routine changes in fabrication processing parameters (e.g., PyC coating rates), in kernel and coating types (see Section 3), and in different coater designs. Although difficult to evaluate in quantitative terms, the authors feel such differences should not be overlooked in such a historical review.[2]

[2] It is important to note that for the present U.S. GT-MHR fuel design, GA has adopted the German coater and coating design for its fuel.

3. SUMMARY OF U.S. AND GERMAN IRRADIATION EXPERIMENTS AND POSTIRRADIATION EXAMINATION RESULTS

3.1 Introduction

Irradiation experiments in support of TRISO-coated particle fuel development programs have been developed in several countries. This review will focus on pertinent experiments performed in the United States and Germany.

The U.S. particle fuel development effort, which included design and testing, coincided with the development of various high temperature gas-cooled reactors (HTGR). This sequence of development is listed in Table 3-1 which also identifies the main fuel forms under consideration at that time. U.S. gas reactors were designed to use prismatic graphite blocks containing fuel compacts, and were primarily intended to produce electricity with the exception that the NP-MHTGR was designed to produce tritium. Over the years, the design has also supported steam cycle, direct cycle, process heat, and weapons material deposition applications.

Table 3.1. U.S. Particle Fuel Development and Testing Sequence.

DATE OF DESIGN CONCEPTION	REACTOR / STATUS	MAJOR FUEL FORM TESTED
1960	Peach Bottom built	BISO coated (Th,U)C_2
1964	Fort St. Vrain built	TRISO coated (Th,U)C_2 fissile TRISO coated ThC_2 fertile
1967	LHTGR design only	TRISO coated UC_2 fissile BISO and TRISO coated ThO_2 fertile
1984	NE-MHTGR commercial design only	TRISO-P coated UCO fissile TRISO-P coated ThO_2 fertile
1989	NP-MHTGR government design only	TRISO-P coated UCO
1995	GT-MHR commercial design only	TRISO coated UCO fissile TRISO coated UCO and/or UO_2 fertile fuel not yet tested

The German particle fuel development effort had been conducted in support of various HTGR designs which employed a pebble bed core. These reactors were intended to produce process heat or electricity. The sequence of fuel development in Germany followed improvement in particle

quality and performance and was largely independent of developments in reactor technology. German fuel development can be categorized according to the sequence of fuels tested as listed in Table 3-2.

Table 3-2. German Particle Fuel Development Sequence.

DATE OF DESIGN CONSIDERATION	FUEL FORM
1972	BISO coated $(Th,U)O_2$
1977	Improved BISO coated $(Th,U)O_2$ TRISO coated UCO fissile particles with ThO_2 fertile particles TRISO coated $(Th,U)O_2$
1981	LEU TRISO coated UO_2

Irradiation test conditions employed by both the U.S. and Germany generally covered the projected fuel operating conditions. Generally, U.S. fuel was to operate at temperatures as high as 1400°C and reach full burnup (commensurate with U-235 enrichment and kernel composition) at fast fluences of 4×10^{25} n/m^2. German fuel was to reach full burnup at fast fluences of 2.4×10^{25} n/m^2 and operate at temperatures up to 1095°C for process heat applications and up to 830°C for electrical production applications. Differences in temperature and fast neutron fluence were due to the different core designs (power density and gas temperature) in which the fuel was to be used. With the exception of irradiation duration, the various experiments performed by each country either bounded expected nominal conditions or were purposely varied to meet other test objectives. In order to obtain results in a timely manner, each country accelerated their irradiation tests. U.S. tests were accelerated by factors of three to ten while German tests were generally accelerated by factors of two to three.

The following sections present irradiation experiment summaries for fuels of "modern" design. For the U.S. experiments, this entails fuel with TRISO coated fissile particles. For German experiments, this definition extends to TRISO coated $(Th,U)O_2$ and LEU TRISO coated UO_2 fuel.

3.2. U.S. Experiments

The particle fuel irradiation experiments and postirradiation examination results described in this section consider only selected tests of key U.S. fuel types. These fuel types include TRISO fissile / BISO fertile particles, weak acid resin (WAR) TRISO fissile / BISO fertile particles, TRISO fissile / TRISO fertile particles, and TRISO-P fissile particles (conventional TRISO-coated

particles with an additional "protective" PyC layer above the OPyC layer). Kernel and coating batches were generally manufactured by General Atomics and Babcock & Wilcox. However, some batches were manufactured by ORNL (identified by batch designators beginning with OR). The following U.S. experiment summaries are listed in chronological order and are not grouped by fuel type. Listed configuration and irradiation data are actual values, not specification values or ranges. Interpretations of postirradiation examination results are from the original sources and no overt attempt has been made to reinterpret the results.

F-30

The F-30 experiment was irradiated in the General Electric Test Reactor (GETR) at Pleasanton, California (Scott and Harmon 1975). The primary objective of this experiment was to demonstrate the irradiation performance of Fort St. Vrain production fuel. Five independently gas swept cells contained the fuel. Cells 1, 3, and 4 contained only fuel compacts, Cell 2 contained only loose particles, and Cell 5 contained both fuel compacts and loose particles. Configuration and irradiation data are given in Tables 3-3 through 3-8.

Postirradiation metallographic examination of seven fuel compacts containing fissile and fertile particles were performed. In addition, five sets of loose fissile particles and five sets of loose fertile particles were examined. Fissile particle failure, defined as a crack completely through the SiC layer, ranged between 0 and 6.1% while fertile particle failure ranged between 0 and 15.1%. Further results of layer failures from the metallographic examination are presented in the following tables. A typical photomicrograph of SiC failure in an F-30 fissile particle is presented in Figure 3-1. Metallography revealed that IPyC layers had remained bonded to the SiC layer throughout irradiation. Figure 3-2 displays a typical photomicrograph of a fissile particle with an IPyC layer crack and a densified buffer.

Table 3-3. F-30 Configuration.

Number of cells	5
Total number of fuel compacts	13
Cylindrical fuel compact diameter	12.45 mm
Cylindrical fuel compact lengths	18.54 and 49.28 mm
Fissile fuel type	HEU (Th,U)C_2 TRISO
Nominal Th/U ratio	4.25
U-235 enrichment	93%
Fissile particle diameter	429 to 560 μm
Fertile fuel type	ThC_2 TRISO
Fertile particle diameter	648 to 771 μm
Number of fissile particle batches	7
Number of fertile particle batches	9
Defective SiC layer fraction* – fissile particles	$< 5 \times 10^{-4}$ to 1.5×10^{-3}
Defective SiC layer fraction* – fertile particles	3×10^{-4} to 1.0×10^{-3}

* The defective SiC layer fractions reported for the U.S. fuel are per particle batch with the exception of HRB-21 and \ the NPR experiments which are per fuel compact.

Table 3-4. F-30 Irradiation Data.

Start date	May 15, 1972				
End date	April 5, 1973				
Duration (full power days)	269				
Cell	1	2	3	4	5
Fissile burnup (%FIMA)	15	19	20	18	12
Fertile burnup (%FIMA)	3	4.5	5	4	1.5
Fast fluence (10^{25} n/m^2, E > 0.18 MeV)	8	10.5	11.5	9.5	12
Time average peak temperature (°C)	1100	1100	1120	1100	1200
BOL Kr-85m R/B	2×10^{-6}	7×10^{-7}	8×10^{-7}	7×10^{-7}	2×10^{-6}
EOL Kr-85m R/B	8×10^{-6}	1×10^{-4}	1×10^{-5}	2×10^{-5}	2×10^{-5}

*

Table 3-5. F-30 Coated Fissile Fuel Particles.

Particle batch	CU6A-6324	CU6A-6326	CU6A-6328	CU6B-2422	CU6B-2427
Fuel form	(Th,U)C_2 TRISO	(Th,U)C_2 TRISO	(Th,U)C_2 TRISO	(Th,U)C_2 TRISO	(Th,U)C_2 TRISO
Thorium to uranium (atom ratio)	4.25	4.25	4.25	4.25	4.25
U-235 enrichment (%)	93	93	93	93	93
Kernel diameter (μm)	178	178	178	226	239
Buffer thickness (μm)	52	59	54	56	55
IPyC thickness (μm)	24	25	23	26	25
SiC thickness (μm)	26	25	25	25	23
OPyC thickness (μm)	35	36	36	43	42
Kernel density (g/cm^3)	not reported	not reported	not reported	not reported	not reported
Buffer density (g/cm^3)	1.08	1.16	1.10	1.18	1.11
IPyC density (g/cm^3)	1.88	1.89	1.89	1.89	1.85
SiC density (g/cm^3)	3.20	3.20	3.21	3.21	3.20
OPyC density (g/cm^3)	1.80	1.83	1.84	1.80	1.78
IPyC BAF (optical)	1.19	1.14	1.18	1.18	1.10
OPyC BAF (optical)	1.12	1.13	1.18	1.08	1.08

Note: Particle batches CU7A-1035 and CU7B-3021 were composites of two or more coating batches and their properties were not reported.

Table 3-6. F-30 Coated Fertile Fuel Particles.

Particle Batch	CT6A-2399	CT6A-2815	CT6A-2835	CT6B-914	CT6B-932
Fuel form	ThC_2 TRISO	ThC_2 TRISO	ThC_2 TRISO	ThC_2 TRISO	ThC_2 TRISO
Kernel diameter (μm)	373	375	362	430	432
Buffer thickness (μm)	62	56	56	53	56
IPyC thickness (μm)	29	35	39	42	35
SiC thickness (μm)	24	28	29	29	23
OPyC thickness (μm)	43	37	39	47	47
Kernel density (g/cm^3)	not reported	not reported	not reported	not reported	not reported
Buffer density (g/cm^3)	1.19	0.91	1.17	1.14	1.14
IPyC density (g/cm^3)	1.89	1.90	1.94	1.90	1.91
SiC density (g/cm^3)	3.20	3.22	3.20	3.21	3.19
OPyC density (g/cm^3)	1.80	1.84	1.76	1.79	1.80
IPyC BAF (optical)	1.18	1.09	1.11	1.11	1.12
OPyC BAF (optical)	1.19	1.13	1.10	1.12	1.13

Note: Particle batches CT7A-3028, CT7A-3033, CT7B-3024 and CT7B-3025 were composites of two or more coating batches and their properties were not reported.

Table 3-7. F-30 Fissile Particle Layer Failures.

Particle Batch	Sample No./Type	Average Irradiation Temp.(°C)	Fast Fluence (10^{25} n/m^2)	Burnup (%FIMA)	Sample Size	OPyC Layer Failure (%)	OPyC 95% Confidence Interval (%)	SiC Layer Failure (%)	SiC 95% Confidence Interval (%)	IPyC Layer Failure (%)	IPyC 95% Confidence Interval (%)
CU6A-6326	3A-14 compact	1050	10.6	19.1	33	0	$0 \le P \le 10.7$	6.1	$0.8 \le P \le 20.1$	3.0	$0 \le P \le 14.6$
CU6A-6328	1C-14 compact	1043	7.9	16.5	228	0.4	$0.1 \le P \le 2.4$	0	$0 \le P \le 1.7$	0	$0 \le P \le 1.7$
CU6A-6328	4B-15 compact	1088	8.9	19.4	161	0	$0 \le P \le 2.3$	0	$0 \le P \le 2.3$	0	$0 \le P \le 2.3$
CU6-6328	5A-14 compact	1052	5.0	12.9	80	0	$0 \le P \le 4.8$	0	$0 \le P \le 4.8$	0	$0 \le P \le 4.8$
CU7A-1035	1A-30 compact	885	5.3	14.6	144	0	$0 \le P \le 2.6$	4.2	$1.9 \le P \le 8.8$	not determined	---
CU6B-2427	5C-11 compact	825	4.2	11.9	16	0	$0 \le P \le 21.0$	0	$0 \le P \le 21.0$	18.8	$3.8 \le P \le 46.0$
CU7B-3021	1D-14 compact	1032	8.7	17.3	90	0	$0 \le P \le 4.3$	0	$0 \le P \le 4.3$	0	$0 \le P \le 4.3$
CU6A-6326	2-2 loose particle	1231	10.3	18.3	205	2.4	$1.0 \le P \le 5.6$	2.4	$1.0 \le P \le 5.6$	1.0	$0.3 \le P \le 3.5$
CU6A-6326	5-2 loose particle	1173	7.3	15.3	421	0.2	$0.04 \le P \le 1.3$	0	$0 \le P \le 0.9$	0.7	$0.24 \le P \le 2.1$
CU6A-6328	2-4 loose particle	1243	10.2	18.2	245	0.4	$0.1 \le P \le 2.3$	1.2	$0.4 \le P \le 3.5$	0.4	$0.1 \le P \le 2.3$
CU6A-6328	5-4 loose particle	1250	7.2	15.0	357	0	$0 \le P \le 1.1$	0	$0 \le P \le 1.1$	0	$0 \le P \le 1.1$
CU6B-2422	2-1 loose particle	1238	10.3	20.1	190	1.0	$0.3 \le P \le 3.8$	1.0	$0.3 \le P \le 3.8$	1.6	$0.5 \le P \le 4.5$

Note: Fast fluence is for $E > 0.18$ MeV.

Table 3-8. F-30 Fertile Particle Layer Failures.

Particle Batch	Sample No./Type	Average Irradiation Temp.(°C)	Fast Fluence (10^{25} n/m^2)	Burnup (%FIMA)	Sample Size	OPyC Layer Failure (%)	OPyC 95% Confidence Interval (%)	SiC Layer Failure (%)	SiC 95% Confidence Interval (%)	IPyC Layer Failure (%)	IPyC 95% Confidence Interval (%)
CT6A-2835	3A-14 compact	1050	10.6	5.7	57	12.3	$5.3 \le P \le 23.2$	3.5	$0 \le P \le 12.2$	10.5	$4.2 \le P \le 21.2$
CT6A-2399	1C-14 compact	1043	7.9	3.3	198	13.6	$9.5 \le P \le 19.1$	0.5	$0.1 \le P \le 2.8$	2.0	$0.8 \le P \le 5.1$
CT6A-2399	4B-15 compact	1079	8.9	4.3	405	26.4	$22.4 \le P \le 30.9$	0	$0 \le P \le 0.9$	4.4	$2.8 \le P \le 6.9$
CT6A-2399	5A-14 compact	1052	6.5	2.1	88	17.0	$8.8 \le P \le 26.2$	2.3	$0 \le P \le 7.9$	56.8	$40.0 \le P \le 75.0$
CT7A-3028 CT7B-3024	1A-30 compact	885	5.3	2.0	111	1.8	$0.5 \le P \le 6.3$	0.9	$0.2 \le P \le 4.9$	5.4	$2.5 \le P \le 11.3$
CT6A-2399 CT6B-932	5C-11 compact	825	4.2	0.9	89	16.8	$8.7 \le P \le 26.1$	0	$0 \le P \le 4.2$	not determined	---
CT7A-3037 CT7B-3025	1D-14 compact	1032	8.7	3.8	96	4.2	$1.5 \le P \le 10.0$	8.3	$4.0 \le P \le 15.0$	14.6	$8.2 \le P \le 22.5$
CT6A-2835	2-1 loose particle	1139	10.3	4.7	146	6.2	$3.3 \le P \le 11.3$	3.4	$1.5 \le P \le 7.8$	58.9	$50.8 \le P \le 66.6$
CT6A-2399	2-3 loose particle	1140	10.2	4.7	166	6.6	$3.7 \le P \le 11.5$	15.1	$10.4 \le P \le 21.3$	92.2	$87.1 \le P \le 95.4$
CT6B-914	2-2 loose particle	1170	10.3	4.7	111	2.7	$0.9 \le P \le 7.6$	14.4	$9.1 \le P \le 22.1$	95.5	$89.9 \le P \le 98.1$
CT6B-914	5-2 loose particle	1064	7.3	2.4	230	0.9	$0.2 \le P \le 3.1$	1.3	$0.4 \le P \le 3.8$	89.1	$84.4 \le P \le 92.5$
CT6B-932	2-4 loose particle	1160	10.2	4.7	133	3.8	$1.6 \le P \le 8.5$	0.8	$0.1 \le P \le 4.1$	100.0	$97.2 \le P \le 100.0$

Note: Fast fluence is for E > 0.18 MeV.

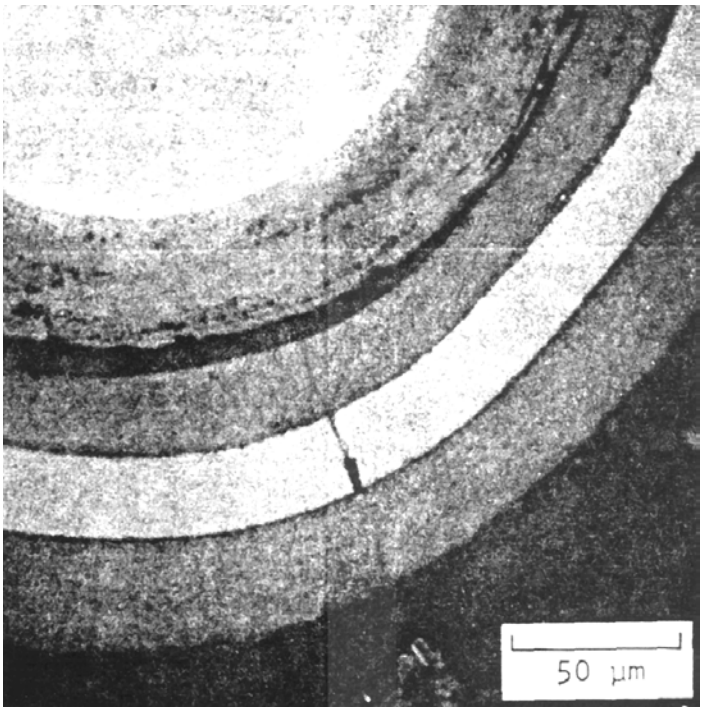

Figure 3-1. A typical SiC layer crack in an F-30 fissile fuel particle.

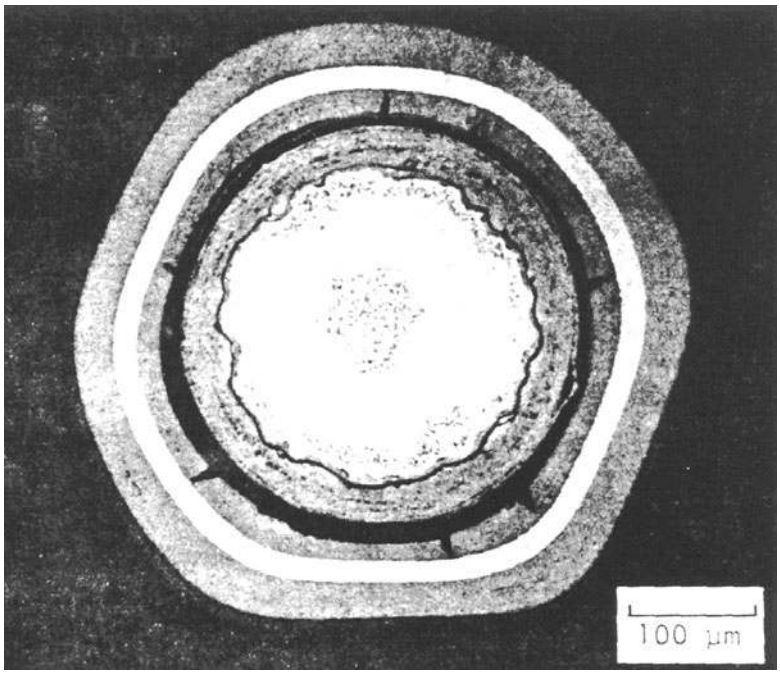

Figure 3-2. A typical IPyC layer crack in a fissile F-30 fuel particle.

HRB-4

The HRB-4 capsule was irradiated in the High Flux Isotope Reactor (HFIR) at Oak Ridge National Laboratory (Scott and Harmon 1975b). The main objective of this experiment was to test candidate fuel materials and manufacturing processes for the proposed Large High Temperature Gas-cooled Reactor (LHTGR). This test consisted of a single gas swept cell containing six fuel compacts vertically positioned. The irradiation of HRB-4 in HFIR coincided with the irradiation of HRB-5 and part of HRB-6. Configuration and irradiation data are given in Tables 3-9 through 3-13.

Table 3-9. HRB-4 Configuration.

Number of cells	1
Number of fuel compacts	6
Cylindrical fuel compact diameter	12.4 mm
Cylindrical fuel compact lengths	25.4 mm
Fissile fuel type	WAR UC_2 TRISO
Fertile fuel type	ThO_2 BISO
U-235 enrichment	5.99 %
Fissile particle diameter	639 μm
Fertile particle diameter	805 μm
Fissile particle batch	OR52A
Fertile particle batch	T01424BIL
Total number of fissile particles	17,780
Total number of fertile particles	4,180

Table 3-10. HRB-4 Irradiation Data.

Start date	October 8, 1972
End date	June 26, 1973
Duration (full power days)	244
Peak fissile burnup (%FIMA)	27.7
Peak fertile burnup (%FIMA)	13.4
Peak fast fluence (10^{25} n/m^2, E > 0.18 MeV)	10.5
Peak temperature (°C)	1250
BOL Kr-85m R/B	1.4×10^{-5}
EOL Kr-85m R/B	3.2×10^{-4}

Table 3-11. HRB-4 Coated Fuel Particles.

Particle batch	OR52A	T01424BIL
Fuel form	WAR UC_2 TRISO	ThO_2 BISO
Carbon to uranium (atom ratio)	not reported	na
U-235 enrichment (%)	5.99	na
Kernel diameter (μm)	367	488
Buffer thickness (μm)	45	83
IPyC thickness (μm)	31	na
SiC thickness (μm)	34	na
OPyC thickness (μm)	30	73
Particle diameter (μm)	639	805
Kernel density (g/cm^3)	not reported	not reported
Buffer density (g/cm^3)	0.95	1.08
IPyC density (g/cm^3)	1.94	na
SiC density (g/cm^3)	3.21	na
OPyC density (g/cm^3)	1.89	1.83
IPyC BAF	1.10	na
OPyC BAF	1.09	1.16
Coating rate (μm/min)	8 to 10	4.0

Note: Entry "na" means not applicable.

Postirradiation examination included gas release measurements of each fuel compact performed in the GA TRIGA reactor. Table 3-12 lists the BOL R/B values performed as part quality control, and the EOL values. The TRIGA gas release measurements were lower than the swept line measurements performed during the actual irradiation. This was in part due to the TRIGA test temperature of 1100°C being lower than the irradiation test centerline temperature of about 1250°C.

Table 3-12. HRB-4 TRIGA Fission Gas Release Results.

COMPACT	BOL Kr-85m R/B	EOL Kr-85m R/B
2A-125	3.8×10^{-6}	1.4×10^{-4}
2B-175	3.0×10^{-6}	1.2×10^{-5}
2C-162	2.5×10^{-6}	8.5×10^{-4}
4A-131	7.9×10^{-6}	1.1×10^{-4}
4B-172	3.6×10^{-6}	2.6×10^{-5}
4C-158	1.8×10^{-6}	8.3×10^{-5}

Metallographic examinations were performed on each fuel compact. A typical photomicrograph of an irradiated HRB-4 fissile particle is presented in Figure 3-3, which shows the formation of gas bubbles in the kernel and the densification of the buffer. IPyC layers of the examined fissile particles had remained bonded to the SiC. The examination indicated that the fissile particles had failed between 0 and 6% of the SiC layers. These failures consisted primarily of radial cracks

through the SiC layer. Between 4 and 73% of the OPyC layers failed during irradiation. There were no tabulations of IPyC layer failures reported. The following table presents further information concerning fissile particle layer failures.

Several of the fissile particles examined displayed evidence of fission product attack. This attack mostly occurred in large concentrations at the IPyC – SiC interface and where fission products in smaller concentrations had diffused up to 25 μm into the SiC. Figure 3-4 presents typical photomicrographs of fission product attack in HRB-4 fissile particles.

Table 3-13. HRB-4 Fissile Particle Layer Failures.

Compact	Fast Fluence (10^{25} n/m^2)	Burnup (%FIMA)	Sample Size	OPyC Layer Failure (%)	OPyC 95% Confidence Interval (%)	SiC Layer Failure (%)	SiC 95% Confidence Interval (%)
2A-125	10.5	27.6	82	31.6	$22.5 \le P \le 46.0$	3.7	$1.0 \le P \le 9.8$
2B-175	10.5	27.7	219	3.7	$1.9 \le P \le 7.0$	0	$0 \le P \le 1.7$
2C-162	10.2	27.6	167	53.9	$46.3 \le P \le 61.3$	1.2	$0.3 \le P \le 4.3$
4A-131	6.3	24.5	128	61.7	$53.1 \le P \le 69.7$	6.3	$3.2 \le P \le 11.8$
4B-172	5.3	22.9	236	5.9	$3.6 \le P \le 9.7$	3.8	$2.0 \le P \le 7.1$
4C-158	4.2	20.7	177	72.6	$65.9 \le P \le 78.9$	1.1	$0.3 \le P \le 4.0$

Notes: Each compact centerline temperature was nominally 1250 °C. Fast fluence is for E > 0.18 MeV.

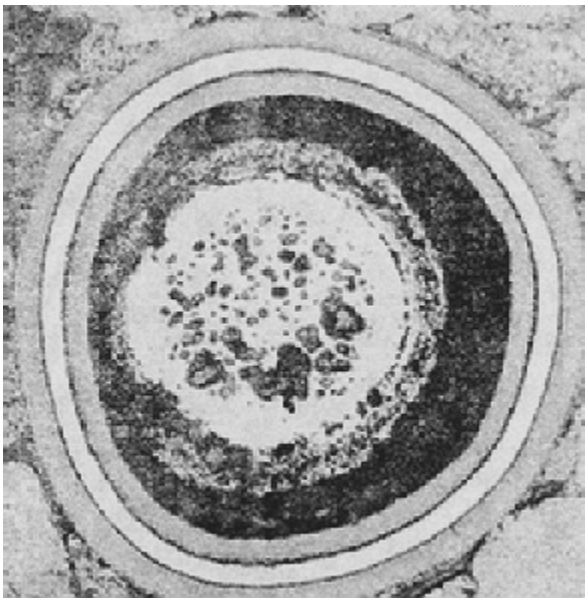

Figure 3-3. Typical HRB-4 fissile particle irradiated to 27.7%FIMA and 10.5 x 10^{25} n/m^2 fast fluence.

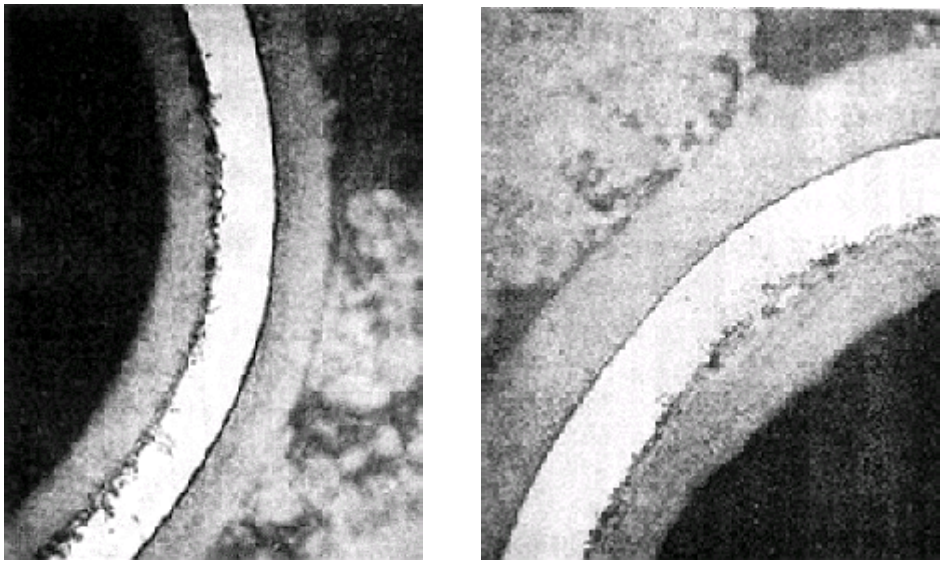

Figure 3-4. Photomicrographs of typical fission product attack in irradiated HRB-4 fissile particles.

HRB-5

The HRB-5 capsule was irradiated in the High Flux Isotope Reactor (HFIR) at Oak Ridge National Laboratory (Scott and Harmon 1975b). The main objective of this experiment was to test candidate fuel materials and manufacturing processes for the proposed Large High Temperature Gas-cooled Reactor (LHTGR). This test consisted of a single gas swept cell containing six fuel compacts vertically positioned. The irradiation of HRB-5 in HFIR coincided with part of the HRB-4 irradiation. Configuration and irradiation data are given in the following tables.

Table 3-14. HRB-5 Configuration.

Number of cells	1
Number of fuel compacts	6
Cylindrical fuel compact diameter	12.4 mm
Cylindrical fuel compact lengths	25.4 mm
Fissile fuel type	WAR UC_2 TRISO
Fertile fuel type	ThO_2 BISO
U-235 enrichment	5.99%
Fissile particle diameter	639 μm
Fertile particle diameter	805 μm
Fissile particle batch	OR52A
Fertile particle batch	T01424BIL
Total number of fissile particles	17,780
Total number of fertile particles	4,180

Table 3-15. HRB-5 Irradiation Data.

Start date	October 8, 1972
End date	February 3, 1973
Duration (full power days)	107
Peak fissile burnup (%FIMA)	15.7
Peak fertile burnup (%FIMA)	4.3
Peak fast fluence (10^{25} n/m^2, E > 0.18 MeV)	4.7
Peak temperature (°C)	1250
BOL Kr-85m R/B	3×10^{-6}
EOL Kr-85m R/B	1×10^{-4}

Table 3-16. HRB-5 Coated Fuel Particles.

Particle batch	OR52A	T01424BIL
Fuel form	WAR UC_2 TRISO	ThO_2 BISO
Carbon to uranium (atom ratio)	not reported	na
U-235 enrichment (%)	5.99	na
Kernel diameter (μm)	367	488
Buffer thickness (μm)	45	83
IPyC thickness (μm)	31	na
SiC thickness (μm)	34	na
OPyC thickness (μm)	30	73
Particle diameter (μm)	639	805
Kernel density (g/cm^3)	not reported	not reported
Buffer density (g/cm^3)	0.95	1.08
IPyC density (g/cm^3)	1.94	na
SiC density (g/cm^3)	3.21	na
OPyC density (g/cm^3)	1.89	1.83
IPyC BAF	1.10	na
OPyC BAF	1.09	1.16
Coating rate (μm/min)	8 to 10	4.0

Note: Entry "na" means not applicable.

Postirradiation examination included gas release measurements of each fuel compact performed in the GA TRIGA reactor. Table 3-17 lists the BOL R/B values performed as part quality control, and the EOL values. The TRIGA gas release measurements were lower than the swept line measurements performed during the actual irradiation. This was in part due to the TRIGA test temperature of 1100°C being lower than the irradiation test centerline temperature of about 1250°C.

Table 3-17. HRB-5 TRIGA Fission Gas Release Results.

Compact	BOL Kr-85m R/B	EOL Kr-85m R/B
2A-123	7.1×10^{-6}	5.3×10^{-6}
2B-184	2.0×10^{-6}	5.3×10^{-5}
2C-149	3.1×10^{-6}	1.0×10^{-4}
4A-115	3.1×10^{-6}	2.9×10^{-4}
4B-181	8.0×10^{-6}	1.8×10^{-4}
4C-153	2.5×10^{-6}	7.9×10^{-6}

Metallographic examinations were performed on each fuel compact. IPyC layers of the examined fissile particles had remained bonded to the SiC. There were no tabulations of IPyC layer failures reported. There was no evidence of fission product attack as seen in the HRB-4 fissile particles. However, the examination indicated that the fissile particles had failed between 0.4 and 17% of the SiC layers. These failures consisted primarily of radial cracks through the SiC layer. A typical photomicrograph of irradiated HRB-5 fissile particles with cracked SiC layers is presented in Figure 3-5. This photomicrograph is also representative of HRB-4 fissile particles with cracked SiC layers. It was reported that a large fraction of these cracked SiC layers were due to metallographic preparation and not a result of fast neutron exposure or fuel burnup effects. The following table presents further information concerning fissile particle layer failures

Table 3-18. HRB-5 Fissile Particle Layer Failures.

Compact	Fast Fluence (10^{25} n/m^2)	Burnup (%FIMA)	Sample Size	OPyC Layer Failure (%)	OPyC 95% Confidence Interval (%)	SiC Layer Failure (%)	SiC 95% Confidence Interval (%)
2A-123	4.7	15.6	210	3.3	$1.6 \leq P \leq 6.7$	7.1	$4.4 \leq P \leq 11.4$
2B-184	4.6	15.7	262	0	$0 \leq P \leq 1.4$	0.4	$0.07 \leq P \leq 2.1$
2C-149	4.5	15.6	70	40.0	$27.5 \leq P \leq 52.0$	17.1	$8.8 \leq P \leq 27.5$
4A-115	2.8	13.2	244	13.9	$10.2 \leq P \leq 18.8$	6.6	$4.1 \leq P \leq 10.4$
4B-181	2.3	12.2	293	0	$0 \leq P \leq 1.3$	5.8	$3.6 \leq P \leq 9.1$
4C-153	1.8	10.7	268	10.8	$7.6 \leq P \leq 15.1$	10.4	$7.3 \leq P \leq 15.0$

Notes: Each compact centerline temperature was nominally 1250°C. Fast fluence is for E > 0.18 MeV.

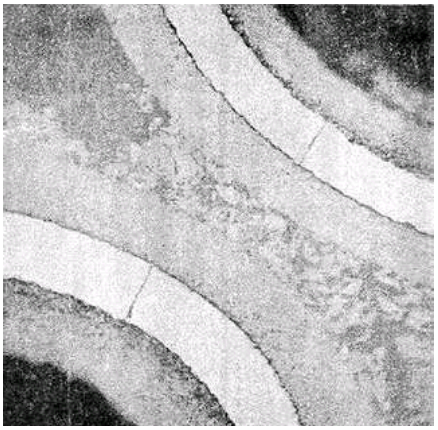

Figure 3-5. Typical irradiated HRB-5 (and HRB-4) fissile particles with cracked SiC layers, particles shown were irradiated to 13.2%FIMA and 2.8 x 10^{25} n/m^2 fast fluence.

HRB-6

The HRB-6 capsule was irradiated in the High Flux Isotope Reactor (HFIR) at Oak Ridge National Laboratory (Scott and Harmon 1975b). The main objective of this experiment was to test candidate fuel materials and manufacturing processes for the proposed Large High Temperature Gas-cooled Reactor (LHTGR). Fissile fuel particles used in HRB-6 came from the same production batch as used in the first core of Fort St. Vrain and were one of the batches previously irradiated in the F-30 experiment. This test consisted of a single gas swept cell containing six fuel compacts vertically positioned. During operation, the sweep gas flow rate was reduced due to high activity in the sweep lines. Due to this gas flow reduction, in-pile fission gas release data was not obtained. The irradiation of HRB-6 in HFIR coincided with part of the HRB-4 irradiation. Configuration and irradiation data are given in the following tables.

Table 3-19. HRB-6 Configuration.

Number of cells	1
Number of fuel compacts	6
Cylindrical fuel compact diameter	12.4 mm
Cylindrical fuel compact length	25.4 mm
Fissile fuel type	HEU (Th,U)C_2 TRISO
Nominal Th/U ratio	4.25
U-235 enrichment	93.15%
Fissile particle diameter	556 μm
Fertile fuel type	ThO_2 BISO
Fertile particle diameter	888 μm
Fissile particle batch	CU6B-2427
Fertile particle batch	T01451BIL-W
Defective SiC layer fraction – fissile particles	< 5 x 10^{-4}

Table 3-20. HRB-6 Irradiation Data.

Start date	February 27, 1973
End date	September 8, 1973
Duration (full power days)	183
Peak fissile burnup (%FIMA)	26.6
Peak fertile burnup (%FIMA)	9.3
Peak fast fluence (10^{25} n/m^2, E > 0.18 MeV)	7.9
Peak temperature (°C)	1100
Minimum TRIGA BOL Kr-85m R/B	5.0×10^{-7}
Maximum TRIGA EOL Kr-85m R/B	2.7×10^{-4}

Table 3-21. HRB-6 Coated Fuel Particles.

Particle batch	CU6B-2427	T01451BIL-W
Fuel form	(Th,U)C_2 TRISO	ThO_2 BISO
Thorium to uranium (atom ratio)	4.25	na
U-235 enrichment (%)	93.15	na
Kernel diameter (μm)	249	506
Buffer thickness (μm)	55	95
IPyC thickness (μm)	25	na
SiC thickness (μm)	23	na
OPyC thickness (μm)	42	95
Particle diameter (μm)	556	888
Kernel density (g/cm^3)	not reported	not reported
Buffer density (g/cm^3)	1.11	1.16
IPyC density (g/cm^3)	1.85	na
SiC density (g/cm^3)	3.20	na
OPyC density (g/cm^3)	1.78	1.81
IPyC BAF	1.10	na
OPyC BAF	1.08	1.16
Coating rate (μm/min)	4.4	4.4

Note: Entry "na" means not applicable.

Postirradiation examination included gas release measurements of each fuel compact performed in the GA TRIGA reactor. Table 3-22 lists the BOL R/B values performed as part of quality control, and the EOL values. However, during the unloading of the HRB-6 capsule, fuel compacts 2A, 2B and 2C were damaged and as many as 30 broken fuel particles were observed. Therefore, the TRIGA gas release measurements at EOL for these compacts would be higher than in-pile sweep line measurements had they been performed.

Table 3-22. HRB-6 TRIGA Fission Gas Release Results.

COMPACT	BOL Kr-85m R/B	EOL Kr-85m R/B
2A	1.0×10^{-6}	7.2×10^{-5}
2B	1.0×10^{-6}	2.2×10^{-4}
2C	8.0×10^{-7}	2.7×10^{-4}
4A	1.0×10^{-6}	1.5×10^{-5}
4B	5.0×10^{-7}	3.0×10^{-5}
4C	1.0×10^{-6}	4.9×10^{-6}

Metallographic examinations were performed on each fuel compact. A typical photomicrograph of an irradiated HRB-6 fissile particle is presented in Figure 3-6, which shows the formation of gas bubbles in the kernel and densification of the buffer. The photomicrograph also shows an incipient crack in the IPyC layer. There were no tabulations of IPyC layer failures reported. IPyC layers of the examined fissile particles had remained bonded to the SiC and there was no evidence of fission product attack. However, the examination indicated that the fissile particles had failed between 0 and 2% of the SiC layers. These failures do not include the fissile particles broken during capsule unloading. It was reported that a large fraction of these failures were due to metallographic preparation. The following table presents further information concerning fissile particle layer failures.

Table 3-23. HRB-6 Fissile Particle Layer Failures.

Compact	Fast Fluence (10^{25} n/m^2)	Burnup (%FIMA)	Sample Size	OPyC Layer Failure (%)	OPyC 95% Confidence Interval (%)	SiC Layer Failure (%)	SiC 95% Confidence Interval (%)
2A	7.9	28.1	71	0	$0 \le P \le 5.0$	0	$0 \le P \le 5.0$
2B	7.9	28.1	57	0	$0 \le P \le 6.0$	1.8	$0 \le P \le 10.0$
2C	7.6	27.5	74	2.7	$0 \le P \le 10.0$	1.4	$0 \le P \le 7.0$
4A	4.7	22.6	57	3.5	$0 \le P \le 10.0$	0	$0 \le P \le 6.0$
4B	3.9	21.2	63	0	$0 \le P \le 9.0$	1.6	$0 \le P \le 9.0$
4C	3.1	19.8	21	0	$0 \le P \le 20.0$	0	$0 \le P \le 20.0$

Notes: Each compact centerline temperature was nominally 1100 °C. Fast fluence is for E > 0.18 MeV

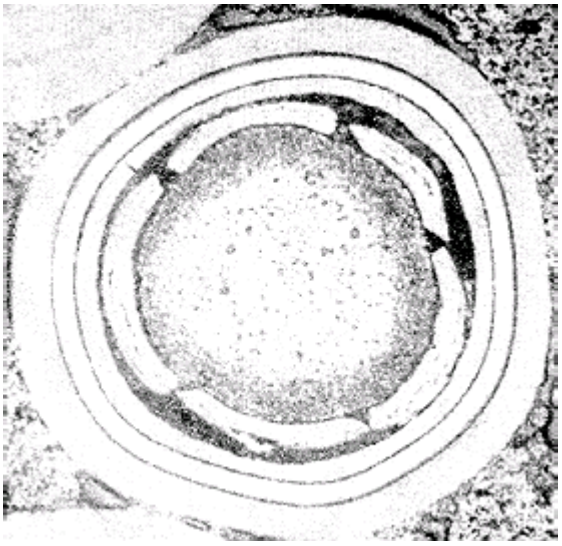

Figure 3-6. Typical HRB-6 fissile particle irradiated to 26.5%FIMA and 7.9 x 10^{25} n/m^2 fast fluence.

OF-2

The OF-2 capsule was irradiated in the Oak Ridge Research Reactor (ORR) (Tiegs and Thoms 1979). The main objectives of the test were to investigate the irradiation performance of various particle fuel forms (mostly WAR UCO with different stoichiometries) and to compare the performance of fuel particles fabricated from different coaters. OF-2 consisted of 88 fuel compacts (and several sets of loose inert particles) contained in a single capsule that was divided into two independently gas swept cells. Various combinations from 15 fissile batches, 16 fertile batches and four compact matrix compositions comprised the fuel compacts (each compact contained fuel from only one fissile batch and one fertile batch). Configuration and irradiation data are given in the following tables.

Visual examination of the OF-2 fuel compacts following irradiation indicated that the compacts characterized with low coke yields (less than 17.4%) had completely debonded with no remaining structure. All of the remaining fuel compacts (with coke yields greater than 17.4%) had remained in good condition.

Table 3-24. OF-2 Configuration.

Number of cells	2
Total number of fuel compacts	88
Cell 1 cylindrical fuel compact dimensions (16 compacts)	15.75 mm diameter, 25.4 mm long
Cell 2 cylindrical fuel compact dimensions (48 compacts)	15.75 mm OD, 3.30 mm ID, 12.70 mm long
Cell 2 cylindrical fuel compact dimensions (24 compacts)	15.75 mm diameter, 50.8 mm long
Fissile fuel type	WAR UC_xO_y TRISO $(Th,U)O_2$ TRISO UC_2 TRISO
U-235 enrichment	not reported
Fissile particle diameter	600 to 753 μm
Fertile fuel type	ThO_2 BISO
Fertile particle diameter	806 to 889 μm
Number of fissile particle batches	15
Number of fertile particle batches	16

Table 3-25. OF-2 Irradiation Data.

Start date	June 21, 1975	
End date	August 1, 1976	
Duration (full power days)	352	
Cell	1	2
Burnup (%FIMA)	75.9 to 79.6	50.0 to 79.5
Fast fluence (10^{25} n/m^2, E > 0.18 MeV)	5.86 to 8.91	1.94 to 8.36
Maximum temperature (°C)	1350	1350
BOL Kr-85m R/B	2×10^{-5}	1×10^{-4}
EOL Kr-85m R/B	1×10^{-4}	5×10^{-6}

Table 3-26. OF-2 Coated Fuel Particles.

Fuel form	WAR UC_xO_y TRISO	$(Th,U)O_2$ TRISO	UC_2 TRISO	WAR UCO TRISO	WAR UCO TRISO	WAR UCO TRISO	WAR UCO TRISO	ThO_2 BISO
Particle batch	various	OR-2321-H	6151-00-035	A-601	A-611	A-615	OR-2208-H	various
Carbon to uranium (atom ratio)	2.61 to 5.54	na	not reported	4.38	5.45	4.12	3.68	na
Oxygen to uranium (atom ratio)	0.01 to 2.04	10	na	0.61	1.75	0.47	0.01	na
Thorium to uranium (atom ratio)	na	4	na	na	na	na	na	na
U-235 enrichment (%)	not reported	not reported	not reported	not reported	not reported	not reported	not reported	na
Kernel diameter (μm)	315.3 to 379.7	361.1	196	354.2	366.4	354.1	366.5	495.9 to 508
Buffer thickness (μm)	23.0 to 74.6	83.3	99	58.8	47.6	51.0	59.2	79.4 to 98
IPyC thickness (μm)	30.7 to 44.0	37.2	33	35.4	36.8	30.7	38.4	na
SiC thickness (μm)	27.9 to 34.3	34.4	32	30.0	30.5	29.5	27.9	na
OPyC thickness (μm)	30.8 to 49.2	41.1	38	35.8	35.5	32.4	40.0	74.7 to 94.2
Particle diameter (μm)	692 to 737	753	600	674	667	641	698	806 to 889
Kernel density (g/cm^3)	3.01 to 5.28	9.9	10.99	3.03	3.10	3.08	3.01	not reported
Buffer density (g/cm^3)	0.87 to 1.33	1.08	1.07	1.217	1.159	1.330	1.11	not reported
IPyC density (g/cm^3)	1.713 to 1.953	1.938	1.92	1.713	1.753	1.857	1.947	na
SiC density (g/cm^3)	3.188 to 3.207	3.206	3.20	3.206	3.204	3.200	3.199	na
OPyC density (g/cm^3)	1.724 to 2.025	1.993	1.85	1.724	1.696	1.910	1.997	not reported
IPyC BAF	not reported	not reported	not reported	not reported	not reported	not reported	not reported	na
OPyC BAF	not reported	not reported	not reported	1.035	1.030	1.069	not reported	not reported
SiC coating rate (μm/min)	0.15 to 0.30	0.22	not reported	not reported	0.15	not reported	0.15	not reported
OPyC coating rate (μm/min)	4.28 to 7.02	6.32	not reported	4.84	5.14	4.00	4.71	3.2 to 21.5

Note: Entry "na" means not applicable.

Postirradiation metallography was performed on three fuel compacts from Cell 1 and on 27 fuel compacts from Cell 2. A significant level of OPyC layer failures were observed in the fissile TRISO-coated particles from Cell 1. However, there were no observed SiC layer failures or any layer failures in the BISO coated fertile and inert particles in these compacts. Examination of 11 fuel compacts from Cell 2, containing the same three fissile particle batches as in Cell 1, also indicated significant levels of OPyC layer failures. The fissile particle batch with the highest OPyC anisotropy (optical BAF = 1.069) had 100% OPyC layer failure, while the other two batches with lower anisotropy (optical BAF of 1.035 and 1.030) had 0 to 33% OPyC layer failures. Further details concerning these OPyC failures are presented in the following table.

Of the 30 fuel compacts metallographically examined, only one compact (which contained WAR UCO fissile particles) displayed cracked SiC layers. Among the 27 fissile particles observed in this compact, 16 displayed cracked SiC layers. These cracks were identified as artifacts of polishing. However, no photomicrographs of these cracks were presented to support this conclusion. Irradiation data from this compact is presented in the following table for completeness.

The metallographic examinations also revealed typical WAR UCO behavior of kernel and buffer densification. This densification was also accompanied by varying degrees of kernel migration.

Figure 3-7 presents a typical WAR UCO photomicrograph which displays kernel and buffer densification, and OPyC layer failure. Examination of OF-2 particles also indicated several incidences of fission product accumulation at the IPyC and SiC interface. A typical photomicrograph of fission product accumulation is presented in Figure 3-8.

Table 3-27. OF-2 Fissile Particle OPyC Layer Failures.

Compact	Fissile Particle Batch	Maximum Temp. (°C)	Burnup (%FIMA)	Fast Fluence (10^{25} n/m^2) E>0.18 MeV	Outer PyC Layer Failure (%)
A-1-2	A-601	1250	60	2.69	3
A-1-5	A-601	1250	69.7	4.72	22
A-1-6	A-601	1250	72.1	5.41	6
A-2-3	A-601	1250	61.5	3.38	19
B-1-2	A-601	1350	77	6.99	0
B-1-3	A-601	1350	78	7.44	7
C-2-2	A-601	1350	79.0	8.50	0
A-1-1	A-611	1250	52	2.10	8
A-1-3	A-611	1250	61.5	3.38	0
A-1-4	A-611	1250	66.2	4.08	7
B-1-4	A-611	1350	78.6	7.83	0
B-1-6	A-611	1350	79.5	8.31	0
C-3-4	A-611	1350	75.9	5.86	33
C-2-1	A-615	1350	79.6	8.91	100

Table 3-28. OF-2 Fissile Particle SiC Layer Cracks.

Compact	Fissile Particle Batch	Maximum Temp. (°C)	Burnup (%FIMA)	Fast Fluence (10^{25} n/m^2) E>0.18 MeV	Cracked SiC Layers (%)
A-3-7	OR-2208-H	1250	65.2	3.92	59

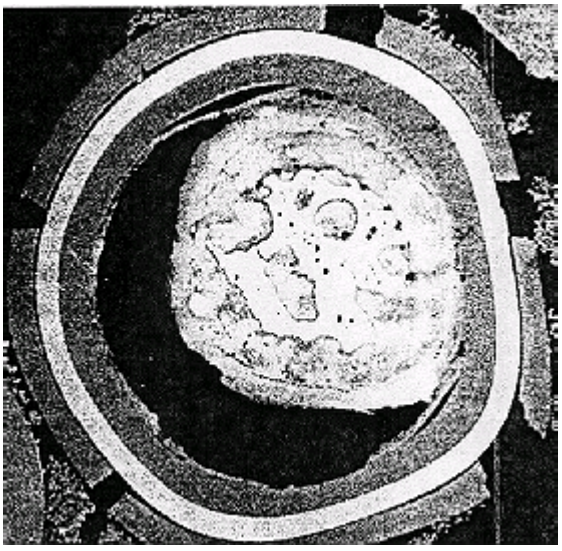

Figure 3-7. Photomicrograph of irradiated OF-2 fissile WAR UCO particle.

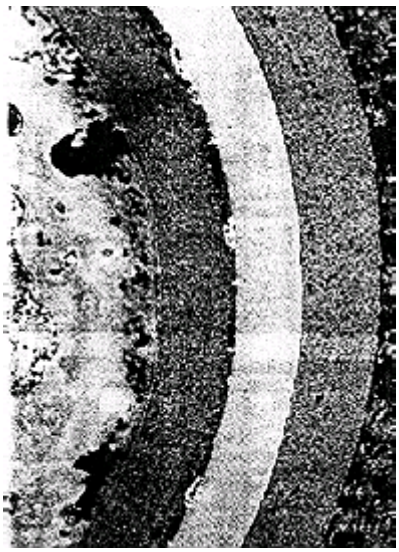

Figure 3-8. Photomicrograph of irradiated OF-2 fissile fuel particles displaying fission product accumulation at IPyC – SiC interface.

HRB-14

The HRB-14 capsule was irradiated in the High Flux Isotope Reactor (HFIR) at Oak Ridge National Laboratory (Young 1980). The main objectives of this experiment were to test low enriched fuel (LEU) particles and to demonstrate reduced matrix - OPyC layer interactions by using cure-in-place fuel compacts. This test consisted of a single gas swept cell equally divided between 20 fuel compacts vertically positioned and molded planchets (wafers) containing BISO coated ThO_2 fertile particles. On-line fission gas release measurements were not reported. Also, irradiation results from the BISO- coated fertile particles were reported separately and are not included in this summary. Configuration and irradiation data are given in the following tables.

Disassembly of the HRB-14 capsule after irradiation produced five fuel compacts with no remaining structure, in essence, five collections of loose particles, four compacts that were partially intact, nine compacts that were intact but displayed significant amounts of debonding, and only two compacts in good shape.

Table 3-29. Lower Half of HRB-14 Configuration.

Number of cells	1
Total number of fuel compacts	20
Cylindrical fuel compact diameter	12.50 mm
Cylindrical fuel compact length	9.52 mm
Fissile fuel type	UC_xO_y TRISO $(Th,U)O_2$ TRISO UO_2 TRISO
U-235 enrichment	19.18 to 19.66%
Fissile particle diameter	760 to 813 μm
Fertile fuel type	ThO_2 TRISO
Fertile particle diameter	786 to 882 μm
Number of fissile particle batches	5
Number of fertile particle batches	8
Defective SiC layer fraction – fissile particles	7.0×10^{-7} to 1.3×10^{-4}
Defective SiC layer fraction – fertile particles	1.6×10^{-5} to 2.9×10^{-3}

Table 3-30. Lower Half of HRB-14 Irradiation Data.

Start date	May 20, 1978
End date	January 4, 1979
Duration (full power days)	214
Peak fissile burnup (%FIMA)	28.6
Peak fertile burnup (%FIMA)	8.5
Peak fast fluence (10^{25} n/m^2, E > 0.18 MeV)	8.3
Maximum temperature (°C)	1190
Minimum temperature (°C)	895
Minimum TRIGA BOL Kr-85m R/B	3.8×10^{-7}
Maximum TRIGA EOL Kr-85m R/B	3.0×10^{-4}

Table 3-31. HRB-14 Coated Fissile Fuel Particles.

Fuel form	UO_2 TRISO	$(Th,U)O_2$ TRISO	$(Th,U)O_2$ TRISO	UCO TRISO	UCO TRISO
Particle batch	6152-01-010	6155-05-010	6155-05-020	6157-08-010	6157-08-020
Carbon to uranium (atom ratio)	na	na	na	0.71	0.69
Oxygen to uranium (atom ratio)	not reported	na	na	0.54	0.51
Thorium to uranium (atom ratio)	na	1.0	1.0	na	na
U-235 enrichment (%)	19.61	19.66	19.66	19.18	19.19
Kernel diameter (μm)	299 ± 8.11	357 ± 9.90	360 ± 10.07	354 ± 15.04	353 ± 15.58
Buffer thickness (μm)	122 ± 20.00	86 ± 13.47	110 ± 12.98	108 ± 15.15	90 ± 15.41
IPyC thickness (μm)	41 ± 3.07	34 ± 4.27	32 ± 3.89	37 ± 4.35	35 ± 4.61
SiC thickness (μm)	32 ± 5.55	36 ± 4.20	36 ± 3.69	36 ± 4.24	40 ± 5.55
OPyC thickness (μm)	40 ± 5.53	46 ± 5.41	48 ± 6.63	48 ± 4.92	49 ± 5.77
Particle diameter (μm)	769 ± 46	760 ± 31	813 ± 32	810 ± 34	786 ± 32
Kernel density (g/cm^3)	10.55	10.40	10.40	11.91	12.03
Buffer density (g/cm^3)	1.15	1.09	1.09	1.20	1.15
IPyC density (g/cm^3)	1.91 ± 0.0047	1.87 ± 0.0061	1.89 ± 0.0163	1.88 ± 0.0093	1.87 ± 0.0100
SiC density (g/cm^3)	3.21	3.21	3.22	3.21	3.21
OPyC density (g/cm^3)	1.87 ± 0.0051	1.87 ± 0.0041	1.86 ± 0.0070	1.90 ± 0.0020	1.91 ± 0.0020
IPyC BAF	1.045 ± 0.0063	1.046 ± 0.0064	1.051 ± 0.0052	1.036 ± 0.0051	1.039 ± 0.0050
OPyC BAF	1.032 ± 0.0042	1.032 ± 0.0045	1.035 ± 0.0044	1.026 ± 0.0048	1.029 ± 0.0050
OPyC coating rate (μm/min)	3.8	4.9	4.4	3.6	3.6

Notes: Entry "na" means not applicable, ± values are one standard deviation

Table 3-32. HRB-14 Coated Fertile Fuel Particles.

Fuel form	ThO_2 TRISO	ThO_2 TRISO	ThO_2 TRISO
Particle batch	Various	6252-17-010	6252-18-010
Kernel diameter (μm)	451 to 475	455 ± 8.93	453 ± 8.75
Buffer thickness (μm)	53 to 90	90 ± 22.32	86 ± 19.23
IPyC thickness (μm)	32 to 40	40 ± 5.10	40 ± 5.10
SiC thickness (μm)	36 to 42	36 ± 3.36	37 ± 3.50
OPyC thickness (μm)	44 to 50	49 ± 7.06	45 ± 6.03
Particle diameter (μm)	786 to 882	882 ± 52	868 ± 44
Kernel density (g/cm^3)	9.78 to 9.90	9.78	9.78
Buffer density (g/cm^3)	0.93 to 1.13	0.93	0.93
IPyC density (g/cm^3)	1.79 to 1.86	1.79 ± 0.0137	1.79 ± 0.0140
SiC density (g/cm^3)	3.21 to 3.22	3.22	3.22
OPyC density (g/cm^3)	1.79 to 1.98	1.95 ± 0.0043	1.83 ± 0.0128
IPyC BAF	1.048 to 1.062	1.050 ± 0.0077	1.048 ± 0.0063
OPyC BAF	1.030 to 1.050	1.050 ± 0.0043	1.035 ± 0.0045
OPyC coating rate (μm/min)	5.0 to 9.0	5.4	5.0

Postirradiation examination included gas release measurements of selected fuel compacts performed at 1100°C in the GA TRIGA reactor. Table 3-33 lists the BOL R/B values performed as part of quality control for those compacts containing fissile particles and their corresponding EOL values.

Table 3-33. HRB-14 TRIGA Fission Gas Release Results.

Compact	Fuel Form	Fissile Batch	Fertile Batch	BOL Kr-85m R/B	EOL Kr-85m R/B
2	$(Th,U)O_2$	6155-05-020	none	8.5×10^{-7}	1.7×10^{-4}
4	$(Th,U)O_2$	6155-05-020	none	2.2×10^{-6}	3.0×10^{-4}
6	UO_2	6152-01-010	6252-18-010	2.5×10^{-6}	2.0×10^{-4}
8	UCO	6157-08-010	6252-18-010	4.6×10^{-6}	3.0×10^{-4}
10	UCO	6157-08-020	6252-18-010	6.0×10^{-7}	2.5×10^{-5}
12	UCO	6157-08-010	6252-18-010	1.1×10^{-6}	9.2×10^{-5}
18	$(Th,U)O_2$	6155-05-010	none	3.8×10^{-7}	8.1×10^{-6}
20	UCO	6157-08-010	6252-18-010	3.8×10^{-6}	1.9×10^{-4}

Note: Compacts are numbered from 1 at core midplane to 20 at capsule bottom.

Metallographic examination was performed on 15 fuel compacts, eight of which contained fissile particles. A few fissile particles were reported to have SiC layer cracks but these cracks were attributed to metallographic preparation. It should be noted that visual inspection of each compact during capsule disassembly indicated that between 0 and 9% of the visible particles (from compact surfaces and loose particles that had fallen off) had failed SiC layers. However, this visual inspection did not distinguish between fissile and fertile particles. Figures 3-9 and 3-10 display photomicrographs of HRB-14 fissile particles that may have cracked SiC layers.

The metallographic examination of fissile particles revealed that between 0 and 3% of the IPyC layers had failed (cracked) and that the IPyC layers had debonded from the SiC in 0 to 7.7% of the particles. Buffer layers did not crack in the UO_2 or $(Th,U)O_2$ fuel but did crack in 10 to 71% of the UCO fuel particles. Kernel extrusion was reported only in UCO fuel. Figure 3-11 displays typical kernel extrusion and Figure 3-12 presents a typical photomicrograph of kernel migration. Further details concerning fissile particle layer failures are presented in the following table.

In several particles of each fuel form, high concentrations of fission products were observed in small localized regions at the SiC – IPyC layer interface. In addition to fission product accumulation, localized chemical attack was also observed in the SiC layers of several $(Th,U)O_2$ and UO_2 fuel particles. This localized attack, which had penetrated about 2 μm into the SiC, was attributed to palladium and was observed in 8% of the particles. UCO fuel particles which did not display localized chemical attack, had uniform attack along the inner SiC layer (usually on one side of the particle). This uniform attack was attributed to rare earths. Figure 3-13 displays typical uniform fission product attack in a UCO fuel particle. It should be noted that with optimized UCO stoichiometry, the kernel retains rare earth fission products and does not display kernel migration as found here with non-optimized UCO kernels containing excess UC_2 leading to rare earth migration.

Metallographic examination of fertile particles indicated that between 0 and 2.4% of the particles in each compact had total coating failure, defined as cracked OPyC and SiC layers. These failures were attributed to pressure vessel failure. Figure 3-14 displays a typical failed fertile particle. Separate tallies of particles where only the SiC layer had failed were not reported. Other fertile particle observations include:

- 1.5 to 29.1% of the particles had failed OPyC layers
- 8 to 70% of the particles had failed IPyC layers
- 11 to 85% of the particles had IPyC layers debonded from the SiC
- 6 to 26% of the particles had cracked buffers
- no kernel migration was observed
- a few kernels had extruded into buffer cracks
- a few particles had palladium attack of the SiC.

Table 3-34. HRB-14 Fissile Particle Layer Failures.

Compact	Fuel Form	Particle Batch	Volume Average Temp.(°C)	Fast Fluence (10^{25} n/m^2)	Burnup (%FIMA)	Sample Size	OPyC Layer Failure (%)	IPyC Layer Failure (%)	Buffer Failure (%)	Kernel Extrusion (%)	Debonded IPyC – SiC (%)
6	UO_2	6152-01-010	1070	7.8	29.5	100	0	3.0	0	0	6.0
16	$(Th,U)O_2$	6155-05-010	990	5.6	15.4	107	0	0	0	0	0
4	$(Th,U)O_2$	6155-05-020	1090	8.1	19.1	87	4.6	0	0	0	3.4
8	UCO	6157-08-010	1055	7.5	28.6	39	0	0	10.3	0	7.7
12	UCO	6157-08-010	1025	6.6	26.4	87	0	1.1	18.4	9.2	1.1
14	UCO	6157-08-010	1010	6.2	26.1	107	0	1.9	15.9	10.3	0.9
20	UCO	6157-08-010	960	4.5	22.9	89	0	0	70.8	20.2	0
10	UCO	6157-08-020	1040	7.1	27.8	83	0	1.2	42.2	2.4	0

Notes: All SiC layer failures were attributed to metallographic preparation Fast fluence is for E > 0.18 MeV

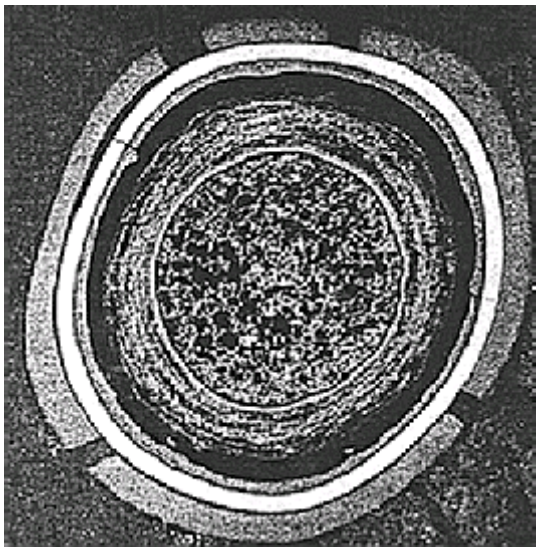

Figure 3-9. Photomicrograph of a $(Th,U)O_2$ particle (batch 6155-05-020) from Compact 4 irradiated at 1090°C to 19.1%FIMA and to a fast fluence (E>0.18 MeV) of $8.1x10^{25}$ n/m^2 displaying OPyC layer failure and possible SiC cracks.

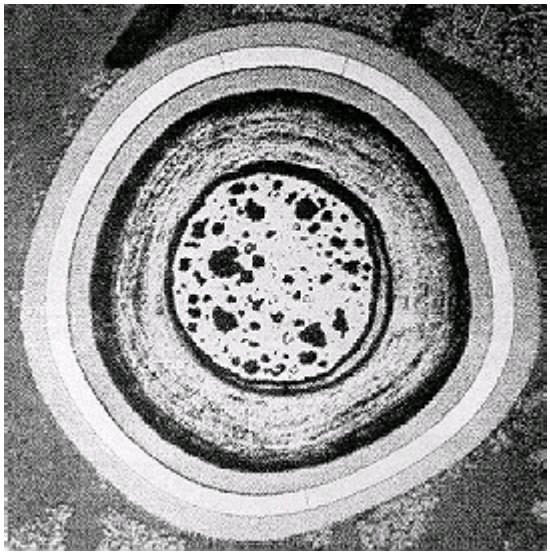

Figure 3-10. Photomicrograph of a UO_2 particle (batch 6152-01-010) from Compact 6 irradiated at 1070°C to 29.5%FIMA and to a fast fluence (E>0.18 MeV) of 7.8×10^{25} n/m^2 displaying possible SiC cracks.

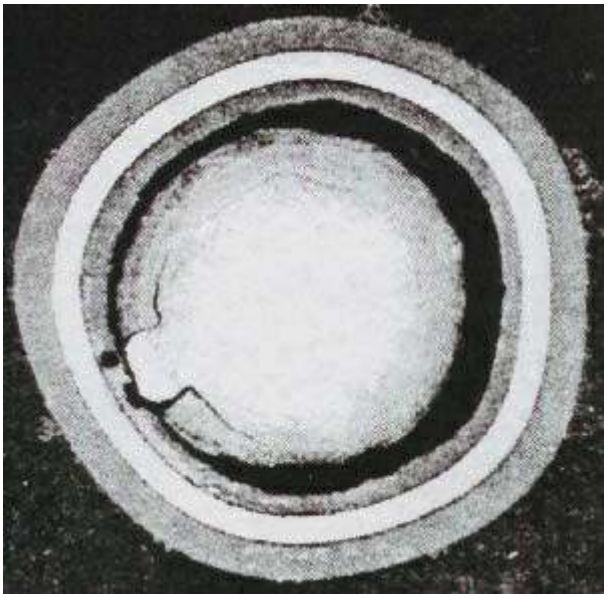

Figure 3-11. Photomicrograph of a UCO particle (batch 6157-08-020) from Compact 10 irradiated at 1040°C to 27.8%FIMA and to a fast fluence (E>0.18 MeV) of 7.1 x 10^{25} n/m^2 displaying kernel extrusion.

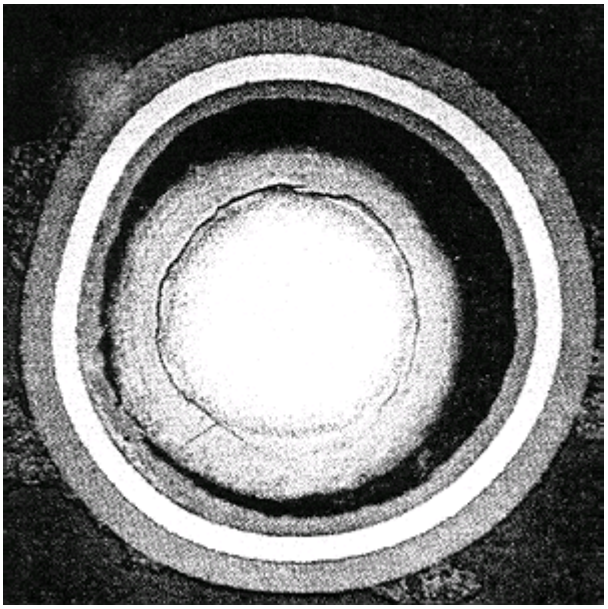

Figure 3-12. Photomicrograph of a UCO particle (batch 6157-08-020) from Compact 10 irradiated at 1040°C to 27.8%FIMA and to a fast fluence (E>0.18 MeV) of 7.1 x 10^{25} n/m^2.

Figure 3-13. Photomicrograph of a UCO particle (batch 6157-08-020) from Compact 10 irradiated at 1040°C to 27.8%FIMA and to a fast fluence (E>0.18 MeV) of 7.1 x 10^{25} n/m^2 displaying fission product attack of the SiC layer.

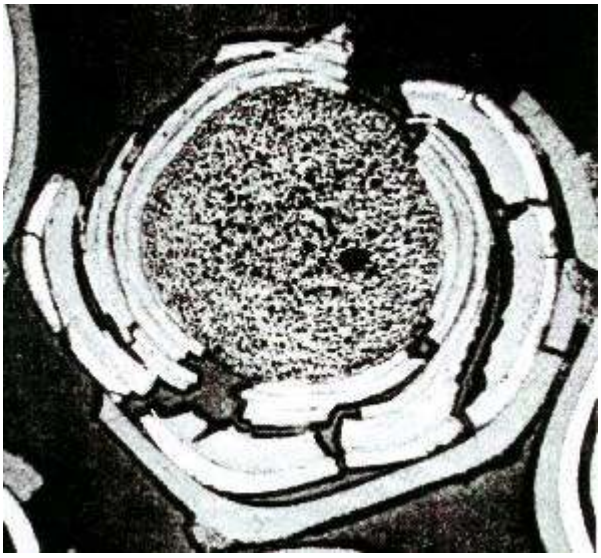

Figure 3-14. Photomicrograph of a ThO_2 fertile particle (batch 6252-17-010) irradiated at 1130°C to 8.5%FIMA and to a fast fluence (E>0.18 MeV) of 8.3 x 10^{25} n/m^2 displaying pressure vessel failure.

HRB-15B

The HRB-15B capsule was irradiated in the High Flux Isotope Reactor (HFIR) at Oak Ridge National Laboratory (Ketterer and Bullock 1981). The primary objective of this experiment was to test a variety of LEU fissile fuel designs and ThO_2 fertile particle designs. This test consisted of a single gas swept cell containing 184 thin graphite trays. Each tray could accommodate up to a maximum of 116 individual, unbonded fuel particles. The loose fissile fuel particles included UC_2, UCO with four different stoichiometries, $(Th,U)O_2$, UO_2, and two types of UO_2* where one type had ZrC dispersed throughout the buffer layer and the other had a pure ZrC coating around the kernel. Each fissile fuel type was tested with both TRISO coating and silicon-BISO coating which consisted of the kernel surrounded by a buffer layer, an IPyC layer and finally a silicon doped OPyC layer. The loose fertile particles tested included TRISO, BISO and silicon-BISO coated ThO_2. Configuration and irradiation data are given in the following tables.

Postirradiation metallography was performed on 20 different particle types consisting of about 20 particles each. These examinations revealed considerable amounts of gas bubble formation in UC_2 and UCO kernels, and buffer densification in TRISO coated particles. Some SiC layer cracking was observed in each TRISO coated fuel type but mostly in the UCO particles. These cracks were reported to have occurred during mount preparation because of the crack orientation and because the visual examination detected no OPyC cracking. Figures 3-15 and 3-16 present photomicrographs of cracked layers in UCO particles. No further tabulation of layer failures was reported.

Table 3-35. HRB-15B Configuration.

Number of cells	1
Total number of particle trays	184
Maximum number of loose particles per tray	116
Particle tray outer diameter	22.3 to 23.6 mm
Particle tray inner diameter	11.1 mm
Fissile fuel type	UCO TRISO and silicon-BISO $(Th,U)O_2$ TRISO and silicon-BISO UC_2 TRISO and silicon-BISO UO_2 TRISO and silicon-BISO UO_2* TRISO and silicon-BISO
U-235 enrichment	~ 19.5%
Fissile particle diameter	742 to 951 μm
Fertile fuel type	ThO_2 TRISO, BISO and silicon-BISO
Fertile particle diameter	773 to 836 μm
Number of fissile particle batches	19
Number of fertile particle batches	22

Note: Two types of UO_2* fuel were tested, one with ZrC dispersed in the buffer and the other with pure ZrC layer around the kernel.

Table 3-36. HRB-15B Irradiation Data.

Start date	July 6, 1978
End date	January 4, 1979
Duration (full power days)	169
Peak fissile burnup (%FIMA)	26.7
Peak fertile burnup (%FIMA)	6.0
Peak fast fluence (10^{25} n/m^2, E > 0.18 MeV)	6.6
Time average temperature (°C)	815 to 915
BOL Kr-85m R/B	2.9×10^{-8}
EOL Kr-85m R/B	5.1×10^{-6}

Table 3-37. Selected HRB-15B Coated Fuel Particles.

Particle batch	6157-08-030	6157-09-010
Fuel form	UCO TRISO	UCO TRISO
Carbon to uranium (atom ratio)	0.49	0.20
Oxygen to uranium (atom ratio)	1.12	1.64
U-235 enrichment (%)	~ 19.5	~ 19.5
Kernel diameter (μm)	359	372
Buffer thickness (μm)	123	136
IPyC thickness (μm)	47	43
SiC thickness (μm)	41	41
OPyC thickness (μm)	44	42
Particle diameter (μm)	863	877
Kernel density (g/cm^3)	not reported	not reported
Buffer density (g/cm^3)	0.98	0.93
IPyC density (g/cm^3)	1.84	1.93
SiC density (g/cm^3)	3.18	3.16
OPyC density (g/cm^3)	1.84	1.85
IPyC BAF	1.030	1.033
OPyC BAF	1.027	1.029

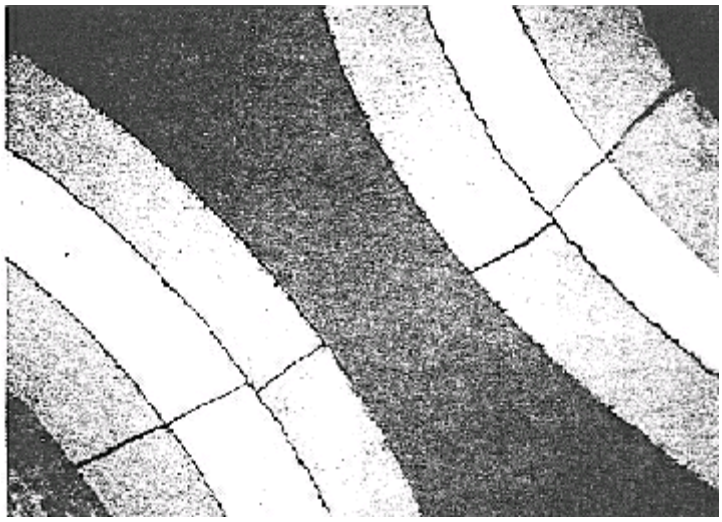

Figure 3-15. Photomicrograph of a UCO particle (batch 6157-08-030) irradiated at 915°C to 26.6%FIMA and to a fast fluence of 6.4 x 10^{25} n/m^2 (E>0.18 MeV) displaying what was reported as cracking artifacts due to mount preparation.

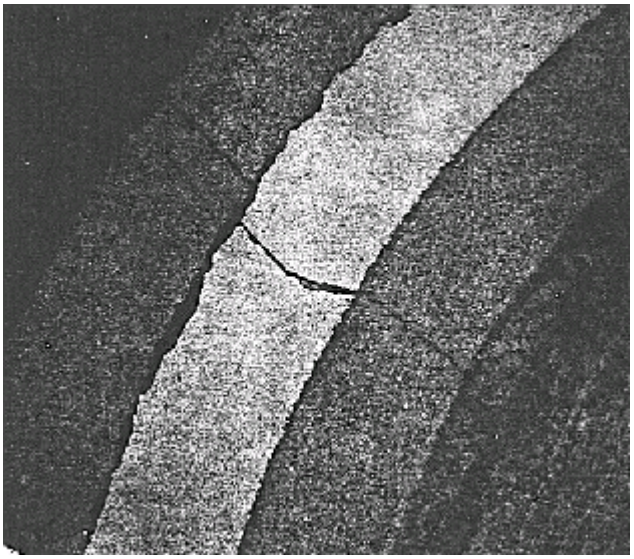

Figure 3-16. Photomicrograph of a UCO particle (batch 6157-09-010) irradiated at 915°C to 22.3%FIMA and to a fast fluence of 3.8 x 10^{25} n/m^2 (E>0.18 MeV) displaying what was reported as cracking artifacts due to mount preparation.

R2-K13

The R2-K13 capsule was irradiated in the R2 reactor at Studsvik, Sweden (Brodda et al. 1985). The main objective of this experiment was to test reference UCO fissile particles and ThO_2 fertile particles. Four independently gas swept cells were positioned on top of one another. The middle two cells contained U.S. fuel. The top and bottom cells each contained a full size German fuel sphere (discussed in the section on German irradiation results). Configuration and irradiation data from the U.S. cells are given in the following tables.

Postirradiation metallographic examination was performed on two fuel compacts. All of the 99 fissile particles examined displayed debonding between the buffer and IPyC layers. In some cases, debonding between the buffer, IPyC and SiC layers were also observed. Likewise, all of the 68 fertile particles examined displayed debonding between the buffer, IPyC and SiC layers. The SiC layers of all the particles examined were observed to be intact.

Table 3-38. R2-K13 U.S. Configuration.

Number of cells	2
Total number of fuel compacts	12
Cylindrical fuel compact diameter	12.52 mm
Cylindrical fuel compact length	25.4 mm
Total number of piggyback sample sets	31
Fissile fuel type	LEU UCO TRISO
Fertile fuel type	ThO_2 TRISO
U-235 enrichment	19.61%
Fissile particle diameter	803 and 824 μm
Fertile particle diameter	781 to 805 μm
Fissile particle batches	2
Fertile particle batches	3
Defective SiC layer fraction – fissile particles	1.9×10^{-4} and 4.4×10^{-4}
Defective SiC layer fraction – fertile particles	$< 2 \times 10^{-6}$ to 1.6×10^{-5}

Table 3-39. R2-K13 U.S. Irradiation Data.

Start date	April 22, 1980	
End date	September 19, 1982	
Duration (full power days)	517	
Cell	2	3
Peak fissile burnup (%FIMA)	22.5	22.1
Peak fertile burnup (%FIMA)	4.6	4.5
Peak fast fluence (10^{25} n/m^2, E > 0.18 MeV)	7.8	7.4
Average center temperature (°C)	1190	985
BOL Kr-85m R/B	1×10^{-5}	2×10^{-7}
EOL Kr-85m R/B	8×10^{-5}	8×10^{-6}

Table 3-40. R2-K13 U.S. Coated Fuel Particles.

Particle batch	6157-11-010	6157-11-020	6252-12COMP	6252-12T-04A	6252-12T-04B2
Fuel form	UCO TRISO	UCO TRISO	ThO_2 TRISO	ThO_2 TRISO	ThO_2 TRISO
Carbon to uranium (atom ratio)	0.5	0.5	na	na	na
Oxygen to uranium (atom ratio)	1.5	1.5	na	na	na
U-235 enrichment (%)	19.61	19.61	na	na	na
Kernel diameter (μm)	353	351	452	454	454
Buffer thickness (μm)	118	117	53	55	52
IPyC thickness (μm)	36	30	33	34	34
SiC thickness (μm)	36	35	38	39	39
OPyC thickness (μm)	48	43	44	47	40
Particle diameter (μm)	824	803	786	805	781
Kernel density (g/cm^3)	11.02	11.12	9.89	9.90	9.90
Buffer density (g/cm^3)	0.97	1.00	1.11	1.09	1.09
IPyC density (g/cm^3)	1.88	1.89	1.85	1.86	1.86
SiC density (g/cm^3)	3.22	3.22	3.22	3.22	3.22
OPyC density (g/cm^3)	1.90	1.93	1.85	1.80	1.90
IPyC BAF	1.057	1.064	1.062	1.063	1.062
OPyC BAF	1.034	1.036	1.037	1.034	1.041
OPyC coating rate (μm/min)	5.3	4.8	5.3	5.8	4.8

Note: “na” means not applicable.

HRB-15A

The HRB-15A capsule was irradiated in the High Flux Isotope Reactor (HFIR) at Oak Ridge National Laboratory (Ketterer et al. 1984). The main objective of this experiment was to test several candidate fuel designs for the proposed LHTGR. This test consisted of a single gas swept cell containing 20 cylindrical fuel compacts positioned vertically, on top of one another. Interspersed between the fuel compacts were 17 bonded wafer/unbonded tray assemblies. Each assembly had a graphite tray holding 54 unbonded particles in separate holes, and serving as a lid, a graphite wafer containing 54 particles bonded in separate holes with carbonaceous matrix material. Configuration and irradiation data are given in the following tables.

Table 3-41. HRB-15A Configuration.

Number of cells	1
Total number of fuel compacts	20
Cylindrical fuel compact diameter	12.54 mm
Number of short fuel compacts/length	3 / 9.53 mm
Number of long fuel compacts/length	17 / 19.05 mm
Number of bonded wafer/unbonded tray assemblies	17
Fissile fuel type	UCO TRISO UC_2 TRISO UC_2 ZrC-TRISO UO_2 TRISO UO_2 ZrC-TRISO UO_2*
Fertile fuel type	ThO_2 TRISO ThO_2 silicon-BISO
U-235 enrichment	~ 19.5%
Fissile particle diameter	736 to 894 μm
Fertile particle diameter	713 to 1014 μm
Fissile particle batches	10
Fertile particle batches	5
Defective SiC layer fraction – fissile particles	1.4×10^{-5} to 7.4×10^{-2}
Defective SiC layer fraction – fertile particles	6.7×10^{-5} to 1.4×10^{-3}

Note: Two types of UO_2 * fuel were tested, one with ZrC dispersed in the buffer and the other with pure ZrC layer around the kernel.

Table 3-42. HRB-15A Irradiation Data.

Start date	July 26, 1980
End date	January 29, 1981
Duration (full power days)	174
Peak fissile burnup (%FIMA)	29.0
Peak fertile burnup (%FIMA)	6.4
Peak fast fluence (10^{25} n/m^2, E > 0.18 MeV)	6.5
Average center temperature (°C)	1150
BOL Kr-85m R/B	6.96×10^{-6}
EOL Kr-85m R/B	3.76×10^{-4}

Table 3-43. Selected HRB-15A Fissile Coated Fuel Particles.

Particle batch	6157-11-010	6162-00-010	6152-04-010	6152-06-010	6151-23-020	6151-23-010
Fuel form	UCO TRISO	UO_2 ZrC-TRISO	UO_2 TRISO	UO_2* TRISO	UC_2 TRISO	UC_2 TRISO
Carbon to uranium (atom ratio)	0.5	na	na	na	2.0	2.0
Oxygen to uranium (atom ratio)	1.5	2.0	2.0	2.0	na	na
U-235 enrichment (%)	~ 19.5%	~ 19.5%	~ 19.5%	~ 19.5%	~ 19.5%	~ 19.5%
Kernel diameter (μm)	353	346	348	379	344	339
Buffer thickness (μm)	118	142	138	100	115	104
IPyC thickness (μm)	36	36	35	39	36	36
SiC or ZrC thickness (μm)	36	45	35	35	39	38
OPyC thickness (μm)	48	60	44	49	48	52
Particle diameter (μm)	824	894	853	825	819	799
Kernel density (g/cm^3)	not reported	not reported	not reported	not reported	not reported	not reported
Buffer density (g/cm^3)	0.97	0.93	0.99	not determined	0.85	0.81
IPyC density (g/cm^3)	1.88	1.86	1.90	1.86	1.91	1.89
SiC or ZrC density (g/cm^3)	3.22	6.68	3.22	3.22	3.21	3.20
OPyC density (g/cm^3)	1.90	1.86	1.85	1.80	1.91	1.79
IPyC BAF	1.057	1.028	1.027	1.032	1.045	1.029
OPyC BAF	1.034	1.026	1.022	1.026	1.031	1.028

Notes: "na" means not applicable. The kernel diameter listed for the UO_2* fuel includes the ZrC layer

Table 3-44. HRB-15A Coated Fertile Fuel Particles

Particle batch	6252-21-010	6252-24-010	6252-25-010	6252-12COMP	6542-43-010
Fuel form	ThO_2 TRISO	ThO_2 TRISO	ThO_2 TRISO	ThO_2 TRISO	ThO_2 silicon-BISO
Kernel diameter (μm)	588	593	591	452	515
Buffer thickness (μm)	98	56	52	53	52
IPyC thickness (μm)	40	19	31	33	na
SiC thickness (μm)	31	38	36	38	na
OPyC thickness (μm)	45	39	40	44	47
Kernel density (g/cm^3)	not reported	not reported	not reported	not reported	not reported
Buffer density (g/cm^3)	1.04	1.07	1.02	1.11	1.03
IPyC density (g/cm^3)	1.93	not determined	1.90	1.85	na
SiC density (g/cm^3)	3.20	3.22	3.22	3.22	na
OPyC density (g/cm^3)	1.90	1.95	1.91	1.85	2.13
IPyC BAF (optical)	1.092	1.211	1.123	1.062	na
OPyC BAF (optical)	1.037	1.037	1.037	1.037	1.109

Postirradiation metallographic examination was performed on five fuel compacts. A summary of the examination results is presented in Tables 3-45 and 3-46. It should be noted that the 5.6% SiC (and OPyC) layer failures listed for the UO_2 particles were attributed to sample preparation. In contrast, the ZrC layer failures observed in the UO_2 ZrC-TRISO-coated particles were also attributed to sample preparation but were not tabulated. A photomicrograph of a UO_2 ZrC-TRISO-coated particle displaying a cracked ZrC layer is presented in Figure 3-17.

The high SiC and IPyC layer failures reported for the fertile ThO_2 particles were attributed to the high IPyC BAF values for these particles. The high BAF was a result of intentionally depositing the IPyC layer at low coating rates in the attempt to produce layers that were impermeable to chlorine (chlorine trapped in the particle during SiC deposition may enhance SiC degradation during irradiation). A representative photomicrograph of a ThO_2 particle displaying a cracked SiC layer is presented in Figure 3-18.

In addition to the examination of the five fuel compacts, about 40 deconsolidated particles from six other fuel compacts underwent metallographic examination. However, the results of these examinations were neither quantified, nor provided in tabular form. This examination did provide photomicrographs of two UC_2 particles which displayed SiC layer cracks. One of these photomicrographs is presented in Figure 3-19. These layer failures were not recognized and hence, no probable cause (sample preparation or otherwise) was reported.

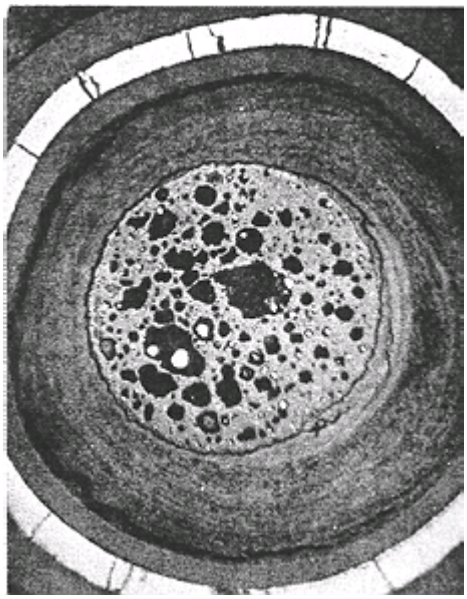

Figure 3-17. Photomicrograph of a UO_2 ZrC-TRISO-coated particle (batch 6162-00-010) irradiated at 1075°C to 27.2%FIMA and to a fast fluence of 6.0×10^{25} n/m^2 (E>0.18 MeV) displaying ZrC layer cracks.

Table 3-45. HRB-15A Fissile Particle Layer Failures.

Particle Batch	Fuel Type	Irradiation Temp. (°C)	Fast Fluence (10^{25} n/m^2)	Burnup (%FIMA)	Sample Size	OPyC Layer Failure (%)	SiC / ZrC Layer Failure (%)	IPyC Layer Failure (%)	Particles With Debonded IPyC (%)	Particles With Kernel Migration (%)	Particles With Kernel Extrusion (%)	Particles With SiC /ZrC Fission Product Attack (%)
6157-11-010	UCO	1110	5.3	25.0	30	3.3	0	0	0	0	26.7	70.0
6162-00-010	UO_2	1075	6.0	27.2	37	0	0	0	0	18.9	0	0
6152-04-010	UO_2	1125	6.4	28.7	18	5.6	5.6	0	0	22.2	0	38.9
6152-06-010	UO_2*	1120	6.5	29.0	22	0	0	4.5	4.5	0	27.3	63.6
6151-23-020	UO_2	1140	6.3	29.0	32	0	0	0	21.9	0	43.8	50.0

Notes: Fast fluence is for E>0.18 MeV. UO_2* has ZrC layer next to kernel

Table 3-46. HRB-15A Fertile Particle Layer Failures.

Particle Batch	Fuel Type	Irradiation Temp. (°C)	Fast Fluence (10^{25} n/m^2)	Burnup (%FIMA)	Sample Size	OPyC Layer Failure (%)	SiC Layer Failure (%)	IPyC Layer Failure (%)	Particles With Debonded IPyC (%)	Particles With Kernel Migration (%)	Particles With Kernel Extrusion (%)	Particles With SiC Fission Product Attack (%)
6252-25-010	ThO_2	1110	5.3	4.2	35	22.9	0	74.3	94.3	0	0	0
6542-43-010	ThO_2 Si-BISO	1075	6.0	5.3	49	4.1	not applicable	not applicable	not applicable	0	0	not applicable
6252-21-010	ThO_2	1125	6.4	6.1	24	25.0	12.5	91.7	95.8	0	0	8.3
6252-21-010	ThO_2	1120	6.5	6.3	35	22.9	8.6	82.9	77.1	0	0	14.3
6252-12 COMP	ThO_2	1140	6.3	6.3	24	2.2	2.2	91.7	95.8	0	0	8.3

Note: Fast fluence is for E>0.18 MeV

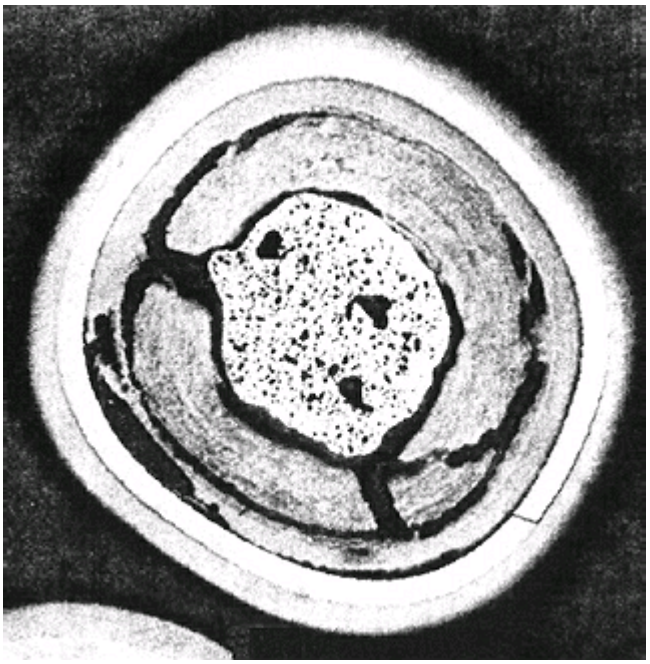

Figure 3-18. Photomicrograph of a fertile ThO_2 TRISO-coated particle (batch 6252-21-010) irradiated at 1120°C to 6.3%FIMA and to a fast fluence of 6.5 x 10^{25} n/m^2 (E>0.18 MeV) displaying SiC layer cracks.

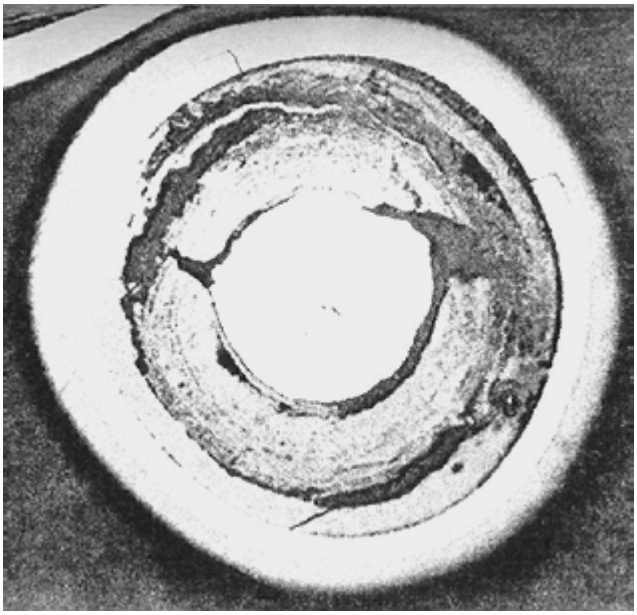

Figure 3-19. Photomicrograph of a UC_2 TRISO-coated particle (batch 6151-23-010) irradiated at 1035°C to 25.7%FIMA and to a fast fluence of 5.1 x 10^{25} n/m^2 (E>0.18 MeV) displaying SiC layer cracks.

HRB-16

The HRB-16 capsule was irradiated in the High Flux Isotope Reactor (HFIR) at Oak Ridge National Laboratory (Ketterer and Myers 1985). The main objective of this experiment was to test a variety of LEU fissile particle fuel designs. This test consisted of a single gas swept cell containing 18 fuel compacts stacked vertically and interspersed with 27 trays of unbonded particles and several encapsulated fission product transport piggyback specimens. Configuration and irradiation data are given in the following tables.

Table 3-47. HRB-16 Configuration.

Number of cells	1
Total number of fuel compacts	18
Cylindrical fuel compact diameter	12.45 mm
Cylindrical fuel compact length	18.70 mm
Number of loose particle trays	27
Number of particles per tray	110 (2 particles per hole)
Fissile fuel type	UCO TRISO UCO ZrC-TRISO UC_2 TRISO UC_2 ZrC-TRISO UO_2 TRISO UO_2* TRISO $(Th,U)O_2$ TRISO
Fertile fuel type	ThO_2 TRISO ThC_2 BISO
U-235 enrichment	19.20 to 19.61%
Fissile particle diameter	742 to 884 μm
Fertile particle diameter	756 and 786 μm
Fissile particle batches	9
Fertile particle batches	2
Defective SiC layer fraction – fissile particles	4.6×10^{-7} to 4.4×10^{-4}
Defective SiC layer fraction – fertile particles	1.6×10^{-5} and 5.0×10^{-4}

Note: UO_2* fuel had ZrC layer next to the kernel

Table 3-48. HRB-16 Irradiation Data.

Start date	June 21, 1981
End date	December 23, 1981
Duration (full power days)	170
Peak fissile burnup (%FIMA)	28.7
Peak fertile burnup (%FIMA)	6.1
Peak fast fluence (10^{25} n/m^2, E > 0.18 MeV)	6.3
Average center temperature (°C)	1150
BOL Kr-85m R/B	2.44×10^{-5}
EOL Kr-85m R/B	2.08×10^{-4}

Table 3-49. Selected HRB-16 Coated Fuel Particles.

Particle batch	6151-23-020	6152-03-010	6152-03-020	6152-04-010	6152-06-010	6157-11-010	6252-12COMP
Fuel form	UC_2 TRISO	UO_2* TRISO	UO_2* TRISO	UO_2 TRISO	UO_2* TRISO	UCO TRISO	ThO_2 TRISO
Carbon to uranium (atom ratio)	2.0	na	na	na	na	0.5	na
Oxygen to uranium (atom ratio)	na	2.0	2.0	2.0	2.0	1.5	na
U-235 enrichment (%)	~ 19.5%	~ 19.5%	~ 19.5%	~ 19.5%	~ 19.5%	~ 19.5%	na
Kernel diameter (μm)	344	312	3128	348	379	353	452
Seal coat + ZrC thickness (μm)	none	26.92	22.0	none	not determined	none	none
Buffer thickness (μm)	115	82	93	138	100	118	53
IPyC thickness (μm)	36	35	39	35	39	36	33
SiC thickness (μm)	39	37	36	35	35	36	38
OPyC thickness (μm)	48	41	40	44	49	48	44
Particle diameter (μm)	819	742	770	853	825	824	786
Kernel density (g/cm^3)	11.75	10.78	10.78	10.90	10.9	11.07	9.88
Buffer density (g/cm^3)	0.85	0.91	0.87	0.99	0.99	0.97	1.11
IPyC density (g/cm^3)	1.91	1.92	1.84	1.90	1.86	1.88	1.85
SiC density (g/cm^3)	3.21	3.20	3.21	3.22	3.22	3.22	3.22
OPyC density (g/cm^3)	1.91	1.87	1.82	1.85	1.80	1.90	1.85
IPyC BAF	1.045	1.036	1.030	1.027	1.032	1.057	1.062
OPyC BAF	1.031	1.031	1.026	1.022	1.026	1.034	1.037

Note: “na” means not applicable

Postirradiation metallographic examination was performed on seven fuel compacts which contained particles from six different fissile batches and one fertile batch. Summaries of the fissile and fertile particle examination results are presented in Tables 3-50 and 3-51. For those fuel compacts containing multiple fissile batches, the following visual criteria were used to identify fuel forms:

- UO_2* had the conspicuous, bright ZrC layer next to the kernel;
- UC_2 had very small gas bubbles (voids) in the kernel, or if present in larger form were very irregular in shape;
- UCO had medium size, mostly circular voids in the center of the kernel and small voids at the periphery of the kernel;
- UO_2 had large, mostly circular voids evenly distributed throughout the kernel.

The metallographic examinations revealed that only the UO_2 particles displayed kernel migration. In fuel compacts 2 and 13, kernel migration was observed in about 28% of the UO_2 particles and in about 60% of the UO_2 particles in compact 14. A photomicrograph of an UO_2 particle from compact 14 displaying kernel migration is presented in Figure 3-20.

All of the UC_2 particles examined (eight total) showed extensive buffer and IPyC layer failure, and significant amounts of fission product accumulation. Two of the UC_2 particles, or 25% of those examined, had SiC layer failures. These SiC failures occurred next to areas of the IPyC where high concentrations of fission products were present. Photomicrographs of one of these SiC failures is presented in Figure 3-21.

Examination of the UCO particles revealed significant amounts of fission product attack of the SiC. The extent of this attack ranged from slight to severe. An example of severe fission product attack, extending through the SiC layer, is presented in Figure 3-22. Although not directly measured, from examinations of a similar batch of UCO particles irradiated in HRB-15A, it was surmised that this fission product attack was also due to palladium.

Of the total of 315 fertile ThO_2 particles examined, over one half displayed IPyC layer failure and nearly 2% displayed SiC layer failure. A photomicrograph of a typical ThO_2 particle displaying IPyC failure and SiC cracking is presented in Figure 3-23.

Table 3-50. HRB-16 Fissile Particle Layer Failures.

Particle Batch	Fuel Type	Fuel Compact	Average Irradiation Temp.(°C)	Fast Fluence (10^{25} n/m^2)	Burnup (%FIMA)	Sample Size	OPyC Layer Failure (%)	SiC Layer Failure (%)	IPyC Layer Failure (%)	Buffer Layer Failure (%)	Particles With Debonded IPyC (%)	Particles With Kernel Extrusion (%)	Particles With SiC Fission Product Attack (%)
6157-11-010	UCO	6	1085	5.56	26.1	15	6.7	6.7	6.7	26.7	0	0	26.7
6157-11-010	UCO	7	1105	5.88	27.0	24	8.3	0	0	8.3	0	100	54.2
6152-04-010	UO_2	2	1020	3.68	19.8	11	0	0	0	0	9.1	36.4	18.2
6152-04-010	UO_2	13	1150	5.94	27.8	7	0	0	0	0	0	14.3	57.1
6152-04-010	UO_2	14	1100	5.61	26.9	10	0	0	10.0	10.0	0	60.0	70.0
6152-03-020	UO_2*	2	1020	3.68	19.8	11	0	0	0	90.9	0	9.1	27.3
6152-03-020	UO_2*	6	1085	5.56	26.1	30	0	0	3.3	100.	3.3	50.0	53.3
6152-06-010	UO_2*	8	1110	6.13	27.9	21	4.8	9.5	4.8	33.3	4.8	33.3	23.8
6152-03-010	UO_2*	9	1110	6.27	28.4	20	10.0	0	20.0	95.0	10.0	70.0	40.0
6152-03-020	UO_2*	13	1150	5.94	27.8	5	0	0	0	100.	20.0	20.0	20.0
6151-23-010	UC_2	2	1020	3.68	19.8	6	0	16.7	83.3	83.3	83.3	0	100.
6152-23-020	UC_2	13	1150	5.94	27.8	2	0	50.0	100.	100.	0	100	50.0

Notes: Fast fluence is for E>0.18 MeV. UO_2* has ZrC layer next to kernel

Table 3-51. HRB-16 Fertile Particle Layer Failures.

Particle Batch	Fuel Type	Fuel Compact	Average Irradiation Temp. (°C)	Fast Fluence (10^{25} n/m^2)	Burnup (%FIMA)	Sample Size	OPyC Layer Failure (%)	SiC Layer Failure (%)	IPyC Layer Failure (%)	Buffer Layer Failure (%)	Particles With SiC Fission Product Attack (%)
6252-12 COMP	ThO_2	2	1020	3.68	2.0	48	0	0	25.0	31.3	6.3
6252-12 COMP	ThO_2	6	1085	5.56	4.7	46	4.4	2.2	50.0	71.7	19.6
6252-12 COMP	ThO_2	7	1105	5.88	5.2	65	3.1	1.5	49.2	67.7	35.4
6252-12 COMP	ThO_2	8	1110	6.13	5.7	52	13.5	5.8	65.4	73.1	36.5
6252-12 COMP	ThO_2	9	1110	6.27	6.0	37	16.2	2.7	62.2	67.6	24.3
6252-12 COMP	ThO_2	13	1150	5.94	5.6	36	0	0	72.2	88.9	50.0
6252-12 COMP	ThO_2	14	1100	5.61	5.1	31	0	0	29.0	54.8	16.1

Note: Fast fluence is for E>0.18 MeV

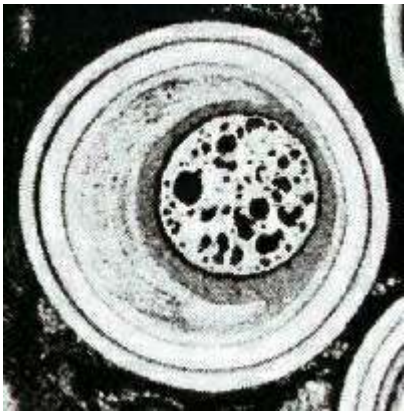

Figure 3-20. Photomicrograph of a UO_2 particle (batch 6152-04-010) irradiated at 1100°C to 26.9%FIMA and to a fast fluence of 5.61 x 10^{25} n/m^2 (E>0.18 MeV) displaying kernel migration.

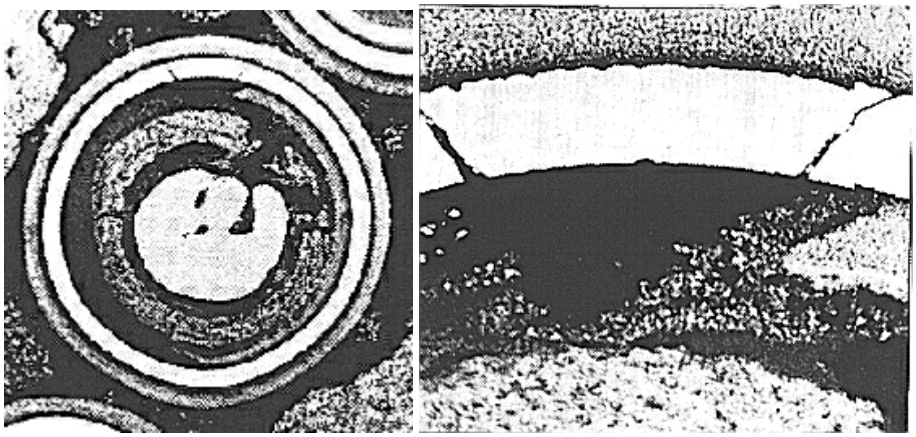

Figure 3-21. Photomicrographs of a UC_2 particle (batch 6151-23-020) irradiated at 1150°C to 27.8%FIMA and to a fast fluence of 5.94 x 10^{25} n/m^2 (E>0.18 MeV) displaying SiC and IPyC layer cracks.

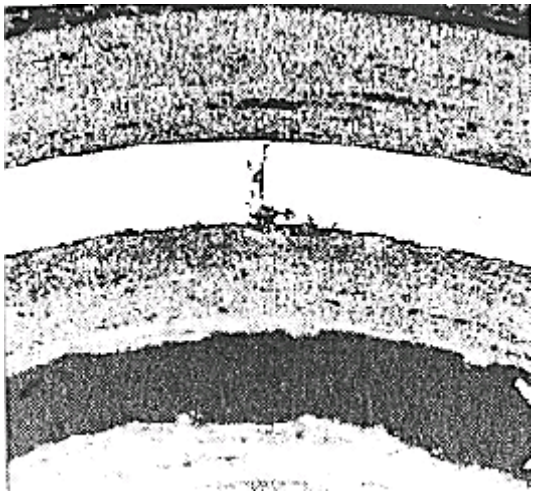

Figure 3-22. Photomicrograph of a UCO particle (batch 6157-11-020) irradiated at 1085°C to 26.1%FIMA and to a fast fluence of 5.56 x 10^{25} n/m^2 (E>0.18 MeV) displaying fission product attack of the SiC layer.

Figure 3-23. Photomicrograph of a fertile ThO_2 TRISO-coated particle (batch 6252-12COMP) irradiated at 1150°C to 5.6%FIMA and to a fast fluence of 5.94 x 10^{25} n/m^2 (E>0.18 MeV) displaying SiC layer cracks.

HRB-21

The HRB-21 capsule was irradiated in the High Flux Isotope Reactor (HFIR) at Oak Ridge National Laboratory (Baldwin et al. 1993a). The objective of the test was to demonstrate the irradiation performance of reference NE-MHTGR fuel. A single gas swept cell contained eight graphite bodies which each held three fuel compacts. Each graphite body also contained three sets of encapsulated (piggyback) specimens. These samples were sealed in niobium tubes up to 52 mm long and 2.2 mm in diameter and contained either absorptivity specimens or loose fuel

particles. The test was originally scheduled to be irradiated for six reactor cycles, however, due to difficulty in maintaining control of test temperature, the experiment was terminated after five reactor cycles. Configuration and irradiation data are given in the following tables.

Table 3-52. HRB-21 Configuration.

Number of cells	1
Number of fuel compacts	24
Number of encapsulated piggyback specimens	24
Cylindrical fuel compact diameter	12.27 to 12.51 mm
Cylindrical fuel compact lengths	49.13 to 49.35 mm
Fissile fuel type	LEU UCO TRISO-P
Fertile fuel type	ThO_2 TRISO-P
U-235 enrichment	19.66%
Fissile particle diameter	904 μm
Fertile particle diameter	988 μm
Fissile particle batch	8876-70-0
Fertile particle batch	8876-58-0
Total number of fissile particles	42,540
Total number of fertile particles	106,240
Defective SiC layer fraction – fissile particles	$\leq 5.4 \times 10^{-6}$
Defective SiC layer fraction – fertile particles	1.7×10^{-5}

Table 3-53. HRB-21 Irradiation Data.

Start date	June 20, 1991
End date	November 21, 1991
Duration (full power days)	105
Peak burnup (%FIMA)	22
Peak fast fluence (10^{25} n/m^2, E > 0.18 MeV)	3.5
Average temperature (°C)	950
Peak temperature (°C)	1300
BOL Kr-85m R/B	1×10^{-8}
EOL Kr-85m R/B	2×10^{-4}

Table 3-54. HRB-21 Coated Fuel Particles.

Particle batch	8876-70-0	8876-58-0
Fuel form	UCO TRISO-P	ThO_2 TRISO-P
Carbon to uranium (atom ratio)	0.20	na
Oxygen to uranium (atom ratio)	1.65	na
U-235 enrichment (%)	19.660	na
Kernel diameter (μm)	351 ± 9.70	512 ± 8.60
Buffer thickness (μm)	105 ± 12.61	67.1 ± 11.52
Buffer – IPyC seal coat thickness (μm)	< 5	< 5
IPyC thickness (μm)	52.8 ± 4.06	56.4 ± 5.06
SiC thickness (μm)	32.6 ± 1.87	36.0 ± 2.48
OPyC thickness (μm)	46.8 ± 4.97	41.1 ± 4.38
OPyC – protective PyC seal coat thickness (μm)	< 5	<5
Protective PyC thickness (μm)	46.4 ± 6.72	45.4 ± 8.49
Particle diameter (μm)	904	988
Kernel density (g/cm^3)	10.65	9.94
Buffer density (g/cm^3)	0.97	1.02
IPyC density (g/cm^3)	1.90 ± 0.002	1.91 ± 0.010
SiC density (g/cm^3)	3.22 ± 0.004	3.19 ± 0.003
OPyC density (g/cm^3)	1.84	1.84
Protective PyC density (g/cm^3)	0.998	0.88
IPyC BAF	1.074	1.106
OPyC BAF	1.038	1.042

Notes: The ± values are one standard deviation, and "na" entries are not applicable.

Postirradiation metallographic examination of three fuel compacts was performed. SiC layer failure for both fissile and fertile particles ranged between 0 and 5%. During irradiation, the on-line ionization chambers recorded several spikes which indicated the failure of about 130 particles. Further results from the metallographic examination concerning layer failures are presented in the following tables.

The metallographic examinations also revealed that the IPyC layer was in contact with the SiC layer. However, in some cases where the IPyC was cracked radially, the IPyC layer was debonded from the SiC. Fission product attack of the SiC layer was also observed. The chemical attack took place at the tips of cracks in the IPyC layer where fission product transport was no doubt enhanced. However, scanning electron microscopy did not detect localized high concentrations of fission products in the SiC but did detect low levels of palladium extending 5 to 10 μm uniformly into the SiC.

Table 3-55. HRB-21 Fissile Particle Layer Failures.

Compact	Average Irradiation Temp. (°C)	Fast Fluence (10^{25} n/m^2)	Burnup (%FIMA)	Sample Size	OPyC Layer Failure (%)	OPyC 95% Confidence Interval (%)	SiC Layer Failure (%)	SiC 95% Confidence Interval (%)	IPyC Layer Failure (%)	IPyC 95% Confidence Interval (%)
1C	800	1.5	14	96	6	$2 \le P \le 12$	0	$0 \le P \le 4$	1	$0 \le P \le 5$
2B	980	2.3	18	70	40	$27 \le P \le 53$	0	$0 \le P \le 6$	3	$0 \le P \le 9$
4A	1000	3.5	22.5	61	98	$91 \le P \le 100$	5	$0 \le P \le 13$	33	$18 \le P \le 48$

Note: Fast fluence is for E > 0.18 MeV

Table 3-56. HRB-21 Fertile Particle Layer Failures.

Compact	Average Irradiation Temp. (°C)	Fast Fluence (10^{25} n/m^2)	Burnup (%FIMA)	Sample Size	OPyC Layer Failure (%)	OPyC 95% Confidence Interval (%)	SiC Layer Failure (%)	SiC 95% Confidence Interval (%)	IPyC Layer Failure (%)	IPyC 95% Confidence Interval (%)
1C	800	1.5	0.5	154	3	$0 \le P \le 6$	0	$0 \le P \le 3$	0.6	$0 \le P \le 3$
2B	980	2.3	1.2	144	37	$27 \le P \le 47$	3	$0 \le P \le 6$	2	$0 \le P \le 5$
4A	1000	3.5	2.2	163	98	$94 \le P \le 100$	5	$0 \le P \le 9$	30	$22 \le P \le 38$

Notes: Fast fluence is for E > 0.18 MeV. The 95% confidence intervals tabulated for HRB-21 and the NPR experiments were calculated using the same standard statistical approach (Burington and May 1970) as used in the early Oak Ridge National Laboratory reports.

NPR-1

The NPR-1 capsule was irradiated in the High Flux Isotope Reactor (HFIR) at Oak Ridge National Laboratory (Baldwin et al. 1993b). The main objective of this experiment was to demonstrate the irradiation performance of reference NP-MHTGR fuel at the upper bounds of burnup, temperature and fast fluence. This experiment was irradiated one month before and then concurrently with the NPR-2 capsule in HFIR. NPR-1 consisted of a single gas swept cell containing 16 fuel compacts in addition to 12 sets of loose particles. The loose specimens were sealed in niobium tubes, 29 mm long and 2.2 mm in diameter. Configuration and irradiation data are given in the following tables.

Table 3-57. NPR-1 Configuration.

Number of cells	1
Number of fuel compacts	16
Number of encapsulated piggyback specimens	12
Cylindrical fuel compact diameter	12.43 mm
Cylindrical fuel compact lengths	49.42 mm
Fuel type	HEU UCO TRISO-P
U-235 enrichment	93.15%
Fuel particle diameter	758 μm
Fuel particle batch	FM19-00001 composite
Total number of fuel particles	77,500
Defective SiC layer fraction	3×10^{-6}

Table 3-58. NPR-1 Irradiation Data.

Start date	July 25, 1991
End date	May 29, 1992
Duration (full power days)	170
Peak burnup (%FIMA)	79
Peak fast fluence (10^{25} n/m^2, E > 0.18 MeV)	3.75
Average temperature (°C)	974
Peak compact temperature (°C)	1240
BOL Kr-85m R/B	1×10^{-8}
EOL Kr-85m R/B	3×10^{-4}

Table 3-59. NPR-1 Coated Fuel Particles.

Particle batch	FM19-00001 composite
Fuel form	UCO TRISO-P
Carbon to uranium (atom ratio)	0.3618 ± 0.0008
Oxygen to uranium (atom ratio)	1.5098 ± 0.0066
U-235 enrichment (%)	93.15 ± 0.01
Kernel diameter (μm)	200 ± 5.2
Buffer thickness (μm)	102 ± 10.2
Buffer – IPyC seal coat thickness (μm)	< 5
IPyC thickness (μm)	53 ± 3.68
SiC thickness (μm)	35 ± 3.12
OPyC thickness (μm)	39 ± 4.01
OPyC – protective PyC seal coat thickness (μm)	< 5
Protective PyC thickness (μm)	47 ± 11.35
Outer seal coat thickness (μm)	<5
Particle diameter (μm)	758 ± 23.5
Kernel density (g/cm^3)	10.52 ± 0.01
Buffer density (g/cm^3)	0.9577 ± 0.05
IPyC density (g/cm^3)	1.923 ± 0.008
SiC density (g/cm^3)	3.2278 ± 0.0007
OPyC density (g/cm^3)	1.855 ± 0.010
Protective PyC density (g/cm^3)	1.06
IPyC BAF	1.05788 ± 0.00543
OPyC BAF	1.05154 ± 0.00622

Note: The ± values are one standard deviation.

Postirradiation metallographic examination of two fuel compacts was performed. The examination indicated that about 0.6% of the SiC layers had failed in one compact and that 0% had failed in the other compact. The on-line gas measurements recorded 526 spikes from the ionization chamber. Assuming each spike corresponds to a particle failure, 0.7% of the total number of particles had all coatings fail. Further results from the metallographic examination concerning layer failures are presented in the following table.

The metallographic examination also revealed that the IPyC layer had remained bonded to the SiC except in the vicinity of SiC cracks where debonding was observed. It was also observed that between 10 and 30% of the particles with failed IPyC layers also displayed cracked SiC layers.

Table 3-60. NPR-1 Fuel Particle Layer Failures.

Compact	Compact Average Temp (°°C)	Fast Fluence (10^{25} n/m^2, E > 0.18 MeV)	Burnup (%FIMA)
A5	987	3.75	79
A8	845	2.4	72

Compact	Layer	Sample Size[(A)]	Failures (%)	95% Confidence Interval (%)
A5	OPyC	39	90	76 ≤ P ≤ 98
	SiC	178	0.6	0 ≤ P ≤ 3
	IPyC	39	31	17 ≤ P ≤ 47
A8	OPyC	53	47	33≤ P ≤ 62
	SiC	260	0	0 ≤ P ≤ 2
	IPyC	53	6	2 ≤ P ≤ 16

Note (a): Data for the OPyC and IPyC layers were reported only for particles examined with kernels remaining in the sample mount.

NPR-2

The NPR-2 capsule was irradiated in the High Flux Isotope Reactor (HFIR) at Oak Ridge National Laboratory (Baldwin et al. 1993b). The main objective of this experiment was to demonstrate the irradiation performance of reference NP-MHTGR fuel at the upper bounds of burnup and fast fluence but at a moderate temperature, close to the expected NP-MHTGR core average. This experiment was irradiated one month after the start of NPR-1 and then concurrently until termination. NPR-2 consisted of a single gas swept cell containing 16 fuel compacts in addition to 16 sets of loose particles. The loose specimens were sealed in niobium tubes, 29 mm long and 2.2 mm in diameter. Configuration and irradiation data are given in the following tables.

Table 3-61. NPR-2 Configuration.

Number of cells	1
Number of fuel compacts	16
Number of encapsulated piggyback specimens	16
Cylindrical fuel compact diameter	12.43 mm
Cylindrical fuel compact lengths	49.42 mm
Fuel type	HEU UCO TRISO-P
U-235 enrichment	93.15%
Fuel particle diameter	758 μm
Fuel particle batch	FM19-00001 composite
Total number of fuel particles	77,500
Defective SiC layer fraction	3 x 10^{-6}

Table 3-62. NPR-2 Irradiation Data.

Start date	August 28, 1991
End date	May 29, 1992
Duration (full power days)	172
Peak burnup (%FIMA)	79
Peak fast fluence (10^{25} n/m^2, E > 0.18 MeV)	3.75
Average temperature (°C)	753
Peak compact temperature (°C)	1030
BOL Kr-85m R/B	5×10^{-9}
EOL Kr-85m R/B	6×10^{-5}

Table 3-63. NPR-2 Coated Fuel Particles.

Particle batch	FM19-00001 composite
Fuel form	UCO TRISO-P
Carbon to uranium (atom ratio)	0.3618 ± 0.0008
Oxygen to uranium (atom ratio)	1.5098 ± 0.0066
U-235 enrichment (%)	93.15 ± 0.01
Kernel diameter (μm)	200 ± 5.2
Buffer thickness (μm)	102 ± 10.2
Buffer – IPyC seal coat thickness (μm)	< 5
IPyC thickness (μm)	53 ± 3.68
SiC thickness (μm)	35 ± 3.12
OPyC thickness (μm)	39 ± 4.01
OPyC – protective PyC seal coat thickness (μm)	< 5
Protective PyC thickness (μm)	47 ± 11.35
Outer seal coat thickness (μm)	<5
Particle diameter (μm)	758 ± 23.5
Kernel density (g/cm^3)	10.52 ± 0.01
Buffer density (g/cm^3)	0.9577 ± 0.05
IPyC density (g/cm^3)	1.923 ± 0.008
SiC density (g/cm^3)	3.2278 ± 0.0007
OPyC density (g/cm^3)	1.855 ± 0.010
Protective PyC density (g/cm^3)	1.06
IPyC BAF	1.05788 ± 0.00543
OPyC BAF	1.05154 ± 0.00622

Note: The ± values are one standard deviation.

Postirradiation metallographic examination of one fuel compact was performed. This examination indicated that about 3% of the SiC layers had failed. The on-line gas measurements recorded 135 spikes from the Geiger-Müller tube. This detector is less sensitive than ionization chambers, and may have missed some transient spikes. However, assuming each spike corresponds to a particle failure, a lower bound of 0.2% can be set for the total number of particles that had failed. Further results from the metallographic examination concerning layer failures are presented in the following table.

The metallographic examination also revealed that the IPyC layer had remained bonded to the SiC except in the vicinity of SiC cracks where debonding was observed. It was also observed that between 10 and 30% of the particles with failed IPyC layers also displayed cracked SiC layers.

Table 3-64. NPR-2 Fuel Particle Layer Failures.

Compact	Compact Average Temp. (°C)	Fast Fluence (10^{25} n/m^2, E > 0.18 MeV)	Burnup (%FIMA)
A4	746	3.75	79

Compact	Layer	Sample Size[(a)]	Failures (%)	95% Confidence Interval (%)
A4	OPyC	84	67	$5 \leq P \leq 77$
	SiC	287	3	$2 \leq P \leq 6$
	IPyC	84	65	$54 \leq P \leq 76$

Note (a): Data for the OPyC and IPyC layers were reported only for particles examined with kernels remaining in the sample mount.

NPR-1A

The NPR-1A capsule was irradiated in the Advanced Test Reactor (ATR) at the Idaho National Engineering and Environmental Laboratory (Baldwin et al. 1993b, Martinson et al. 1993). The primary objective of the test was to demonstrate the irradiation performance of reference NP-MHTGR fuel at the upper bounds of nominal operating conditions. The same reference fuel was also irradiated in the NPR-1 and NPR-2 tests. For NPR-1A, 20 fuel compacts were placed vertically in a single, gas swept cell. Originally, the test was scheduled for 104 days of irradiation but was terminated after 64 days due to indications of a significant number of fuel particle failures. Configuration and irradiation data are given in the following tables.

Table 3-65. NPR-1A Configuration.

Number of cells	1
Number of fuel compacts	20
Cylindrical fuel compact diameter	12.37 to 12.50 mm
Cylindrical fuel compact lengths	49.33 mm
Fuel type	HEU UCO TRISO-P
U-235 enrichment	93.15%
Fuel particle diameter	758 μm
Fuel particle batch	FM19-00001 composite
Total number of fuel particles	75,360
Defective SiC layer fraction	3×10^{-6}

Table 3-66. NPR-1A Irradiation Data.

Start date	October 2, 1991
End date	January 3, 1992
Duration (full power days)	64
Peak burnup (%FIMA)	64
Peak fast fluence (10^{25} n/m^2, E > 0.18 MeV)	2.1
Average temperature (°C)	977
Peak temperature (°C)	1220
BOL Kr-85m R/B	4×10^{-9}
EOL Kr-85m R/B	1.8×10^{-5}

Table 3-67. NPR-1A Coated Fuel Particles.

Particle batch	FM19-00001 composite
Fuel form	UCO TRISO-P
Carbon to uranium (atom ratio)	0.3618 ± 0.0008
Oxygen to uranium (atom ratio)	1.5098 ± 0.0066
U-235 enrichment (%)	93.15 ± 0.01
Kernel diameter (μm)	200 ± 5.2
Buffer thickness (μm)	102 ± 10.2
Buffer – IPyC seal coat thickness (μm)	< 5
IPyC thickness (μm)	53 ± 3.68
SiC thickness (μm)	35 ± 3.12
OPyC thickness (μm)	39 ± 4.01
OPyC – protective PyC seal coat thickness (μm)	< 5
Protective PyC thickness (μm)	47 ± 11.35
Outer seal coat thickness (μm)	<5
Particle diameter (μm)	758 ± 23.5
Kernel density (g/cm^3)	10.52 ± 0.01
Buffer density (g/cm^3)	0.9577 ± 0.05
IPyC density (g/cm^3)	1.923 ± 0.008
SiC density (g/cm^3)	3.2278 ± 0.0007
OPyC density (g/cm^3)	1.855 ± 0.010
Protective PyC density (g/cm^3)	1.06
IPyC BAF	1.05788 ± 0.00543
OPyC BAF	1.05154 ± 0.00622

Note: The ± values are one standard deviation.

Postirradiation metallographic examination of one fuel compact was performed. This examination indicated that about 1% of the SiC layers had failed. Based upon the on-line gas measurements, it was estimated that a total of about 48 particles had failed which corresponds to 0.06% of the total particle population. Further results from the metallographic examination concerning layer failures are presented in the following table.

Table 3-68. NPR-1A Fuel Particle Layer Failures.

Compact	Compact Average Temp. (°C)	Fast Fluence (10^{25} n/m^2, E > 0.18 MeV)	Burnup (%FIMA)
A9	1052	1.91	64

Compact	Layer	Sample Size[(a)]	Failures (%)	95% Confidence Interval (%)
A9	OPyC	17	47	$25 \le P \le 75$
	SiC	83	1	$0 \le P \le 5$
	IPyC	17	18	$5 \le P \le 42$

Note (a): Data for the OPyC and IPyC layers were reported only for particles examined with kernels remaining in the sample mount.

3.3. German Experiments

The particle fuel irradiation experiments described in this section consider only tests using "modern" German fuel (Gontard and Nabielek 1990). This fuel includes high-enriched $(Th,U)O_2$ TRISO-coated particles fabricated since 1977 and low enriched UO_2 TRISO-coated particles fabricated since 1981. The physical attributes of the fuel used in these tests are listed in the following table.

Table 3-69. Characteristics of Modern German TRISO Fuel Particles.

Particle batch	EUO 2308	EUO 2309	HT 354-383	EO 1607	EO 1674
Experiments irradiated in	FRJ2-K13 FRJ2-P27 HFR-P4 HFR-K3 Sl-P1	FRJ2-P27 HFR-P4	FRJ2-K15	R2-K12 BR2-P25	R2-K13
Kernel form	UO_2	UO_2	UO_2	$(Th,U)O_2$	$(Th,U)O_2$
U-235 enrichment (%)	9.82	9.82	16.76	89.57	89.01
Kernel diameter (μm)	497 ± 3%	497 ± 3%	501 ± 10.8	494 ± 3%	496 ± 3%
Kernel density (g/cm^3)	10.81	10.81	10.85	10.12	10.10
Buffer thickness (μm)	94	93	92 ± 14.3	85	89
IPyC thickness(μm)	41	37	38 ± 3.4	39	37
SiC thickness (μm)	36	51	33 ± 1.9	37	33
OPyC thickness (μm)	40	38	41 ± 3.8	39	39
Particle diameter (μm)	895	922	906 ± 28.8	888	890
Buffer density (g/cm^3)	1.00	1.00	1.013	1.09	1.06
IPyC density (g/cm^3)	[1.9]	[1.9]	[1.9]	1.93	1.90
SiC density (g/cm^3)	3.20	3.20	3.20	3.20	3.19
OPyC density (g/cm^3)	1.88	1.87	1.88	1.93	1.90
IPyC BAF	1.053		1.029		
OPyC BAF	1.019		1.020		

Notes: The ± entries are one standard deviation. Entries in square brackets, [ ] are estimated values.

The following German fuel irradiation experiment summaries present the mixed oxide tests first followed by the UO_2 tests. U.S. nomenclature is used in the description of the German test configurations (capsule is used in place of the German irradiation rig and cell is used in place of the German capsule).

R2-K12

The R2-K12 cells were irradiated in the R2 reactor at Studsvik, Sweden. The main objective of this experiment was to test mixed oxide $(Th,U)O_2$ and fissile UC_2/fertile ThO_2 fuel elements. Four full size spherical fuel elements were irradiated in four independently gas swept cells. Two cells contained mixed oxide fuel spheres, while the other two cells contained the fissile/fertile fuel spheres. Since the two-particle fissile/fertile system was not developed further by the Germans, only the mixed oxide results were reported. Configuration and irradiation data from the mixed oxide cells are given in the following tables.

Cold gas tests on each fuel sphere during the postirradiation examination indicated that all the particles had remained intact. The fuel sphere from Cell 1 was partially deconsolidated and visual inspection revealed two kernels "without coating". Segments from each of the two fuel spheres were metallographically examined which revealed a reaction zone on the inner side of the buffer layer, and tangential cracks between the buffer and inner pyrocarbon layer. Only one particle exhibited a radial crack in the buffer layer beyond the reaction zone. All of the SiC and PyC layers examined had remained intact.

Table 3-70. R2-K12 Configuration.

Number of cells	2
Number of fuel spheres	2
Spherical fuel element diameter	59.9 mm
Fuel zone diameter	47 mm
Fuel type	HEU $(Th,U)O_2$ LTI - TRISO
Particle batch	EO 1607
U-235 enrichment	89.57%
U-235 per fuel element	1.002 g
Th per fuel element	4.961 g
Heavy metal per fuel element	6.076 g
Number of particles per spherical fuel element	10,960
Defective SiC layers (U/U-total)	$< 1 \times 10^{-5}$

* The defective SiC layer fractions reported for German fuel are per pebble with the exception of loose particle experiments which are per particle batch.

Table 3-71. R2-K12 Irradiation Data.

Start date	November 28, 1978	
End date	February 12, 1980	
Duration (full power days)	308	
Cell	1	2
Burnup (%FIMA)	11.1	12.4
Fast fluence (10^{25} n/m^2, E > 0.10 MeV)	5.6	6.9
Center temperature (°C)	1100	1280
Surface temperature (°C)	950	1120
BOL Kr-85m R/B	3.9×10^{-9}	4.6×10^{-9}
EOL (report date) Kr-85m R/B	3.0×10^{-7}	2.0×10^{-7}

R2-K13

The R2-K13 cells were irradiated in the R2 reactor at Studsvik, Sweden. The main objective of this experiment was to test mixed oxide (Th,U)O_2 fuel elements and supply fuel for subsequent safety tests. R2-K13 was a combined experiment with the U.S. Four independently gas swept cells were positioned one atop of another. The top and bottom cells each contained a full size German fuel sphere. The middle two cells contained U.S. fuel and is discussed in Section 3.2. Configuration and irradiation data from the German cells are given in the following tables.

Cold gas tests on each fuel sphere during the postirradiation examination indicated that all the particles had remained intact. These tests are conducted after the fuel has been stored (for about 14 days) at room temperature and a quasi-steady-state release of fission gas has been reached. The fuel is then swept with a carrier gas which is monitored for various fission gases (usually Kr-85 m) and heated to about 60°C. Sudden increases in the amount of detected fission gas is then detected. The amount of increase is proportional to the gas source, and in a calibrated system, indicates the number of failed particles.

Table 3-72. R2-K13 Configuration.

Number of cells	2
Number of fuel spheres	2
Spherical fuel element diameter	59.77 mm
Fuel zone diameter	47 mm
Fuel type	HEU (Th,U)O_2 LTI - TRISO
Particle batch	EO 1674
U-235 enrichment	89.01%
U-235 per fuel element	1.02 g
Th-232 per fuel element	10.125 g
Heavy metal per fuel element	11.27 g
Number of particles per spherical fuel element	19,780
Defective SiC layers (U/U-total)	$< 5 \times 10^{-6}$

Table 3-73. R2-K13 Irradiation Data.

Start date	April 22, 1980	
End date	September 19, 1982	
Duration (full power days)	517	
Cell	1	4
Burnup (%FIMA)	10.2	9.8
Fast fluence (10^{25} n/m^2, E > 0.10 MeV)	8.5	6.8
Center temperature (°C)	1170	980
Surface temperature (°C)	960	750
BOL Kr-85m R/B	2.2×10^{-9}	1.5×10^{-9}
EOL Kr-85m R/B	7.0×10^{-8}	5.0×10^{-8}

BR2-P25

The BR2-P25 capsule was irradiated in the BR2 reactor at Mol, Belgium. The primary objective of this experiment was to test (Th,U)O_2 mixed oxide fuel. One independently gas swept cell contained 12 compacts. Each compact was cylindrical in shape and contained a small fuel sphere. Configuration and irradiation data are given in the following tables.

During the postirradiation examination, Compacts 3 and 7 were electrolytically deconsolidated with no particle failures being evident. Ceramographic examination of cross sections from Compacts 4 and 8 revealed some radial cracks in the buffer layers, however, no defective particles were found.

Table 3-74. BR2-P25 Configuration.

Number of cells	1
Number of compacts	12
Cylindrical compact diameter	26.58 to 27.74 mm
Cylindrical compact height	29.87 to 30.03 mm
Diameter of spherical fuel zone	20 mm
Fuel type	HEU (Th,U)O_2 LTI - TRISO
Particle batch	EO 1607
U-235 enrichment	89.57%
U-235 per fuel compact	0.136 g
Th-232 per fuel compact	0.6744 g
Heavy metal per fuel compact	0.8264 g
Number of particles per compact	1490
Number of particles per cell	17,880
Defective SiC layers (U/U-total)	$< 1 \times 10^{-5}$

Table 3-75. BR2-P25 Irradiation Data.

Start date	October 30, 1978
End date	December 19, 1981
Duration (full power days)	350
Burnup (%FIMA)	13.9 to 15.6
Fast fluence (10^{25} n/m^2, E > 0.10 MeV)	6.2 to 8.1
Maximum temperature (°C)	1070
Minimum temperature (°C)	1010
BOL Kr-85m R/B	2×10^{-7}
EOL Kr-85m R/B	1×10^{-6}

HFR-P4

The HFR-P4 capsule was irradiated at the High Flux Reactor (HFR) in Petten, Holland. The primary objective of this experiment was to compare the fuel performance of particles with 36 and 51 μm thick SiC layers irradiated at 1000°C, beyond burnups of 12%FIMA and beyond fast fluences of 6 x 10^{25} n/m^2 (E > 0.10 MeV). The performance of the 36 μm SiC layer fuel was also to be evaluated at an irradiation temperature of 1200°C. Three independently gas swept cells each contained 12 compacts. Each compact was cylindrical in shape and contained a small fuel sphere. Configuration and irradiation data are given in the following tables. Note that the burnup and fast fluence goals were met while irradiation temperature goals were not.

Postirradiation examination revealed that the test articles had remained intact. However, some failures were found on the upper compacts which were caused by the thermocouples and gas inlet tubes.

Table 3-76. HFR-P4 Configuration.

Number of cells	3
Number of compacts per cell	12
Cylindrical compact diameter	23 to 29 mm
Cylindrical compact height	32 mm
Diameter of spherical fuel zone	20 mm
Fuel type	LEU UO_2 LTI – TRISO
Particle batch – Cells 1 and 3	EUO 2308
Particle batch – Cell 2	EUO 2309
U-235 enrichment	9.82%
Number of particles per compact	1630
Number of particles per capsule	19,600
Defective SiC layers (U/U-total)	< 1 x 10^{-6}

Table 3-77. HFR-P4 Irradiation Data.

Start date	June 10, 1982		
End date	November 28, 1983		
Duration (full power days)	351		
Capsule	1	2	3
SiC layer thickness (μm)	36	51	36
Maximum temperature (°C)	940	945	1075
Minimum temperature (°C)	915	920	1050
Maximum burnup (%FIMA)	14.7	14.9	14.0
Peak fast fluence (10^{25} n/m^2, E > 0.10 MeV)	8.0	8.0	8.0
BOL Kr-85m R/B	3.5 x 10^{-9}	-	3.6 x 10^{-9}
EOL Kr-85m R/B	8 x 10^{-8}	8 x 10^{-8}	8 x 10^{-9}

SL-P1

The SL-P1 experiment was irradiated at the Siloë Reactor in Grenoble, France. The objective of the experiment was to test reference LEU fuel up to the potential limits for burnup and fast fluence at 800°C. One gas swept cell contained 12 compacts. Each cylindrical compact contained one small fuel sphere. Configuration and irradiation data are given in the following tables. The operational objectives for this experiment were met. Postirradiation examination revealed that none of the compacts showed mechanical failure.

Table 3-78. SL-P1 Configuration.

Number of cells	1
Number of compacts	12
Cylindrical compact diameter	30.1 mm
Cylindrical compact height	30.8 mm
Diameter of spherical fuel zone	20 mm
Fuel type	LEU UO_2 LTI - TRISO
Particle batch	EUO 2308
U-235 enrichment	9.82%
Number of particles per compact	1634
Number of particles per cell	19,600
Defective SiC layers (U/U-total)	$< 1 \times 10^{-6}$

Table 3-79. SL-P1 Irradiation Data.

Start date	June 24, 1982
End date	December 23, 1983
Duration (full power days)	330
Burnup (%FIMA)	8.6 to 11.3
Fast fluence (10^{25} n/m^2, E > 0.10 MeV)	5.0 to 6.8
Compact mean temperature (°C)	743 to 794
BOL Kr-85m R/B	5.8×10^{-7}
EOL Kr-85m R/B	1.2×10^{-6}

HFR-K3

The HFR-K3 capsule was irradiated at the High Flux Reactor in Petten, Holland. The primary objective of this experiment was to determine the performance of reference LEU fuel from an accelerated test. Four full size spherical fuel elements were irradiated in three independently gas swept cells. The cells were positioned vertically, one atop of the other, with the middle cell containing two fuel spheres. To minimize flux gradient effects on the test fuel, the entire test rig was rotated 90° several times during the irradiation. Configuration and irradiation data are given in the following tables. No failures were reported as a result of the postirradiation examination.

Table 3-80. HFR-K3 Configuration.

Number of cells	3
Number of fuel spheres	4
Spherical fuel element diameter	59.98 mm
Fuel zone diameter	47 mm
Fuel type	LEU UO_2 LTI - TRISO
Particle batch	EUO 2308
U-235 enrichment	9.82%
Number of particles per spherical fuel element	16,400
Defective SiC layers (U/U-total)	4×10^{-5}

Table 3-81. HFR-K3 Irradiation Data.

Start date	April 15, 1982			
End date	September 5, 1983			
Duration (full power days)	359			
Cell / Sphere	A / 1	B / 2	B / 3	C / 4
Burnup (%FIMA)	7.5	10.0	10.6	9.0
Fast fluence (10^{25} n/m^2, E > 0.10 MeV)	4.0	5.8	5.9	4.9
Center temperature (°C)	1200	920	920	1220
Surface temperature (°C)	1020	700	700	1020
BOL Kr-85m R/B	1×10^{-9}	9×10^{-10}	9×10^{-10}	2×10^{-9}
EOL Kr-85m R/B	2×10^{-7}	1×10^{-7}	1×10^{-7}	3×10^{-7}

FRJ2-K13

FRJ2-K13 cells were irradiated at the DIDO reactor in Jülich, Germany. The objective of this test was to supply irradiated reference fuel for subsequent safety tests. Fuel performance was also to be examined under the controlled irradiation conditions of significant burnup with negligible fast neutron fluence. Four full size spherical fuel elements were irradiated in two independently gas swept cells. The cells were vertically positioned one atop of another with the fuel spheres similarly positioned within the cells. Configuration and irradiation data are given in the following tables. No failures were reported as a result of the postirradiation examination.

Table 3-82. FRJ2-K13 Configuration.

Number of cells	2
Number of fuel spheres	4
Spherical fuel element diameter	59.98 mm
Fuel zone diameter	47 mm
Fuel type	LEU UO_2 LTI - TRISO
Particle batch	EUO 2308
U-235 enrichment	9.82%
Number of particles per spherical fuel element	16,400
Defective SiC layers (U/U-total)	4×10^{-5}

Table 3-83. FRJ2-K13 Irradiation Data.

Start date	June 24, 1982			
End date	February 12, 1984			
Duration (full power days)	396			
Cell / Sphere	A / 1	A / 2	B / 3	B / 4
Burnup (%FIMA)	7.5	8.0	7.9	7.6
Fast fluence (10^{25} n/m^2, E > 0.10 MeV)	0.2	0.2	0.2	0.2
Center temperature (°C)	1125	1150	1150	1120
Surface temperature (°C)	985	990	990	980
BOL Kr-85m R/B	2×10^{-9}	2×10^{-9}	8×10^{-10}	8×10^{-10}
EOL Kr-85m R/B	2×10^{-8}	2×10^{-8}	7×10^{-9}	7×10^{-9}

FRJ2-K15

FRJ2-K15 cells were irradiated at the DIDO reactor in Jülich, Germany. The main objectives of this test were to demonstrate the high burnup potential of reference fuel used in AVR reload 21-1, and to perform in-core temperature transient tests. Fuel performance was also to be examined under the controlled irradiation conditions of significant burnup with negligible fast neutron fluence. Three full size spherical fuel elements were irradiated in three independently gas swept cells. Configuration and irradiation data are given in the following tables.

This experiment was still in progress when preliminary results were reported. As of the report date, burnup had reached about 14%FIMA and the intent was to continue the test to about 15%FIMA. Postirradiation examination activities are currently being planned and are not yet available.

Capsules 2 and 3 underwent a temperature transient test at a burnup of about 10%FIMA. The temperature of the sphere surfaces was raised to 1100°C and held for 11 hours. The Kr-85m R/B ratio from each capsule increased to a maximum of about 10^{-8} at the start of the transient and then dropped back to the pre-transient levels after the temperature was returned to the nominal test condition.

Table 3-84. FRJ2-K15 Configuration.

Number of cells	3
Number of fuel spheres	3
Spherical fuel element diameter	60.4 mm
Fuel zone diameter	47 mm
Fuel type	LEU UO_2 LTI - TRISO
Particle batch	HT 354-383
U-235 enrichment	16.76%
Number of particles per spherical fuel element	9,500
Defective SiC layers (U/U-total)	$< 5 \times 10^{-5}$

Table 3-85. FRJ2-K15 Irradiation Data.

Start date	September 4, 1986		
Report date	May 20, 1990		
Duration (full power days)	590		
Cell	1	2	3
Burnup (%FIMA)	14.1	15.3	14.7
Fast fluence (10^{25} n/m^2, E > 0.10 MeV)	0.2	0.2	0.1
Center temperature (°C)	970	1150	990
Surface temperature (°C)	800	980	800
BOL Kr-85m R/B	2.0×10^{-10}	2.47×10^{-10}	2.0×10^{-10}
EOL Kr-85m R/B	1.0×10^{-8}	5.0×10^{-9}	3.0×10^{-9}

FRJ2-P27

FRJ2-P27 cells were irradiated at the DIDO reactor in Jülich, Germany. The main objectives of this test were to investigate fission product release at various cyclic temperatures and to determine the effectiveness of thicker SiC layers on the retention of Ag-110m. Three independently gas swept cells each contained three compacts and two coupons (trays). The compacts were cylindrical in shape and contained (an unspecified) outer fuel free zone. The coupons were graphite disks with holes, annularly spaced, for the insertion of 34 particles. Two coupons contained the thicker SiC particles (51 μm vs. 36 μm) where one was placed in Cell 1 and the other in Cell 3. Configuration and irradiation data are given in the following tables.

Postirradiation examination revealed that all specimens and components were in excellent condition. Cold gas tests of all compacts and coupons determined that there was only one defective/failed particle present. This particle was from a Capsule 2 coupon (with nominal SiC thickness). Ceramographic examination revealed that the particle was inserted in the coupon “without coating” and that kernel interactions led to a compression of the inner side of the buffer to a thickness of about 10 μm.

Table 3-86. FRJ2-P27 Configuration.

Number of cells	3
Number of compacts per cell	3
Number of coupons per cell	2
Cylindrical compact diameter	27.9 to 28.03 mm
Cylindrical compact height	29 mm
Coupon diameter	27 mm
Coupon height	2.2 mm
Diameter of coupon fuel annulus	23 mm
Fuel type	LEU UO_2 LTI - TRISO
Particle batch for compacts and 4 coupons	EUO 2308
Particle batch for 2 coupons (thick SiC)	EUO 2309
U-235 enrichment	9.82%
Number of particles per compact	2424
Number of particles per coupon	34
Number of particles per cell	7340
Defective SiC layers (U/U-total)	$< 3 \times 10^{-6}$

Table 3-87. FRJ2-P27 Irradiation Data.

Start date	February 17, 1984		
End date	February 10, 1985		
Duration (full power days)	232		
Cell	1	2	3
Burnup (%FIMA)	7.6	8.0	7.6
Fast fluence (10^{25} n/m^2, E > 0.10 MeV)	1.4	1.7	1.3
Maximum temperature (°C)	1080	1320	1130
Minimum temperature (°C)	880	1220	1080
BOL Kr-85m R/B	1.0×10^{-6}	8.6×10^{-7}	2.0×10^{-8}
EOL Kr-85m R/B	1.6×10^{-6}	1.0×10^{-5}	1.2×10^{-7}

HFR-K6

The HFR-K6 capsule was irradiated at the High Flux Reactor in Petten, Holland (Conrad 2001, IAEA 1997). This experiment was a proof test for HTR MODUL reference fuel. Four full size spherical fuel elements were irradiated in four independently gas swept cells. A typical reactor temperature history was simulated in the test with 17 temperature cycles (corresponding to 17 passes through the core). For one third of a cycle, the fuel sphere center temperature was held at 800 °C, and for two thirds of a cycle, the center temperature was 1000 °C. In addition, three temperature transients (sphere center temperature held at 1200 °C for five hours) were performed at beginning of life, middle of life and end of life. Limited configuration and irradiation data are given in the following tables (this experiment was conducted at the end of the German program and full experimental documentation could not be located). There were no particle failures reported as a result of the irradiation.

Table 3-88. HFR-K6 Configuration.

Number of cells	4
Number of fuel spheres	4
Spherical fuel element diameter	60 mm
Fuel type	LEU UO_2 - TRISO
U-235 enrichment	10.6%
Number of particles per spherical fuel element	14,600

Table 3-89. HFR-K6 Irradiation Data.

Start date	1990			
End date	May 4, 1993			
Duration (full power days)	634			
Cell	1	2	3	4
Burnup (%FIMA)	7.2	9.3	9.7	9.2
Fast fluence (10^{25} m^{-2}, E > 0.10 MeV)	3.2	< 4.8	4.8	< 4.8
Temperature	cycled	cycled	cycled	cycled
EOL Kr-85m R/B	$\leq 3 \times 10^{-7}$	$\leq 3 \times 10^{-7}$	$\leq 3 \times 10^{-7}$	$\leq 3 \times 10^{-7}$

HFR-K5

The HFR-K5 capsule was irradiated at the High Flux Reactor in Petten, Holland (Conrad 2001, IAEA 1997). This experiment was a proof test for HTR-500 reference fuel. Four full size spherical fuel elements were irradiated in four independently gas swept cells. A typical reactor temperature history was simulated in the test with 17 temperature cycles (corresponding to 17 passes through the core). For one third of a cycle, the fuel sphere center temperature was held at 800 °C, and for two thirds of a cycle, the center temperature was 1000 °C. In addition, three temperature transients (sphere center temperature held at 1200 °C for five hours) were performed at beginning of life, middle of life and end of life. Limited configuration and irradiation data are given in the following tables (this experiment was conducted at the end of the German program and full experimental documentation could not be located). There were no particle failures reported as a result of the irradiation.

Table 3-90. HFR-K5 Configuration.

Number of cells	4
Number of fuel spheres	4
Spherical fuel element diameter	60 mm
Fuel type	LEU UO_2 - TRISO
U-235 enrichment	10.6%
Number of particles per spherical fuel element	14,600

Table 3-91. HFR-K5 Irradiation Data.

Start date	1991			
End date	May 16, 1994			
Duration (full power days)	564			
Cell	1	2	3	4
Burnup (%FIMA)	6.7	8.8	9.1	8.7
Fast fluence (10^{25} m^{-2}, E > 0.10 MeV)	2.9	< 4.3	4.3	< 4.3
Temperature	cycled	cycled	cycled	cycled
EOL Kr-85m R/B	$\leq 3 \times 10^{-7}$	$\leq 3 \times 10^{-7}$	$\leq 3 \times 10^{-7}$	$\leq 3 \times 10^{-7}$

3.4. SUMMARY AND DISCUSSION

Irradiation Performance

Numerous in-pile irradiation experiments have been conducted in both the U.S. and Europe as part of the U.S. and German TRISO-coated particle fuel development efforts. These irradiations were conducted at a variety of burnups, temperatures, and fluences. The rate of accumulation of burnup and fast fluence (i.e., the degree of acceleration) in the irradiation relative to that expected in the reactor is also an important parameter. Note that for most of these fuels, the time to reach goal burnup and fast fluence is ~ 1095 days (3 years) whereas in the irradiations the time to reach peak conditions were accelerated by factor of 2 to 10. A summary of salient features of the irradiations is found in Table 3-92.

Figure 3-24 compares the beginning of life Kr-85m R/B for German and U.S. irradiations discussed earlier in this section. This measurement was selected as a metric of as-manufactured quality. Other measures were considered but were discarded because in some cases the measurements of defect level in U.S. fuel were measured at the particle stage prior to compacting or were not reported consistently in all U.S. irradiations (e.g. TRIGA R/B). The Kr-85m R/B is a function of irradiation temperature, but this dependency is much smaller than the overall variation shown in the figure. The results show that German fuel had consistently lower initial defects than the U.S. fuel in the 1980s and further that it improved over that time as was the case for fuel used in AVR; in fact the lowest ever R/B measured in an in-reactor irradiation is from German fuel (~ 10^{-10}). The initial defect level in U.S. fuel was much higher and showed great variability in the time from 1970-1980. The level did not significantly change until the early 1990s when serious effects at reduction of initial contamination were undertaken in the fabrication campaign. Unfortunately, those very low levels of contamination were followed by in-reactor fuel failures at the percent level.

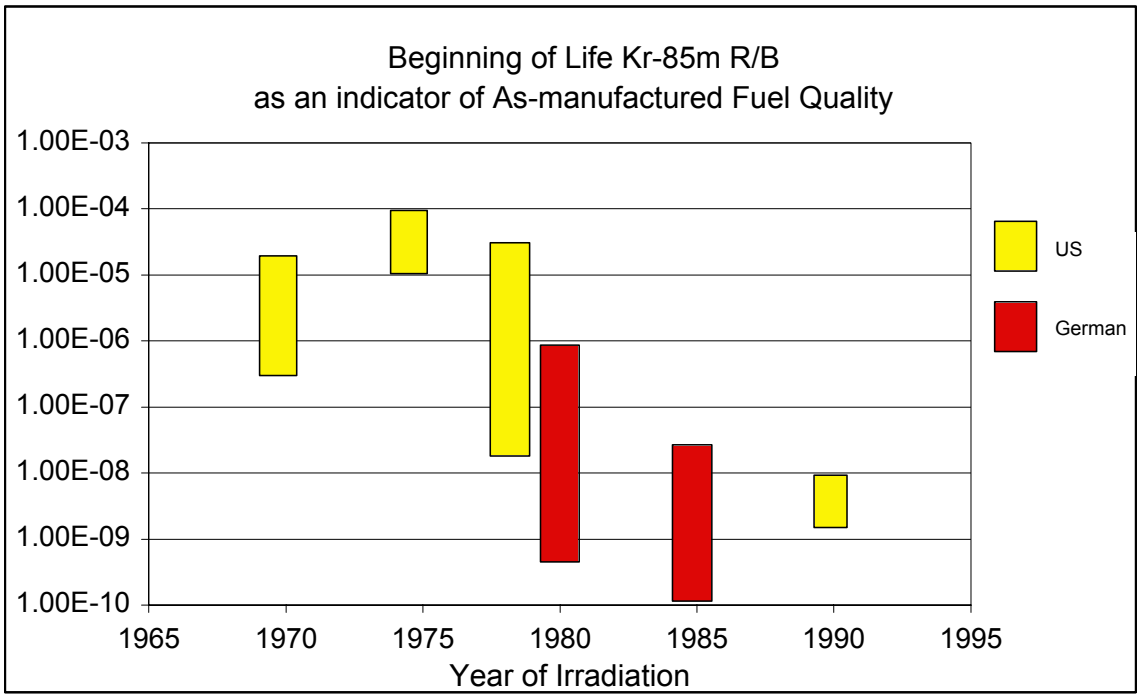

Figure 3-24. Comparison of BOL Kr-85m R/B from German and U.S. irradiations.

Our detailed review indicates that the U.S. and German irradiation programs were implemented quite differently with very different results. The German program's focus was on UO_2-TRISO fuel for AVR/THTR and all future designs such as HTR Modul, whereas the U.S. program examined many different variants (different coatings, different kernels). In fact, comparing only the irradiations of reference modern fuel forms for each country –UCO irradiations in the US and UO_2 irradiations in Germany – highlights the limited performance data available on UCO TRISO-coated particle fuel in the U.S. relative to UO_2 in Germany. Figure 3-25 presents the maximum on-line Kr-85m release to birth ratio (R/B) measured in the U.S. and German irradiations. (In most cases, the maximum R/B was measured at the end of life, however, in some irradiations, the final portion of the experiment was conducted at lower temperatures which caused the R/B to decrease. The R/B results indicate that the German fuel exhibits about a factor of 1000 less fission gas release under irradiation than U.S. fuel under a broad range of conditions (temperature, burnup, fluence)

More detailed plots of the R/B in the German and U.S. irradiations as functions of burnup, temperature and fast fluence in Figure 3-26 reveal no systematic trend.

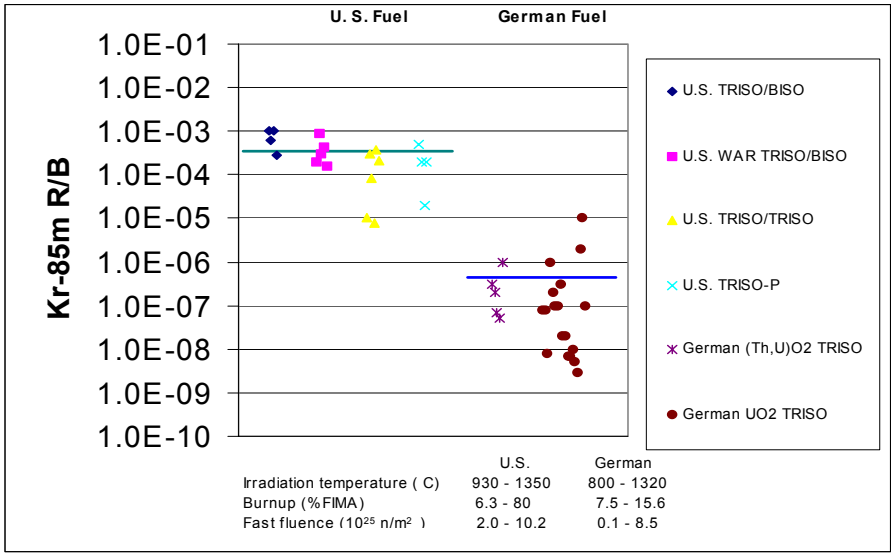

Figure 3-25. Comparison of-end-of-life Kr-85m R/B from historic German and U.S. irradiations.

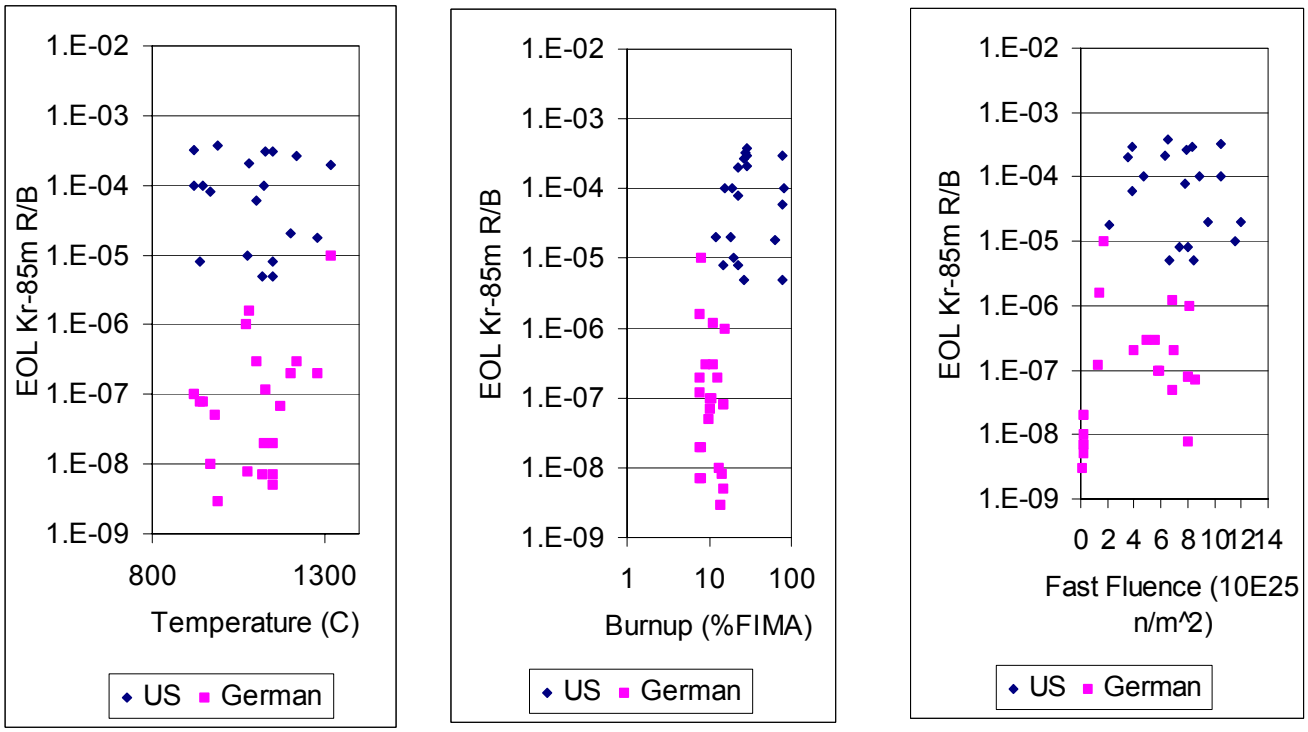

Figure 3-26. Comparison of end-of-life Kr-85m release to birth ratios (R/B) for German and U.S. fuel irradiations as functions of temperature, burnup, and fast fluence.

Furthermore, the results from the postirradiation examinations confirm the more extensive and more reliable gas release data. German fuel is excellent. Out of about 380,000 UO_2 and 80,000 $(Th,U)O_2$ particles tested there were no in-pile and more reliable failures and only a few "damaged" particles due to experimental anomalies. Gas release was attributed only to as-manufactured defects and heavy metal contamination. By contrast, percent level failures of fuel and in many cases very high levels of failures of individual layers of the TRISO-coated particles were observed following irradiation of U.S. fuel in most experiments. Figure 3-27 presents the layer failures observed during postirradiation examination of U.S. coated particle fuel. The values in the figure represent the maximum observed layer failure across all batches in the experiment. The lack of a bar in the figure in most cases signifies that no data were tabulated for that layer. In rare instances, no failures were observed.

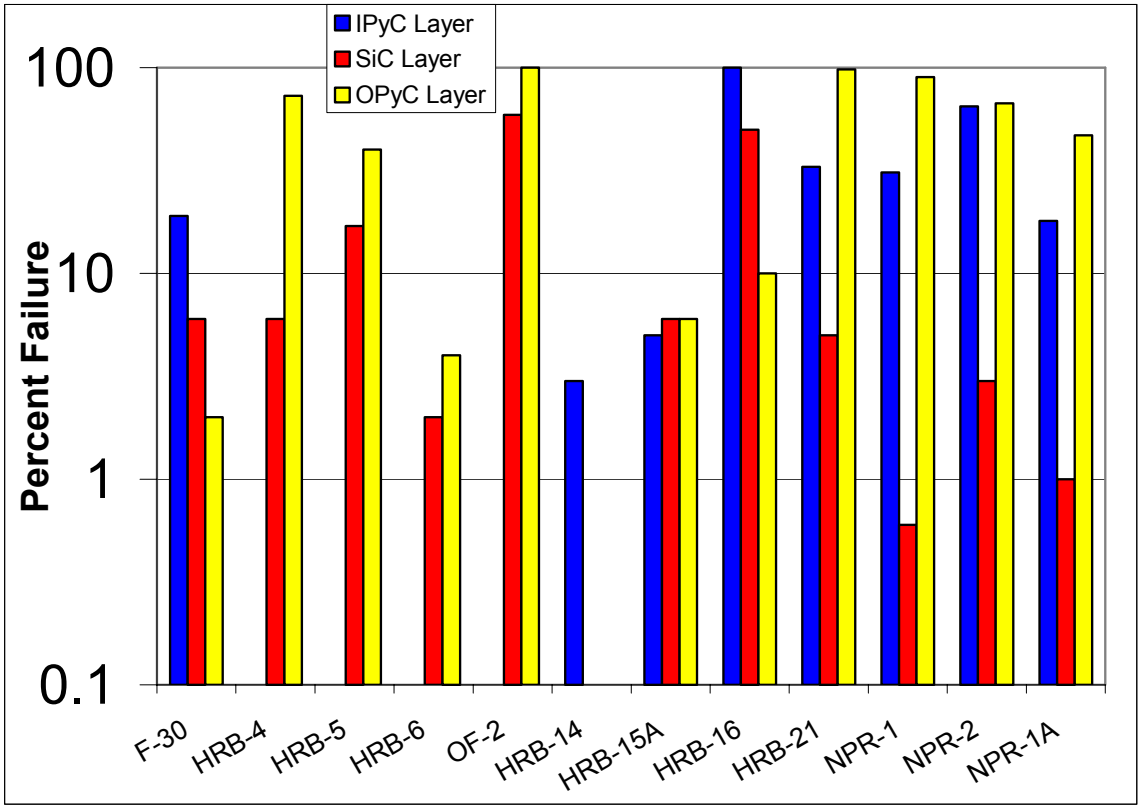

Figure 3-27. Failures observed during postirradiation examination of U.S. coated particle fuel over the past 25 years.

Detailed review of the U.S. irradiation database indicates a number of different failure mechanisms of the individual layers of the TRISO coating contributed to the less than satisfactory U.S. fuel performance. Failures of the coating layers were attributed to: (a) pressure vessel failure (b) kernel migration (amoeba effect), (c) fission product attack of the SiC layer, (d) irradiation-induced IPyC

cracking and/or debonding leading to cracking in the SiC layer, and (e) matrix-OPyC interaction and irradiation-induced OPyC failure. The PyC related mechanisms are strongly related to the anisotropy and porosity in the coatings. The anisotropy has a strong influence on the shrinkage and swelling behavior of the PyC layers under irradiation. However, the anisotropy measurements, especially optical methods (OPTAF), are not reliable predictors of PyC failure under irradiation as indicated by the lack of correlation between the measured BAF and PyC failure (e.g., OF-2, HRB-5, HRB-6), and the high level of PyC failure observed in most irradiations. As discussed in Section 5, the porosity of the layer has an impact on the strength of the interfacial bond between the SiC and PyC.

Fission product and impurity attack of the SiC and kernel migration are thermally driven phenomena that are strongly influenced by burnup, temperature, and the temperature gradient across the particle. The temperature gradient is a strong function of the power density in the fuel body.

A U.S. fuel compact has a higher packing fraction of particles (up to 50%) than German pebbles (~10%). The U.S. core design uses a higher fuel power density than the German fuel designs. This difference required more severe testing conditions for the U.S. fuel. In addition, as shown in Table 3-92, the U.S. irradiations were accelerated 3 to 10 times real time compared to the 2 to 3 times level of acceleration used for most of the German irradiations. Thus, some of the phenomena that were observed in U.S. irradiations may be related to the more demanding U.S. core design and to the accelerated nature of the irradiation. These differences in power density in each reactor drove the fuel designs. The Germans could use oxide fuel with little threat to fuel integrity by kernel migration or fission product attack because of the lower temperatures and temperature gradients in the fuel. By contrast, the US prismatic design with its high fuel operating temperature and power density (and resulting higher temperature gradient) resulted in the development of UCO kernel to minimize kernel migration and fission product mobility in the fuel. Had the U.S. and German irradiations been conducted under similar conditions, the disparity in results may have been less but these differences certainly cannot entirely account for the factor of 1000 in performance indicated in Figure 3-25.

Table 3-92. Summary of Particle Fuel Irradiation Experiments.

Test/cell	Fuel forms	Irrad.time (d)/ Accel. Level	Peak temp. (°C)	Peak fissile & fertile burnup (%FIMA)	Peak fluence (10^{25} n/m^2)	EOL Kr-85m R/B (10^{-6})
U.S. Experiments						
F-30/1	HEU (Th,U)C_2 TRISO & ThC_2 TRISO	269/4x	1100	15.0 / 3.0	8.0	8
F-30/2			1100	19.0 / 4.5	10.5	100
F-30/3			1120	20.0 / 5.0	11.5	10
F-30/4			1100	18.0 / 4.0	9.5	20
F-30/5			1200	12.0 / 1.5	12.0	20
HRB-4	LEU WAR UC_2 TRISO & ThO_2 BISO	244/4.5x	1250	27.7 / 13.4	10.5	320
HRB-5	LEU WAR UC_2 TRISO & ThO_2 BISO	107/10x	1250	15.7 / 4.3	4.7	100
HRB-6	HEU (Th,U)C_2 TRISO & ThO_2 BISO	183/6x	1100	26.6 / 9.3	7.9	270
OF-2/1	WAR UCO UC_2 (Th,U)O_2 TRISO & ThO_2 BISO	352/3x	1350	79.6 / 4.3	8.9	100
OF-2/2			1350	79.5 / 4.3	8.4	5
HRB-14	LEU UCO UO_2 (Th,U)O_2 TRISO & ThO_2 BISO	214/5x	1190	28.6 / 8.5	8.3	300
HRB-15B	LEU UCO UC_2 (Th,U)O_2 UO_2 TRISO and Si BISO & ThO_2 TRISO, BISO, and Si-BISO	169/6.5x	915	26.7 / 6.0	6.6	5
R2-K13/2	LEU UCO TRISO & ThO_2 TRISO	517/2x	1190	22.5 / 4.6	7.8	80
R2-K13/3			985	22.1 / 4.5	7.4	8
HRB-15A	LEU UCO UC_2 UO_2 TRISO and ZrC-TRISO & ThO_2 TRISO and Si-BISO	174/6.3x	1150	29.0 / 6.4	6.5	380
HRB-16	LEU UCO UC_2 UO_2 (Th,U)O_2 TRISO and ZrC-TRISO & ThC_2 ThO_2 TRISO and BISO	170/6.3x	1150	28.7 / 6.1	6.3	210
HRB-21	LEU UCO & ThO_2 TRISO-P	105/10x	1300	22.0 / 2.2	3.5	200
NPR-1	HEU UCO TRISO-P	170/6.3x	1240	79.0	3.8	300
NPR-2	HEU UCO TRISO-P	172/6.3x	1030	79.0	3.8	60
NPR-1A	HEU UCO TRISO-P	64/6.3x	1220	64.0	2.1	18
German Experiments						
R2-K12/1	HEU (Th,U)O_2 TRISO	308/3x	1100	11.1	5.6	0.300
R2-K12/2			1280	12.4	6.9	0.200
R2-K13/1	HEU (Th,U)O_2 TRISO	517/2x	1170	10.2	8.5	0.070
R2-K13/4			980	9.8	6.8	0.050
BR2-P25	HEU (Th,U)O_2 TRISO	350/3x	1070	15.6	8.1	1.000
HFR-P4/1	LEU UO_2 TRISO	351/3x	940	14.7	8.0	0.080
HFR-P4/2			945	14.9	8.0	0.080
HFR-P4/3			1075	14.0	8.0	0.008
SL-P1	LEU UO_2 TRISO	330/3x	794	11.3	6.8	1.200
HFR-K3/1	LEU UO_2 TRISO	359/3x	1200	7.5	4.0	0.200
HFR-K3/2			920	10.0	5.8	0.100
HFR-K3/3			920	10.6	5.9	0.100
HFR-K3/4			1220	9.0	4.9	0.300
FRJ2-K13/1	LEU UO_2 TRISO	396/2.75x	1125	7.5	0.2	0.020
FRJ2-K13/2			1150	8.0	0.2	0.020
FRJ2-K13/3			1150	7.9	0.2	0.007
FRJ2-K13/4			1120	7.6	0.2	0.007
FRJ2-K15/1	LEU UO_2 TRISO	533/2x	970	13.2	0.2	0.010
FRJ2-K15/2			1150	14.6	0.2	0.005
FRJ2-K15/3			990	13.9	0.1	0.003
FRJ2-P27/1	LEU UO_2 TRISO	232/4.7x	1080	7.6	1.4	1.600
FRJ2-P27/1			1320	8.0	1.7	10.000
FRJ2-P27/1			1130	7.6	1.3	0.120
HFR-K5/1	LEU UO_2 TRISO	563/2x	Cycled Proof Test	6.7	2.9	<0.3
HFR-K5/2				8.8	<4.3	<0.3
HFR-K5/3				9.1	4.3	<0.3
HFR-K5/4				8.7	< 4.3	<0.3
HFR-K6/1	LEU UO_2 TRISO	634/1.7x	Cycled Proof Test	7.2	3.2	<0.3
HFR-K6/2				9.3	< 4.8	<0.3
HFR-K6/3				9.7	4.8	<0.3
HFR-K6/4				9.2	<4.8	<0.3

Note: U.S. fluence is for E > 0.18 MeV and German fluence is for E > 0.10 MeV.

4. HIGH TEMPERATURE ACCIDENT PERFORMANCE

4.1. Introduction

The release of fission products from TRISO-coated irradiated fuels heated to elevated temperatures to simulate accident conditions is reviewed. For a small high temperature gas cooled reactor, the temperature evolution during a loss of coolant accident with complete depressurization is calculated to reach 1600 °C (including a 100° C uncertainty margin) for a duration of about 30 hours, as shown in Figure 4-1. The preponderance of the experimental data is from tests with fuels of German manufacture, but insights are also provided by a few experiments using U.S. and Japanese fuels. There is some evidence of particle failure by internal pressure (pressure vessel failure), but of most interest is degradation of the SiC layer in the TRISO coating during accident performance testing at elevated temperatures. Results of testing in the temperature ranges 1500-1800°C are discussed first, followed by testing at higher temperatures. Releases of cesium are sensitive to the integrity of the SiC layer so much attention is paid to this fission product. Releases of krypton are sensitive to pressure vessel failure, but otherwise trail releases of cesium due to holdup by PyC layers. Releases of other fission products such as strontium, europium, and cerium are treated where data are available. Silver, although not a safety concern due to its low yield, has potential consequences for reactor maintenance, and diffuses readily through the SiC layer, even at 1200°C. The influences of irradiation characteristics (fuel burnup, neutron fluence, irradiation temperature), SiC microstructure (grain size and orientation), and fuel fabrication processes (SiC coating rate) on fission product release are investigated.

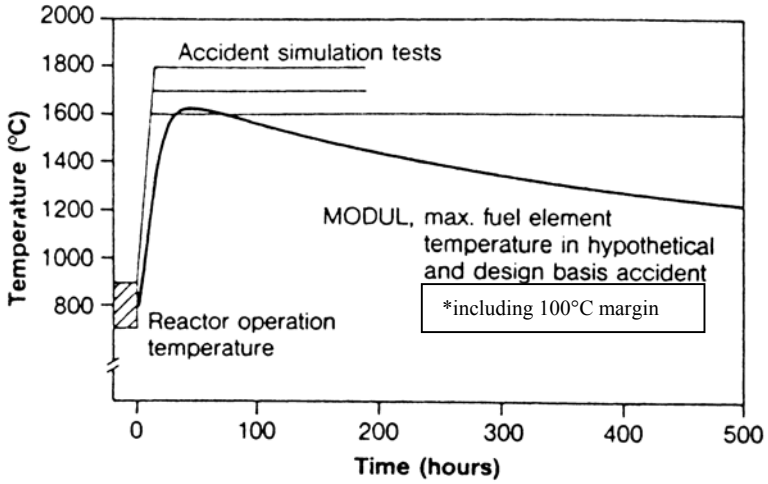

Figure 4-1. Temperature evolution during a depressurized reduction cooling of a small HTR, and in heating tests with irradiated fuel elements.

4.2 Accident testing at 1500-1800°C

U.S. Results

One of the few U.S. contributions to the accident performance literature is (Bullock 1984) in which fission product releases are reported after anneals at 1200, 1350, and 1500°C for UO_2, UC_2, UCO, and UO_2*(1) and UO_2*(2) fuel particles irradiated in the HRB-15B capsule in HFIR. In the UO_2*(1) fuel the kernel was coated with a ZrC layer and, in the UO_2*(2) fuel, ZrC was dispersed in the buffer layer surrounding the kernel. The fuel burnup was in the range 21-25 %FIMA and the fast neutron fluence was in the range 3.4-5.5 x 10^{25} n/m^2. The irradiation was quite accelerated with a residence time of 169 effective full power days at 100 MW reactor power. Only the fission product release data at 1500°C are discussed here, as cesium was not released at the lower temperatures. No fission product releases were measured at any temperature from UO_2*(1) fuel particles. Ten particles of each fuel type were annealed for 11,866 hours at 1500°C. Integral releases for each 10-particle batch were measured from individual particles by gamma counting each particle before and after the test and, as a function of time, by periodic gamma monitoring of fission product collectors during the anneal. The agreement of the integral releases from each 10-particle batch by these two methods was excellent.

Cesium was released from only the UO_2 and UC_2 fuel particles as is shown in Figure 4-2. These same two fuel batches released the greatest fractions of silver as illustrated in Figure 4-3. The time signatures of the releases of cesium and silver from the UO_2 fuel particles in Figures 4-2 and 4-3 indicate a diffusion release mechanism through the SiC layer. However, the release of cesium from the UC_2 fuel batch is sudden in Figure 4-2 and the release of silver shows a rapid increase at the same time as the sudden release of cesium, as indicated in Figure 4-4. The distribution of fission product releases among particles within the fuel batches in Table 4-1 indicate that the release of cesium from the UO_2 fuel particles is from two of the ten particles and from only one particle in the UC_2 fuel batch. This same table shows that the release of silver was 100% from the UO_2 fuel batch, and 82% from the UC_2, with 6 of the 10 UC_2 particles releasing 100% of their silver inventories, 2 particles releasing 85-95%, 1 particle releasing 50%, and 1 particle retaining 100%. Particle-to-particle variations in fission product release are the norm in the data of Table 4-1.

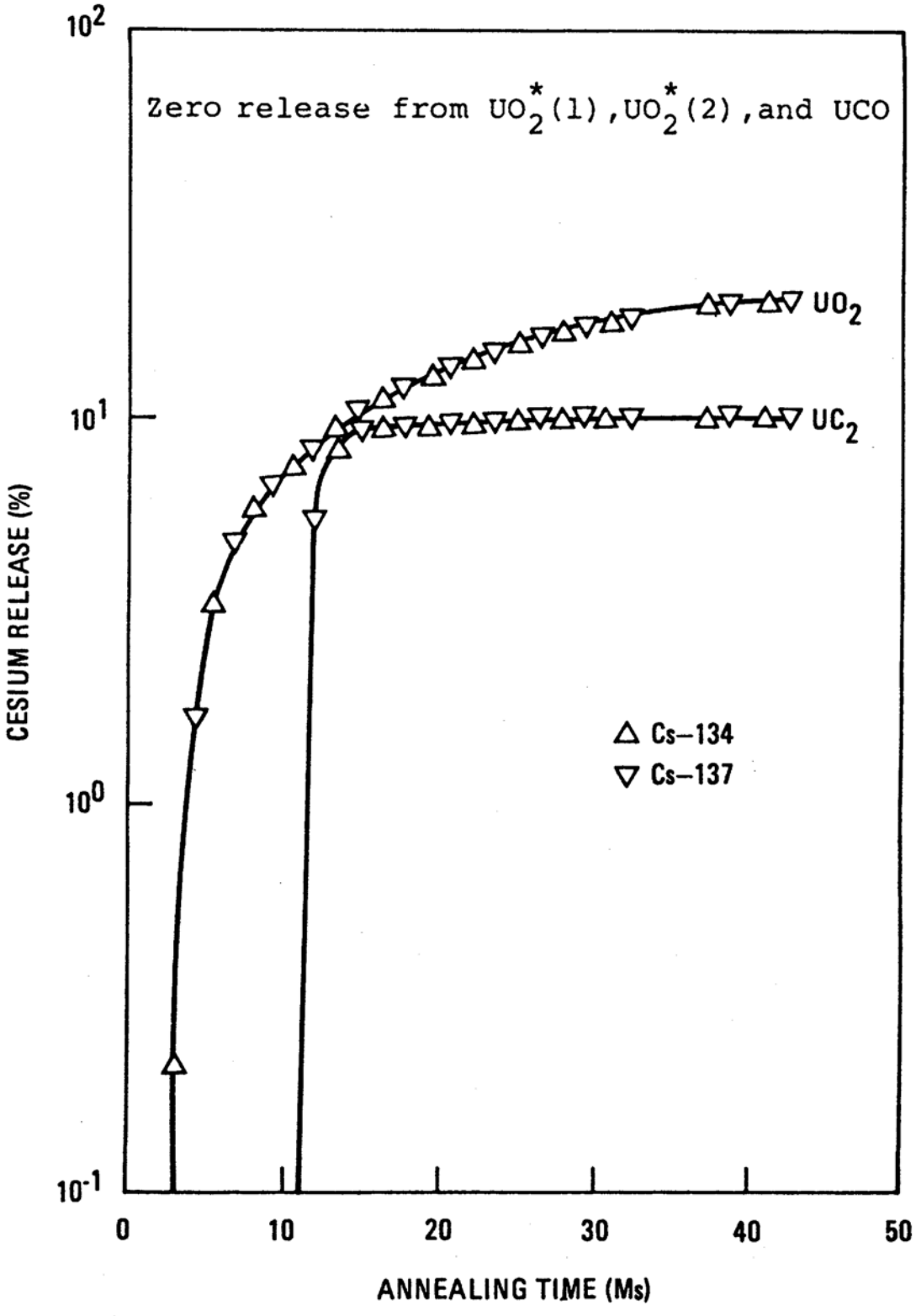

Figure 4-2. Release of Cs from various types of TRISO-coated fuel particles at 1500ºC.

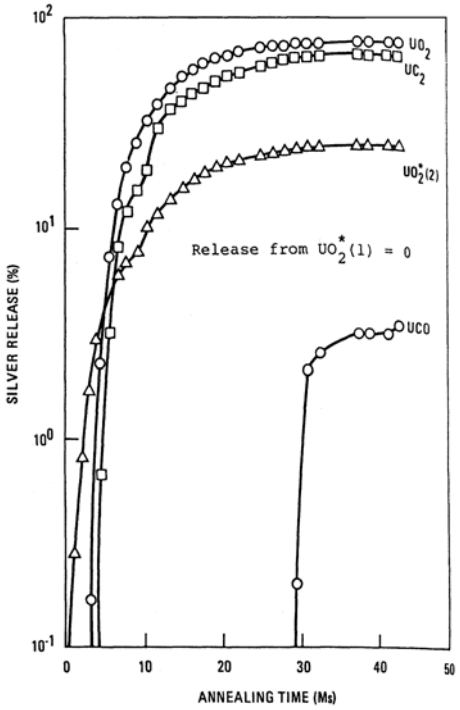

Figure 4-3. Release of ^{110}Ag from various types of TRISO-coated fuel particles at 1500ºC.

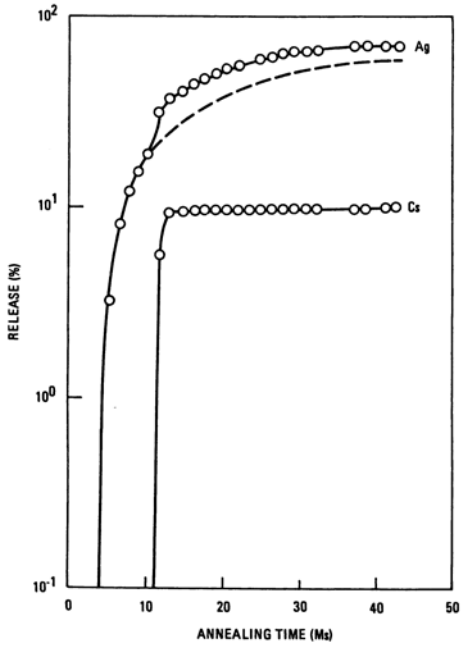

Figure 4-4. Abrupt 10% increase in ^{110}Ag release from UC_2 particles at 1500ºC when one of the ten test particles released its entire Cs inventory.

Table 4-1. Distribution of fission-product release within particle batches during postirradiation annealing.

Annealing Temperature ºC	TRISO particle type a)	Release Breakdown from the 10 particles within a test batch for: Cs-134 Cs-137	Ag-110m	Eu-154	Ce-144
1500	UC_2	9 = 0% 1 = 99% 10 = 12%	1 = 0% 1 = 50% 85%<2<95% 6 = 100% 10 = 82%	15%<5<25% 45%<3<55% 2 = 100% 10 = 46%	12%<3<18% 18%<3<25% 70%<3<80% 1 = 99% 10 = 45%
1500	UO_2	8 = 0% 2 = 99% 10 = 24%	10 = 100%	Uniform release of 16%	10 = 0%
1500	$UC0_4O_{1.6}$	10 = 0%	7 = 0% 10%<3<20% 10 = 3%	Uniform release of 37%	10 = 1%b))
1500	UO_2*(2)	10 = 0%	7 = 0% 70%<3<80% 10 = 27%	2 = 0% 0%<5<10% 15%<3<25%	10 = 0%
1350	$UC0_4O_{1.6}$	10 = 0%	10 = 0%	Uniform release of 23%	10 = 0%
1350	UO_2*(2)	10 = 0%	7 = 0% 45%<3<55% 10 = 19%	10 = 4% b)	10 = 0%
1200	$UC0_4O_{1.6}$	10 = 0%	10 = 0%	Uniform release of 6%	10 = 0%
1200	UO_2*(2)	10 = 0%	10 = 2% b)	10 = 0%	10 = 0%

a) There was zero release within about ± 5% as determined from individual particle counting before and after annealing for all isotopes from each of the 10 particles in all test combinations not listed, i.e., UO_2*(1) at all temperatures, and UC_2, UO_2, and $UC0_4O_{1.6}$ at 1350 and 1200ºC. Since no release on collectors was detected at the 0.01% level from the combined 10 particles within each of these test batches, it can be assumed that release from any one of these particles was certainly less than 0.01% and was probably not more than 0.001%

b) These total releases from 10 particles were too small and too uniformly distributed among particles to allow the determinations of individual release values.

The microstructures in Figure 4-5 show that the SiC layer in the UO_2 batch exhibits large columnar grains, whereas the UCO batch exhibits a strong laminar grain structure in the SiC. The UC_2 and UO_2*(1) batches exhibit laminar structures in the SiC that are somewhat weaker than in the UCO batch. The results in Table 4-1 indicate that silver release at 1500°C is greatest (100%) in the case of columnar SiC, least (3%) for strongly laminar SiC, and intermediate (82%) for somewhat less strong laminar SiC. Although Cs was released from only three particles of the 50 particles annealed at 1500°C, two of these particles had columnar SiC and one had a somewhat weak laminar SiC. The sensitivity of cesium release to SiC grain structure was recognized in (Myers 1984) where the diffusivity of cesium through columnar SiC was given as an order of magnitude greater than through laminar SiC. The diffusion equations of (Myers 1984) are accessible in Table A-3 of (IAEA 1997).

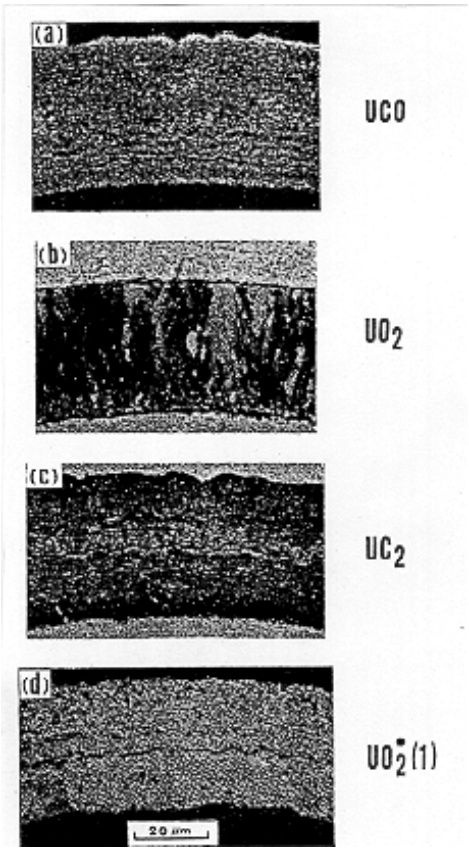

Figure 4-5. Microstructures of etched SiC barrier layers in various types of TRISO-coated particles.

As shown in Figure 4-6, releases of europium are greatest (37-46%) for the fuel batches containing UC_2 in the kernel, compared with fuel batches containing only UO_2 in the kernel (9-16%). As shown in Table 4-1, cerium release is 45% in UC_2, only about 1% in UCO, and nil in UO_2 particles. These behaviors are related to the thermodynamics of rare-earth oxides and carbides according to (Homan et al. 1977) where oxides formed in UO_2 (such as Eu_2O_3 and Ce_2O_3) are less likely to escape from the kernel than are the more mobile rare-earth carbides formed in UC_2. In UCO, europium forms a carbide and cerium forms an oxide (Homan et al. 1977).

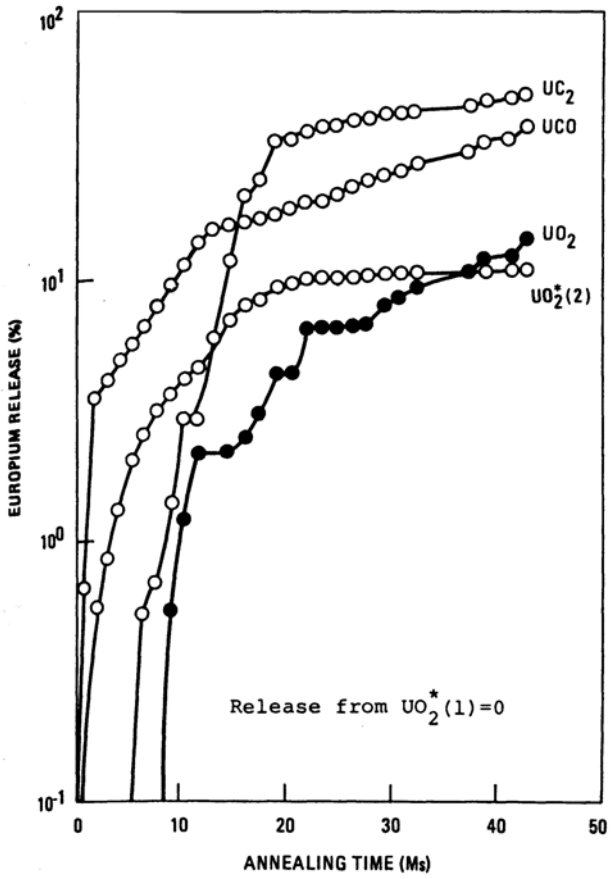

Figure 4-6. Release of ^{154}Eu from various types of TRISO-coated fuel particles of 1500ºC.

In summary, the work of (Bullock 1984) with admittedly relatively few particles, indicates that under a long annealing time at 1500°C, (a) silver and cesium releases are at a maximum in the case of SiC with a columnar grain structure, (b) europium releases are largest in UC_2 fuels, but can be significant in UCO and, to a lesser extent, in UO_2 fuels, and (c) cerium release is significant only in UC_2 fuel.

German Results

The safety tests carried out by the Germans were performed primarily on whole spherical fuel elements containing approximately 16,000 fuel particles and in some cases on fuel compacts containing approximately 1,600 fuel particles. Irradiation data (Schenk et al. 1990, Schenk and Nabielek 1991, and IAEA 1997) are presented in Table 4-2 for spherical fuel elements (60 mm in diameter) and in Table 4-3 for compacts (cylinders manufactured from spherical elements with a fuel zone 20 mm in diameter). These two tables also contain the maximum integral fractional releases of krypton and cesium measured during the heating tests. The spherical fuel elements listed in Table 4-2 all experienced burnup and fluence within the historic pebble bed burnup and fluence envelope (9%FIMA and 2.2 x 10^{25} n/m^2), with the exception of HFR-K3/3 (10.6%FIMA and 6.0 x 10^{25}

n/m^2), AVR 82/20 (8.6%FIMA and 2.4 x 10^{25} n/m^2), and AVR 82/9 (8.9%FIMA and 2.5 x 10^{25} n/m^2). In contrast, all the compacts were irradiated beyond the PBMR envelope.

Table 4-2. Results of accident simulation tests with irradiated spherical fuel elements.

Fuel Element	Burnup (%FIMA)	Fast Fluence (10^{25} n/m^2)	Heating Test		Fractional Release	
			Temp. (ºC)	Duration (h)	^{85}Kr	^{137}Cs
AVR 71/22	3.5	0.9	1600	500	4×10^{-7}	2×10^{-5}
HFR-K3/1	7.5	4.0	1600	500	2×10^{-6}	1×10^{-4}
FRJ-K13/2	8.0	0.1	1600	160	6×10^{-7}	4×10^{-5}
AVR 82/20	8.6	2.4	1600	100	2×10^{-7}	6×10^{-5}
AVR 82/9	8.9	2.5	1600	500	5×10^{-7}	8×10^{-4}
AVR 74/11	6.2	1.6	1700	185	3×10^{-5}	8×10^{-5}
FRJ-K13/4	7.6	0.1	1600 1800	138 100	3×10^{-7} 7×10^{-5}	3×10^{-6} 1×10^{-2}
HFR-K3/3	10.6	6.0	1800	100	7×10^{-4}	6×10^{-2}
AVR 76/18	7.1	1.9	1800	200	1×10^{-4}	5×10^{-2}
AVR 74/10	5.5	0.9	1800	90	2×10^{-3}	1×10^{-1}
AVR 70/33	1.6	0.4	1800	175	2×10^{-3}	2×10^{-2}

Table 4-3. Results of accident simulation tests at 1600-1800ºC with irradiated fuel compacts.

Fuel Compact	Irradiation Conditions			Heating Test		Fractional Release	
	Burnup (%FIMA)	Fast Fluence (10^{25} n/m^2)	Temp. (ºC)	Temp.(ºC)	Duration (h)	^{85}Kr	^{137}Cs
HFR-P4/ 3/ 7	13.9	7.5	1075	1600	304	1×10^{-3}	4×10^{-3}
HFR-P4/ 1/ 8	13.8	7.2	940	1600	304	5×10^{-5}	2×10^{-3}
HFR-P4/ 2/ 8	13.8	7.2	945	1600	304	8×10^{-5}	1×10^{-3}
HFR-P4/ 1/ 12	11.1	5.5	940	1600	304	5×10^{-7}	3×10^{-4}
SL-P1/ 6	10.7	6.7	800	1600	304	7×10^{-7}	4×10^{-4}
SL-P1/ 10	10.3	6.0	800	1700	304	9×10^{-5}	6×10^{-2}
SL-P1/ 9	10.7	6.3	800	1700	304	4×10^{-5}	1×10^{-1}
HFR-P4/ 3/ 12	12.0	5.5	1075	1800	279	1×10^{-3}	5×10^{-1}

Krypton integral releases as a function of time at various temperatures are shown in Figure 4-7. In Figure 4-7(a), krypton releases are below the level of one particle failure at 1600°C, whereas that level of release is exceeded at 1700 and 1800°C for spherical fuel elements. The occasional vertical lines in the releases at temperatures above 1600°C are associated with pressure vessel failure of particles. Pressure vessel failure is a function of burnup (fission gas inventory and in UO_2 fuel, CO inventory), fuel irradiation temperature, (fission gas pressure and oxygen to fission ratio in UO_2 fuel (Proksch and Strigl 1982)), and fuel particle design and properties (buffer void volume and SiC strength). Figure 4-7(b) shows the larger releases associated with burnups in excess of the traditional

pebble bed envelope. Krypton-85 release can be used as an indicator of iodine-131 release based on reactivation of irradiated fuels immediately before heating tests (Verfondern et al. 1990). Figure 4-7c shows krypton release is negligible (10^{-6}) for compacts with 10-12%FIMA at 1600°C, but becomes significant (10^{-4}) at about 200 hours at 1700°C, and at about 150 hours at 1800°C. Cesium releases as a function of time at temperature are shown in Figure 4-8 where it can be seen, that 5 compacts with burnup in the range 10.7-13.9%FIMA exhibit higher releases than 5 spherical fuel elements with burnup in the range 3.5-8.9%FIMA. The reason for this behavior at conditions beyond the PBMR is not well understood, but has been attributed to increased permeability of SiC irradiated to high fluence and/ or burnup (related perhaps to fission product attack during postirradiation heatup as discussed later).

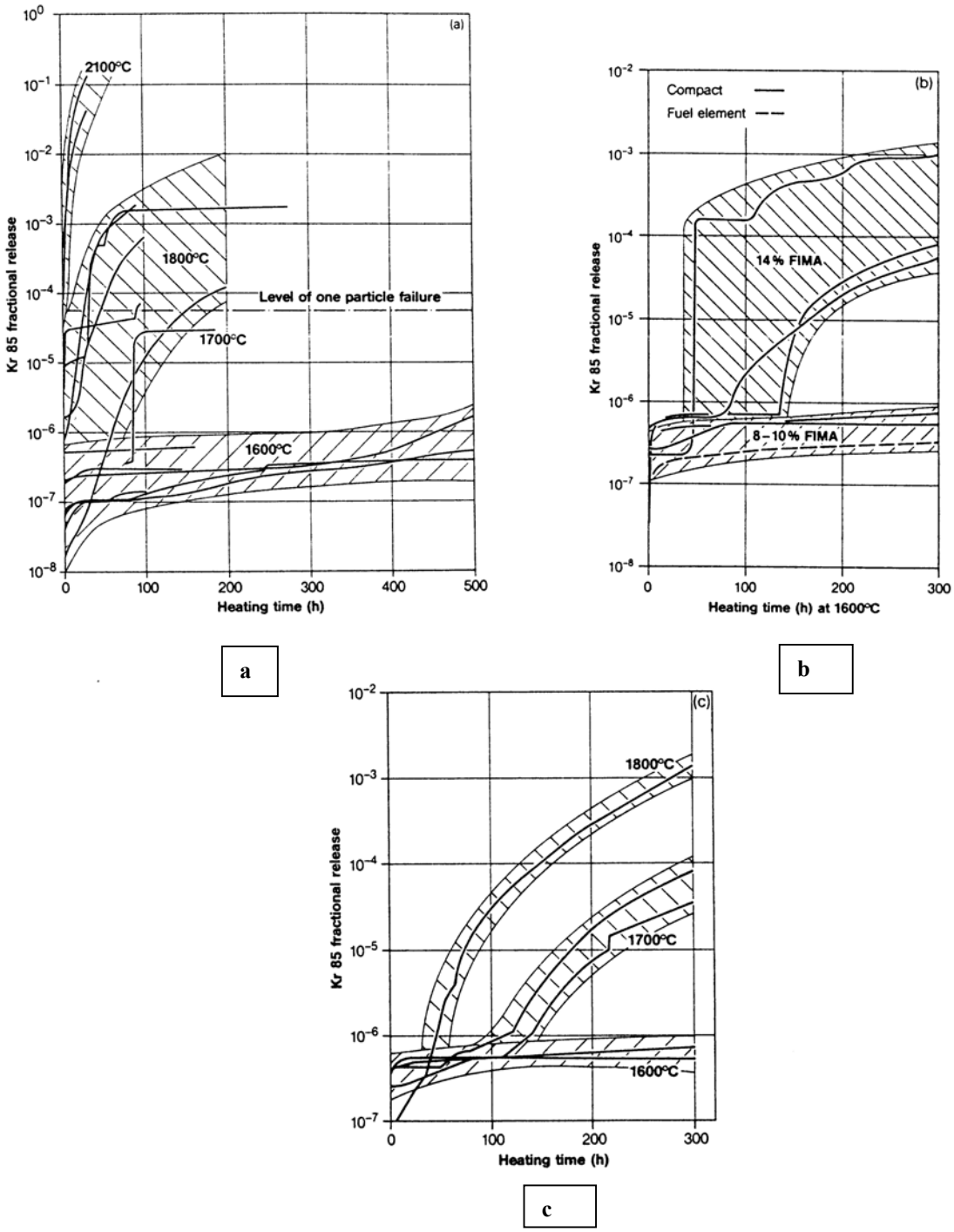

Figure 4-7. Accumulated fractional release of ^{85}Kr as a function of heating time at constant temperature. (a) Heating tests with spherical fuel elements at 1600-1800ºC. (b) 1600ºC heating tests with compacts of 8-14%FIMA. (c) 1600-1800ºC heating tests with compacts of 10-12%FIMA.

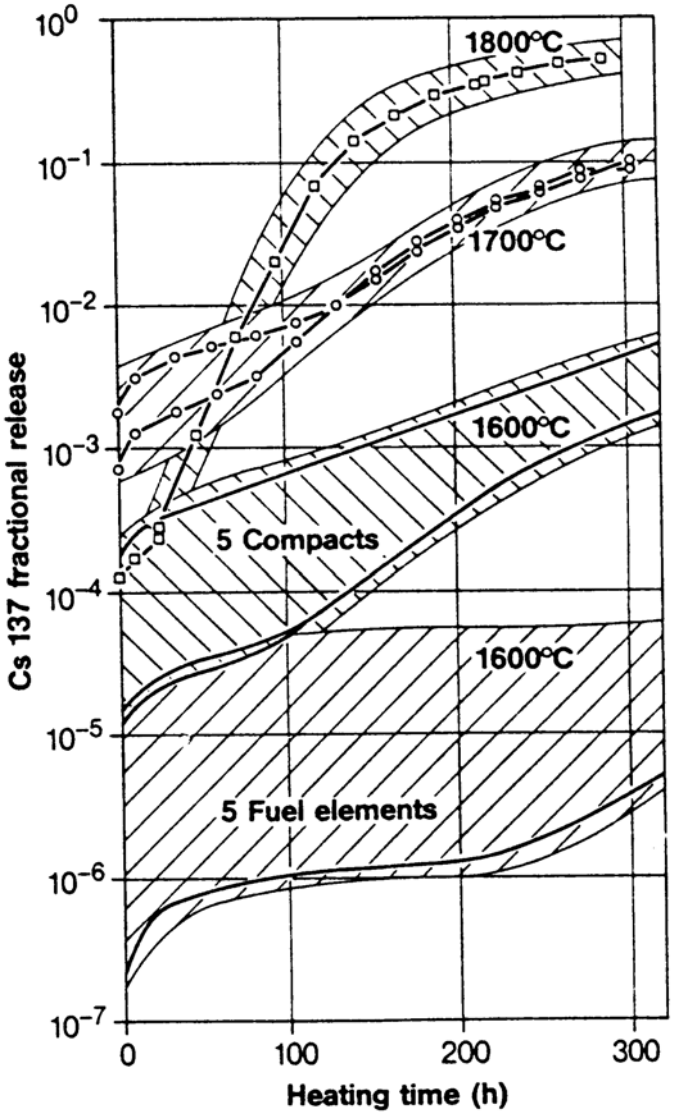

Figure 4-8. Cesium release during heat of spherical fuel elements (1600ºC) and compacts (1600-1800ºC).

Integral fractional releases of silver, cesium, krypton and strontium are shown as a function of time at 1600°C for sphere HFR-K3/1 in Figure 4-9. The release of silver is on the order of 1-2% at the outset of heating as considerable silver was released from fuel particles to the matrix during irradiation at temperatures in the range 1000-1200°C for 358 days. The release of cesium is considerably greater than the release of krypton, which is held up by PyC, and strontium, which is retained in the UO_2 kernel and the graphite matrix to a greater extent than cesium. The distribution of metallic fission products averaged over a number of UO_2 TRISO fuel element spheres examined after accident testing (Schenk and Nabielek 1991) is shown in Table 4-4

Table 4-4. Averaged Fission Product Distribution for Spherical Fuel Elements After Accident Simulation Tests.

Fuel Type	Heating Temp. (°C)	Time at Temp. (h)	Nuclide	Fractional Fission Product Content in:			Fractional Release from Fuel Element
				Kernel	Coating	Matrix [A3-3]	
UO_2 TRISO	1600	Up to 500	^{137}Cs ^{90}Sr ^{110m}Ag	5×10^{-1} 9.5×10^{-1} 8×10^{-1}	5×10^{-1} 5×10^{-2} 2×10^{-1}	$2 \times 10^{-5} \ldots 1 \times 10^{-3}$ $2 \times 10^{-3} \ldots 5 \times 10^{-3}$ 9×10^{-4}	5×10^{-5} 1×10^{-6} $1 \times 10^{-3} \ldots 3 \times 10^{-2}$
UO_2 TRISO	1800	Up to 200	^{137}Cs ^{90}Sr ^{110m}Ag	2×10^{-2} 7×10^{-1} 9×10^{-2}	6×10^{-1} 8×10^{-2} 2×10^{-1}	1.5×10^{-1} 2×10^{-1} 3×10^{-2}	5×10^{-2} 3×10^{-3} 7×10^{-1}
(Th,U) O_2 BISO	2000	5	^{137}Cs ^{90}Sr	1×10^{-2} 5×10^{-2}	3×10^{-1} 2×10^{-2}	$[2 \times 10^{-2}]$[a] $[1 \times 10^{-2}]$	7×10^{-1} 9×10^{-1}
(Th,U) O_2 TRISO	2150	Heatup from 1250°C in 56 h	^{137}Cs	2×10^{-2}	5×10^{-1}	$[3 \times 10^{-2}]$	2×10^{-1}

[a] Brackets denote spheres with A3-3 matrix.

In Figure 4-9, the radial profiles of silver and cesium in the graphite matrix exhibit strong concentration gradients typical of materials which are diffusing, whereas the strontium profile is much more flat, indicating little diffusive release from the matrix. In this same figure, the release of cesium is observed to climb strongly after 200 hours of heating. Cesium release from HEU (Th, U)O_2 TRISO fuel element R2-K13/1, irradiated to 10.2%FIMA and 8.5×10^{25} n/m^2, was 1.5% after 1000 h at 1600°C (Schenk and Nabielek 1991). Ceramographic sections in Figure 4-10 show evidence of increasing degradation in the SiC layer for longer times at 1600°C and higher burnup, the most degraded being the SiC in sphere HFR-K3/1. Microprobe profiles through particles after heating, in Figure 4-11 show the buildup of fission product palladium at the IPyC/SiC interface in spheres HFR-K3/1 and HFR-K3/3. It is hypothesized (Schenk et al. 1990) that corrosion by palladium degrades the SiC leading to accelerated diffusion of cesium through grain boundaries. It has also been hypothesized that palladium attack of SiC occurs via grain boundaries and this hypothesis is being investigated by experiment in a doctoral thesis at MIT (MacLean 2001).

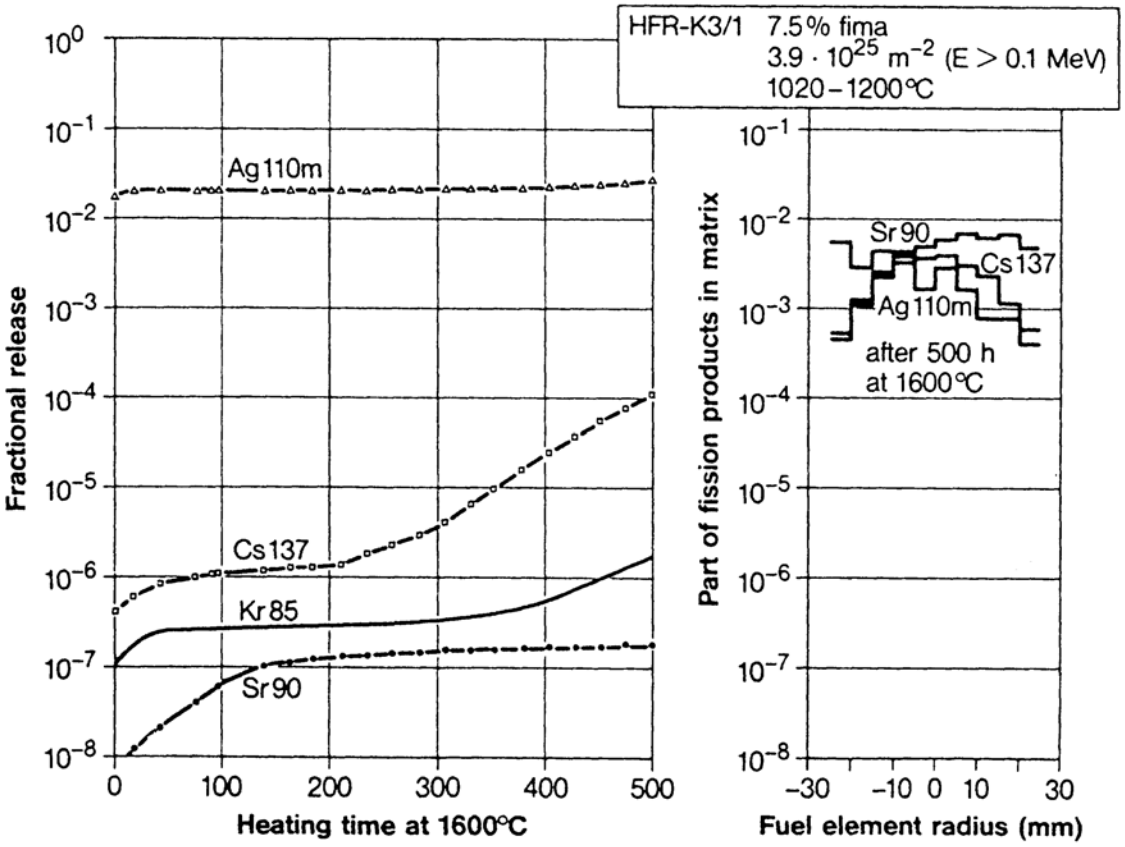

Figure 4-9. Fission product release and distribution in sphere HFR-K3/1 after irradiation at 1000-1200°C C for 359 days and 1600ºC heating.

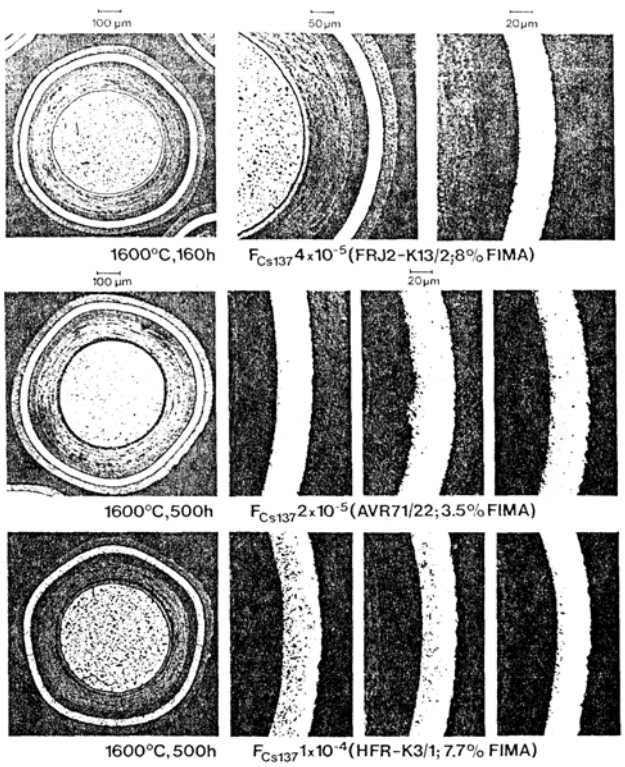

Figure 4-10. Ceramographic sections through particles heated at 1600º (complete particle followed by enlarged views from 3 different particles).

It has been further hypothesized (Schenk et al. 1990) that with grain sizes in SiC of nearly the same dimension as the layer thickness, variations in grain orientation and size may cause random variations in cesium release from particle to particle. Indeed, such variations have been observed in HFR-K3/3 (See Figure 4-11a) by IMGA analysis (Baldwin and Kania 1990), within HEU (Th,U)O_2 TRISO fuel element R2-K13/1 (Schenk and Nabielek 1991), and by (Bullock 1984).

Japanese Results

Individual UO_2-TRISO fuel particles deconsolidated from a compact of Japanese manufacture were heated at 1700°C for 270 hours and 1800°C for 222 hours at ORNL (Minato et al. 2000). The fuel had been irradiated in HFIR in the HRB-22 capsule to a burnup of 4.8%FIMA and a fast neutron fluence of 2.1 x 10^{25} n/m^2 for a duration of 89 EFPD and a time-averaged maximum temperature of 1100°C. Releases of silver, cesium, europium, and krypton were measured as a function of time as shown in Figures 4-12 and 4-13 for batches of 25 particles at each temperature. The krypton release in Figure 4-13 shows that one particle failed early in the heating also releasing antimony.

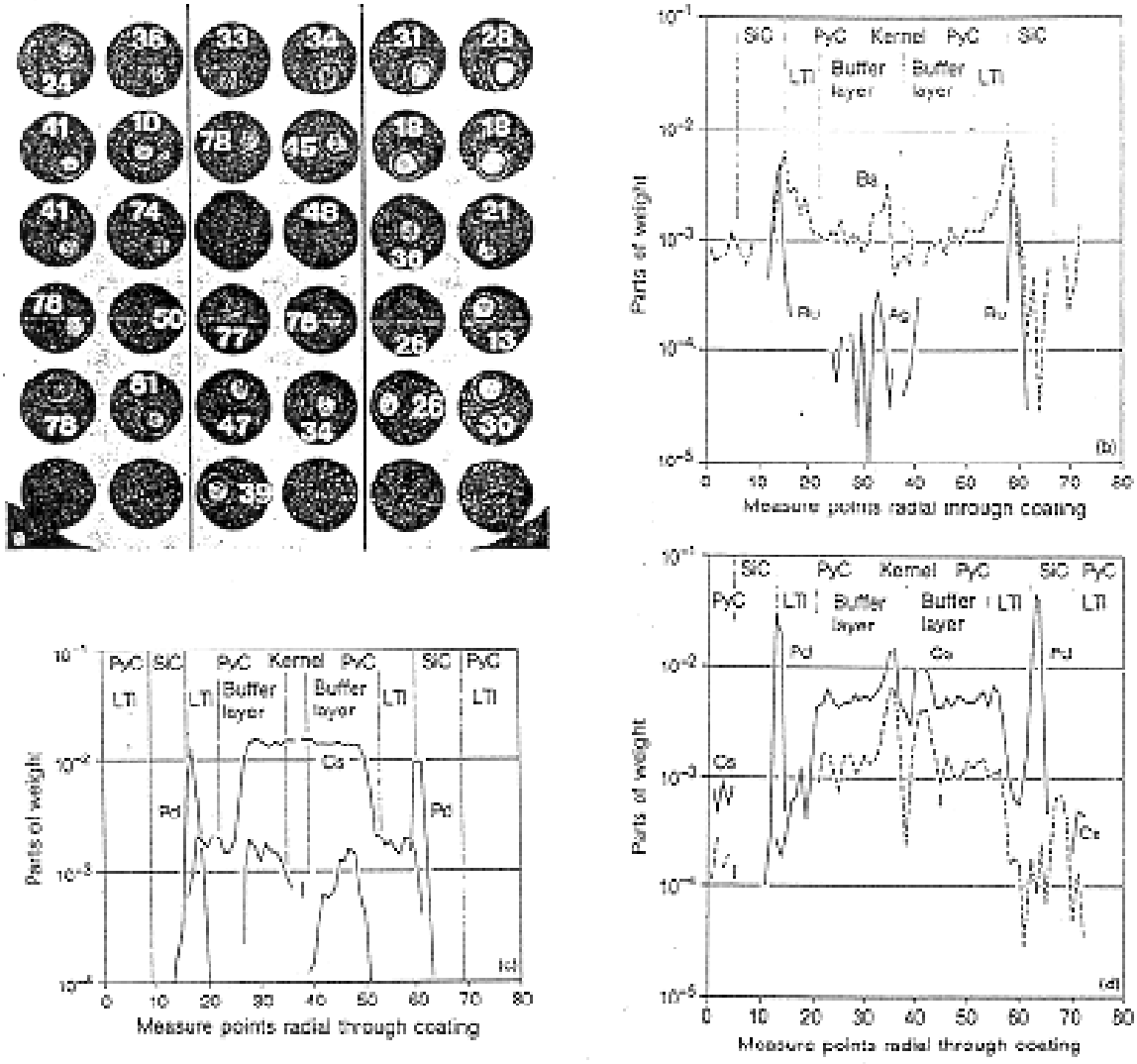

Figure 4-11. Microprobe profiles of fission product elements through coatings of particles from HFR-K3. (a) Arrangement of sectioned particles (HFR-K3/3) for microprobe measurements. The numbers show the percentage of cesium loss from every single particle after heating at 1800ºC. (b) Ba, Ru, Ag profile in a particle with 78% Cs loss after 1800ºC test. (c) Cs, I, Pd profile in a particle from HFR-K3/1 (0.01% Cs loss from sphere) after 1600ºC test. (d) Cs, I, Pd profile in a particle (78% Cs loss) from HFR-K3/3.

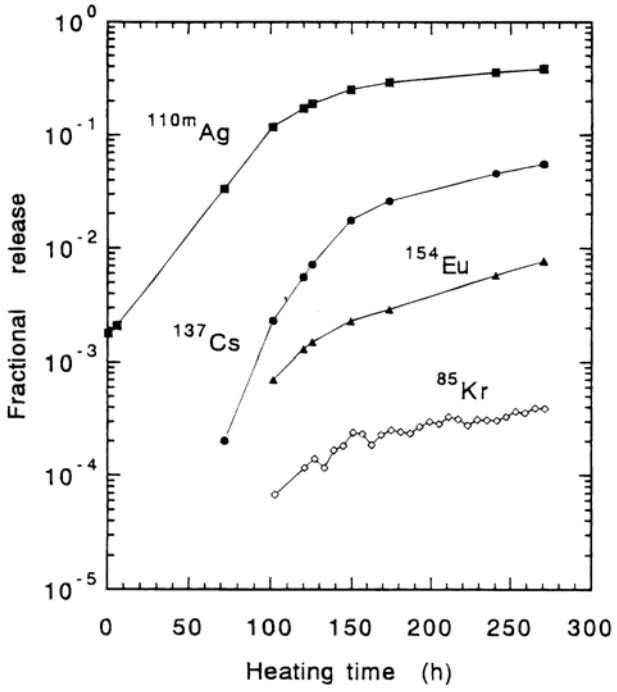

Figure 4-12. Time-dependent fractional releases of fission products during the ACT3 heating test at 1700°C for 270 h, obtained by the on-line measurements of fission gas release and intermittent measurements of metallic fission product release.

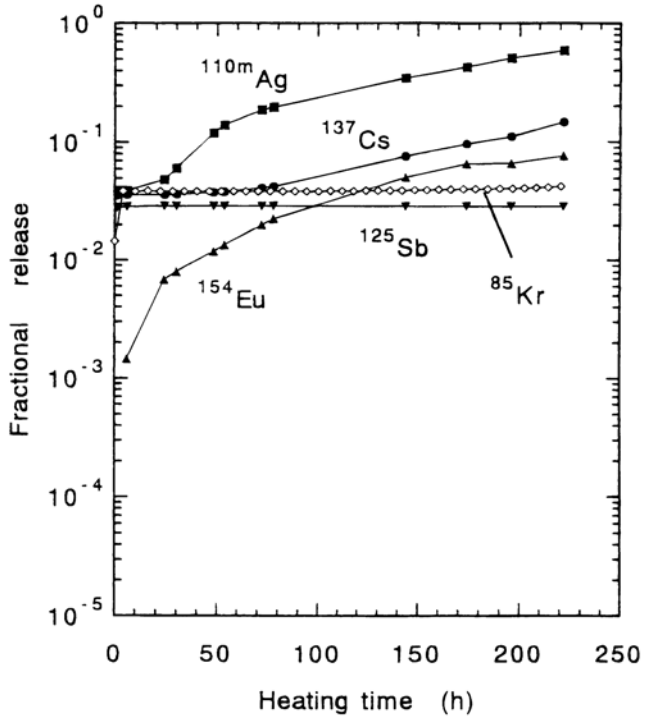

Figure 4-13. Time-dependent fractional releases of fission products during the Act 4 heating test at 1800ºC for 222 h, obtained by the on-line measurements of fission gas release and intermittent measurements of metallic fission product release.

Fission product inventories of the individual fuel particles were measured before and after the heating tests with the IMGA apparatus and results of these measurements are shown for silver, cesium and europium in Figures 4-14 (1700°C) and 4-15 (1800°C). Both these figures exhibit large variations in fission product release from particle to particle. At 1700°C, silver release varies from 10 to 100%, cesium from 0 to 20% and europium from 5 to 30%. At 1800°C, not including the failed particle, the silver release varied from 24 to 100%, cesium from 0 to 55%, and europium from 0 to 69%. Individual particles were examined at JAERI by X-ray microradiographs, ceramography, and electron microprobe.

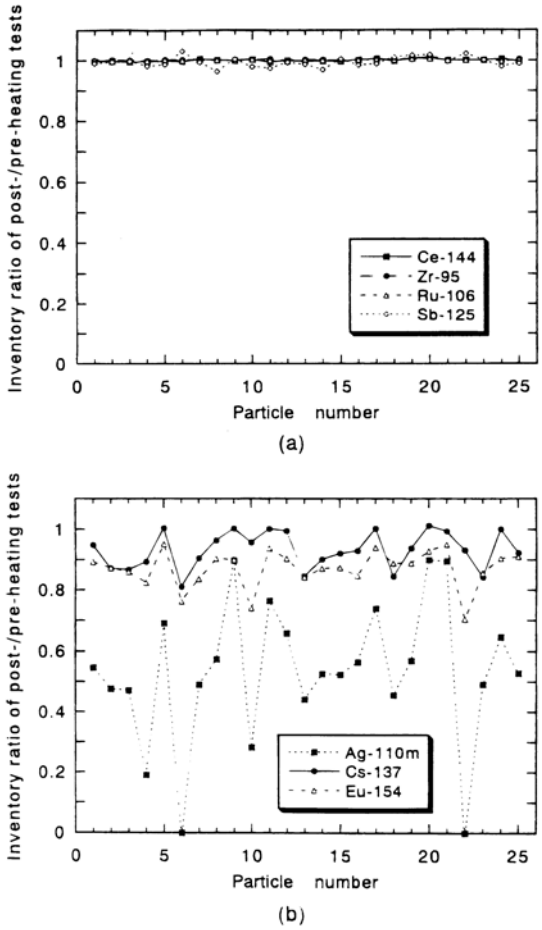

Figure 4-14. Inventory ratios of post-to pre-heating tests in individual particles in ACT3 measured with the IMGA system: (a) ^{95}Zr, ^{106}Ru, ^{125}Sb, and ^{144}Ce; (b) ^{110m}Ag, ^{137}Cs, and ^{154}Eu.

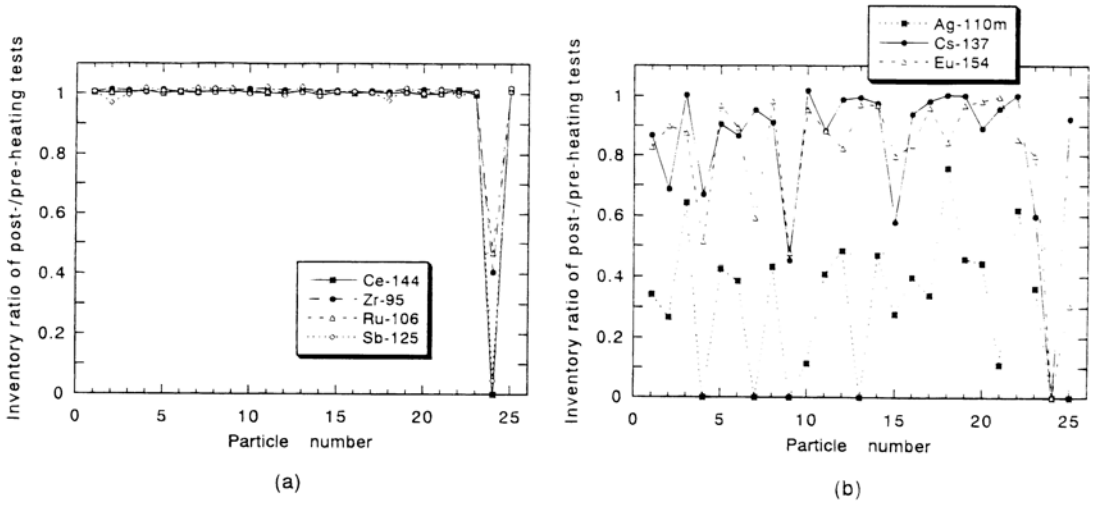

Figure 4-15. Inventory ratios of post- to pre- heating test in individual particles in ACT4 measured with the IMGA system: (a) ^{95}Zr, ^{106}Ru, ^{125}Sb, and ^{144}Ce; (b) ^{110m}Ag, ^{137}Cs, and ^{154}Eu.

Accumulations of fission products in the buffer show up as bright spots in X-ray microradiographs of fuel particles from which large fission product releases were measured, as shown in Figures 4-16 (1700°C) and 4-17 (1800°C). In Figure 4-16, particle ACT3-5 had relatively little fission product release and shows no evidence of fission product accumulation in the buffer, whereas particle ACT3-6 had relatively large releases and shows a bright spot in the buffer. A similar trend is shown in Figure 4-17 for a relatively non-releasing particle (ACT4-3) and two strongly releasing particles (ACT 4-9 and ACT 4-13). These figures also show that the buffers of the low-releasing particles are intact whereas those of the heavily releasing particles are severely cracked. In addition, the kernels of the releasing particles in Figures 4-16 and 4-17 exhibit larger pores than the kernels of the non-releasing particles. The SiC layers of all the particles show signs of degradation as seen in Figures 4-16, 4-17, and 4-18. Accumulations of fission products, especially palladium, were found in all particles at the IPyC/SiC interface, as shown in Figure 4-19, and sometimes within the SiC layer.

The Japanese work corroborates results from Germany and the U.S. in that wide variations are measured in fission product release from particle to particle, palladium buildup at the IPyC/ SiC interface is observed in both releasing and non-releasing particles, and fission product releases increase in the increasing test temperature.

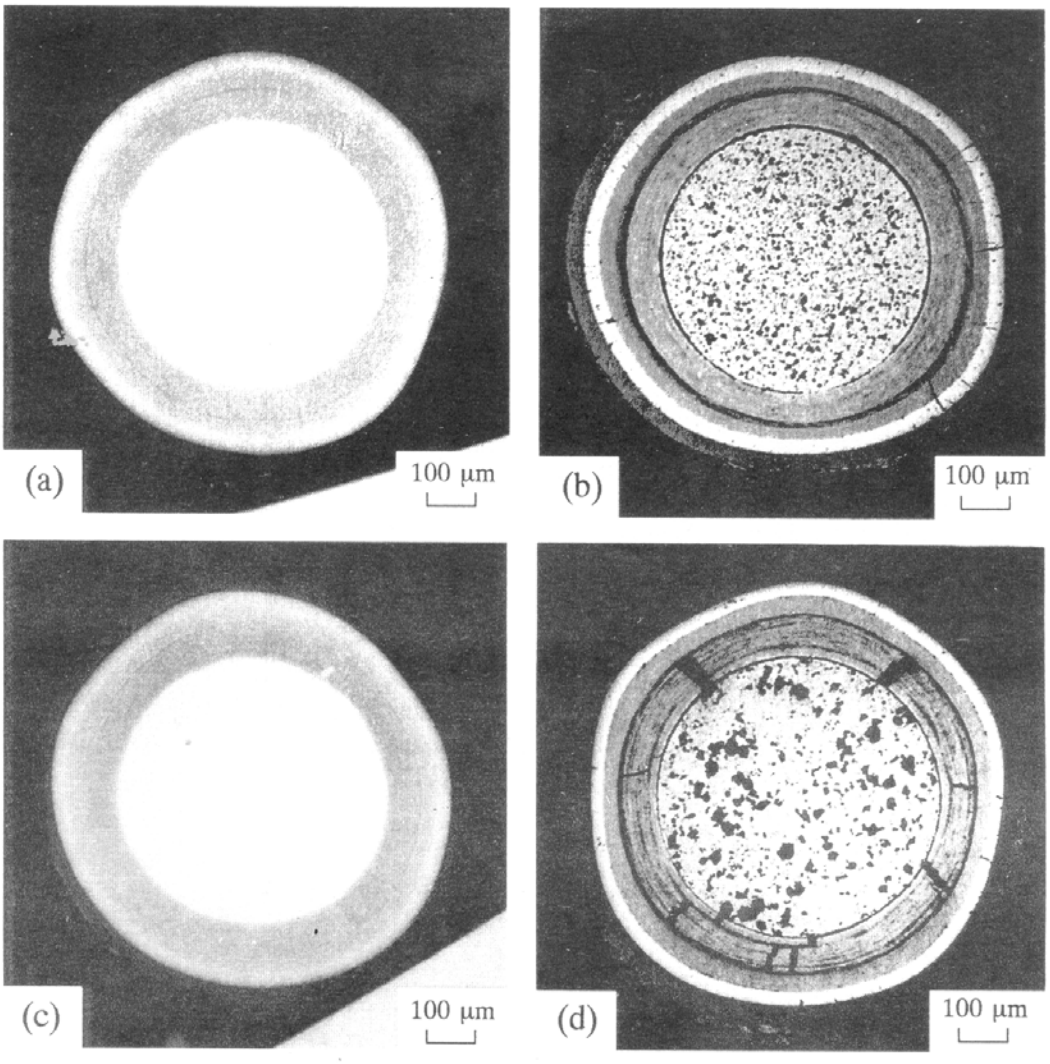

Figure 4-16. X-ray microradiographs and ceramographs of the particles after the ACT3 heating test: (a) and (b) show particle ACT3-5; (c) and (d) show particle ACT3-6.

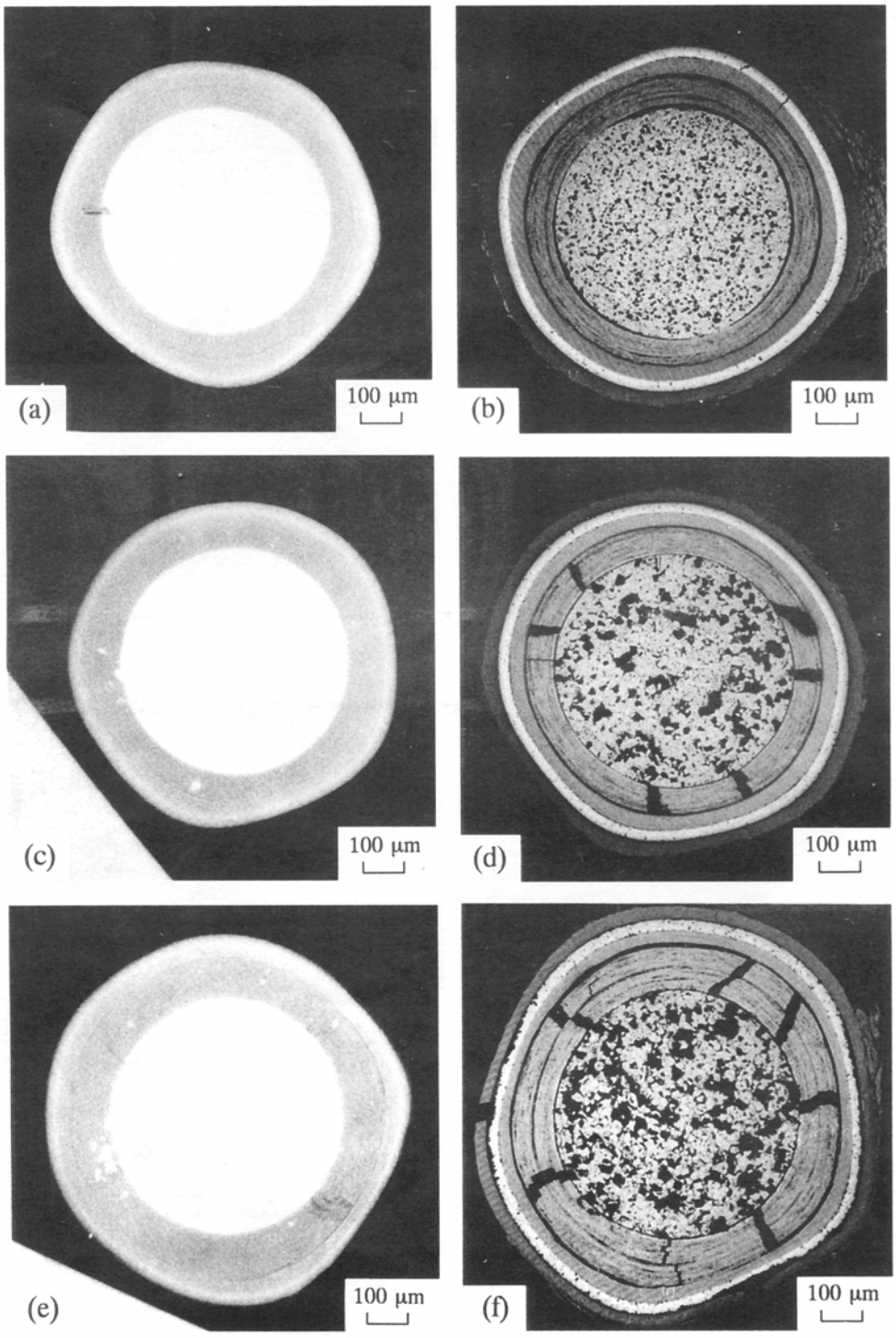

Figure 4-17. X-ray micrographs and ceramographs of the particles after the ACT4 heating test: (a) and (b) show particle ACT4-3; (c) and (d) show particle ACT4-9; and (e) and (f) show particle ACT4-13.

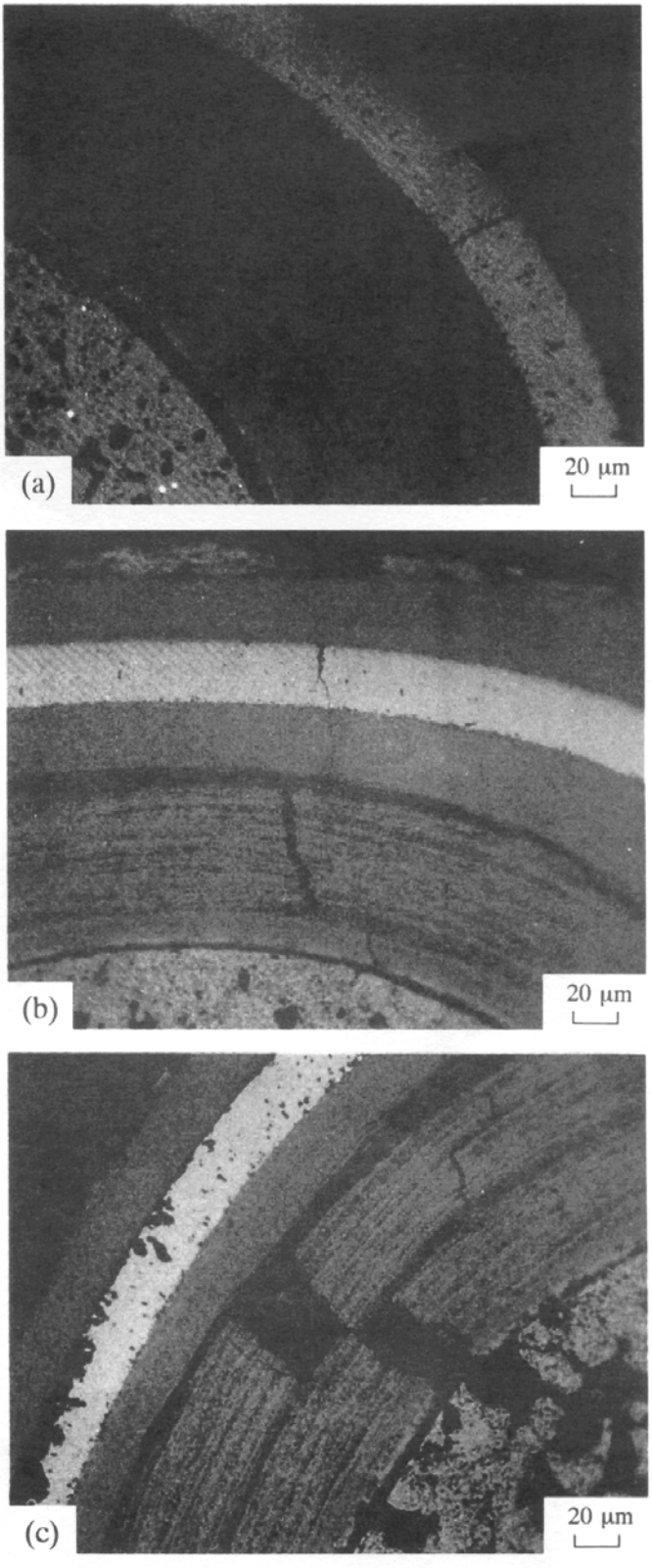

Figure 4-18. Ceramographs of coating layers of the particles after the ACT4 heating test: (a) shows particle ACT4-3, (b) shows particle ACT4-9, and (c) shows particle ACT4-13.

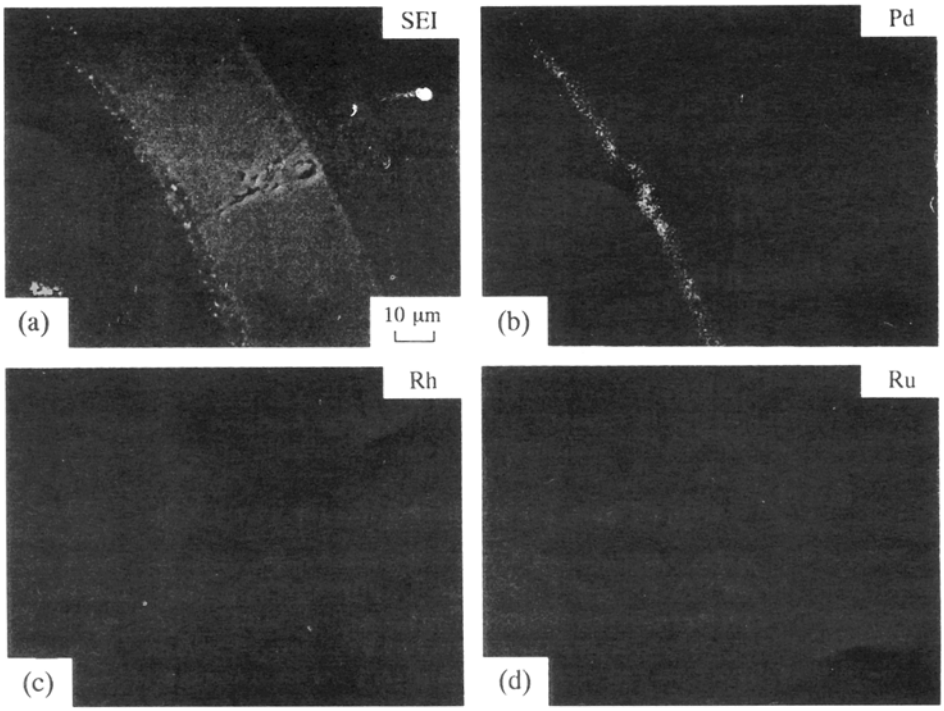

Figure 4-19. Electron probe microanalysis of coating layers of particle ACT4-3 after the ACT4 heating test shown in Figure 4-18a: (a) secondary electron image; X-ray image images for (b) palladium, (c) rhodium, and (d) ruthenium.

4.3 Accident Testing at 1900-2500°C

The primary mechanism for coating failure and fission product release at extreme temperatures in the range 1900 to 2500°C is thermal decomposition of the SiC layer (Nabielek et al. 1989). This comprehensive article includes measurements of the rate of SiC thermal decomposition using unirradiated German fuel particles, coating failure fractions from unirradiated German fuel spheres in isothermal heating tests, fission product releases from irradiated GA fuel particles in temperature ramp tests, and fission product releases from irradiated German spherical fuel elements under isothermal and ramp heating tests.

The thermal decomposition reaction is

$$SiC\ (s) = Si\ (g) + C\ (s)$$

and results in the development of interconnected pathways through which volatile fission products such as cesium and fission gases are readily transported. Figure 4-20 is a section of a fuel particle after heating to 2500°C in 30 hours, showing the degradation of the SiC layer

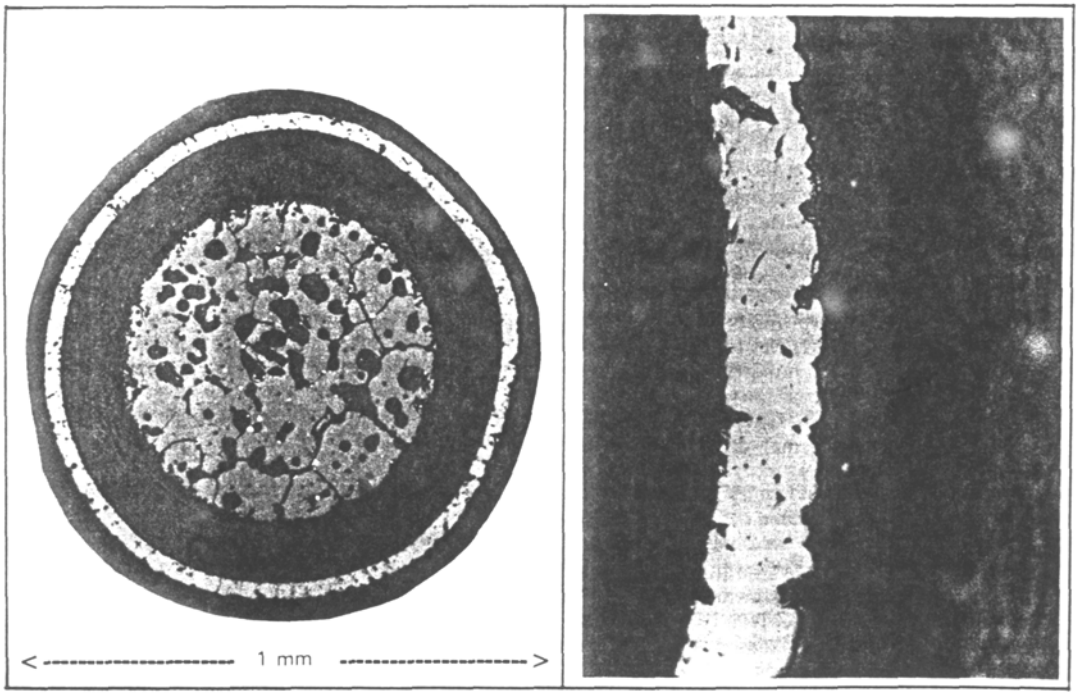

Figure 4-20. Section of particle after heating to 2500ºC in 30 hours. The dark areas in the white SiC layer show partial decomposition with a corresponding loss of ability to retain fission products.

The thinning of SiC was determined by measuring the weight loss after heating unirradiated fuel particles (from which the OPyC had been removed by burning) in vacuum. The thinning was found to be linear with time at a specific temperature and to vary with temperature in an Arrhenius relationship

$$dv/dt = (dv_o/ dt) \exp (-Q/RT)$$

where dv/dt is the rate of thinning and the activation energy, Q, was determined to be between 540 and 560 kJ/mol. The rate of decomposition was found to be independent of the SiC microstructure (e.g., columnar or laminar grain boundary orientation) and SiC manufacturing conditions. At 2200°C, the rate of thinning is 8 x 10^{-10} m/s.

Single unirradiated German spherical fuel elements were heated in vacuum and the fraction of fuel particles with failed SiC layers was determined by measuring the thorium and uranium leached by acid solutions after burning the graphite matrix, the OPyC layers, and IPyC layers exposed by failed SiC. The results shown in Figure 4-21 indicate that no systematic trend was found between ThO_2, $(Th,U)O_2$, and UO_2 fuels.

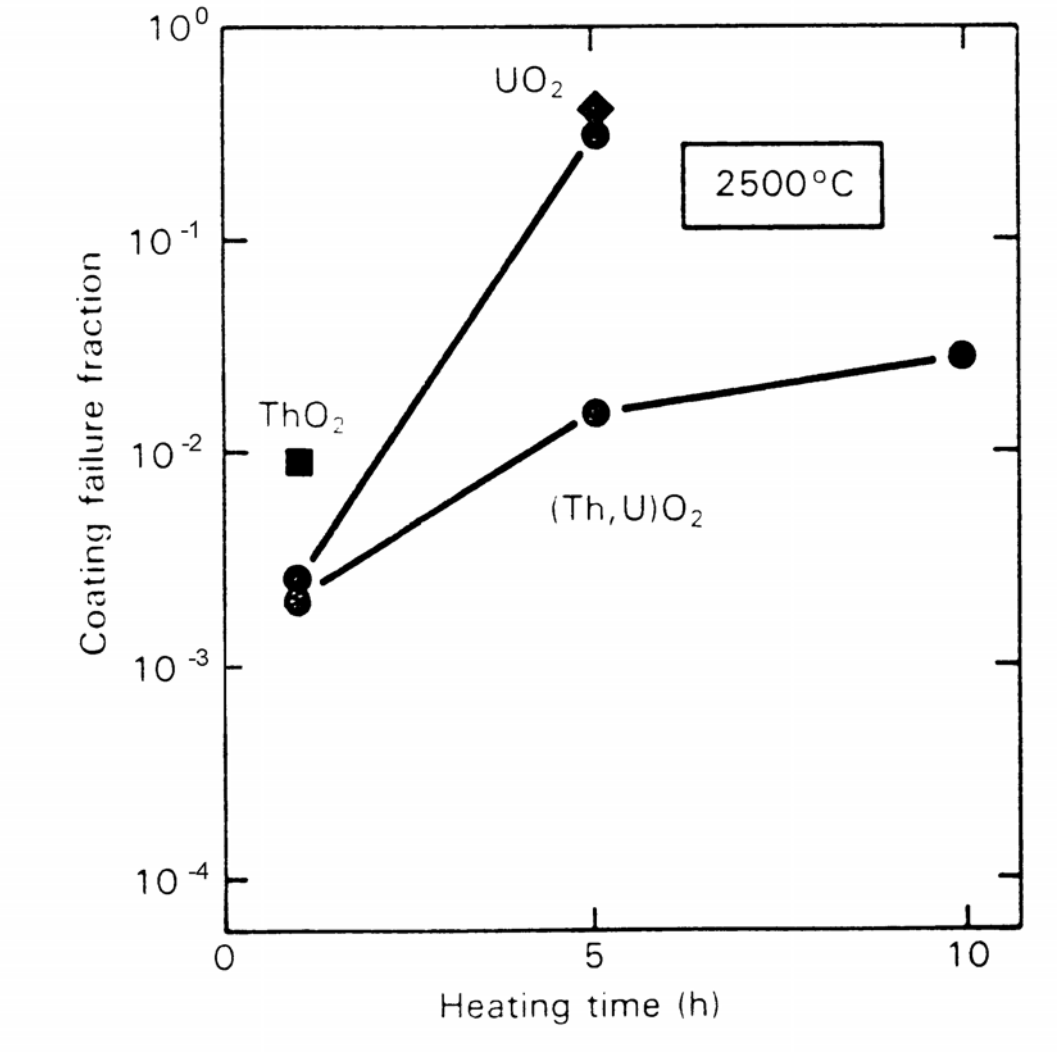

Figure 4-21. TRISO particle coating failure as a function of heating time in HOBEG experiments with unirradiated sperical fuel elements.

The release of krypton measured in linear ramp heating tests carried out with batches of 200 unbonded, irradiated TRISO fuel particles at GA showed no burnup dependence (Figure 4-22), nor correlation with kernel type, UC_2 or ThO_2, (Figure 4-23), or kernel enrichment (Figure 4-24). Only the thermal degradation of the SiC layer, characterized by the development of porosity throughout the SiC as well as cracks penetrating the entire layer (Figure 4-25) appears to contribute to the release of fission products at these high temperatures. Intact OPyC layers (Figure 4-25) slow the diffusive release of noble gases from fuel particles, but not the releases of metallic fission products such as silver and cesium. These fission product release effects are shown in Figure 4-26

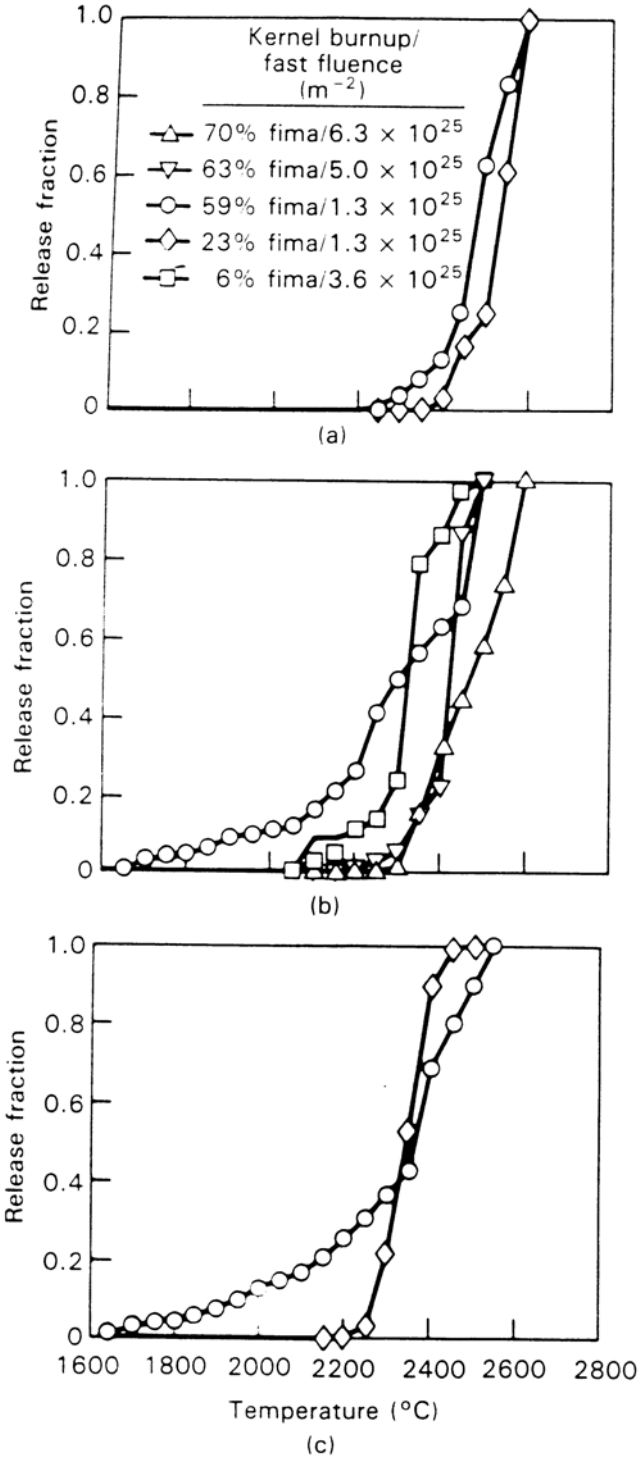

Figure 4-22. Krypton release as a function of heating temperature during linear ramp tests, with heatup to 2600ºC in (a) 8 h, (b) 30 h, and (c) 80 h. No systematic trend of burnup dependence can be observed with the UC_2 TRISO-coated particles used here.

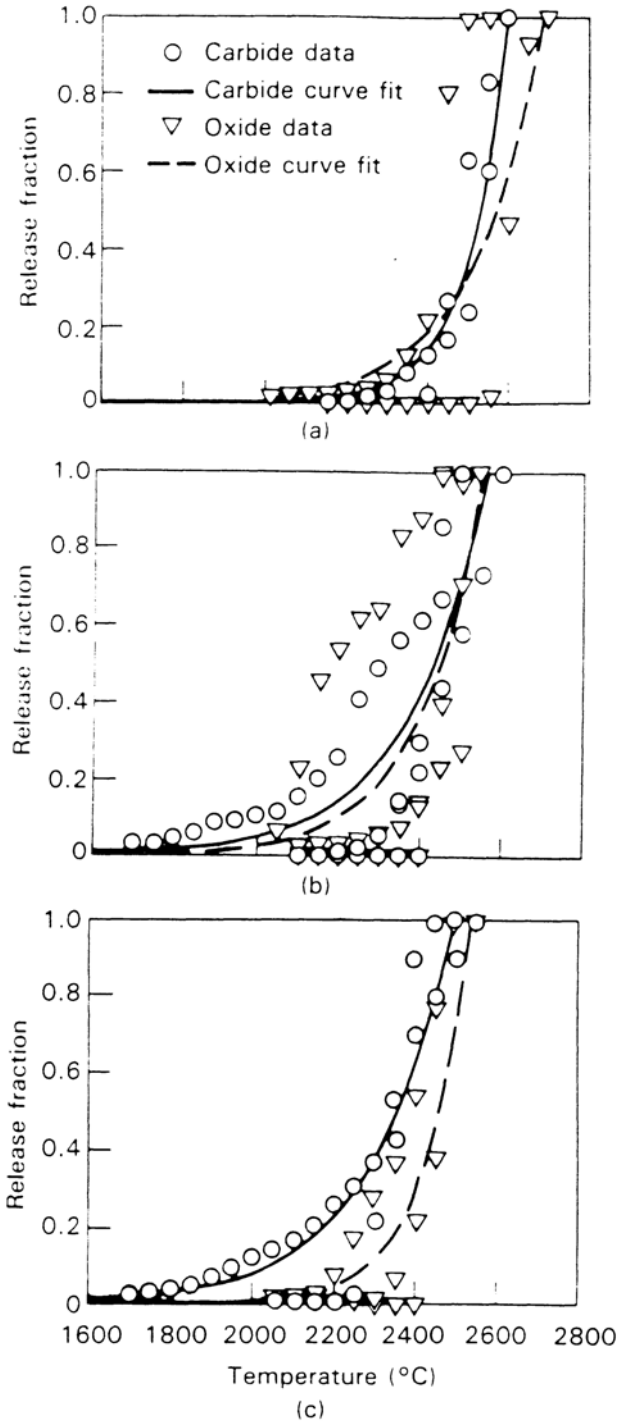

Figure 4-23. Krypton release as a function of heating temperatures during linear ramp tests, with heatup to 2600ºC in (a) 8 h, (b) 30h, and (c) 80 h. A comparison of the oxide and carbide fuel performance at extreme temperatures shows no significant correlation with the chemical composition of the kernel.

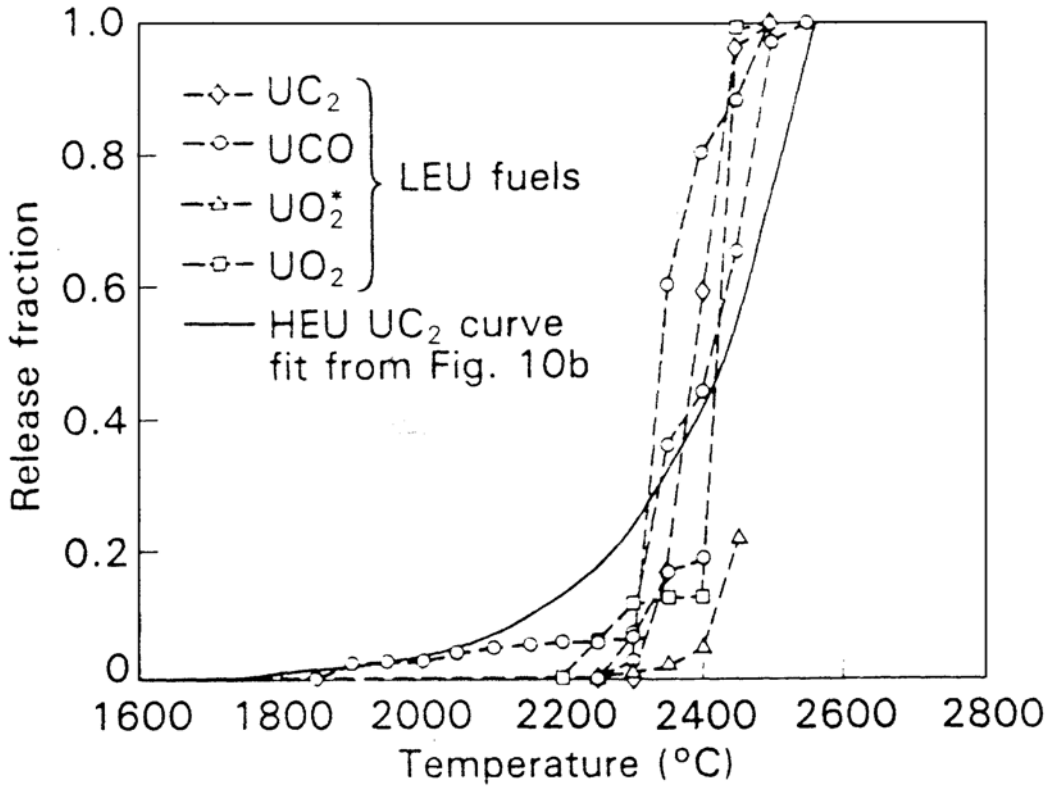

Figure 4-24. Krypton release as a function of heating temperature during linear ramp tests. Release from low-enriched fuels is consistent with the average release obtained from high-enriched UC_2 TRISO-coated particles.

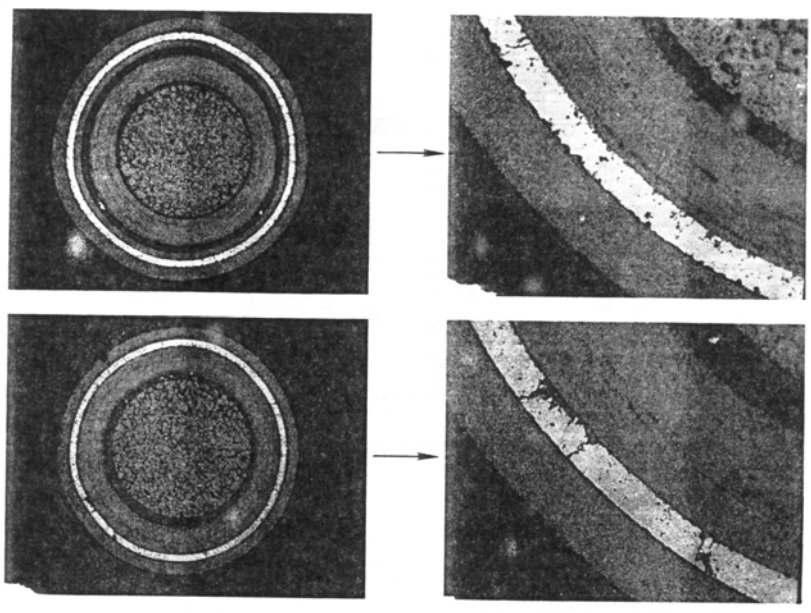

Figure 4-25. Ceramography of TRISO ThO_2 particles irradiated to 4.1%FIMA and heated at a rate of 20ºC/h to 2230ºC.

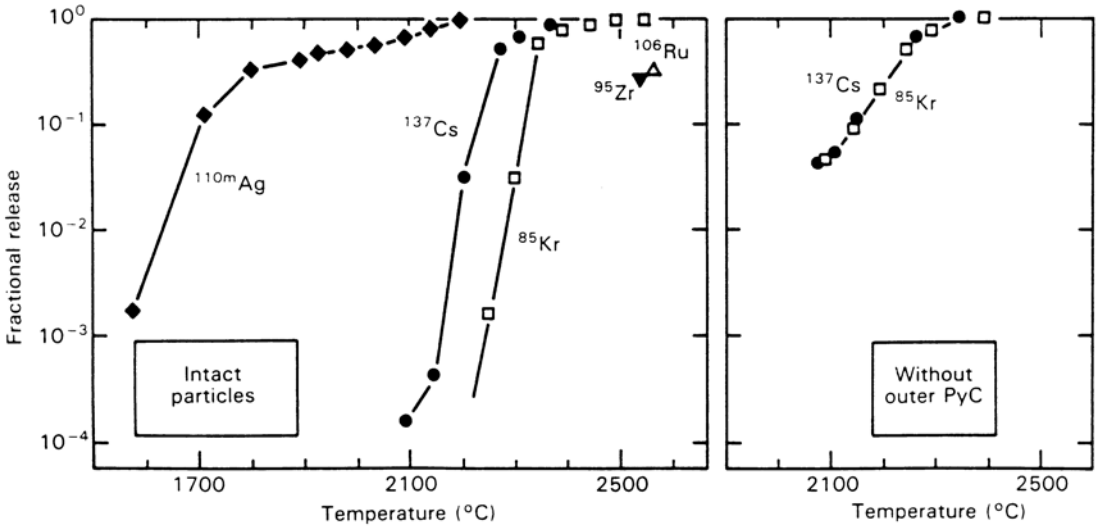

Figure 4-26. Typical fission product release profiles during linear temperature ramp. In both cases, 200 irradiated particles were heated to 2500ºC. The left diagram shows intact particles and the right diagram shows particles where the OPyC layers have been removed.

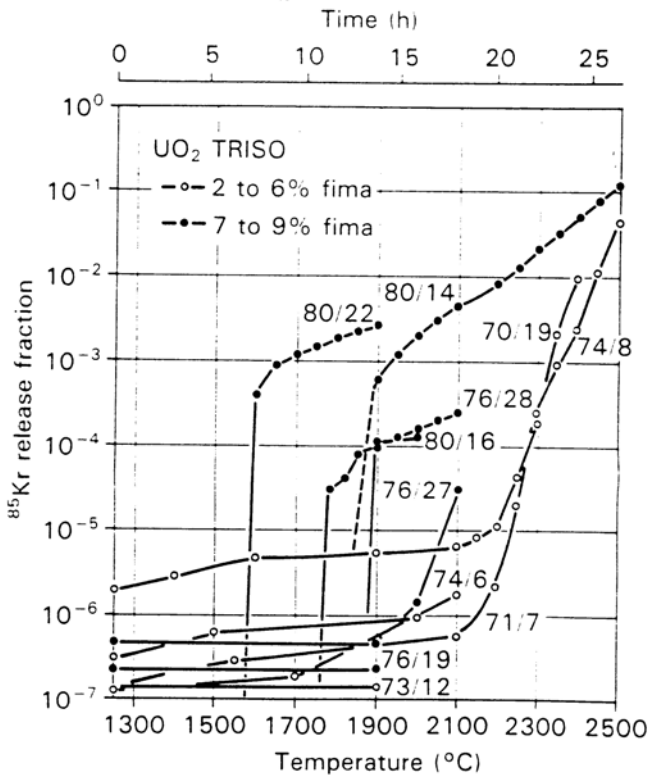

Figure 4-27. Krypton release as a function of heating temperature during linear ramp tests with spherical fuel elements containing UO_2 TRISO-coated particles of 2 to 6 and 7 to 9%FIMA burnup (AVR fuel elements).

Heating of irradiated German spherical fuel elements reveals some small effects of burnup on krypton release at high temperatures. Pressure vessel failures are evident early in ramp tests in fuel elements with higher burnup as shown in Figure 4-27. In isothermal heating tests with irradiated elements, initial krypton releases appear to be affected by coating failures as a result of high internal gas pressure at higher burnup, but at longer times thermal decomposition of the SiC layer dominates the releases minimizing the burnup effect (see Figure 4-28).

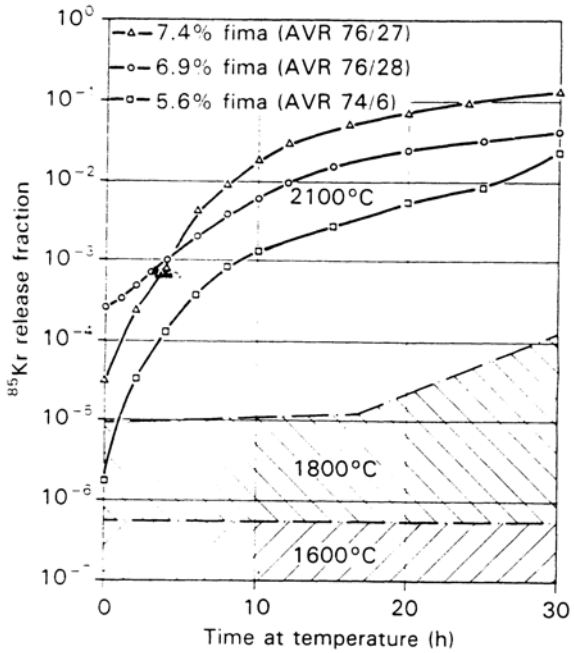

Figure 4-28. Krypton release during isothermal heating tests with spherical fuel elements containing 16,400 UO_2 TRISO particles each. A small influence of burnup can be observed.

4.4 Air Ingress

Fuel particle failure resulting from air ingress has been reported in (IAEA 1997) from a Japanese experiment with unirradiated fuel and a German experiment with irradiated fuel. Figure 4-29 shows that the burning of carbonaceous materials in a Japanese compact is complete after 20 hours at 1400°C. For a German irradiated spherical element, Figure 4-30 shows that burning of the graphite is complete after 100 hours at 1100°C. Once the carbonaceous materials surrounding the fuel particles have been burned away, the SiC-coated particles are susceptible to oxidation. Results from the Japanese tests, shown in Table 4-5, indicate that the failure fraction is 6.9×10^{-4} in unirradiated

compacts after 20 hours at 1400°C. It should be noted in Table 4-5 that the particle failure fractions are greater in compacts than in tests using particles not in compacts. A possible explanation is that the exothermic oxidation of carbonaceous materials in the compacts generated temperatures in the compacts greater than the furnace temperatures (IAEA 1997). The results from tests with irradiated German fuel particles and spherical fuel elements in Table 4-6 indicate a particle failure level of 1.2 x 10^{-3} after 140 hours at 1400°C and 7.3 x 10^{-4} after 70 hours at 1400°C. The time evolution of the fractional release of ^{85}Kr is shown in Figure 4-29 for the AVR 92/ 22 fuel sphere held at 1400°C for 140 hours.

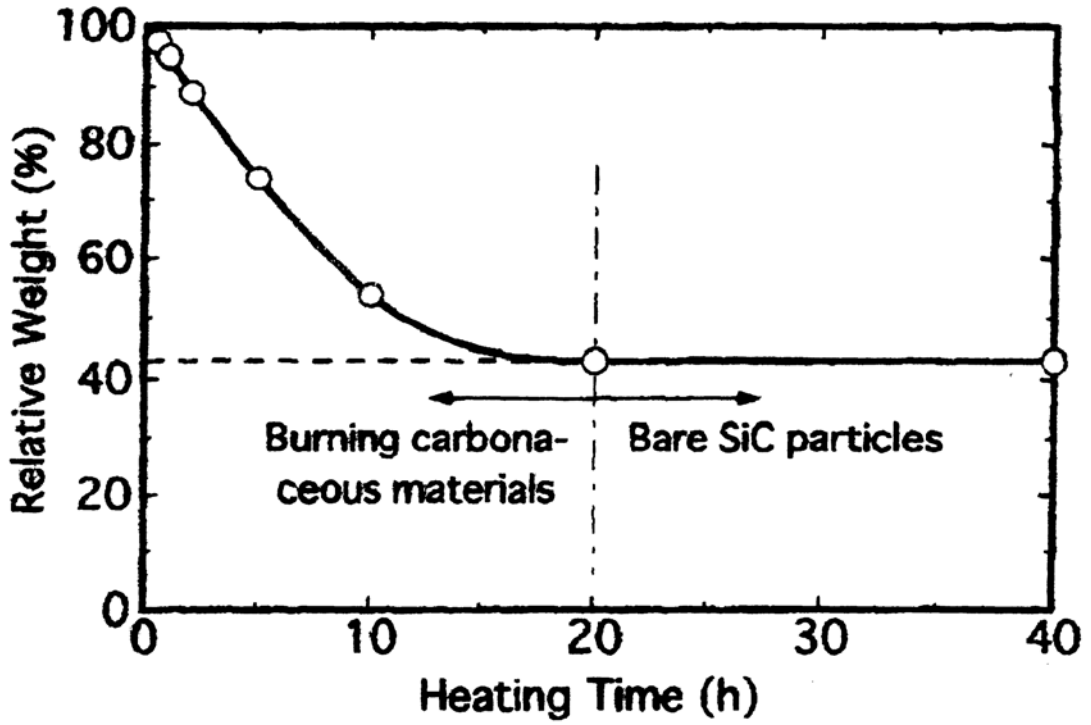

Figure 4-29. Weight change of a fuel compact during air oxidation at 1400ºC.

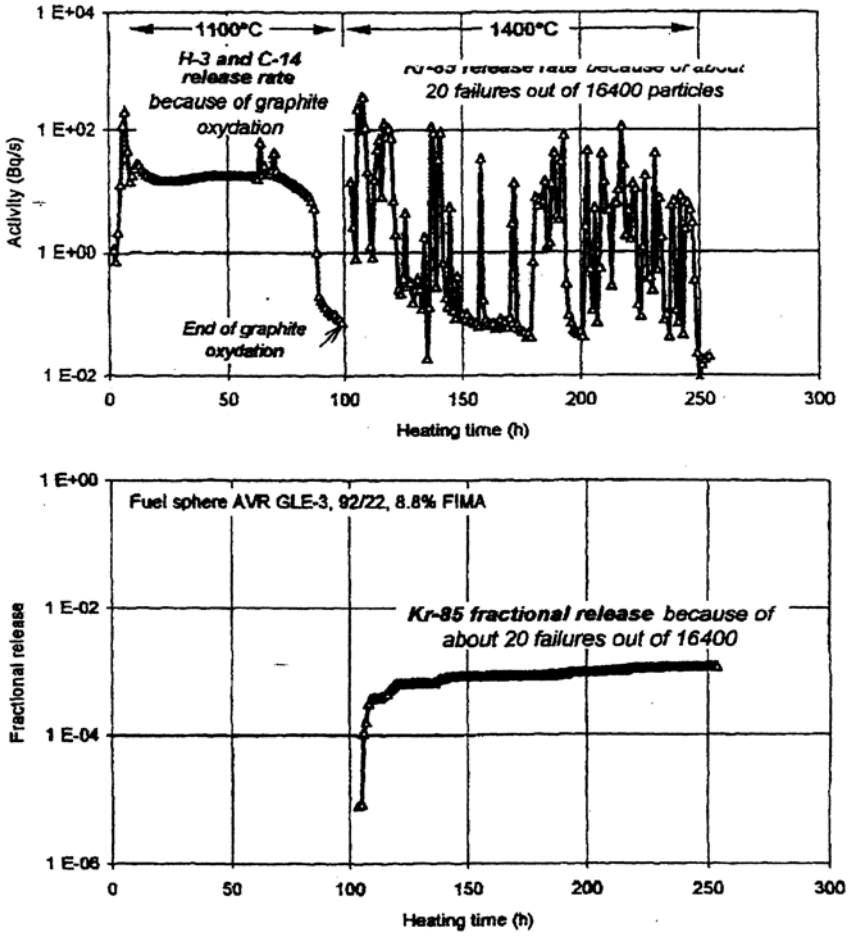

Figure 4-30. Oxidation of a fuel sphere in air: (Top) AVR 92/8, 9%FIMA (Bottom) AVR 92/22, 8.8 %FIMA

Table 4-5. Coated particle failure of non-irradiated fuel under air at high temperatures.

	Sample	# of Coated Particles Tested	Test Conditions:		No. of Failed Coated Particles	Failure Fraction
			Temp (°C)	Time(h)		
1	Coated particles	3151	900	40	1	2.3×10^{-4}
2	Coated particles	3127	1000	40	0	5.1×10^{-6}
3	Coated particles	3136	1200	40	0	1.0×10^{-6}
4	Coated particles	3123	1300	600	2	5.4×10^{-4}
5	Coated particles	3114	1400	40	1	3.2×10^{-5}
6	Fuel compact	10461	900	54	13	1.2×10^{-3}
7	Fuel compact	10599	1400	20	8	6.9×10^{-4}

Table 4-6. Heating tests with intact particles and fuel spheres in air (UO_2TRISO).

Fuel Sample	# Of Particles	Burnup (%FIMA)	Test Conditions			Kr-85m Release		
			Heatup (h)	Max. Temp. (ºC)	Time (h)	1st Failed Particle After	No. of Failed Particles	Fraction of Failed Particles
92/29, 12	10	9.2	14	1400	400	397 h	1	0.1
73/8, 11	10	4.7	15	1500	25	8 h	10	1
92/29, 13	10	9.2	15	1500	25	3 h	10	1
92/29, 11	10	9.2	28	1620	1	at 1613 ºC	10	1
AVR 89/12	16,400	9.4	13	1300	410	258 h	4	2.4×10^{-4}
AVR 92/22	16,400	8.8	14	1400	140	1 h	20	1.2×10^{-3}
AVR 89/14	16,400	9.0	14	1400	70	2 h	12	7.3×10^{-4}

Oxygen partial pressures in an air ingress accident in a high temperature gas reactor considerably less than 2×10^{-2} MPa (corresponding to oxygen in air at atmospheric pressure) will likely have an impact on fuel failure. Firstly, a lower partial pressure of oxygen will slow the rate of combustion of graphite, extending the time required to expose SiC-coated fuel particles to the oxidizing environment. Unfortunately, no data are readily available on this effect, but it could be quite significant. Secondly, there is a potentially adverse effect of low oxygen partial pressure according to a thermodynamic study by (Minato and Fukuda 1993) due to the reaction

$$SiC\ (s) + 1/2O_2\ (g) = SiO\ (g) + C\ (s). \qquad \textbf{(Eq. 1)}$$

In this reaction, solid SiC reacts to form gaseous SiO with the result that the SiC layer is thinned as a function of time. At higher oxygen partial pressures the reaction

$$SiC\ (s) + O_2\ (g) = SiO_2\ (s) + C\ (s) \qquad \textbf{(Eq. 2)}$$

takes place, in which solid SiC is transformed over time to solid SiO_2, which remains protective of the fuel. According to (Minato and Fukuda 1973), the transition from the reaction in Equation 2 (termed "passive") to the reaction in Equation 1 (termed "active") occurs along the line identified as SiC + C in Figure 4-31. For example, if the oxygen partial pressure were 1 x 10^{-2} MPa (1 x 10^4 Pa), corresponding to air at 0.5 atm, SiC oxidation would occur in the passive regime (Equation 2) as the temperature increased up to 1400°C (~6 x $10^{-4}K^{-1}$) beyond which the oxidation would transition to the active regime governed by Equation 1. According to Figure 4-31, the transition from passive to active oxidation of SiC occurs at lower temperatures for lower values of initial oxygen pressure.

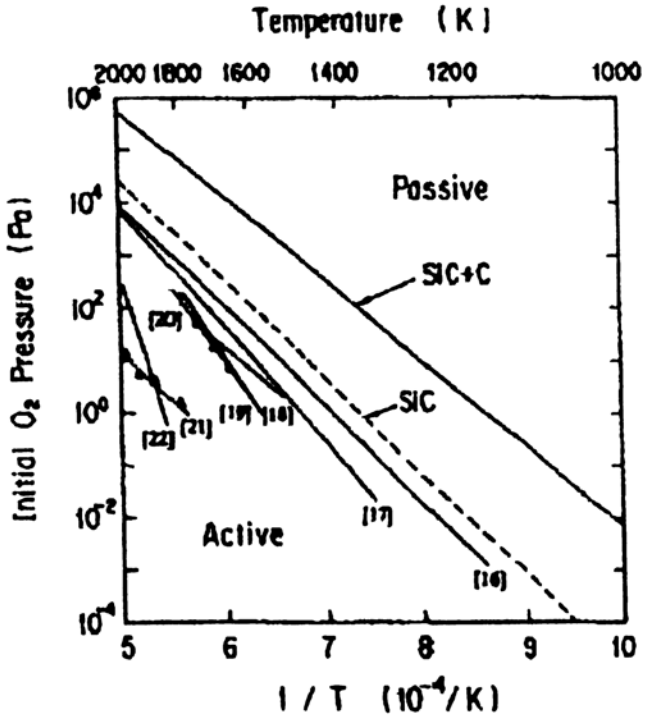

Figure 4-31. Active-to-passive oxidation transitions for SiC and SiC+C calculated in the SiC-C-O_2-He system as a function of temperature and initial O_2 pressure. Literature data for SiC are presented for comparison.

The dashed line identified as SiC in Figure 4-31 corresponds to the transition between the reactions

$$SiC\ (s) + O_2\ (g) = SiO\ (g) + CO\ (g) \qquad \textbf{(Eq. 3)}$$

and

$$SiC\ (s) + 3/2O_2\ (g) = SiO_2\ (s) + CO\ (g). \qquad \textbf{(Eq. 4)}$$

Equation 3 corresponds to the active regime of SiC oxidation and Equation 4 to the passive regime. Given that Equations 3 an 4 require more oxygen per mole of SiC than do Equations 1 and 2, one might have thought that the SiC + C line would have appeared below the SiC line in Figure 4-31. Due to the formation of CO in Equations 3 and 4, these reactions are thermodynamically favored over the reactions in Equations 1 and 2. Therefore, it may be that the dashed SiC line in Figure 4-31 is controlling, in which case the transition from passive SiC oxidation to active SiC oxidation at 1400°C occurs at an oxygen partial pressure of about 3×10^{-4} MPa (300 Pa), equivalent to air at 0.015 atm.

Without experimental data on spherical fuel element oxidation and fuel failure at lower oxygen pressures, it is difficult to weigh the competing effects of slower oxidation of graphite to expose SiC-coated particles against the transition to the active oxidation regime. If quite low oxygen partial pressures are predicted in an air ingress accident in a gas reactor, it is likely that kinetic effects will dominate, causing greatly reduced rates of graphite oxidation, and therefore, very low fuel particle fractional failure due to lack of SiC-layer exposure. In the case of a gas reactor, it may be that fuel failure in an air ingress accident is limited by the supply of oxygen available to oxidize the carbonaceous components of the spherical fuel elements.

4.5 Reactivity-Initiated Accident Testing

RIA tests on HTGR fuel have been conducted at the NSSR reactor in Japan ((Fukuda et al. 1990, IAEA 1997) and the HYDRA and IGR reactors in Russia (IAEA 1997). Reactivity insertion by rapid withdrawal of control rods in the HTTR reactor design was calculated to produce an energy insertion of 1.26×10^4 J/(g UO_2) over a duration of about 8 s. In the NSRR, pulse widths at half maximum power ranged from 10–30 ms and energy depositions ranged from 200–2300 J/(g UO_2). Fuel enrichments from 4 to 20% were used in the NSRR to achieve the range of energy depositions in TRISO coated UO_2 fuel particles. In these tests unirradiated loose particles and unirradiated fuel compacts have been used. Fuel failure fraction as a function of energy deposition is shown in Figure 4-32 from the NSRR tests on unirradiated fuel compacts. The failure fraction was about 1% at an energy deposition of 1000 J/(g UO_2) and almost 100% by 1500 J/(g UO_2). At an energy deposition of 2300 J/(g UO_2), the central region of the UO_2 fuel kernels was vaporized (Figure 4-33) and the uranium was found by microprobe to have deposited near the boundary of the coated particles and the graphite matrix (Fukuda, et al., 1990). At an energy deposition less than 2300 J/(g UO_2) radial cracks were present through the coating layers (Figure 4-33). Small cracks appeared on the surface of

compacts subjected to an energy deposition of 2300 J/(g UO_2), whereas compacts subjected to lesser energy depositions showed no surface damage.

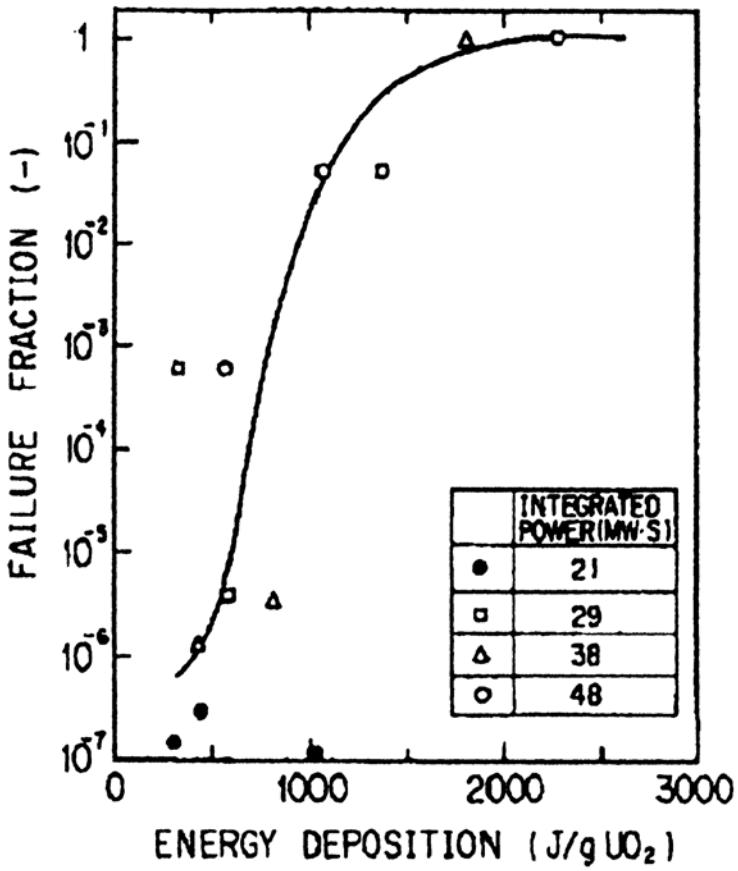

Figure 4-32. Relation between failure fraction of the coated particles and energy deposition by NSSR irradiation.

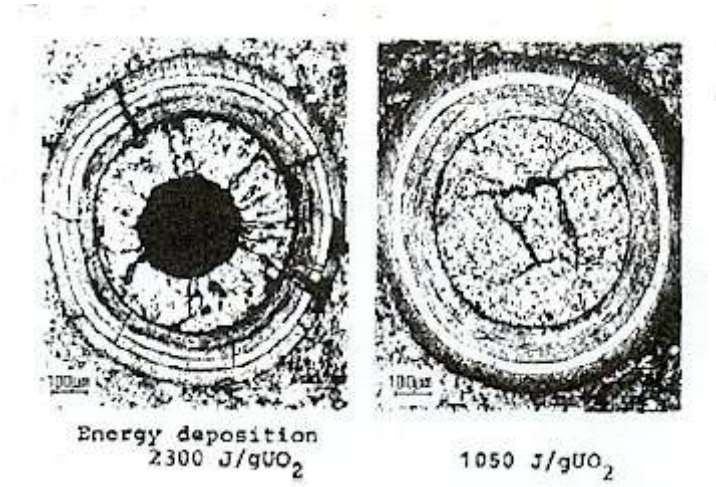

Figure 4-33. Cross-section of coated particles irradiated in NSSR.

In the HYDRA tests, the pulse duration was 1-2 ms and the energy deposition was in the range 100-1700 J/(g UO_2). Samples consisted of loose particles, tablets of particles in graphite about 10 mm in diameter and 5 mm in thickness, and 60 mm diameter spherical fuel elements. As can be seen in

Tables 4-7 and 4-8, the wide variety of fuel particles tested contained UO_2 kernels of diameters from 400 to 900 μm, varying numbers of pyrocarbon layers and thicknesses, and SiC layer thicknesses ranging from 60 to 140 μm.

Table 4-7. Characteristics of the coated fuel particles irradiated as loose particles and as tablets in the HYDRA tests.

Coated Particle Batch U-235	Fuel Kernel		Protective Coating							
	Uo_2		PyC-1		PyC-2		SiC		PyC-4	
Enrich. (%)	Diameter (μm)	Density (g/cm^3)	Thickn. (μm)	Density (g/cm^3)	Thickn. (μm)	Density (g/cm^3)	Thickn. (μm)	Density (g/cm^3)	Thickn. (μm)	Density (g/cm^3)
1 KM 36	490	9.77	92	1.1	70	1.88	60	3.18	61	1.84
2 KM 36	490	10.8	99	1.02	77	1.83	65	3.21	60	2.09
3 KM[(1)] 10	532	7.86	91	1.1	70	1.94	60	3.20	56	1.9

	Uo_2		PyC-1		PyC-2		SiC + PyC		SiC		SiC + PyC	
	Diameter (μm)	Density (G/cm^3)	Thickn. (μm)	Density (g/cm^3)	Thickn. (μm)	Density (g/cm^3)	Thickn. (μm)	Density (g/cm^3)	Thickn. (μm)	Density (g/cm^3)	Thickn. (μm)	Density (g/cm^3)
21-9X-84 21	900	9.1	105	1.1	14	1.5	91	2.4	100	3.18	56	2.4
36-27X-89 36	500	9.4	56	1.1	10	1.5	50	2.4	60	3.18	42	2.4

(1) Part of the samples of the 3KM batch underwent irradiation after three hours of preliminary annealing at 1700ºC.

Table 4-8. Characteristics of the coated fuel particles contained in the fuel elements irradiated in the HYDRA tests.

Batch	Kernel, Coating	Density (g/cm^3)	Diameter, Thickness (μm)
36-X-80	UO_2	8.59	400-630
	PyC-1	1.1 ± 0.1	20
	PyC-2	1.5	7
	PyC-3	1.1 ± 0.1	15
	PyC-4	1.9	70
	SiC	3.2	140
	PyC-6	1.2	15
	PyC-7	1.7	56
100	UO_2	9.8	560
	PyC-1	1.0	30
	PyC-2	1.5	67
	PyC-3	1.8	(PyC-2 + PyC-3)
	SiC	3.0	60
	PyC-5	1.8	70
21-X-78	UO_2	≈9.1	400-630
	PyC-1	≈1.1	30
	PyC-2	-	18
	PyC-3	≈1.6	35
	SiC	≈3.1	80
	PyC-4	≈1.75	84

The HYDRA results shown in Figure 4-34, along with those of (Fukuda, et al., 1990) shown previously in Figure 4-32, are unfortunately difficult to interpret because the symbols referring to the fuel particle types are not well defined. [3]

[5] One could guess that "CP (γk = 10.8 g/cm^3)" refers to particle batch 2 KM (see Table 4-7) containing a UO_2 kernel having a density of 10.8 g/cm^3. "CP (γk = 7.9 g/cm^3)" may refer to particle batch 3 KM (see Table 4-7) containing a UO_2 kernel having a density of 7.86 g/cm^3. "CP with (PyC + SiC) coating" may refer to particle batch 21- 9X - 84 and/or 36 - 27X - 89 (see Table 4-7) containing some sort of combined SiC + PyC layer on either side of the SiC layer. The identity of the points in Figure 5-33 labeled "EFE" is less obvious, but they may be spherical fuel elements.

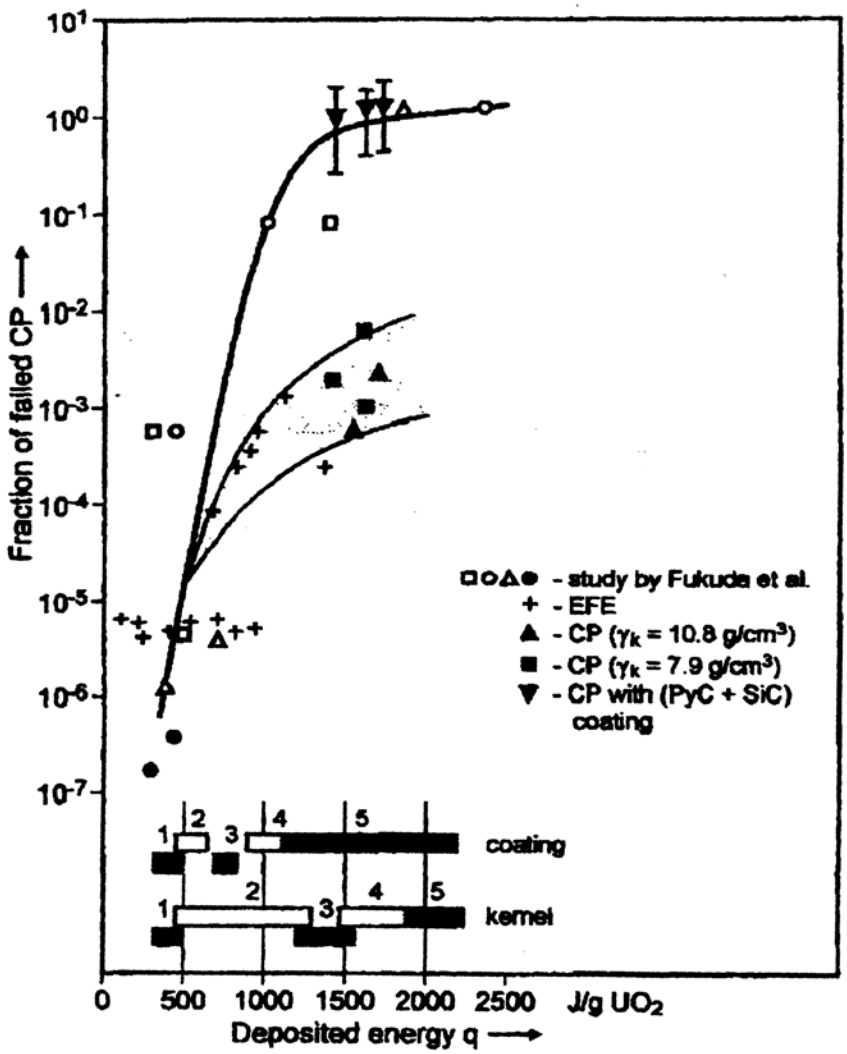

Figure 4-34. Dependence of the failed coated particle fraction on specific energy deposition in the single irradiation.

The stages depicted in Figure 4-34 are:
1) Heating up to approximately 1500-1800ºC
2) Heating up to approximately 2000º C; kernel fuel dispersion
3) Heating up to melting; carbidization possible
4) Melting: carbidization possible
5) Evaporation; carbidization possible

In Figure 4-34, the data plotted with the symbol identified as "CP with (PyC + SiC) coating" fall on the line from (Fukuda et al. 1990) in support of HTTR licensing, whereas the data from the other fuel batches and the fuel elements show much smaller fuel particle failure fractions. The explanation may be that particle batch 36-27X-89, one of those with (PyC + SiC) coating layers, has a buffer thickness of only 56 μm, whereas the other particle batches have buffer thickness > 90 μm (see Table 4-7). The fuel for the Japanese HTTR reactor design, probably similar to that tested by (Fukuda et al. 1990), has a buffer thickness of 60 μm comparable to that of batch 36-27X-89.

It is reported that the smaller free volume in the particles of batch 36-27X-89 resulted in a higher internal pressure, causing coating failures that were observable by visual inspection of loose particles

and tablets from this batch; however, failures in any of the other particle batches tested were not apparent by visual inspection (IAEA 1997). Posttest ceramography of coated fuel particles revealed extensively cracked kernels at 1050 J/(g UO_2) and evidence of melting in the kernels at energy depositions above 1300 J/(g UO_2).

The effect of a reduced buffer thickness causing increasing fuel particle failure fraction by about two orders of magnitude is apparent in Figure 4-34 by comparing the results from the "CP with (PyC + SiC) coating" data points and those of the "CP (γk = 10.8 g/cm^3)"and "CP (γk = 7.9 g/cm^3)". One caveat is that the spherical fuel elements (see Table 4-8) contain fuel particles with very thin (20-30 μm) low-density pyrocarbon layers (buffers), but the "EFE" data points in Figure 4-34 are in the same grouping as fuel particles with buffer layers > 90 μm. If the "EFE" data points can be rationalized and the buffer thickness effect validated, the 95 μm buffer thickness in the German type TRISO-coated fuel should translate into a roughly two order of magnitude reduction in fuel particle failure relative to the results of (Fukuda et al. 1990) shown in Figure 4-32. Therefore, one might expect a failure rate of 1x 10^{-4} at 1000 J/(g UO_2) and 1 x 10^{-2} at 1500 J/(g UO_2) for PBMR fuel.

Two series of tests were carried out in the IGR reactor to study the integrity of spherical fuel elements under longer pulse durations than those in the HYDRA reactor (IAEA 1997). Quantitative analysis of the coated fuel particle failure was not performed. In the first series, irradiations of three pulses were made sequentially of durations, 1.6, 1.0 and 0.7 s and the maximum energy deposition rates were 150, 300, and 629 kW per fuel element. In the second series, following a low power pulse to check temperature and neutron flux measuring systems, three pulses of durations varying from 7 to 30 s at an energy deposition rate of 46 kW per fuel element were conducted. The characteristics of the coated particles in the fuel elements are shown in Table 4-9 and the irradiation conditions and principal results are presented in Table 4-10. The number of elements tested is not mentioned. Fuel element integrity was maintained after the first test series, but, after the second test series, cracks were observed in the fuel-free zone of the fuel elements and parts of the fuel elements were split into 2-3 fragments. Ceramography of the fuel elements revealed complete destruction of the coated particles, including cracking of the PyC layers and cracking, delamination and thermal decomposition of the SiC layers. The free volume of the coated particles in the IGR tests (0.07 mm^3) was about the same as those of the KM batches (0.06-0.08 mm^3) tested in HYDRA. The fuel particle destruction was caused by the order of magnitude higher energy deposition in the IGR tests (3-9 x 10^4 J/(g UO_2)) vs. the HYDRA tests (1.7 x 10^3 J/(g UO_2)) (IAEA 1997)

Table 4-9. Characteristics of the coated fuel particles contained in the fuel elements irradiated in the IGR tests. (1) Made on the basis of UO_2 with 21% enrichment of U-235.

	Kernel	**PyC-1**	**PyC-2**	**PyC-3**	**SiC-4**	**PyC-5**
Size (μm)	520	100	20	65	45	70
Density (g/cm^3)	10.1	1.0	1.5	1.9	3.2	1.8

Table 4-10. Pulse irradiation conditions in the IGR tests.

Characteristics	1st Series	2nd Series
Power (kW/fuel element)	620	46
Energy deposition (J/(g UO_2))	2.6×10^4	9×10^4
Pulse duration (on peak half-width)	0.7	30
Temperature (K) spherical fuel element surface spherical fuel element center kernel (in center of fuel element)(1)	 860 1490 3360	 2000 ± 200 3000 3200
Strain on surface of fuel element (MPa)(1)	70	70
Spherical fuel element state after testing	intact	Spherical fuel elements and particle coatings have failed

(1) Calculational data

4.6 Summary

The principal barrier to fission product release in TRISO-coated particles, the SiC layer, can be compromised by three mechanisms in elevated temperature safety tests: (a) pressure vessel failure, (b) corrosion by fission products, primarily palladium, and (c) thermal decomposition.

Pressure vessel failure is a function of fuel burnup and irradiation temperature and can be controlled by limiting these parameters and by the mechanical design of the fuel particle. Fission product corrosion of SiC is a function of burnup (affecting fission product inventory), power per fuel particle during irradiation (affecting temperature and temperature gradient in the particle), and microstructure of the SiC. Burnup and power per particle can be controlled by reactor design and operating parameters. SiC microstructure (grain size and orientation) can be controlled by deposition temperature during fuel fabrication. Thermal decomposition of SiC at elevated temperatures (>1900°C) is solely a function of temperature and is independent of reactor operating parameters and fuel fabrication parameters.

German fuel elements with burnup ≤ 9 %FIMA and neutron fast fluence ≤ 2.2 x 10^{25} n/m^2 (PBMR conditions) release krypton at a level equivalent to less than one fuel particle failure (6 x 10^{-5}) for heating times up to 500 hours at 1600°C. Krypton releases can exceed 6 x 10^{-5} at higher annealing temperatures (≥1700°C) and for more severe irradiation conditions at 1600°C.

Cesium releases from German fuel elements irradiated within the PBMR limits remain below the level of one particle inventory for heating times up to 300 hours at 1600°C. At longer times, cesium releases in excess of 6 x 10^{-5} have been measured at 1600°C for fuel irradiated within the PBMR limits. Cesium releases can greatly exceed the 6x10^{-5} level for fuel with more severe irradiation conditions tested at 1600°C and for fuels with irradiation conditions within (and beyond) the PBMR limits at temperatures ≥ 1700°C.

In general, the largest releases during post-irradiation heating tests are from silver followed by cesium. The releases of krypton and strontium are much lower due to the holdup of krypton by intact PyC layers and the holdup of strontium in the UO_2 kernel and in the graphite matrix of the fuel element. The release of europium is largest from UC_2 fuel, but can be significant in UCO and to a lesser extent UO_2 fuels. Cerium release is significant only in UC_2 fuel.

Limited tests on air ingress and reactivity induced energy deposition have been performed. The databases are not nearly as complete as the long-term heatup tests. More systematic testing may be required to address the behavior of TRISO-coated fuel under these more severe conditions.

5. IMPLICATION OF DIFFERENCES IN THE U.S. AND GERMAN FABRICATION PROCESSES, IRRADIATION DATA AND POSTIRRADIATION EXAMINATION RESULTS ON TRISO-COATED FUEL PERFORMANCE AND FAILURE MECHANISMS

5.1 Implications of Fabrication Differences on Fuel Performance

A comparison of the microstructures of the layers of the TRISO coatings in German and U.S. fuel and the detailed review of the fabrication processes in Section 2 has revealed many differences. There are three specific technical differences in the coating layers produced by the respective fabrication

processes that have important impacts in terms of performance under irradiation and accident conditions: pyrocarbon anisotropy and density, IPyC/SiC interface structure, and SiC microstructure. Each has important implications on the behavior of the fuel under irradiation and safety testing, and is discussed in the following sections.

Pyrocarbon anisotropy and density. The density and anisotropy of PyC is determined by the deposition conditions in the coater (Martin 2000). A variety of coating conditions have been historically used to produce U.S. PyC. In many cases, low coating gas concentrations were used resulting in very low deposition rates for pyrocarbons between 1 and 4 μm/min. Under these conditions, one obtains high-density but anisotropic pyrocarbons with a laminar-like structure (see Figure 5-1). The high density of the IPyC was deemed important to prevent chlorine attack of the kernel during deposition of the SiC layer. By contrast, the German fuel manufacturers favored higher coating gas concentrations and correspondingly high coating rates resulting in more isotropic pyrocarbons. (For a general discussion of the relationship between deposition conditions and microstructure of the PyC, see reference Martin 2000.) These different microstructures lead to different behavior under irradiation. The higher density, more anisotropic U.S. PyC is more susceptible to cracking under irradiation.

Postirradiation examination of many of the U.S. capsules indicate large shrinkage cracks in the inner pyrocarbon layer which has been shown (Miller 2001) to lead to stress concentrations in the SiC layer and subsequent failure of the layer. Photographs of such irradiation induced shrinkage cracks in the F-30 and NPR-1 irradiations are shown in Figure 5-2 and discussed further in Section 5.2. Our review indicates that U.S. anisotropy measurements on PyC, especially by optical methods (OPTAF), appear not to correlate with the larger body of data on the role of coating rate in producing isotropic PyC and furthermore are very unreliable predictors of PyC failure under irradiation. More reliable methods on anisotropy characterization are needed to correlate acceptable processing parameters to anisotropy and to PyC survivability under irradiation.

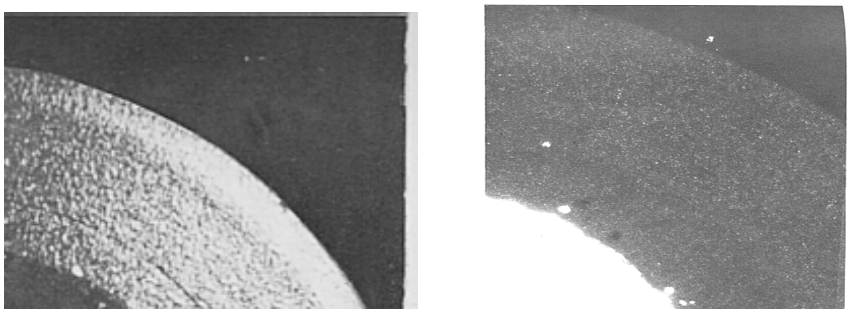

a. Laminar PyC
Low coating gas concentrations

b. Isotropic PyC
Higher coating gas concentrations

Figure 5-1. Effect of the coating rate on the PyC microstructure (Martin 2000).

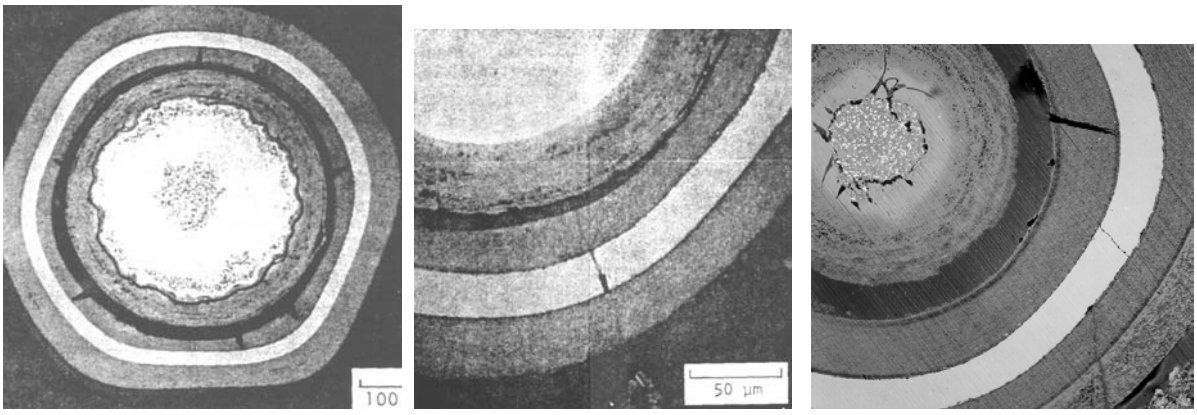

Figure 5-2. Irradiation induced cracking of IPyC in F-30 irradiation (left and center photographs) and NPR irradiation (right photograph).

Nature of the IPyC/SiC interface. Another important difference between U.S. and German TRISO-coated fuel is the nature of the IPyC/SiC interface. Differences in fabrication process of the IPyC and SiC coating layers (e.g., coating rates, temperatures) appear to lead to a difference in the surface porosity and microstructure between the German and U.S. IPyC. Photomicrographs of the IPyC/SiC interface in German and U.S. fuel are shown in Figure 5-3. This figure shows that the interface in German fuel is more tightly bonded because SiC is deposited into a PyC that appears to have more surface porosity. For the U.S. fuel, apparently the less surface porosity in the IPyC and/or the underlying PyC microstructure results in a smoother, less strong bond. The TRISO coating of German fuel never exhibits debonding under irradiation whereas the review of the irradiation results in Section 3 indicates that the TRISO coating in U.S. fuel debonds quite frequently. The debonding is believed to be related to the strength of the IPyC/SiC interface. Partial debonding can lead to stress intensification in the SiC layer that may cause failure (see Section 5.2).

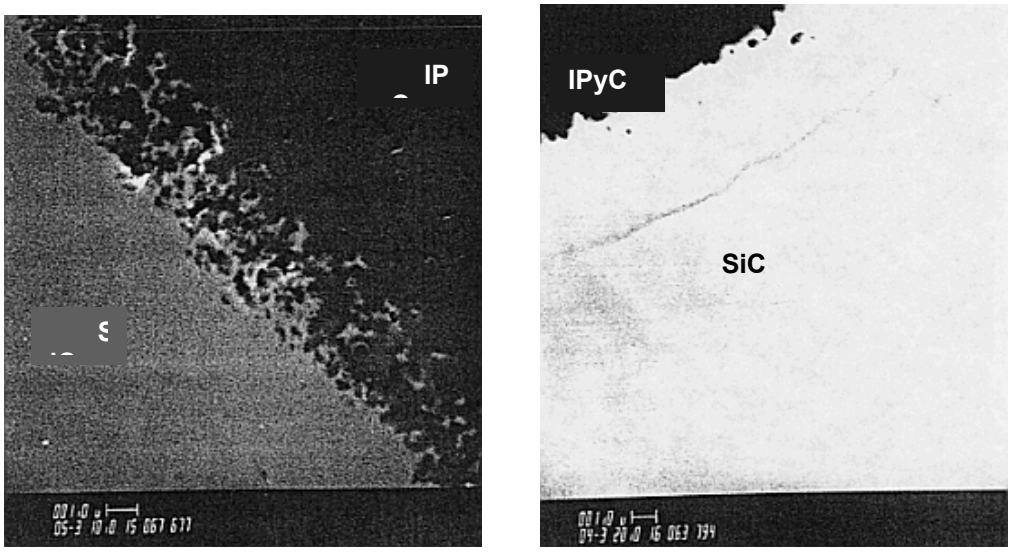

Figure 5-3. Comparison of SiC/IPyC interface in German (left) and U.S. (right) fuel.

SiC microstructure. The microstructures of German and U.S. SiC are different because of the different temperatures used in the coating process. The deposition of the SiC layer is performed at significantly higher temperature in the GA process (1650°C) compared to the German process (1500°C). Price (1977) explains that the SiC grain size increases with increasing deposition temperature. Although the same SiC phase is obtained (i.e., beta SiC) within the 1500-1650°C range, the size of the grains can differ considerably. At lower temperatures the grains are smaller. On the other hand, at higher temperatures the grains can be as large as the SiC layer thickness, which may result in poor retention of the fission products under high-temperature conditions typical of accident situations. It is reported by Saurwein and Schilling (1993) that the NPR-PTF fuel particles presented columnar SiC grains as long as 30 μm (comparable with the thickness of the SiC-layer), while only smaller grains (about 2 μm) were found in the German fuel.

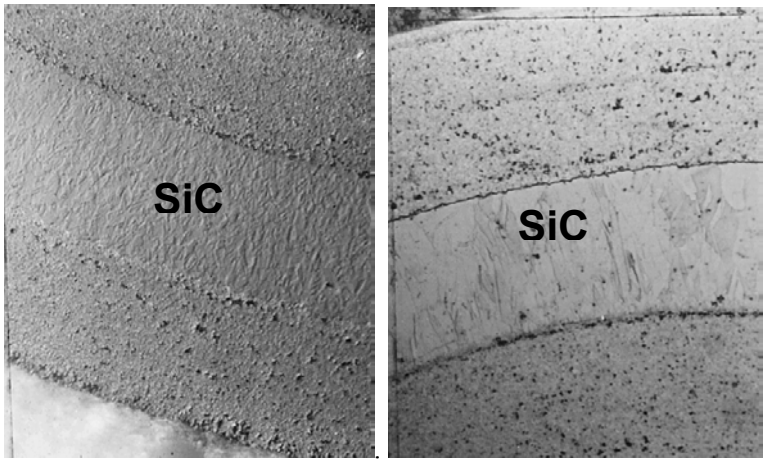

Figure 5-4. Comparison of microstructure of German (left) and U.S. (right) produced SiC.

A comparison of the microstructures is shown in Figure 5-4. These differences could be important from a performance perspective because the smaller-grained German SiC with its longer grain pathway to the surface should in principle retain metallic fission products better than the large columnar U.S. SiC. Data from accident testing presented in Section 4 and from the HRB-15A experiment (GA 1984) suggests that Ag release is a function of the microstructure of the SiC. Figure 5-5 compares photomicrographs of two different types of SiC morphologies produced on U.S. UCO fuel. The fuel was irradiated to 26%FIMA and a peak fluence of 5.4 x 10^{25} n/m^2 at a temperature of ~ 1100°C. Approximately 90% of the Ag was released from the large columnar grained SiC whereas only ~ 30% was released in the smaller grained SiC microstructure. Figure 5-6 is a photomontage of different SiC microstructures of U.S. coated particles with different kernels heated at 1500°C following irradiation. Release of Ag was 100% from the UO_2 particles with large columnar grained SiC, and 24% for cesium. The weaker laminar SiC structure, which was applied to the UC_2 kernel also showed very high Ag (82%) and Cs (12%) releases. The laminar SiC microstructures associated with UCO showed very little release of Ag and none for Cs. In addition, the effect of grain size and morphology on Cs retention in SiC has been studied (Myers, 1984). The diffusivity of cesium through columnar SiC was given as an order of magnitude greater than through laminar SiC. The ability of make definitive statements about the role of SiC microstructure in fission product release from the coated particle is complicated by the fact that these data were obtained on fuels with different kernel types whose ability to retain metallic fission products may be different.

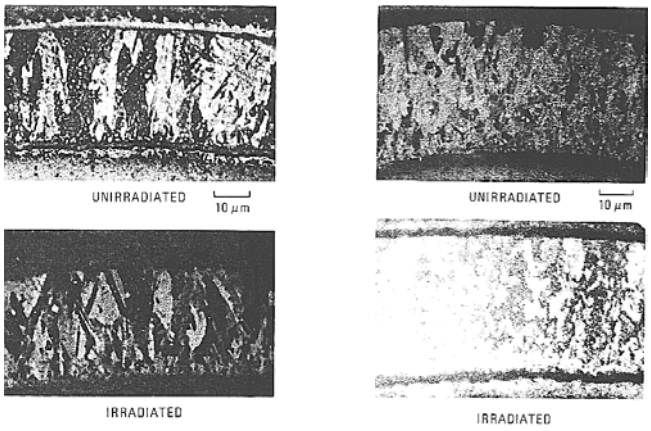

Figure 5-5. Photomicrographs of large thru-wall columnar SiC grains and smaller SiC grains produced in UCO fuel irradiated in U.S. HRB-15A. Ag releases from these two fuels were different.

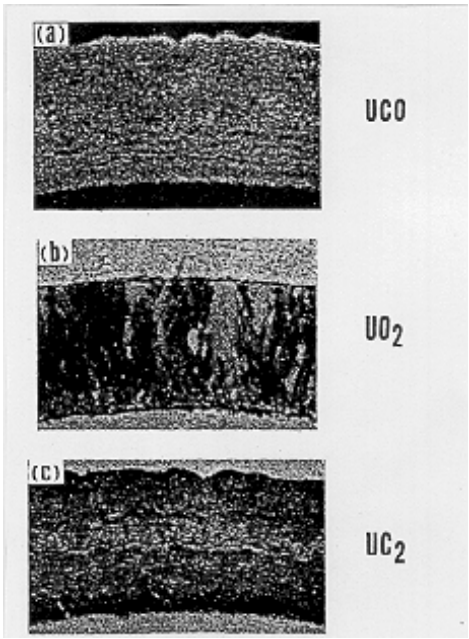

Figure 5-6. Microstructures of different SiC layers on coated particles.

5.2 Failure Mechanisms

A review of the irradiation and safety testing of coated particle fuel in Sections 3 and 4 reveals a number of potential failure mechanisms. These failure mechanisms are functions of temperature,

burnup, fluence, and temperature gradient across the particle. Mechanisms that may result in particle failure, which ultimately leads to fission product release, can be listed as:

(1) Pressure vessel failure caused by internal gas pressure
(2) Pyrocarbon layer cracking and/or debonding due to irradiation induced shrinkage which ultimately leads to the failure of the SiC layer
(3) Fuel kernel migration (amoeba effect) which leads to interactions with the coating layers.
(4) Fission product/ coating layer chemical interactions
(5) Matrix/ OPyC interaction
(6) As-manufactured defects produced during fabrication of fuel particles or during pressing of fuel compacts/spheres
(7) Thermal decomposition of the SiC layer at very high temperatures
(8) Enhanced SiC permeability and/ or SiC degradation

In this section, these mechanisms and the variables that control them are briefly described.

Pressure Vessel Failure

Under irradiation coated particle fuel is subjected to a number of forces that put stress on the TRISO coating. One of the earliest recognized mechanisms is overpressure due to gas generation under irradiation. During irradiation, fission gases are released from the kernel to the porous buffer layer. The pressure that is generated exerts tensile forces on the IPyC and SiC layer of the particle. In addition to fission gas, in coated particle fuel with UO_2 kernels, there is excess oxygen released during fission. (The rare earth and other fission products tie up about 1.6 atoms of oxygen per fission, leaving an excess of 0.4). This excess oxygen will react with the buffer to form CO gas. Both the fission gas and CO production are functions primarily of burnup and temperature. In UCO fuels, CO is not produced, provided enough uranium carbide is added to the kernel to ensure that there is no excess oxygen available from fission to react with the buffer layer over the burnup life of the fuel. The key variables that affect this mechanism are burnup and temperature. Fluence does not significantly affect these processes. Particles are generally sized with a large enough buffer to ensure that nominal particles do not fail by overpressure. Particle failure is postulated to occur in the event that during the coating process, particles are coated with an insufficient or missing buffer layer (i.e., void volume to accommodate the gases). Thus, fabrication specifications limit the number of particles produced with thin or missing buffer layers and impose limits on the statistical variation in kernel diameter and buffer thickness. Photomicrographs displaying overpressure failures for a fertile, UO_2 and UC_2 particle are presented in Figure 5-7. No indications of pressure vessel failure were observed in the German experiments. This is a much analyzed, but seldom seen failure mechanism.

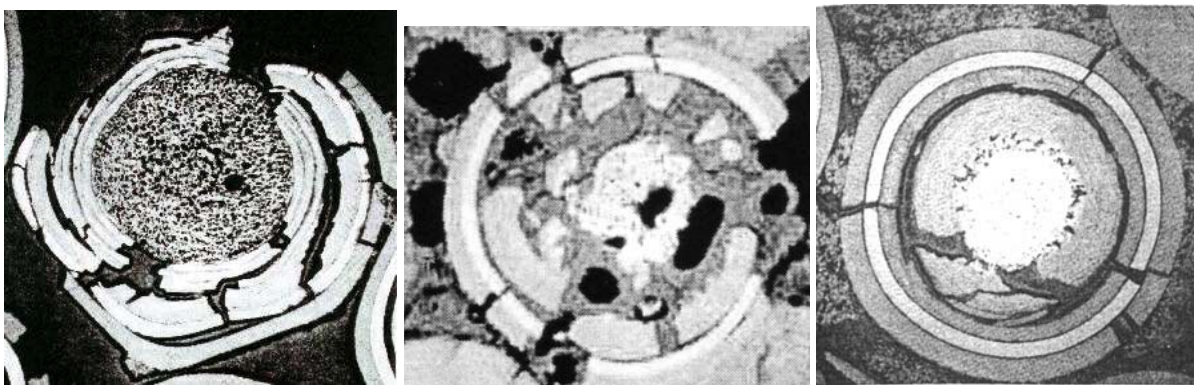

Figure 5-7. Pressure vessel failure in a fertile fuel particle from HRB-14, a UO_2 particle from HRB-8 and a UC_2 particle from P13T.

Irradiation-induced IPyC Cracking and Debonding

Under irradiation, PyC shrinks in both the radial and tangential direction. At modest fluences (~ 2 x 10^{25} n/m^2) depending on the density, temperature and anisotropy of the material, it begins to swell in the radial direction and continues to shrink in the tangential direction. This behavior puts the PyC layers into tension in the tangential direction. At longer irradiation times, irradiation induced creep works to relieve the tensile stress in the PyC layer. If the PyC is strongly attached to the SiC layer, the PyC shrinkage provides a strong compressive stress in the SiC layer that offsets the tensile stresses generated by gas production. In fact, the particles are designed such that in intact particles, the SiC layer remains in compression throughout the irradiation.

The shrinkage, swelling and creep behavior of the pyrocarbons is quite complex. Detailed stress calculations are used to model the evolution of stress and strain in all layers of the TRISO coating. In many of U.S. irradiations reviewed in Section 3, including the most recent from the DOE New Production Reactor Program, the shrinkage was much larger than anticipated and led to tangential stresses in the PyC high enough to cause cracking in the layer. These cracks led to tensile stress concentrations in the SiC layer high enough to cause failure of that layer (Miller et al. 2001, Leikind 1993). A plot of the tangential stress in the SiC layer of a TRISO-coated particle with an initially cracked IPyC is shown in Figure 5-8. The stress in the SiC at the IPyC crack tip increases with irradiation time (fast fluence) as the IPyC shrinks. At longer times, stress relaxation due to irradiation-induced creep of the IPyC occurs. Photomicrographs of such shrinkage cracks found in the F-30 irradiation used to qualify fuel for Fort St. Vrain and the NPR irradiations are shown in Figure 5-2. Postirradiation examination of German fuel did not reveal any shrinkage cracks in the IPyC

layer as has been observed in U.S. irradiations. Thus, the experimental evidence to date suggests that this mechanism is most likely not important for very isotropic PyC. This is by far the most common fuel failure mechanism observed in GA fuel (See Section 3.2).

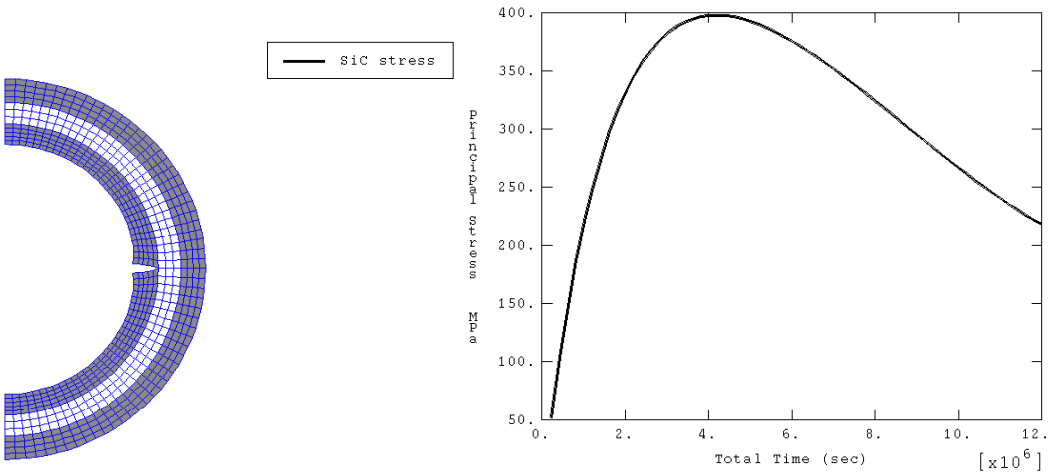

Figure 5-8. Stress history in the SiC of a TRISO-particle with cracked IPyC (Miller et al. 2001).

As discussed in Section 5.1, this failure mechanism has been attributed to high anisotropy in the PyC layer because of deposition of the layer at too low of a coating gas concentration and thus coating rate during manufacture of the fuel.

In addition to irradiation-induced shrinkage, debonding at the IPyC/SiC interface has been observed in many U.S. irradiations. As discussed in Section 5.1, this debonding is believed to be related to the nature of the IPyC/SiC interface. Weakly bonded coating layers as in U.S. fuel can partially detach because of the radial tensile stresses generated by the PyC shrinkage under irradiation. A particle for which partial debonding of the IPyC from the SiC has occurred can develop relatively large tensile stresses in the SiC (although significantly smaller than in the case of a cracked IPyC). The stress history for an initially partially debonded fuel particle is illustrated in Figure 5-9. Tensile stresses occur at the point of IPyC/SiC contact as the IPyC shrinks under irradiation. Irradiation induced creep relieves the stress at longer times. When these stresses are used in concert with the Weibull statistics to calculate the SiC failure probability, it is found that the SiC fails at a low, but not insignificant, rate.

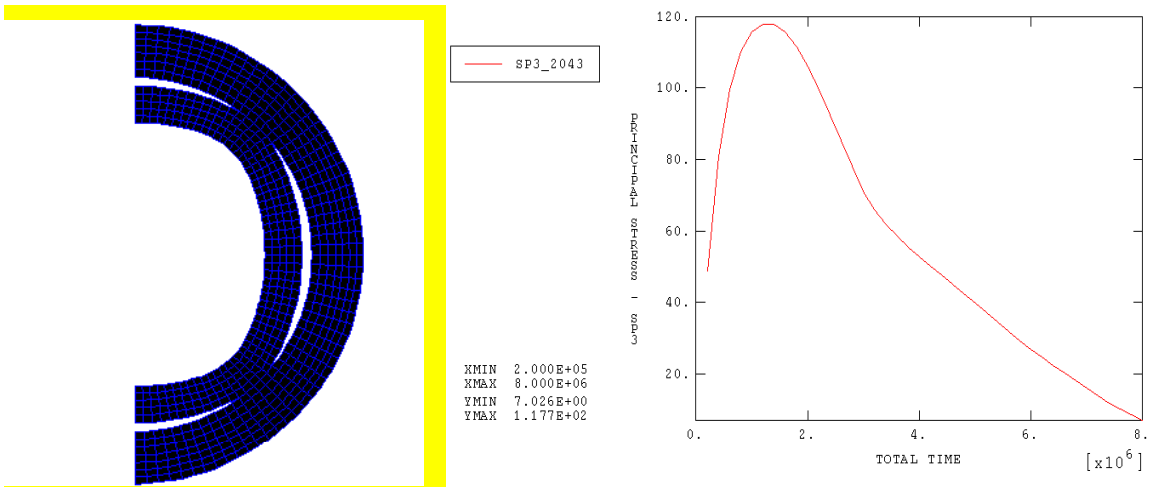

Figure 5-9. Stress time history for the SiC layer near a partially debonded area..

The loading and unloading of the particles after deposition of each layer in U.S. fuel has been hypothesized to lead to thermal shock of the fuel particles that could produce microcracks in the IPyC layer that might grow and cause fuel failure under irradiation. We have analyzed such an event as discussed in Appendix A and concluded that the thermal stresses induced by this discontinuous fabrication process are well below the failure strength of IPyC.

Kernel Migration

Kernel migration is defined simply as movement of the kernel in the coated particle toward the TRISO coating. If the migration is excessive, the kernel will penetrate the TRISO coating leading to failure of the particle. Kernel migration, also known as the amoeba effect, is actually a misnomer. Kernel migration is associated with carbon transport in the particle in the presence of a temperature gradient. In the fuel kernel there is an equilibrium between C, UO_2 and CO. When there is a thermal gradient across the particle, the equilibrium is different on each side of the particle. The different equilibrium conditions leads to mass transport of carbon down the temperature gradient. This movement of carbon appears in photomicrographs of fuel as a movement of the kernel up the temperature gradient and hence the name kernel migration as shown in Figure 5-10. This phenomenon is strongly dependent on the temperature and temperature gradient in the fuel with secondary dependence on burnup. In prismatic cores with UO_2 fuel, where power densities in the particles are greater, the potential for kernel migration is greater. In pebble bed cores, the power densities and hence the thermal gradients are much smaller. Kernel migration was observed in a number of U.S. irradiations (HBR-4, OF-2, HRB-14, HRB-16), but has not been observed in German

irradiation experiments or in AVR and THTR operation due to the low power densities and the lack of a sufficiently steep thermal gradient. For prismatic cores, this phenomenon prompted the U.S. to change their kernel design from UO_2 to UCO, an oxycarbide kernel, in which no CO is produced and thus the equilibrium and carbon transport phenomena mentioned above are not expected to occur. In most recent irradiation experiments with U.S. UCO fuel with a proper C/O ratio kernel migration has not observed. In the design of irradiation experiments, it is important to limit the thermal gradient across the fuel specimen or power per particle to values that are typical of those in the reactor application to ensure that no false positives are observed. As a result, German researchers recommend that the level of acceleration of any coated particle fuel irradiation be no greater than three times real time.

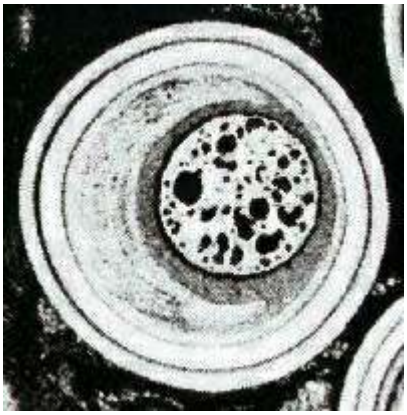

Figure 5-10. Photomicrograph of kernel migration.

Fission Product Coating Layer Chemical Interactions

Past irradiation experiments indicate that fission products can be transported from the kernel to the inner surface of the SiC where they interact and can damage and potentially fail the SiC layer. In older uranium carbide kernels rare earth fission product migration was of concern. In UO_2 kernels, palladium is very important as are some other noble fission products. In UCO kernels, the oxycarbide form of the kernel generally ties up all fission products with the exception of the metals (e.g., Ag, Cs, Pd) as either carbides or oxides which tend to limit their mobility in the UCO system. However, Pd transport has still been observed in UCO coated particle fuel. In addition, although not a failure mechanism, the migration of silver in both UO_2 and UCO has been observed. The silver can migrate through apparently intact particles and be released into the reactor coolant system where it will deposit on cold surfaces. For direct cycle gas reactors, this may be in the turbine, which has important maintenance (worker dose) implications. Studies have been conducted to understand the mechanism

for the Ag migration through and Pd attack of the SiC. The migration of the fission products is thought to be a function of temperature and burnup as well as temperature gradient. Although a complete understanding of the phenomena is not available, the role of temperature gradient is recognized as being critical. The degree of fission product attack is generally correlated with the temperature gradient in the fuel. Thus, these fission product attack mechanisms are expected to play a more important role in prismatic reactors where power densities in the particle are larger than corresponding particles in a pebble bed reactor. A representative photomicrograph of this attack in U.S. fuel is shown in Figure 5-11.

Also of note here is the fact that the enrichment of the fuel is important in defining the magnitude of the Ag and Pd problem. The difference in yield of Ag and Pd between U and Pu is on the order of 25 to 50. Thus, in LEU fuels where at the end of life significant fission comes from Pu, the concentration of Ag and Pd can be much greater than in HEU fuel of similar burnups. As in the case of kernel migration, it is important to limit the thermal gradient or power per particle in the design of irradiation experiments to values that are typical of that in the reactor application to ensure that no false positives are observed. As a result, German researchers recommend that the level of acceleration of any coated particle fuel irradiation be no greater than three times real time.

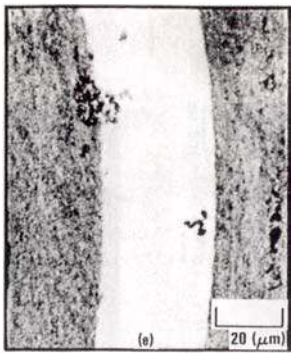

Figure 5-11. Photomicrograph demonstrating fission product attack of the SiC layer.

Chemical reactions between fission products and SiC layers have not been observed in German fuel at the conclusion of the irradiation experiments. However, during high temperature safety tests, palladium was identified as the primary fission product causing SiC degradation.

Matrix-OPyC Interaction

In many of the U.S. irradiations, high levels of OPyC failure were observed (e.g., HRB-4, HRB-5, OF-2) by cracking or debonding from the SiC layer. These failures were attributed to intrusion of the liquid carbonaceous matrix material in the OPyC during compact fabrication followed by shrinkage under irradiation. Specifications on the U.S. matrix material and its injection were developed based on the irradiation experiments to limit this failure mechanism. In addition, in other U.S. irradiations, irradiation-induced failure was observed, and attributed to a combination of unacceptable microporosity and anisotropy of the layer. Fuel fabrication specifications were developed in the U.S. to limit this failure mechanism to 3% of all OPyC layers, a level considered acceptable based on fuel performance modeling at the time. No similar behavior was observed in German fuel because of the use of powder-based matrix material that is more difficult to penetrate the OPyC and the higher isotropy of German PyC.

As-Manufactured Defects

In the absence of any of the above failure mechanisms, any fission gas and metal release during irradiation is attributed to heavy metal contamination outside of the SiC layer and to initially defective particles. Initially, defective particles can be the result of undetected defective particles that have not been removed during fabrication, attack of the particles during fabrication or irradiation by impurity metals (e.g., Fe), or particles that have failed as a result of the formation of the particles into a compact in a prismatic design or a pebble in the pebble bed design. The high level of as-manufactured defects in GA fuel is believed to be related to the introduction of impurities from the graphite furnace that attack the SiC layer during final heat treatment at 1700°C (Don McEachern 2002).

Numerous process improvements have been made to minimize these defects so that the fuel process specifications can be met. For example, in German fuel, particles are tabled at numerous points during fabrication to remove out-of-round particles (after kernel, TRISO-coating deposition, and particle overcoating). Metal screens are no longer used in some fabrication lines to limit metal pickup during fabrication. During the NPR program, stringent control of key aspects of the process was used in prismatic fuel to limit heavy metal contamination. In pebble bed fuel, a soft overcoating is put on the particle after the OPyC layer reduce out of roundness and to limit stresses induced by particle-to-particle contact during pebble manufacture. In prismatic fuel, recent process development work has been carried out to reduce particle stresses during compact formation.

During the three decades of German particle fuel production, the fraction of as-manufactured defects has continuously dropped to very low levels (< 1 x 10^{-6}). This is evident by the low BOL Kr-85m R/B values (reaching a minimum value of 2 x 10^{-10} in the FRJ2-K15 experiment) from each of the German experiments. Even at these low defect levels, as-manufactured defects were the most common source of particle abnormalities reported. In all, one fuel kernel was reported to be without coating in the FRJ2-P27 experiment and two kernels were reported to be without coating in the R2-K12 experiment. The particle failures cited in the HFR-P4 experiment were caused by contact with thermocouples and gas inlet tubes and thus, may be considered as failures due to fabrication of the test capsule and not as an intrinsic fault of the fuel.

SiC Thermal Decomposition

At very high temperatures (> 2000°C), thermodynamics and data from high temperatures heating tests show that the SiC layer undergoes thermal decomposition. This phenomenon is primarily a function of temperature and time and has not played a major role in fuel failure at lower accident temperatures (1600-1800°C).

Enhanced SiC Permeability and/or SiC Degradation. Although not formally a failure mechanism, there is some limited evidence presented in Section 4 that fast neutron fluence and/or burnup plays a role in the permeability or degradation of the SiC layer with respect to fission products under high temperature heating. Pebbles exposed to higher fluence (4.6 x 10^{25} n/m^2) and higher burnup (14%FIMA) have exhibited a greater release of fission products (e.g., cesium) in heating tests than similar pebbles exposed to less severe conditions. This phenomenon could become very important as coated particle fuel is pushed to higher burnup.

6. SUMMARY AND CONCLUSIONS

This review has concluded that there has historically been a difference in the quality of U.S. and German fuel. This difference has been traced to technical differences in the fabrication processes used in Germany and the U.S. as well as different philosophies used to implement the irradiation and testing programs in the two countries.

A review of the fabrication processes used in Germany and the U.S. to make coated particle fuel indicates that the scale of fuel fabrication and development efforts in the last 25 years were quite different. German fabrication of modern TRISO fuel was industrial/production scale incorporating improvements from fuel manufactured for the German AVR and THTR reactors. Only ~ 100 defects were measured in 3.3 million particles produced. The post Fort St. Vrain U.S. Program was a mixture of lab scale and larger scale fabrication. The initial defect levels varied greatly and were generally much greater than those produced in Germany.

A comparison of the fabrication processes has revealed many differences in the overall process. Three specific technical differences in the nature of the TRISO coating that can be attributed to differences in the fabrication processes are: pyrocarbon microstructure and density, the nature of the IPyC/ SiC interface, and SiC microstructure.

A review of the U.S. and German irradiation programs over the last 25 years indicates that the irradiation programs were implemented quite differently with vastly different results. The German program's focus was on UO_2-TRISO fuel for AVR and all future designs such as HTR Modul. The U.S. program produced and tested many different variants (different coatings, different kernels) using different coaters and different coating conditions, with apparently few lessons learned from one irradiation to the next, and insufficient feedback to the fabrication process. The on-line gas release data indicate that German fuel exhibits about a factor of 1000 less fission gas release under irradiation than U.S. fuel under a broad range of conditions (i.e., temperature, burnup, fluence). Furthermore, the postirradiation examination confirms the more extensive gas release data. German fuel is excellent. Out of ~ 380,000 LEU UO_2 and ~ 80,000 HEU $(Th,U)O_2$ particles tested there were no in-pile failures and only a few "damaged" particles due to experimental anomalies. Gas release was attributed only to as-manufactured defects and heavy metal contamination. U.S. fuel did not perform very well. Percent level failures of fuel, and in many cases very high levels of failures of individual layers of the TRISO coating were observed following irradiation in most experiments. A variety of

failure mechanisms were noted which were related to effects of accelerated irradiation and attributes of the fabrication process.

Extensive testing has been done on German TRISO-coated fuel to characterize the behavior under long term depressurized conduction cooldown. Much less work has been done on U.S. UCO fuel. The German data show excellent behavior for fuel irradiated to burnups of less than 9%FIMA and fast fluences less than 4×10^{25} n/m^2 annealed at 1600°C. Greater releases were observed at higher temperature or 1600°C in fuel irradiated to 14%FIMA and fluences above 4.6×10^{25} n/m^2. The work has resulted in better understanding of the mechanisms that challenge the integrity of SiC with respect to retention of fission products of the expected source term from the fuel for such events.

7. REFERENCES

Adams, C.C., April 1994, *Fuel Particle Coating Process Topical Development Plan*. Attachment to Report GA/DOE-065-94.

Allen, P.L., et al., 1977, "Nuclear Fuel Coated Particle Development in the Reactor Fuel Element Laboratories of the U.K. Atomic Energy Authority," *Nuclear Technology,* Vol.35, pp.246-253.

Baldwin, C.A., and M.J. Kania, 1990, "Fission Product Retention in TRISO Coated UO_2 Particle Fuels Subjected to HTR Simulated Core Heating Tests: Behavior of Gas Cooled Reactor Fuel Under Accident Conditions,"*IAEA Specialists Meeting*, Oak Ridge, Tennessee, November 5-8.

Baldwin, C. A., et al., 1993a, *Interim Postirradiation Examination Data Report for Fuel Capsule HRB 21*, ORNL/M-2850.

Baldwin, C. A., et al., 1993b, *The New Production Reactor Fuel Post Irradiation Examination Data Report for Capsules NPR 1, NPR 2, and NPR 1A*, ORNL/M-2849.

Baumeister, T., 1978, *Marks' Standard Handbook for Mechanical Engineers*, 8th Edition, pp.4-10/4-11.

Besenbruch, G., 1993, "Improvements and Changes for Coating System," *FCT Meeting, Oak Ridge, Tennessee, September 1.*

Besenbruch, G., et al., 2001,"HTR Fuel Compacts without Defective Particles," *Proceedings of the HTR-TN International Fuel Seminar, Brussels, Belgium, February 1-2.*

Brodda, B. G., et al., 1985, *The German-U.S. Cooperative Experiment R2-K13 Part I: Irradiation of UCO and ThO_2 TRISO Particles in Prismatic Block Segments*, KFA-HBK-IB-09/85.

Bryan, M.F., 1992, *Evaluation of NP-MHTGR Performance Test Fuel Quality Control Data*, INEEL. Report EGG-NPR-10130.

Bullock, R.E., 1984, "Fission-Product Release During Postirradiation Annealing of Several Types of Coated Fuel Particles," *J. Nucl. Matter*, Vol. No. 125, pp. 304.

Bullock, R.E., September 1993, "Proposed Fixes for TRISO-P Fuel," CEGA Interoffice Correspondence, CEGA-M-93-1178.

Burington, R.S., and D.C. May, Jr., 1970, Handbook of Probability and Statistics with Tables, 2nd ed., McGraw-Hill, New York.

Caldwell, C.S., 1993, "Kernel Fabrication Line. Kernel Stoichiometry," *FCT Meeting, Oak Ridge, Tennessee, September* 1.

CEGA, 1993, *NP-MHTGR, Material Models of Pyrocarbon and Pyrolytic Silicon Carbide Report,* CEGA-002820.

Conrad, R., and K. Bakker, 2001, "Irradiation of Fuels for High Temperature Gas-Cooled Reactors at the HFR Petten," *International HTR Fuel Seminar, Brussels, Belgium, February 1-2.*

Czechowicz, D.G., February 1992, "Influence of UCO Composition on CO Generation for NP-MHTGR Fuel–Consequence of High CO Pressure on Fuel Performance," CEGA Interoffice Correspondence, CEGA-M-92-0580.

EG&G, 1991, *Product Specification for NPR-MHTGR Performance Test Fuel Report* ES-51393 Rev.2. Project 015448.

Fukuda, K., K. Hayashi, and K. Shiba, 1990, "Fuel Behavior and Fission Product Release under HTGR Accident Conditions-Fission Product Transport Processes in Reactor Accidents*," Proceedings Conference, Dubrovnik, 1989*), J. T. Rogers, Ed., Hemisphere Publ., pp. 197-204.

Fukuda, K. et al., 1991, "R&D of HTTR Coated Particle Fuel," *Journal of Nuclear Science and Technology*, Vol. 28, No. 6, pp. 570-581.

Fukuda, K. et al., 1989, *R&D of HTGR Fuel at JAERI,* Report IAEA-TECDOC-577.

GA, 1984, *Capsule HRB-15A Postirradiation Examination Report,* General Atomics, Report GA-A16758, pp. 4-9, 4-10.

GA, 1985, *Capsule HRB-16 Postirradiation Examination Report,* General Atomics, Report HTGR-85-053 pp. 174-176, 177-184.

Gallix, R. 1993, *Evaluation of the Particle Coating Process,* General Atomics, Report PC-000351 (Revision 1).

Gontard, R., and H. Nabielek, 1990, *Performance Evaluation of Modern HTR TRISO Fuels*, HTA-IB-05/90.

Gontard, R. and H. Nabielek, 1990, *Performance Evaluation of Modern HTR TRISO Fuels,* Forschungszentrum Jülich GmbH (KFA), Report HTA-IB-05/90, Chapters 1 and 2.

Goodin, D.T., " CEGA/GA Evaluations of TRISO-P Fuel Failure," *FCT Meeting*, Oak Ridge, Tennessee, August 31, 1993.

Heit, W. et al., 1985, "Status of Qualifications of High-Temperature Reactor Fuel Element Spheres," *Nuclear Technology*, Vol. 69, pp. 44-69.

Hobbins, R.R., et al., 1993, "NP-MHTGR Fuel Development Program Results", Idaho National Engineering Laboratory, Lockheed Idaho Technologies Company. (Private communications).

Homan, F.J., et al., 1977, "Stoichiometric Effects on Performance of High-Temperature Gas-Cooled Reactor Fuels from the U-C-O System," *Nuclear Technology,* Vol. 35, pp. 428-441.

Huschka, H., and P. Vygen, "Coated Fuel Particles: Requirements and Status of Fabrication Technology," *Nuclear Technology,* Vol. 35, pp. 238-245.

IAEA, November 1997, *Fuel Performance and Fission Product Behaviour in Gas Cooled Reactors*, IAEA-TECDOC-978.

Incropera, F.P., and D.P.De Witt, 1990, *Fundamentals of Heat and Mass Transfer*, 3rd Edition, John Wiley & Sons Publishing, pp. A-7.

Johnson, D., 1993, *Coating Process Improvement Task Close Out Report,* General Atomics. Report PC-000367 (Revision 0).

Ketterer, J. W., and R.E. Bullock, 1981, *Capsule HRB-15B Postirradiation Examination Report*, GA-A15940 UC-77.

Ketterer, J., et al., 1984, *Capsule HRB-15A Postirradiation Examination Report*, GA-A16758 UC-77.

Ketterer, J. W., and B.F. Myers, 1985, *Capsule HRB-16 Postirradiation Examination Report*, HTGR-85-053.

Lackey, W.J., D.P. Stinton, and J.D. Sease, 1977, "Improved Gas Distributor for Coating High-Temperature Gas-Cooled Reactor Fuel Particles," *Nuclear Technology*, Vol. 35, pp. 227-237.

Leikind, B.J et al., 1993, *MHTGR TRISO-P Fuel Failure Evaluation Report*, DOE-HTGR-903990.

MacLean, H., 2001, "Fission Product Interaction in Pebble Bed Reactor Fuel," *Thesis Committee Meeting*, Massachusetts Institute of Technology, October 5.

Martin, D.G., April 2000, *Pyrocarbon in High Temperature Nuclear Reactor in Irradiation Damage in Graphite due to Fast Neutrons in Fission and Fusion Systems*, Report IAEA-TECDOC-1154.

Martinson, Z. R., et al., 1993, *Test NPR-1A Results Report*, EDF-NPR-MHTGR-0656.

McCardell, R.K., et al., 1990, *NP-MHTGR Fuel Development Program Plan*, Idaho National Engineering Laboratory, Report EGG-NPR-8971 (Revision A).

McCardell, R.K., et al., 1992, *NP-MHTGR Fuel Development Program Plan*. Idaho National Engineering Laboratory, Report EGG-NPR-8971 (Revision C).

McEachern, D.,April 2002, Personal communication.

Mehner, A.W., et al., 1990, "Spherical Fuel Elements for Advanced HTR Manufacture and Qualification by Irradiation Testing," *Journal of Nuclear Materials,* Vol. 171, pp. 9-18.

Miller, G.K., et al., 2001, "Consideration of the Effects on Fuel Particle Behavior from Shrinkage Cracks in the Inner Pyrocarbon Layer," *Journal of Nuclear Materials*, Vol. 295, pp. 205-212.

Minato, K., and K. Fukuda, October 1993, "Thermodynamic Analysis of the Behaviour of HTGR Fuel and Fission Products under Accidental Air or Water Ingress Conditions*," Proceedings of a Technical Committee Meeting, Response of Fuel, Fuel Elements and Gas Cooled Reactor Cores under Accidental Air or Water Ingress Conditions, Beijing, China, October 25-27*, IAEA- TEC DOC-784.

Minato, K., et al., 1994, "Internal Flaws in The Silicon Carbide Coating of Fuel Particles for High-Temperature Gas-Cooled Reactors," *Nuclear Technology*, Vol. 106, pp. 342-349.

Minato, K., et al., 1995, "Failure Mechanisms of Fuel Particle Coating for High-Temperature Gas-Cooled Reactors During the Coating Processes," *Nuclear Technology*, Vol. 111, pp. 260-269.

Minato, K., et al., 1997, "Improvements in Quality of As-Manufactured Fuels for High-Temperature Gas-Cooled Reactors," *Journal of Nuclear Science and Technology*, Vol. 34, No. 3, pp. 325-333.

Minato, K., et al., 2000, "Fission Product Release Behavior of Individual Coated Fuel Particles for High-Temperature Gas-Cooled Reactors," *Nuclear Technology,* Vol. 131, pp. 36-47

Myers, B.F., 1984, *Cesium Diffusion in Silicon Carbide During Post Irradiation Anneals*, Technical Note KFA-HBK-TN-01184, Research Center Jülich.

Nabielek, H., et al., 1984, "Fuel for Pebble-Bed HTRs," *Nuclear Engineering and Design,* Vol. 78, pp. 155-166.

Nabielek, H., et al., 1989, "The Performance of High-Temperature Reactor Fuel Particles at Extreme Temperatures," *Nucl.Technol*., Vol. 84, pp. 62.

Nickel, H., March 1981, "CVD in Nuclear Energy – Pyrocarbon Deposition in Fluidized Beds," *Presented at the Workshop on Plasma Chemistry in Technology. Ashkelon, Israel, March 30.*

Nickel, H., et al., February 2001, "Long Time Experience with the Development of HTR Fuel Elements in Germany," *Proceedings of the HTR-TN International Fuel Seminar, Brussels, Belgium.*

Nuclear News, February 2001, "China's First High-Temperature Reactor Goes Critical," pp. 34-35.

Proksch, E., and A. Strigl, 1982, "Production of Carbon Monoxide During Burn-Up of UO_2 Kerneled HTR Fuel Particles," *J. Nucl. Mater*., Vol. 107, pp. 280.

Saurwein, J., and L. Shilling, September 1993*, Final Report – Testing of As-manufactured NPR-PTF, German, and U.S. Historical Fuel*, General Atomics, Issue/Release Summary, Doc. No. 910647 N/C.

Saurwein, J., September 1994, "Comparison of German QC and GA QC Methods Proposed for MHR-1 and MHR-2 Capsule Fuel," *Presentation to the GT-MHR Fuel Review Committee, General Atomics.*

Sawa, K., et al., 1999, "Fabrication of the First-Loading Fuel of the HTTR," *Journal of Nuclear Science and Technology*, Vol. 36, No. 8, pp. 683-690.

Scheffel, W.J., September 1993, "Proposed Fuel Specification Changes," *FCT Meeting, Oak Ridge, Tennessee.*

Scott, C. B., and D.P. Harmon, 1975a, *Postirradiation Examination of Capsule F-30*, GA-A13208.

Scott, C. B., and D.P. Harmon, 1975b*, Postirradiation Examination of Capsules HRB-4, HRB-5, and HRB-6*, GA-A13267 UC-77.

Schenk, W. and H. Nabielek, 1991, "High-Temperature Reactor Fuel Fission Product Release and Distribution at 1600 to 1800 °C," *Nucl. Technol*., Vol. 96, pp. 323.

Schenk, W., G. Pott, and H. Nabielek, 1990, "Fuel Accident Performance for Small HTRs," *J. Nucl. Mater.*, Vol. 171, pp.19.

Shaber, E.L., October 1992, "Fuel Fabrication History,"*INEEL Presentation*.

Spence, R., 1981. "Sol-Gel Spherical Fuel," *American Society for Metals Conference: Metallurgical Technology of Uranium and Uranium Alloys. Gatlinburg,Tennessee*, *May 26-28.*

Stansfield, O., 1970, "Optical Anisotropy in Pyrolytic Carbon and Graphite," *J. Nucl. Mater*., Vol.34, pp. 215-220

Stinton, D.W., Laday, R. Spence, 1982, "Production of Spherical UO_2-UC_2 for Nuclear Fuel Application Using Thermochemical Principles," *American Ceramics Soc*., Vol. 65, pp. 321-4.

Tang, C. et al., September 2000, "Research and Development of Fuel Element for Chinese 10MW High Temperature Gas-Cooled-Reactor," *Journal of Nuclear Science and Technology*, Vol.37, No.9, pp.802-806.

Tiegs, T. N., and K.R. Thoms, 1979*, Operation and Postirradiation Examination of ORR Capsule OF-2: Accelerated Testing of HTGR Fuel*, ORNL-5428.

Todreas, N.E., and M.S. Kazimi, 1993, *Nuclear Systems,* Taylor & Francis, pp. 295-296.

TPRC, 1973, *Thermophysical Properties of* Matter, Volume 10, Thermal Diffusivity, IFI/Plenum, New York – Washington, pp.502-503.

Verfondern, K., W. Schenk, and H. Nabielek, 1990, "Passive Safety Characteristics of Fuel for a Modular High-Temperature Reactor and Fuel Performance Modeling under Accident Conditions," *Nuclear Technology*, Vol. 91, pp.235.

Voice, E.H., and D.N. Lamb, 1969, "The Deposition and Structure of Pyrolitic Silicon Carbide," DP-677, OECD High Temperature Reactor Dragon Project; U.K. Atomic Energy Establishment, Winfrith.

Wolf, L. et al., 1975, "Fuel Elements of the High Temperature Pebble Bed Reactor," *Nuclear Engineering and Design*, Vol.34, pp.93-108.

Yoshimuta, S. et al., 1991, "Production Process and Quality Control for the HTTR Fuel*," Proceedings of an IAEA organized Specialists Meeting, Oak Ridge, Tennessee, November 5-8, 1990.*

Young, C.A., 1980, *Pre- and Postirradiation Evaluation of Fuel Capsule HRB-14*, General Atomics Report, GA-A15969, UC-77.

Xu, A. et al., 1993, "A Total Gelation Process for the Preparation of Dense UO_2 Microspheres for HTGR," *Proceedings of the First Pacific Rim International Conference on Advanced Materials and Processing (PRICM-1), Hangzhou, CHINA, Jun 23-27, 1992,* pp.1035-1039.

Xu, S.J. et al., 1995, "Effect of Deposition Temperature on the Properties of Pyrolytic SiC," *J. Nucl. Mater*, Vol. 223, pp. 12-16.

.

APPENDIX A – THERMAL-SHOCK CALCULATIONS

Some problems might arise due to the repeated loading and unloading of the particles during the coating process for the GA fuel

1. The cold particles (25°C) are injected in the hot coater (1230°C) with no preheating. This generates large thermal stresses that might crack the coating. Because thermal stresses are self-limiting, the cracks would not grow, but remain very localized and would close when the particle temperature becomes uniform again, which would make them invisible during the fuel QC inspection. However, when the coatings are stressed under irradiation by either fission gas release or neutron-induced shrinkage, these micro-cracks would grow and result in fuel failure (Gallix 1993).

2. The hot particles (1230°C) are dropped into a cold hopper (25°C) and develop tensile thermal stresses at the point of contact (Gallix 1993). Again because thermal stresses are self-limiting, the cracks would be very localized and invisible during the fuel QC inspection, but ready to grow when the coatings are stressed under irradiation (Gallix 1993).

3. The hot particles are dropped from 4 feet and may crack upon impact with the bottom of the hopper (Gallix 1993).

While large cracks from mechanism 3) above would be detectable during QC tests, cracks from mechanisms 1) and 2) might not, because their formation is controlled by thermal stresses, which are self-limiting and can be accommodated by local yielding, thus resulting in small very-localized cracks. Simple calculations were performed to simulate the loading and unloading transients, and to assess the magnitude of the thermal stresses generated during these transients. These calculations are presented in this appendix.

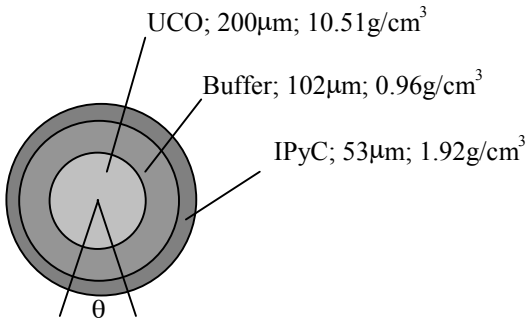

Figure A-1. Schematic of the fuel particle in the coater.

The fuel particle was modeled as a sphere with three regions, i.e., a UCO kernel, a buffer layer and an IPyC of typical thickness and density (see Figure A-1). Four additional material properties were needed for each region to conduct the thermal stress calculations, i.e., the specific heat, the thermal conductivity, the elastic Young's modulus, and the elastic Poisson's ratio.

The kernel composition is 35 at.% U, 12.5 at.% C, and 52.5 at.% O. The specific heat of the kernel $C_{p,UCO}$ was calculated with the Kopp's approximation for multi-component solids (Baumeister 1978):

$$C_{p,UCO} = \frac{\sum_{i=1}^{3} a_i C_i}{\sum_{i=1}^{3} a_i M_i} \qquad \textbf{(A-1)}$$

where a_i, M_i and C_i are the atomic fraction, the atomic weight, and the molar specific heat of the i-th component, respectively. The thermal conductivity of the kernel, k_{UCO}, was then calculated from thermal diffusivity data (TPRC 1973) by means of the well-known definition:

$$k_{UCO} = \alpha_{UCO} \rho_{UCO} C_{p,UCO} \qquad \textbf{(A-2)}$$

where α_{UCO} and ρ_{UCO} are the kernel thermal diffusivity and density, respectively. The Young's modulus and Poisson's ratio for the UCO kernel were arbitrary assumed to be 40 MPa and 0.13, respectively, to simulate a very soft material.

The specific heats for IPyC and the buffer layers were assumed to be equal on a per-unit-mass basis, and were found in (Incropera and De Witt 1990). The thermal conductivity of the IPyC was found in (Martin 2000), and arbitrarily reduced by 75% for the buffer layer. The Young's modulus and Poisson's ratio for the IPyC layer were found in (CEGA 1993). The Young's modulus and Poisson's

ratio for the buffer layer were arbitrary assumed to be 400 MPa and 0.13, respectively, to simulate a relatively soft material.

The calculations were performed with ABAQUS, a finite-element code for structural analysis. A total of 1080 axisymmetric four-nodes elements were used to model the particle, of which 360 elements represented the kernel, 420 the buffer layer, and 300 the IPyC. The temperature and the stress distributions in the three regions were calculated for the following transient, which effectively simulates the loading and unloading of the particles, at the beginning and the end of the IPyC coating deposition, respectively:

Loading. At t=0 a temperature of 1230°C is set at the outer surface of the particle, which is initially at uniform room temperature (25°C). This boundary condition simulates the violent heat-up of the particle upon injection in the hot coater.

Heat-up. A few milliseconds are needed for the particle to reach the new equilibrium temperature of 1230°C.

Unloading. The particle surface is thermally insulated except for a region of the surface defined by a cone of known opening θ (see Figure A-1), where a temperature of 25°C is imposed. This boundary condition simulates the contact of the particle with the cold surface of the hopper.

Cool-down. A few milliseconds are needed for the particle to reach the new equilibrium temperature of 25°C.

The main variables of the calculations are the BAF of the IPyC layer (which affects the development of the thermal stresses), and the cone opening, θ. Two values of the BAF and two values of the cone opening were selected, i.e., 1.06 and 1.2 for the BAF, 30° and 6° for θ. Therefore, a total of four transients were run. The transients were analyzed in terms of maximum principal stress in the IPyC (which always occurs at the inner surface of the IPyC) as a function of time. An example of the variation of the maximum principal stress with time is illustrated in Figure A-2, for BAF=1.06 and θ=30°. As expected, the stresses peak immediately after the abrupt changes in temperature at the particle surface, i.e., when large temperature gradients are present in the IPyC. Also, higher stresses are generated at particle unloading (cool-down) than at particle loading (heat-up).

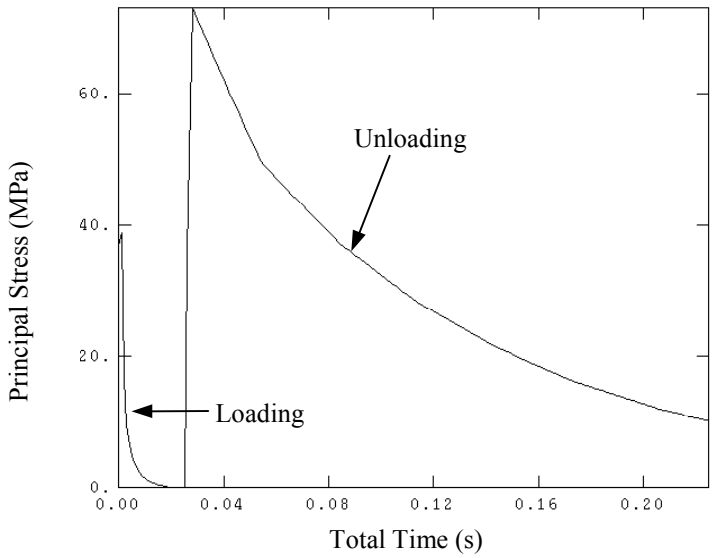

Figure A-2. Thermal stresses in the IPyC of a fuel particle during loading to and unloading from the coater.

The peak stress for all four BAF/θ combinations is reported in Table A-1. It can be seen that the stresses increase with the cone opening and anisotropy. Considering that the cracking strength of the IPyC is about 300 MPa, it can be concluded that thermal shock from loading and unloading of the particles in the coater does not crack the IPyC.

Table A-1. Results of the thermal shock calculations.

BAF	θ	IPyC Peak Stress (MPa)
1.06	6°	40
1.06	30°	70
1.20	6°	50
1.20	30°	80